3-2005

Application of Functionally Graded Materials in Aircraft Structures

William G. Cooley

APPLICATION OF FUNCTIONALLY GRADED MATERIALS IN AIRCRACT STRUCTURES

THESIS

William G. Cooley, Captain, USAF

AFIT/GAE/ENY/05-M04

DEPARTMENT OF THE AIR FORCE
AIR UNIVERSITY

AIR FORCE INSTITUTE OF TECHNOLOGY

Wright-Patterson Air Force Base, Ohio

The views expressed in this thesis are those of the author and do not reflect the official policy or position of the United States Air Force, Department of Defense, or the U.S. Government.

AFIT/GAE/ENY/05-M04

APPLICATION OF FUNCTIONALLY GRADED MATERIALS IN AIRCRACT STRUCTURES

THESIS

Presented to the Faculty

Department of Aeronautics and Astronautics

Graduate School of Engineering and Management

Air Force Institute of Technology

Air University

Air Education and Training Command

In Partial Fulfillment of the Requirements for the

Degree of Master of Science in Aeronautical Engineering

William G. Cooley, BS

Captain, USAF

March 2005

AFIT/GAE/ENY/05-M04

APPLICATION OF FUNCTIONALLY GRADED MATERIALS IN AIRCRACT STRUCTURES

William G. Cooley, BS

Captain, USAF

Approved:

//signed//	
Dr. Anthony Palazotto (Chairman)	Date
//signed//	
Dr. Robert Canfield (Member)	Date
//signed//	
Dr. Richard Cobb (Member)	Date

Abstract

Functionally Graded Materials (FGM) have *continuous* variation of material properties from one surface to another unlike a composite which has stepped (or discontinuous) material properties. The gradation of properties in an FGM reduces the thermal stresses, residual stresses, and stress concentrations found in traditional composites.

An FGM's gradation in material properties allows the designer to tailor material response to meet design criteria. For example, the Space Shuttle utilizes ceramic tiles as thermal protection from heat generated during re-entry into the Earth's atmosphere. However, these tiles are prone to cracking at the tile / superstructure interface due to differences in thermal expansion coefficients. An FGM made of ceramic and metal can provide the thermal protection *and* load carrying capability in one material thus eliminating the problem of cracked tiles found on the Space Shuttle.

This thesis will explore analysis of FGM flat plates and shell panels, and their applications to real-world structural problems. FGMs are first characterized as flat plates under pressure and thermal loading in order to understand the effect variation of material properties has on structural response. Next, FGM shell panels under thermal loading are analyzed. In addition, results are compared to published results in order to show the accuracy of modeling FGMs using ABAQUS software. Conclusions drawn from FGM characterization are used to develop a patch to retrofit a cracked aircraft exhaust wash structure and reduce thermally induced cracking.

Acknowledgments

I would like to express my sincere appreciation to my faculty advisor, Dr. Anthony Palazotto, for his guidance and support throughout the course of this thesis effort. The insight and experience was certainly appreciated. I would, also, like to thank my sponsor, Dr. Ravinder Chona, from the Air Force Research Laboratory for both the support and latitude provided to me in this endeavor.

William G. Cooley

Table of Contents

Page

List of Figures

Page

Page

Page

Page

Page

Page

Page

List of Tables

APPLICATION OF FUNCTIONALLY GRADED MATERIALS IN AIRCRAFT STRUCTURES

I. Introduction

Background

"Functionally Graded Materials (FGM) are a class of composites that have *continuous* variation of material properties from one surface to another and thus alleviate the stress concentration found in laminated composites. The gradation in properties of the materiel reduces thermal stresses, residual stresses, and stress concentrations." [3]

A functionally graded structure is defined as, "those in which the volume fractions of two or more materials are varied continuously as a function of position along certain dimension(s) of the structure to achieve a require function." [2] Because the properties change throughout the dimension (typically the thickness) of a material, FGMs can provide designers with tailored material response and exceptional performance in thermal environments. For example, the Space Shuttle utilizes ceramic tiles as thermal protection from heat generated during re-entry into the Earth's atmosphere. However, these tiles are laminated to the vehicle's superstructure and are prone to cracking and debonding at the superstructure/tile interface due to abrupt transition between thermal expansion coefficients. In other words, the ceramic tile expands a different amount than the substructure it is protecting. The difference in expansion causes stress concentrations at the interface of the tile and superstructure which results in cracking or debonding. Figure 1 demonstrates the stress concentrations found in conventional thermal protection panels at the tile / superstructure interface. It also shows how an FGM can alleviate those

stress concentrations by gradually changing material properties through-the-thickness of the material but still provide the thermal protection found in conventional thermal shielding.

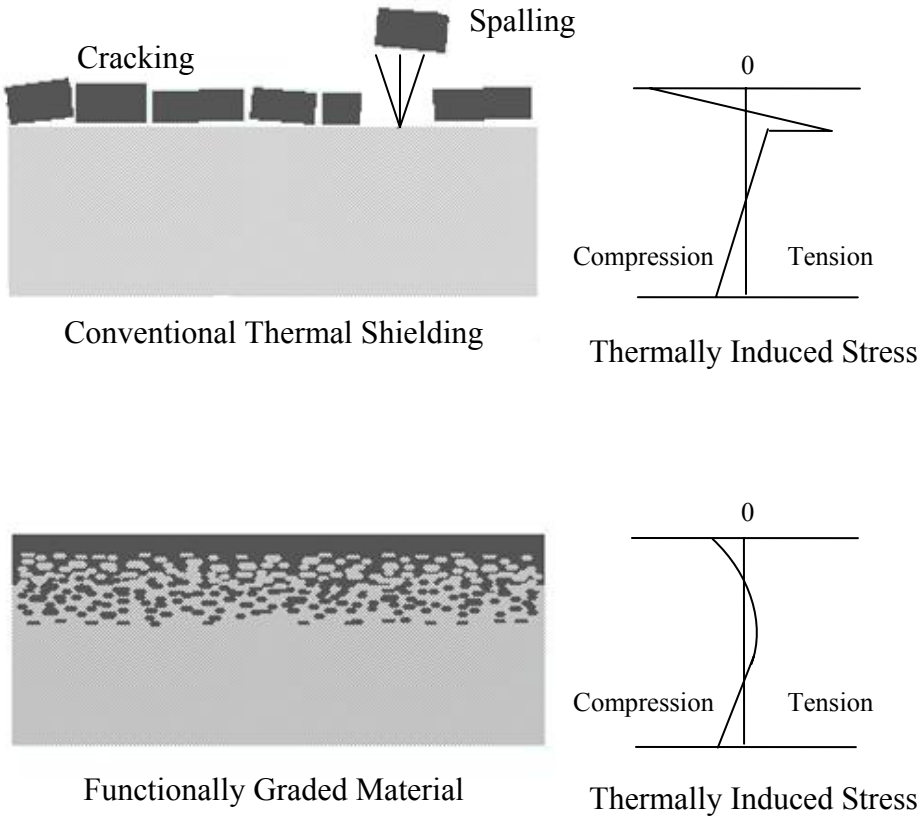

Figure 1. Thermal Protection

An FGM composed of ceramic on the outside surface and metal on the inside surface eliminates the abrupt transition between coefficients of thermal expansion, offers thermal/corrosion protection, *and* provides load carrying capability. This is possible because the material composition of an FGM changes *gradually* through-the-thickness;

therefore, stress concentrations from abrupt changes in material properties (i.e., coefficients of thermal expansion) are eliminated.

Research Focus

This thesis will explore FGM applications in severe thermal environments, such as aerospace and space vehicles. FGM performance is first characterized under thermal environments and mechanical loading in order to understand the unique characteristics of FGMs and to compare FGM structural response to traditional metal structure. Conclusions from FGM characterization are used to support the goal of this thesis: the design of a patch used to retrofit a cracked aircraft exhaust wash structure.

An exhaust wash structure separates exhaust gas from aircraft structure for vehicles which have internally exhausted engines, i.e., stealth aircraft and UAVs with engines that don't exhaust directly to the atmosphere. Hot, high speed engine exhaust flows over the top surface of exhaust wash structures which, in turn, causes large deflections. Cracking typically forms at the boundary of the exhaust wash structure where it is attached to stringers and stiffeners which limit deflection and rotation. Because the hot gas causes the panel to expand, and the boundary region is held rigid by stiffeners, a large moment develops at the boundary and cracking results.

An FGM patch applied to the underside of the exhaust wash structure can be designed such that thermally induced deflection of the FGM patch is in a direction opposite to the exhaust wash structure deflection. An FGM patch can be tailored because of the change in material properties through-the-thickness, namely the coefficient of thermal expansion. It is hypothesized that a carefully designed FGM patch can reduce

thermally induced deflections and halt further crack growth by changing the stress field at the boundary of the exhaust wash structure. Additionally, it is hypothesized that an FGM exhaust wash structure can provide substantial reduction in thermally induced deflection and stress.

Research Outline

In order to design an FGM patch for an exhaust wash structure, research is initially carried out to characterize FGMs under thermal and mechanical loading. Flat plates are analyzed under a range of thermal loads and simple supports in order to understand unique characteristics of an FGM. Displacement plots, stress contours, and temperature profiles are used to compare FGM plate response to a traditional metal structure. A secondary goal is to verify the accuracy of the modeling technique chosen by comparing displacement plots to published results.

Before characterizing FGM curved panels, localized buckling must be explored. Knowing that shell panels under thermal loading are prone to localized buckling [5], a study of local buckling is carried out in ABAQUS. The goal of this segment is to explore localized buckling and compare results to published work in order to gain confidence in solutions where localized buckling is expected. The exhaust wash deck is subject to local buckling because the boundary of the panel is rigidly held in place by stringers and stiffeners. These stringers and stiffeners essentially clamp the edge of the panel and cause buckling because thermally induced expansion can not manifest itself into displacement at the panel edges. A study of localized buckling explores a curved panel under a concentrated force using plots of non-linear center deflection (past local

buckling). These plots are compared to published results in order to gain confidence in ABAQUS' ability to handle localized buckling.

Once confidence in localized buckling solutions is developed, curved shells under thermal loading are examined in order to characterize FGMs as shell panels and to evaluate their performance in buckling scenarios. Additionally, the effect of curvature is compared to the flat plate thermal analysis in order to understand the effect curvature has on structural response.

Finally, using results from the characterization of FGMs, a patch is developed to retrofit an exhaust wash structure. A baseline structural response is first performed on the exhaust wash structure. This baseline is used to evaluate the effectiveness of numerous FGM patches. Patches are evaluated using studies of various materials, patch thickness, boundary conditions, and edge tapering. Plots of deflection and contour plots of stress are used to evaluate the effectiveness of the patch.

II. Methodology

Chapter Overview

The purpose of this chapter is to establish the methodology used to model FGMs with finite elements. Coordinate systems, boundary conditions, theoretical formulation and details of the finite element analysis are discussed or defined. Relevant research is presented in its appropriate section.

Research Focus and Development

Because an engine exhaust wash structure can be either flat or curved, and can be exposed to mechanical loading or steady-state isothermal loading, FGM performance under all of these conditions is studied. This data is obtained through a progressive analysis of flat plates to curved panels and from thermal loading to pressure loading in order to study each loading criteria and structure type separately.

Flat plates are first analyzed as simply supported structures under a range of steady-state isothermal loads (applied as surface temperatures). The suitability of an FGM under this environment is studied using displacement plots, stress contours, and temperature profiles. The goal of this segment of research is to identify FGM performance under thermal loading and to compare performance to traditional structure. In addition, displacement plots are compared to published results in order to demonstrate the accuracy of modeling FGMs in ABAQUS.

Before studying thermally loaded shell panels, a curved shell panel with a concentrated force is studied in order to understand how ABAQUS handles localized buckling. It is desirable to know if ABAQUS can *accurately* handle localized buckling

using traditional analysis techniques or if a full buckling analysis is required. A simply supported panel with a concentrated force applied at the center is analyzed and non-linear plots of displacement are compared to published results.

Once confidence in modeling curved panels under localized buckling is obtained, a simply supported curved panel under steady-state isothermal thermal loading is analyzed. The goal of this segment is to compare the FGM performance in a flat plate to a curved panel and, notably, the effect curvature has on FGM performance. The curved panel has same material properties as the flat plate and also has the same geometry as the flat plate, with the exception of curvature. The suitability of an FGM under this environment is again studied using displacement plots, stress contours, and temperature profiles. At this point, performance of characteristics of FGMs in flat plates and curved shells is known, and ABAQUS' ability to model plates and panels is verified.

Conclusions from aforementioned research are now used to design a patch to retrofit a cracked aircraft exhaust wash structure. The structure cracks because thermally induced deflection is resisted by a clamped boundary condition, which causes high stresses near the edges of the panel. A patch applied to the structure can counteract the deflection by creating a deflection in direction opposite to the previous un-patched structure. First, a baseline study of the structural characteristics of the exhaust wash panel is performed. This baseline is then compared to a variety of patches and is used to evaluate the effectiveness of a patch. The following patch characteristics are studied in order to attempt to optimize a solution: patch thickness, material properties, boundary condition, and edge taper.

At this point it is appropriate to begin an in-depth exploration of FGMs and the finite method modeling technique.

Theoretical Formulation of FGM

An FGM is defined to be a material which has a continuous gradation through-the-thickness (h). One side of the material is typically ceramic and the other side is typically metal. A mixture of the two materials composes the through-the-thickness characteristics. This material variation is dictated by a parameter, "n." At n = 0 the plate is a fully ceramic plate while at n = ∞ the plate is fully metal. Material properties are dependent on the n value and the position in the plate and vary according to a power law.

"The typical material property P is varied through the plate thickness according to the expressions (a power law)

$$P(z) = (P_t - P_b)V + P_b \qquad V_f = \left(\frac{z}{h} + \frac{1}{2}\right)^n \tag{1}$$

Where P_t and P_b denote the particular property being considered at the top and bottom faces of the plate, respectively, and n is the parameter that dictates the material variation profile through-the-thickness." [3] The variation of the volume fraction, V_f, of ceramic through-the-thickness of the plate is an indicator of the volumetric fraction of ceramic at a given location. This volume fraction is based on the mixture of metal and ceramic and is an indicator of the material composition (volumetric wise) at any given location in the thickness. If the volume fraction of ceramic is defined as V_f then the volume fraction of metal is the remainder of the material, or 1- V_f. E, G, ρ, α, and k vary according to the power law and their calculated values are entered into ABAQUS accordingly.

The “n” value is of significance because it is an exponent of the volume fraction equation. “n” essentially dictates the *amount* and *distribution* of ceramic in the plate. With higher values of “n” the plate tends toward metal (the lower surface) while lower values of “n” tend toward ceramic (the upper surface). Designers can vary the “n” value to tailor the FGM to specific applications. This thesis will characterize “n” for each of the models studied in order to provide designers with general value of “n” that will best suit their needs.

Figure 2 details the change in volume fraction through-the-thickness for the values of “n” studied (n=0.0 (fully ceramic), n=0.2, n=0.5, n=1.0, n=2.0, n=∞ (fully metal)).

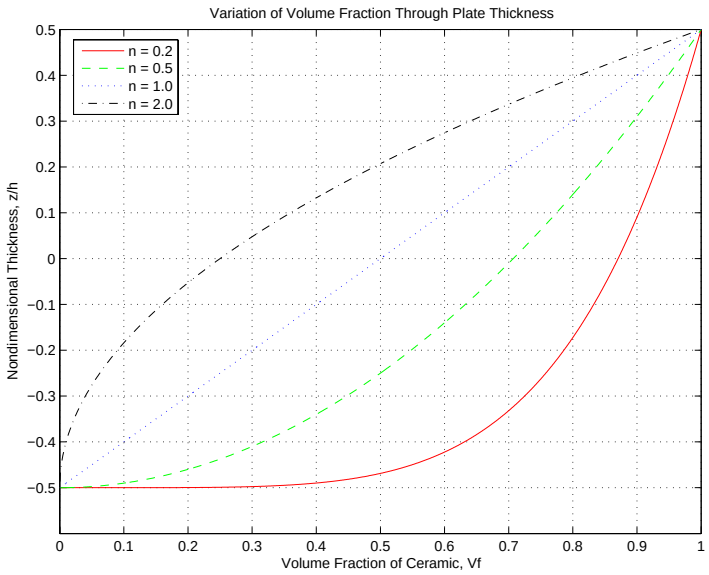

Figure 2. Variation of Volume Fraction

Note that lower values of “n” push the curve toward the right, or toward a fully ceramic plate (bottom surface material). In fact, at n=0, the curve would actually be a vertical line corresponding to a volume fraction of ceramic equal to 1. Additionally,

higher values of "n" push the curve toward the left, or toward a metal plate (top surface material). At n=∞, a straight line would exist at a ceramic volume fraction of 0 indicating a fully metal material.

A more detailed representation of "n" is shown in Figure 3 through Figure 6. where shaded graphs show the reader the gradual change in material properties. Note: black indicates metal material and white indicates ceramic material. The gray shaded region between black and white is a visual indicator of the mixture of metal and ceramic. Dark gray is a metal rich mixture while light gray is a ceramic rich mixture. Additionally, a graph of the ceramic volume fraction, V_f, is presented. It is noted that the area left of the curve indicates ceramic while area right of the curve indicates metal.

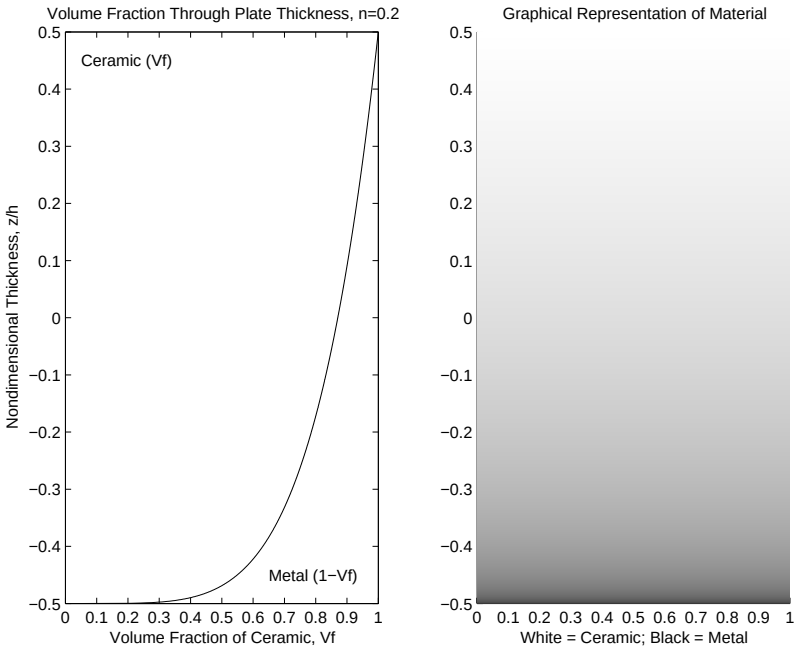

Figure 3. Graphical Representation of n=0.2

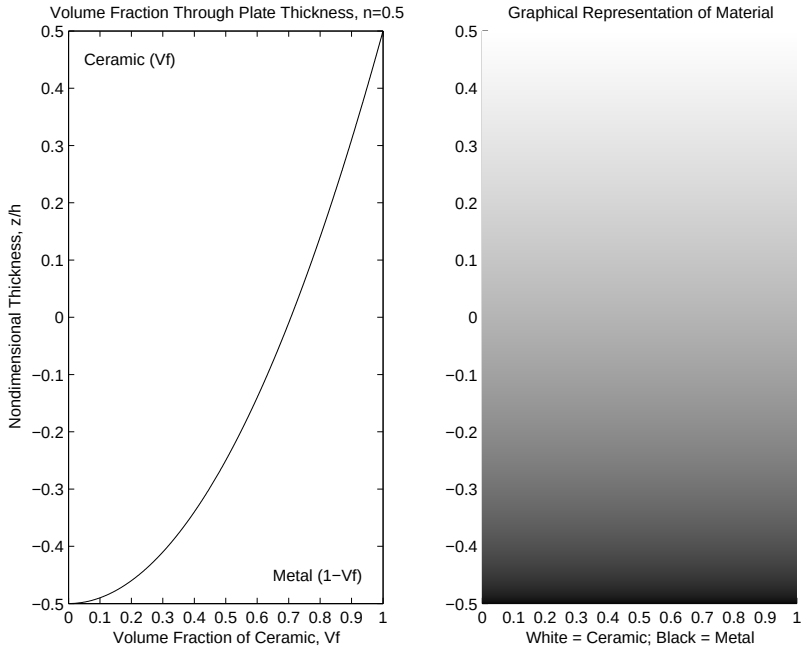

Figure 4. Graphical Representation of n=0.5

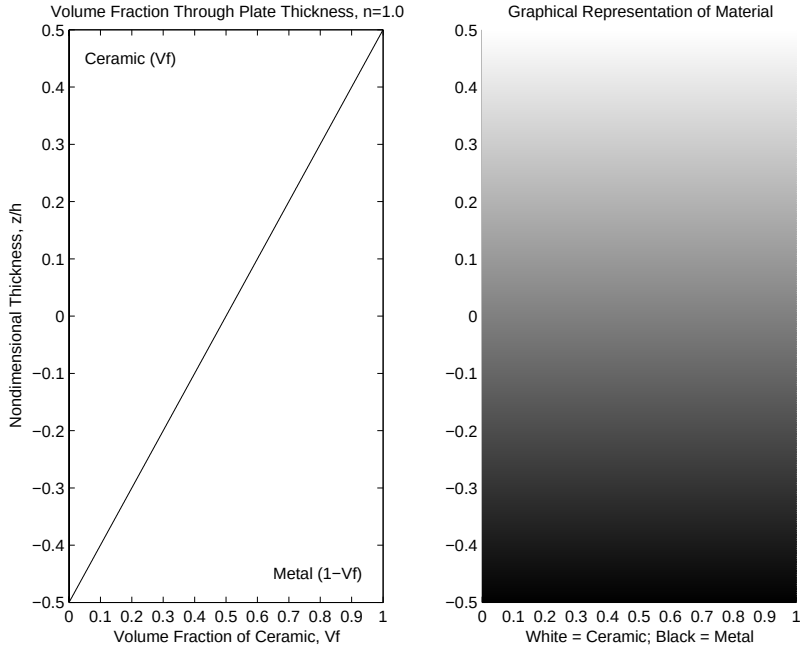

Figure 5. Graphical Representation of n=1.0

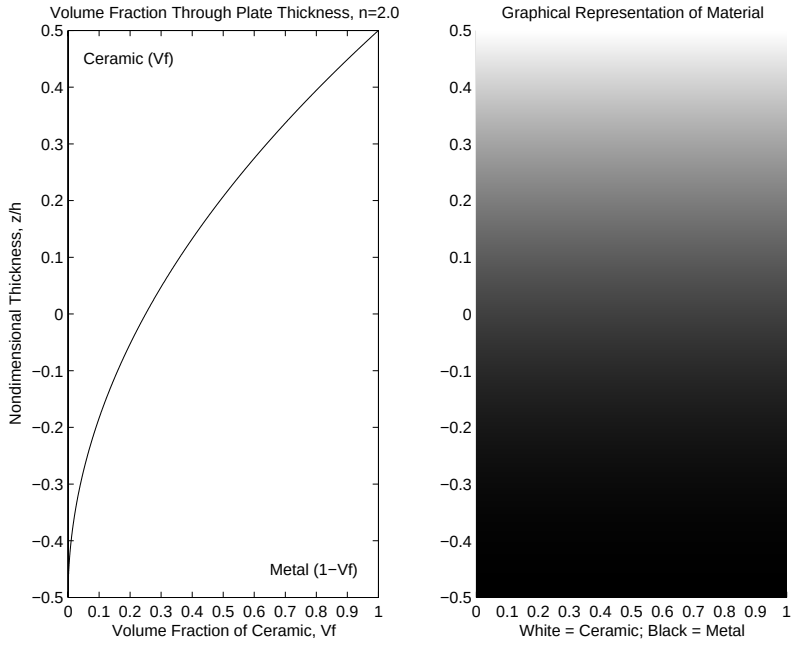

Figure 6. Graphical Representation of n=2.0

It is noted that at n=0.2 there is very little metal in the material and a sharp transition from majority metal to majority ceramic is located at z/h = -0.4. As the "n" value increases the material composition tends more toward metal. At n=1.0 there is a linear transition from metal to ceramic.

It is apparent that structural designers requiring significant thermal protection should consider low values of "n" which will yield a ceramic rich plate. Designers that desire corrosion protection with high load carrying capability should consider higher values on "n" which yield a metal rich plate.

Physical Creation of FGMs

Most FGMs are created using a powdered metallurgy process. Powdered ceramic and powdered metal are mixed in a hopper according to volume ratios. This mixture is

then sprayed onto a sheet and quickly sintered using a laser. This method is repeated to build a plate which is functionally graded through-the-thickness. This gradation in material properties is possible because the powdered materials can be mixed according to a power law. [4] Figure 8 shows a scanning electron microscope picture of an YSZ / NiCoCrAlY FGM. Note how the material properties gradually change through-the-thickness. Also, note the mixture of the two materials though the thickness and how regions of the two materials are shown. Figure 7 shows a diagram of material composition through-the-thickness, which can be directly compared to Figure 8, and gives meaning to the SEM picture.

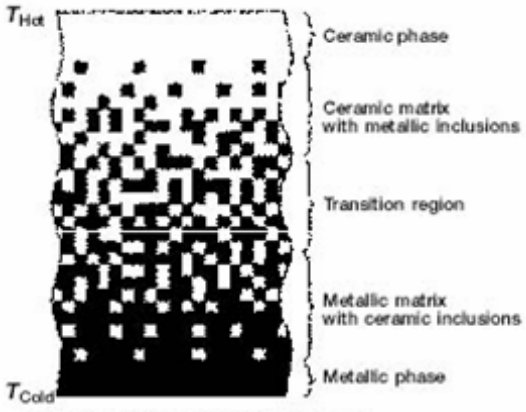

Figure 7. Diagram Depicting FGM Gradation

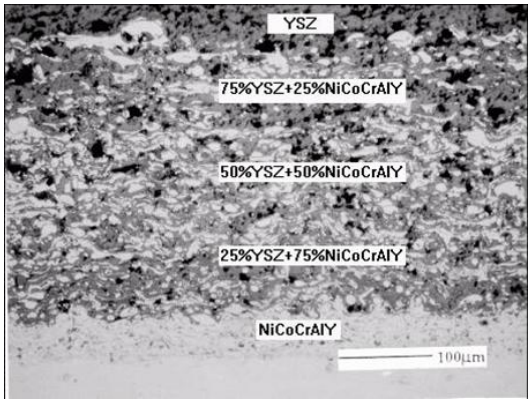

Photo courtesy of Nanyang Technical University

Figure 8. SEM Picture of a YSZ / NiCoCrAlY FGM

Finite Element Modeling Technique

The SI units system is used throughout this thesis. Units are as follows: length [m], pressure [N/m^2], temperature [°C], expansion [1/°C], density [kg/m^3], conductivity [W/m·ºC], and heat transfer film coefficient [$W/m^2 \cdot °C$]

Displacements in the x, y, and z directions are noted by u, v, and w, respectively. Rotation about the x and y axes are noted by dw/dx and dw/dy, respectively.

Because the material properties of the FGM change throughout the thickness, the numerical model must be broken up into various "slices" in order to capture the change in properties. These "slices" capture a finite portion of the thickness and are treated like isotropic materials. Material properties are calculated at the mid-plane of each of these "slices" using the power law equation previously outlined. The "slices" and their associated properties are then layered together to establish the through-the-thickness variation of material properties. Although the layered "slices" do not reflect the gradual change in material properties, a sufficient number of "slices" can reasonably approximate the material gradation. Figure 9 shows how the thickness has been discretized into nine slices, that ply one is at the bottom of the plate, and that the origin of the z axis is at the mid-plane of the plate with +z in the direction of the top surface.

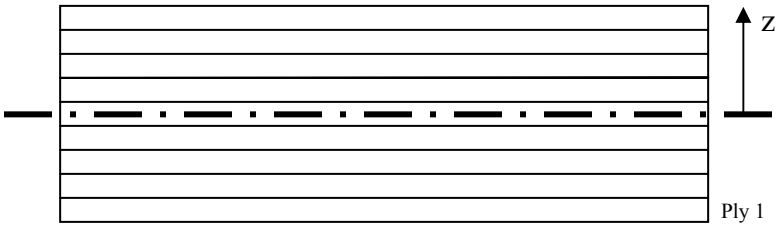

Figure 9. Origin of Z-Axis

Nine total "slices" are used throughout this thesis and was chosen because it is the maximum number of "slices" that ABAQUS can handle in a 2D shell analysis. ABAQUS limits the user to 20 temperature degrees-of-freedom when using 2D shells. If three through-the-thickness temperature degrees-of-freedom are chosen for each "slice,"

then nine “slices” results in 19 temperature degrees-of-freedom. While fewer “slices” could have been used on a case by case basis, nine was chosen in order to simplify the model development.

Models used to characterize FGMs were meshed as eight rows and eight columns. Columns are in the width-wise direction and rows are in the length-wise direction (see Figure 17 on page 34). Slices are in the thickness-wise direction. Models used to analyze the exhaust wash structure were meshed with 36 rows and 12 columns. Element types used for heat transfer analysis and structural analysis are discussed in their respective sections. Pictures of the models are shown in their respective Analysis and Results sections.

Finite Element: Heat Transfer Methodology and Element Discussion

This thesis explores two types of steady state thermal loading, isothermal temperatures applied to the top and bottom surfaces of the FGM (used on models characterizing FGMs under thermal loading), and convection on the top and bottom surface (only used in exhaust wash structure analysis). Both are analyzed using similar techniques.

All thermal loading used to characterize FGMs is steady-state isothermal loading. A hot, uniform temperature is applied to the top surface of the FGM while a cold, uniform temperature is applied to the bottom surface. An isothermal load (no variation across the surface) is applied to the top and bottom surfaces of the FGM using a temperature boundary condition. At time = ∞, heat has transferred itself from the hot top surface to the cold bottom surface. The through-the-thickness temperature profile

generated by this heat flow will depend on the material properties, particularly the thermal conductivity. Figure 10 shows a diagram of the conductive heat transfer process used for characterizing FGM's response to thermal loading.

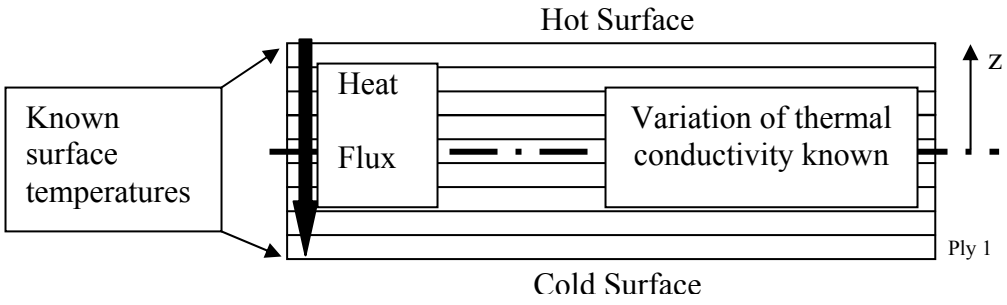

Figure 10. Conductive Heat Transfer Diagram

Since FGMs have material properties which change though-the-thickness, the thermal conductivity changes through-the-thickness. For example, a majority ceramic FGM has an overall low thermal conductivity and will result in high temperatures near the hot, top of the plate with much lower temperatures in the bottom of the plate. In effect, the ceramic top surface insulates the lower surface (metal). On the contrary, a majority metal FGM will result in the high top surface temperatures extending much deeper into the thickness. Finally, a pure ceramic or pure metal plate will result in a linear temperature profile because both materials are homogeneous and the thermal conductivity does not change through-the-thickness.

The through-the-thickness temperature profile depends on the material properties. Homogeneous material properties have no variation in material properties through-the-thickness so heat flow is linear between the top (hot) surface and the bottom (cool) surface. However, FGMs have changing material properties so solving heat flow inside

the thickness (conduction) is not linear. Shell conduction for non-homogeneous materials can be solved with two methods: 1) either an analytical solution using Fick's law where the thermal conductivity is integrated through-the-thickness to obtain a temperature as a function of thickness position, or 2) using finite element software.

When surface temperatures and thermal conductivity are know, the through-the-thickness temperature profile can be calculated using Fick's law. Solving Fick's law will result in a temperature field through-the-thickness, T(z).

$$-\frac{d}{dz}\left(k(z)\frac{dT}{dz}\right)=0 \qquad \begin{aligned} T\left(\frac{h}{2}\right) &= T_{topsurface} \\ T\left(-\frac{h}{2}\right) &= T_{bottomsurface} \end{aligned} \tag{2}$$

In a homogeneous material, the thermal conductivity doesn't change through-the-thickness, so Fick's law becomes:

$$T(z)=\frac{z}{h}\left(T_{topsurface}-T_{bottomsurface}\right)+\frac{1}{2}\left(T_{bottomsurface}+T_{topsurface}\right) \tag{3}$$

Solving Fick's law for an FGM is very time consuming because the k(z) depends on V_f, which in turn is raised to the power of "n". T(z) would have to be solved for every FGM. This thesis presents a variety of FGMs with numerous "n" values and several thicknesses therefore it is impractical to solve Fick's law for every FGM model. Additionally, a binary file detailing every nodal temperature at each of the "slice" temperature integration points would have to be created for each model. This file is required for ABAQUS to solve a thermal-stress analysis; however, ABAQUS has the ability to solve heat transfer using nearly the same finite element model used in a structural analysis.

Instead of manually calculating a temperature profile using Fick's law, a steady state heat transfer analysis is performed in ABAQUS to obtain the through-the-thickness temperature profile. The known top and bottom surface temperatures are entered into ABAQUS as temperature boundary conditions. ABAQUS then solves the shell conduction problem with a combination of piecewise quadratic interpolation of temperature through-the-thickness of the shell and linear interpolation on the reference surface of the shell. The results are a binary file detailing the nodal temperatures at each temperature integration point (reference Figure 12 on page 20). The creation of the file and heat transfer analysis is handled by ABAQUS automatically.

The element type used in all heat transfer analyses in this thesis is 4-node heat transfer quadrilateral shell (ABAQUS element type DS4). It only has temperature degrees-of-freedom which are determined by the shell lay-up. For example, Figure 11 shows a three layered shell with three temperature integration points per layer. It has seven total temperature degrees-of-freedom. [3 slices * (3 integration points – 1) + 1 = 7 total temperature degrees-of-freedom].

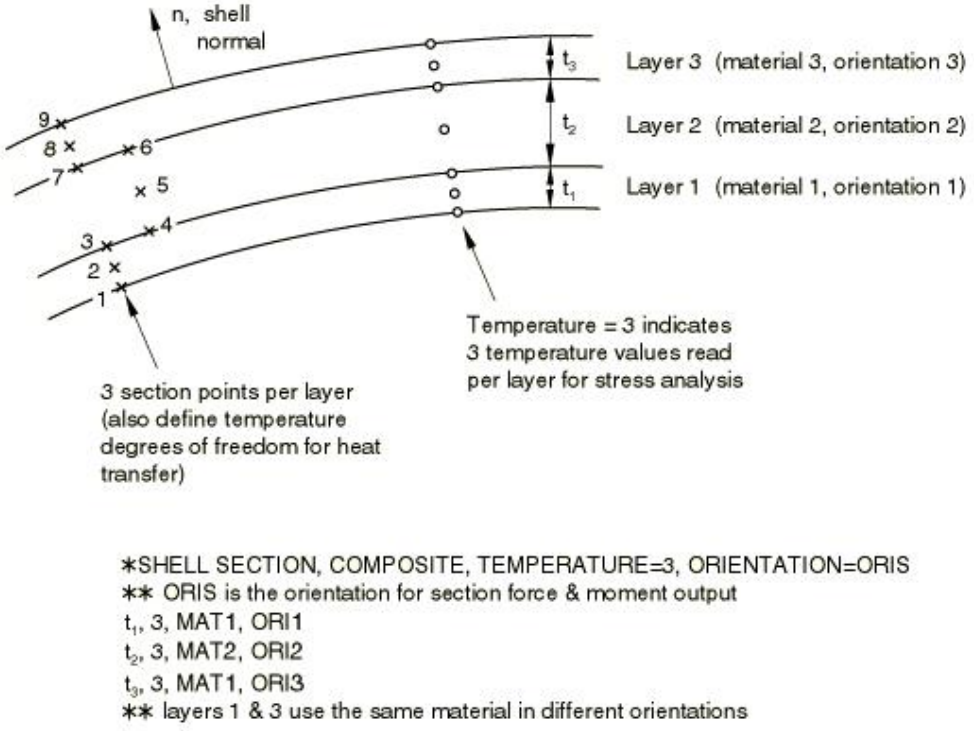

Figure 11. ABAQUS Shell Section Orientation (Photo Courtesy of ABAQUS [6])

Temperature degrees-of-freedom (DOF) start at DOF 11 in the ABAQUS software and the total number of temperature DOFs depend on the number of temperature integration points per layer which is set to three by default or can be selected by the user. Note: there is an only one integration point at the union of two layers; in other words, the layers share the same temperature point (reference Figure 11). In addition, it is noted that shell sections are defined to have layer 1 at the bottom of the lay-up. Special attention must be paid to entering section properties starting with the bottom layer. It is easy to get confused and enter the section properties starting with the top surface.

A heat transfer analysis is performed with no displacement boundary conditions (only temperature boundary conditions); the DS4 element does not have displacement or

rotational degrees-of-freedom. Therefore, a thermal stress-displacement analysis is performed with two different models. The first model is strictly a heat transfer analysis to obtain the nodal temperatures at the temperature integration points. This data is written to a reference file which is used in the second model, a strictly structural analysis with displacement and rotation boundary conditions, as shown in Figure 12 (Appendix B and Appendix C shows input files from both models).

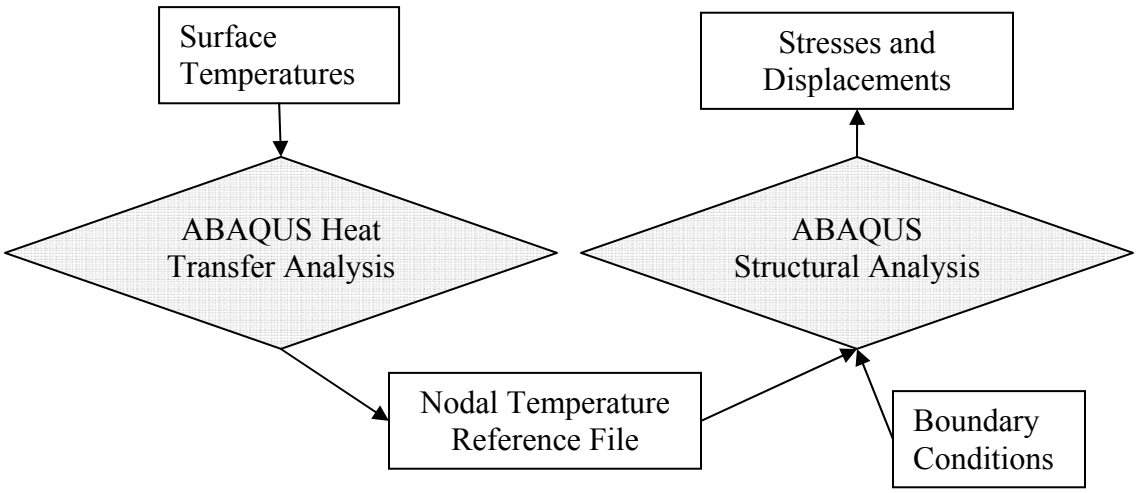

Figure 12. Diagram of Thermal Stress-Displacement Analysis

The quadrilateral element DS4 uses a uses a 2 × 2 Gauss integration scheme with a 2 × 2 nodal integration scheme for the internal energy and specific heat term. An example of the DS4 element is show in Figure 13. Nodes are numbered in a counter-clockwise fashion starting tin the lower left hand corner of the element. The integration points are noted with and "X".

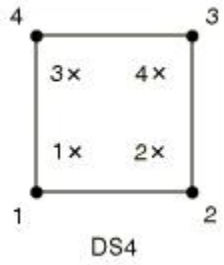

Figure 13. Heat Transfer Element (DS4)

This thesis explores two types of heat transfer: conduction (as outlined in the preceding section) and convection (only on the exhaust wash deck). Convective heat transfer on the exhaust wash structure is in the form of engine exhaust wash. In previous analyses, surface temperatures were prescribed; however, the exhaust wash problem has prescribed gas temperatures and convective heat transfer coefficients. Convection is heat transfer caused circulation currents of a gas or liquid in contact with the surface. These hot gases will transfer heat to a surface. This heat transfer depends on the gas temperature and the heat transfer coefficient, h. High speed gas has a higher heat transfer coefficient than a low speed gas. In other words, a high speed gas can supply more heat to a surface than a low speed gas can.

The exhaust wash panel has hot gas with a high film heat transfer coefficient on the top surface and cold gas with a low film heat transfer coefficient on the bottom surface, as shown in Figure 14.

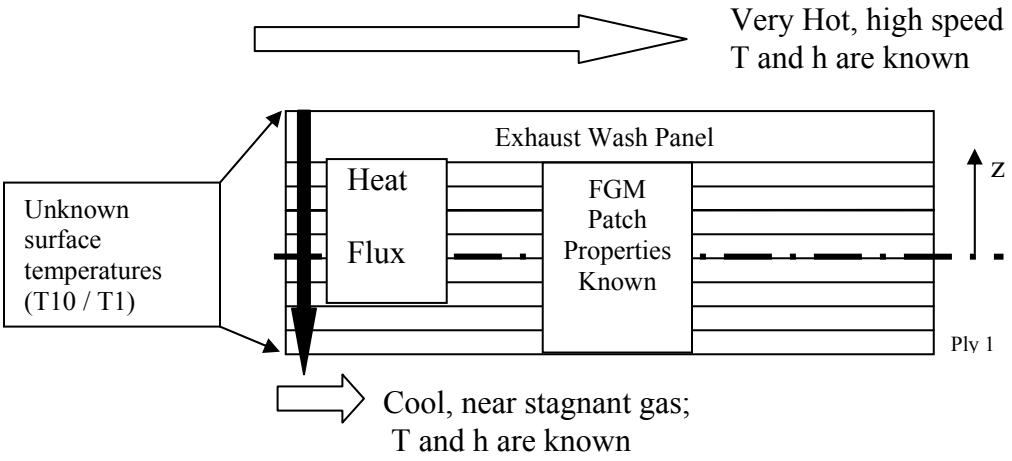

Figure 14. Convective Heat Transfer Diagram

The hot, high speed gas is the aircraft engine exhaust while the cool, low speed gas is the air found in the cavity between the exhaust wash panel and the underlying aircraft structure. If effect, this gas is enclosed, therefore it has a very low heat transfer coefficient.

In a 2D shell analysis, ABAQUS does not provide provisions for convection so surface temperatures are manually calculated using the gas temperatures, heat transfer coefficients, and thermal conductivity of the material.

In a steady state analysis, it is known that the heat flux (q) is uniform throughout the thickness of the material. In other words, the heat flux from the hot gas to the top surface of the FGM is equal to the heat flux from the bottom surface of the FGM to the cold gas. A convective heat flux is equal to the heat transfer coefficient times the difference between gas and surface temperature, or $q = h_{gas}\left(T_{hot} - T_{cold}\right)$. Also, conduction within the material is equal to thermal conductivity divided by the thickness times the difference in surface temperatures, or $q = \frac{K}{t}\left(T_{hot} - T_{cold}\right)$. [9] However, since the

thermal conductivity changes through-the-thickness, the FGM is discretized into eight "slices" and the thermal conductivity is calculated for each "slice." The exhaust wash structure is treated as one additional "slice." This process allows for simultaneous equations to be solved in order to obtain the surface temperatures and heat flux. Two convection equations (heat flux from the hot gas to the exhaust wash top surface and heat flux from the FGM bottom surface to the cold gas), 9 conductive equations within the FGM and structure (one for every slice), and 10 unknown "slice" surface temperatures are solved simultaneous knowing that the heat flux for each equation is equal, as shown below:

$$q = h_{HotGas}\left(T_{HotGas} - T_{10}\right) \quad \text{Convection from the hot gas to the top surface of the exhaust wash panel} \tag{4}$$

$$q = \frac{K_{structure}}{t_{structure}}\left(T_{10} - T_9\right) \quad \text{Conduction from the top of the exhaust wash panel to the bottom of the exhaust wash panel (or top of eighth FGM slice)} \tag{5}$$

$$q = \frac{K_{FGMslice8}}{t_{slice}}\left(T_9 - T_8\right) \quad \text{Conduction from the top of the eighth FGM slice to the bottom of the eight FGM slice} \tag{6}$$

$$q = \frac{K_{FGMslice7}}{t_{slice}}\left(T_8 - T_7\right) \quad \text{Conduction from the top of the seventh FGM slice to the bottom of the seventh FGM slice} \tag{7}$$

$$q = \frac{K_{FGMslice6}}{t_{slice}}\left(T_7 - T_6\right) \quad \text{Conduction from the top of the sixth FGM slice to the bottom of the sixth FGM slice} \tag{8}$$

$$q = \frac{K_{FGMslice5}}{t_{slice}}\left(T_6 - T_5\right) \quad \text{Conduction from the top of the fifth FGM slice to the bottom of the fifth FGM slice} \tag{9}$$

$$q = \frac{K_{FGMslice4}}{t_{slice}}\left(T_5 - T_4\right) \quad \text{Conduction from the top of the fourth FGM slice to the bottom of the fourth FGM slice} \tag{10}$$

$q = \frac{K_{FGMslice3}}{t_{slice}}(T_4 - T_3)$	Conduction from the top of the third FGM slice to the bottom of the third FGM slice	(11)
$q = \frac{K_{FGMslice2}}{t_{slice}}(T_3 - T_2)$	Conduction from the top of the second FGM slice to the bottom of the second FGM slice	(12)
$q = \frac{K_{FGMslice1}}{t_{slice}}(T_2 - T_1)$	Conduction from the top of the first FGM slice to the bottom of the first FGM slice	(13)
$q = h_{ColdGas}(T_{ColdGas} - T_1)$	Convection from the bottom surface of the FGM to the cold gas	(14)

Note: the unknown temperatures are the surface temperatures of the "slices" noted in Figure 14.

Once the surface temperatures have been calculated, a steady state heat transfer analysis with ABAQUS is used to obtain a though-the-thickness temperature profile. Once again, the through-the-thickness temperature profile could be manually calculated and entered into an ABAQUS reference file, however, this process is time consuming and offers opportunities for human error. Once the temperature profile is solved using ABAQUS, the profile is applied to a second structural analysis to find the material response to the convection. On a final note, the heat transfer element used is DS4, which is the same element used in the previous section where surface temperatures where known. The same element can be used because surface temperatures are solved then entered as a temperature boundary condition.

Finite Element: Structural Analysis Methodology and Shell Element Discussion

In a structural analysis, fully integrated, general-purpose, finite-membrane-strain shell element is used (ABAQUS element S4). This element has displacement, rotation, and temperature degrees-of-freedom. A picture of the S4 element is shown in Figure 15.

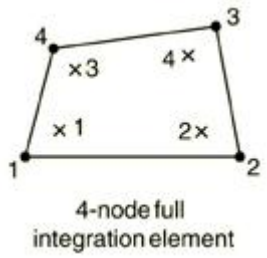

Figure 15. Structural Element S4

"Element S4 is a fully integrated finite-membrane-strain shell element. Since the element's stiffness is fully integrated, no spurious membrane or bending zero energy modes exist and no membrane or bending mode hourglass stabilization is used. Similarly, element S4 assumes that the transverse shear strain (and force, since the transverse shear treatment is elastic based on the initial elastic modulus of the material) is constant over the element. Therefore, all four stiffness integration locations will have the same transverse shear strain, transverse shear section force, and transverse shear stress distribution." [6]

"It is well known that a standard displacement formulation will exhibit shear locking for applications dominated by in-plane bending deformation. However, a standard displacement formulation for the out-of-plane bending stiffness is not subject to similar locking response. Hence, S4 uses a standard displacement formulation for the

element's bending stiffness, and the theory presented above for the rotation kinematics and bending strain measures applies to S4. The membrane formulation used for S4 does not rely on the fact that S4 is a shell element." [6]

This thesis explores both thermal and pressure loading when characterizing FGMs and model both flat plates and curved shells. Element type S4 is used throughout this thesis as the structural element.

Thermal loading is treated as an uncoupled process and solved in two steps. The first step is to perform a steady state heat transfer analysis to obtain nodal temperatures. The second step is to perform a structural analysis where all nodes were taken to have stress free reference state of 20º C. The difference in applied temperature and the stress free temperature causes expansion of the material according to its thermal expansion coefficient.

To help illustrate this, Figure 16 shows a side view of a panel. The undeformed width of the panel is L. As temperature is applied to the panel, it will expand according to its thermal expansion coefficient and the temperature delta applied to it, or $\alpha \cdot \Delta T$. However, the expansion is resisted by the displacement controlled boundary conditions. This combination of expansion and boundary condition causes the panel to deflect out of plane, as shown in Figure 16.

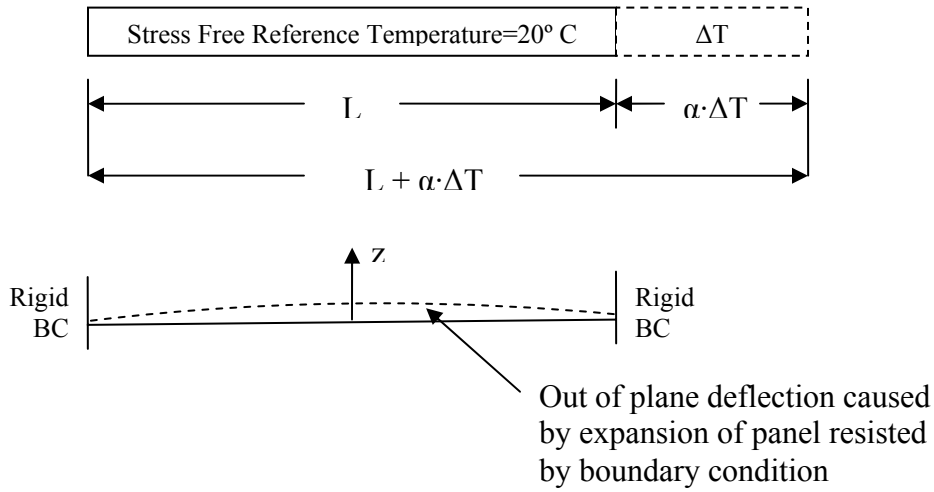

Figure 16. Plate Deflection Diagram

Stresses resulting from the panel deformation are extrapolated to the nodes in order to produce contour plots of stresses. Displacement plots are created using nodal displacements.

Unlike coupled thermal-displacement analysis, a distributed pressure or concentrated force analysis is completed in one step. Both boundary conditions and loading are applied in a single model. Resulting stresses are then extrapolated to the nodes to produce contour plots of stresses. Displacement plots are created using nodal displacements.

Non-Linearity Background and Analysis

Knowing that plates and shells subject to thermal loading will likely experience deformation that is over 50% of the thickness, it is of interest to compare linear and non-linear solutions when characterizing FGMs. Major sources of non-linearity are geometric

stiffening and material non-linearity (yielding). Geometric stiffening is caused by structural deformation which affects the structural stiffness. "An example of geometric nonlinearity is a thin flat disk, clamped around its circular boundary, and loaded by lateral pressure. If lateral deflection at the center is more than about half the thickness, the disk develops membrane stretching forces that carry a considerable portion of the load." [1]

In the previous example, the stiffness matrix and reaction matrix are dependent on the displacement. Both matrices must be updated after every iteration in order to account for these stress stiffening effects. In other words, as the structure undergoes large displacements, the structural stiffness is affected by the displacement, as shown in the equation below:

$$[K + K(\delta, \delta^2)]\{\delta\} = \{F\} \tag{15}$$

The non-linear stiffness matrix (Greens' strain) is proportional to the displacement and the square of the displacement, as shown below for strain in the x direction [1]:

$$\varepsilon_{11} = \frac{\partial u_1}{\partial x_1} + \frac{1}{2}\left(\left[\frac{\partial u_1}{\partial x_1}\right]^2 + \left[\frac{\partial u_2}{\partial x_1}\right]^2 + \left[\frac{\partial u_3}{\partial x_1}\right]^2\right) \tag{16}$$

In order to evaluate the non-linear portion of the stiffness matrix, displacements are required. However, these displacements are affected by the non-linear portion of the stiffness matrix therefore the non-linear analysis becomes an interactive process.

In ABAQUS, non-linear geometry is turned on using "NLGEOM = YES" in the "Step" card. (See Appendix B and Appendix C for sample ABAQUS input files). This

flag tells ABAQUS to check the stiffness matrix to ensure that the internal and external forces balance as the load is incremented toward the desired load. This balance on internal and external forces is accomplished by:

1) Project a line from the current load/displacement position to the desired load, P. The slope of the line is equal to the stiffness matrix (calculated at the current load/position, $[K] = \int [B]^T [E][B] dVol$).

2) Find the displacement at the desired load (intersection of desired load and line from step 1)

3) Calculate the internal forces using the current stiffness matrix and displacement found in step 2.

4) The residual force is the desired load minus internal forces found in step 3.

5) If step the residual force is "too big" then calculate a new stiffness matrix based on the new displacement and load at new displacement then repeat step 1. A convergence criterion determines how "big" the residual force can be. The tolerance value is set to 0.5% of an average force in the structure, averaged over time.

If the internal / external forces and displacement don't balance with the stiffness matrix, as outlined above, then ABAQUS updates the stiffness matrix using the incremental displacement and tries again. This increment control is handled automatically by ABAQUS; however the user can provide a means for direct control.

(Appendix E outlines a non-linear load-displacement analysis as taken from the ABAQUS user's manual).

Solutions to non-linear thermal displacement problems follow the same as outlined above with a few exceptions. First, instead of incrementing load, ABAQUS increments temperature, (θ). Second, ABAQUS splits up the stiffness matrix into the portions that depend on displacement (K_{uu}) and the portion that depends on temperature ($K_{\theta\theta}$), as outlined by the equation below:

$$\begin{bmatrix} K_{uu} & 0 \\ 0 & K_{\theta\theta} \end{bmatrix} \begin{Bmatrix} \Delta u \\ \Delta\theta \end{Bmatrix} = \begin{Bmatrix} \Delta R_u \\ \Delta R_\theta \end{Bmatrix} \tag{17}$$

Where $[K_{uu}] = \int [B]^T [E][B] dVol$ and $[K_{\theta\theta}] = \int [B]^T [E][\alpha\Delta T] dVol$,

$\Delta R_\theta = \int [B]^T [E]\{\alpha\}\Delta\theta \cdot dVol$ and R_u = BC Reactions + Applied force

ABAQUS/Standard generally uses Newton's method as a numerical technique for solving the nonlinear equilibrium equations because convergence is much faster than with other solvers (usually modified Newton or quasi-Newton methods) for the types of nonlinear problems most often studied with ABAQUS. [6]

"ABAQUS/Standard uses a scheme based predominantly on the maximum force residuals following each iteration. By comparing consecutive values of these quantities, ABAQUS/Standard determines whether convergence is likely in a reasonable number of iterations. If convergence is deemed unlikely, ABAQUS/Standard adjusts the load increment; if convergence is deemed likely, ABAQUS/Standard continues with the iteration process. In this way excessive iteration is eliminated in cases where convergence is unlikely, and an increment that appears to be converging is not aborted because it

needed a few more iterations. One other ingredient in this algorithm is that a minimum increment size is specified (0.01), which prevents excessive computation in cases where buckling, limit load, or some modeling error causes the solution to stall. This control is handled internally, with user override if needed. Several other controls are built into the algorithm; for example, it will cut back the increment size if an element inverts due to excessively large geometry changes. These detailed controls are based on empirical testing." [6]

Finite Element Software, Pre-Processor, and Post-Processor

Since ABAQUS software is utilized as the FEA processor, ABAQUS CAE is obviously desired as the pre-processor and post-processor. However, due to the unique techniques required to models FGMS, Matlab is used as a pre-processing tool to create input files more efficiently.

Material properties vary through-the-thickness and are discretized into "slices." For every "slice" and for each of the six "n" values analyzed in this thesis, material properties must be calculated and entered into ABAQUS. This task quickly becomes overwhelming because each of the six "n" values studied are modeled with nine "slices," each of which has four material properties entered into ABAQUS (E, ρ, α, and k). The end result is calculating and manually entering 216 material properties into ABAQUS for every model studied. This task is not only inefficient considering the number of models studied but would introduce significant opportunities for human error.

Matlab is used to automatically generate ABAQUS input files. This powerful tool allows one to focus on the study of FGMs rather than the mundane task of entering

properties by hand. A program is created for each model studied; the input parameters include: load parameters (any number of pressures, loads, temperatures, etc), model geometry, mesh requirements, material properties, values of "n", and the number of "slices" to be modeled. The program outputs requested ABAQUS input files, both for heat transfer and structural analysis. The end result is a very powerful tool that allows for quick and accurate designed FGM models. Without the use of Matlab, it would be very time-consuming to change a parameter (say the number of "slices") and study its effects. ABAQUS CAE is utilized, however, to verify the input file created by the Matlab program. Appendix A details the use of Matlab and ABAQUS in flow chart format.

Similar to the overwhelming task of entering material properties into ABAQUS, significant time is spent plotting displacements and stresses for each of the analysis. For example, a flat plate under thermal loading is studied and plots of displacements vs. applied temperature for each of the six values of "n" are carried out. If one considers each of the 13 temperatures modeled and each of the five boundary conditions one would have to manually capture and plot 390 data points. This task is again overwhelming considering the number of models created in this thesis. Instead, Matlab is utilized as a post-processor to create plots and graphs. The program reads each of the ABAQUS output files and stores the output parameters (displacement and stress). Displacement plots can then be created with more than one "n" value, something that ABAQUS CAE can not accomplish. ABAQUS CAE will only create plots and graphs for the model currently being analyzed. Therefore, it is not only impractical to manually save plots and graphs from ABAQUS CAE but impossible to create a single graph showing the material

response of every “n” value analyzed. Appendix A outlines this process in flow chart format.

Flat Plate Coordinate Systems and Boundary Conditions

Flat plates were modeled as 2D simply supported structures; around the perimeter only deflection and rotations about the edge were allowed. Five simple supports were modeled: SS1, SS2, SS3, SS4 and Hinged-Free. The origin of the rectangular coordinate system is located at the corner of the plate and the z axis is located at the mid-surface of the plate. See Figure 17 thru Figure 21 for details on each of the simple supports studied.

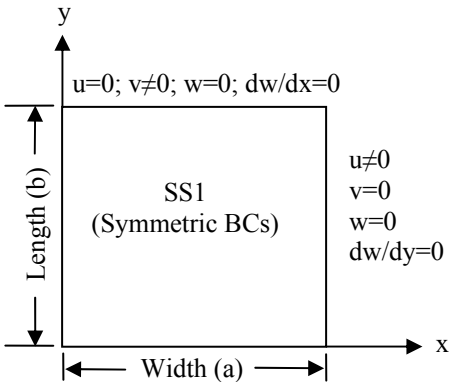

Figure 17. SS1 Plate Boundary Condition

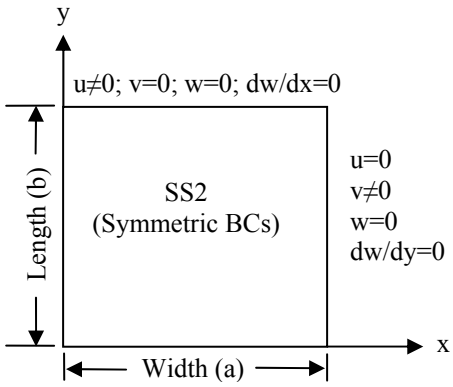

Figure 18. SS2 Plate Boundary Condition

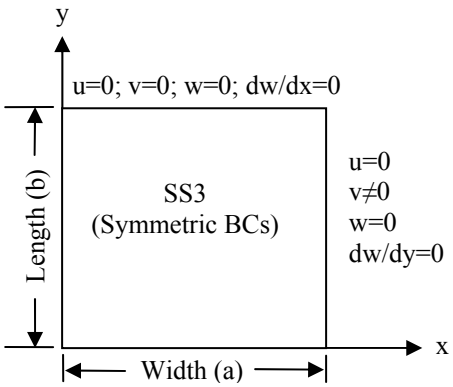

Figure 19. SS3 Plate Boundary Condition

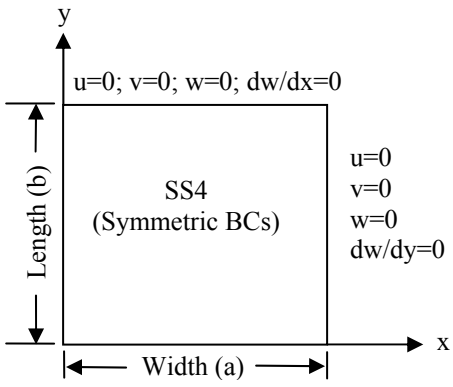

Figure 20. SS4 Plate Boundary Condition

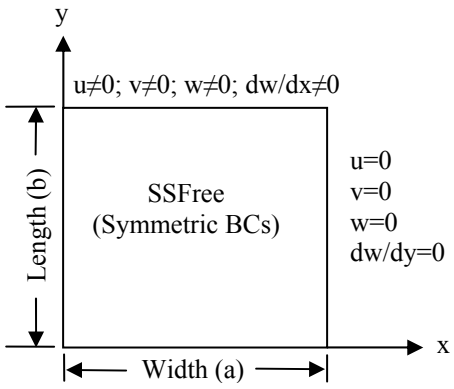

Figure 21. SSFree Plate Boundary Condition

Curved Panel Coordinate Systems and Boundary Conditions

Curved panels were modeled in the rectangular coordinate system using shell panels. Displacements along the straight edge are fixed (rotation is allowed) while displacements and rotations along the curved edge are free. The origin of the rectangular coordinate system is at the front face and centerline of the panel with the global z axis located at the mid-plane of the material. The local z axis (at the mid-plane of the material) is still utilized for calculating material properties (refer to Figure 9). Figure 22 shows the locations the panel boundary conditions and global axis system.

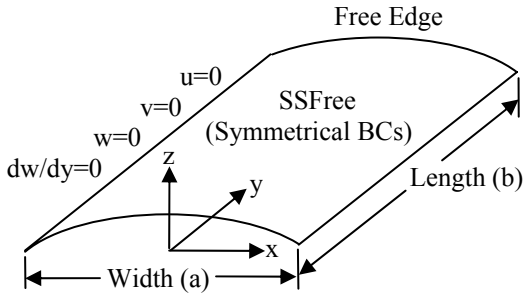

Figure 22. SSFree Panel Boundary Condition

Exhaust Wash Structure Coordinate Systems and Boundary Conditions

The exhaust wash structure is modeled in the rectangular coordinate system as a 2D shell panel structure and follows the same conventions as the curved panel as noted in Figure 22 with the exception of the boundary conditions. The edges are clamped and all displacements and rotations are fixed; the free edge has no restraints.

Summary

FGMs have material properties that change through-the-thickness according to a power law. In order to model FGMs in ABAQUS, the material thickness is broken into "slices" in order to capture the change in material properties. The "slices" are then treated as individual homogeneous materials and are layered together and modeled similar to a composite structure. Material properties for each "slice" are calculated according to a power law with the "slice" mid-plane as the z coordinate in the equation. The power law is based off the volumetric mixture ratio of the two materials.

All models are based in the rectangular coordinate system and are simply supported, with the exception of the exhaust wash deck. Table 1 summarizes the boundary conditions along the length and width for each boundary condition.

Table 1. Summary of Boundary Conditions

BC Name	BC Abbreviation	Width-wise BCs	Length-wise BCs
Simple Support 1	SS1	v = w = 0 dw/dy=0	u = w = 0 dw/dx=0
Simple Support 2	SS2	u = w = 0 dw/dy=0	v = w = 0 dw/dx=0
Simple Support 3	SS3	u = w = 0 dw/dy=0	u = v = w = 0 dw/dx=0
Simple Support 4	SS4	u = v = w = 0 dw/dy=0	u = v = w = 0 dw/dx=0
Simple Support-Free	SSFree	u = v = w = 0 dw/dy=0	All displacements are free All rotations are free
Clamped-Free	ClampedFree	u = v = w = 0 All rotations = 0	All displacements are free All rotations are free

III. Analysis and Results

Chapter Overview

This chapter will present results from finite element models for flat plates under thermal loading and pressure loading. Additionally, curved panels under thermal loading and concentrated force loading are examined. Finally, an aircraft exhaust wash structure is analyzed and retrofitted with a patch.

Flat Plate under Thermal Loading

The goal of analyzing flat plates under thermal loading is to characterize the effect "n" has on the structural response to thermal loading. Following work published by J.N. Reddy [3], a flat Aluminum-Zirconia with sides a=0.2 m and thickness h = 0.01 m is exposed to various surface temperatures. The top surface is exposed to isothermal temperatures in a range 0ºC to 600ºC and the bottom temperature is exposed to a constant temperature of 20ºC. Note: each top surface temperature examined is treated as an independent model. "n" values of 0 (ceramic), 0.2, 0.5, 1.0, 2.0, and ∞ (metal) are examined. Material properties for the bottom and top surface are listed below:

Aluminum (Bottom surface)

E = 70 GPa; $\nu = 0.3$; $\rho = 2{,}707$ Kg/m^3; $\alpha = 23$ μm/m·ºC ; k = 204 W/m·K

Zirconia (Top surface)

E = 151 GPa; $\nu = 0.3$; $\rho = 3{,}000$ Kg/m^3; $\alpha = 10$ μm/m·ºC ; k = 2.09 W/m·K

A 2D shell analysis with a 8x8 mesh and 9 slices is used to solve the problem. A steady state heat transfer analysis is first performed to obtain nodal temperatures. Figure 23 details the temperature profile through the thickness.

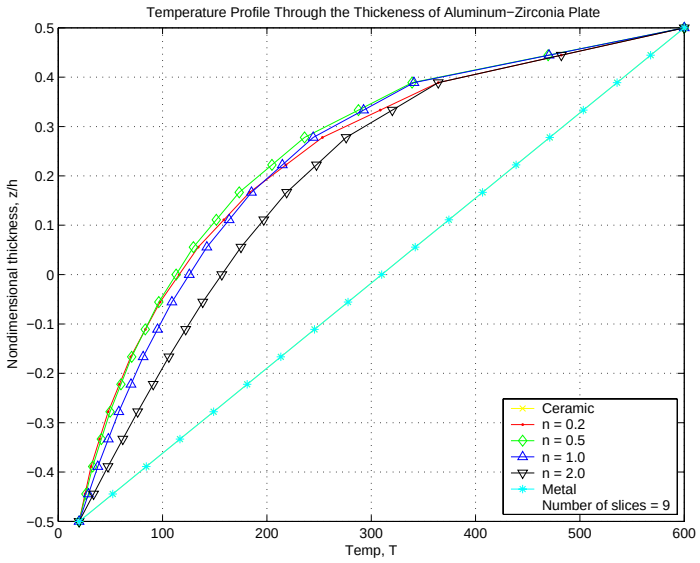

Figure 23. Plate Through-the-Thickness Temperature Profile

The non-dimensional thickness represents the location in the plate thickness and is non-dimensionalized in order to generalize the temperature profile for comparison to any other non-dimensionalized temperature profile plot. A non-dimensional thickness of zero is the mid-plane of the material while a non-dimensional thickness of 0.5 is the top of the plate. It is noted that that metal and ceramic plates have linear temperature variations through-the-thickness because they are composed of homogenous materials. However, FGM plates tend to have non-linear temperature profiles with much lower temperatures in the bottom 75% of the thickness because the ceramic at the top surface insulates the metal beneath.

The second step was to analyze the structural response to the applied temperature profile created in the heat transfer analysis. Nodal temperatures are applied to a structural problem with prescribed boundary conditions. The difference in applied

temperature and stress free reference temperature causes the material to expand, thus creating stress and out of plane displacements.

This analysis was performed for both linear and non-linear geometries and for all simply supported boundary conditions. Both linear and non-linear plots of non-dimensionalized displacement (w/h) vs. top surface temperature are shown in Figure 24 through Figure 33. The thickness is again non-dimensionalized to allow for comparison to any other non-dimensionalized plot. Note: the bottom surface is fixed at 20°C, each of the studied boundary conditions is located in the legend, and linear deflections are in the left column, while non-linear deflections are in the right column.

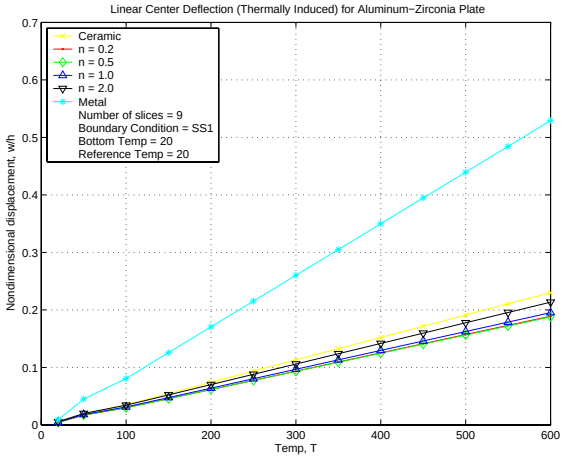

Figure 24. Plate-Thermally Induced Deflection for SS1 (Linear)

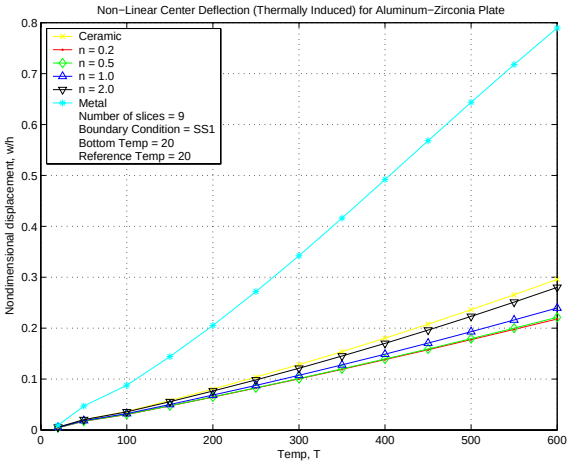

Figure 25. Plate-Thermally Induced Deflection for SS1 (Non-Linear)

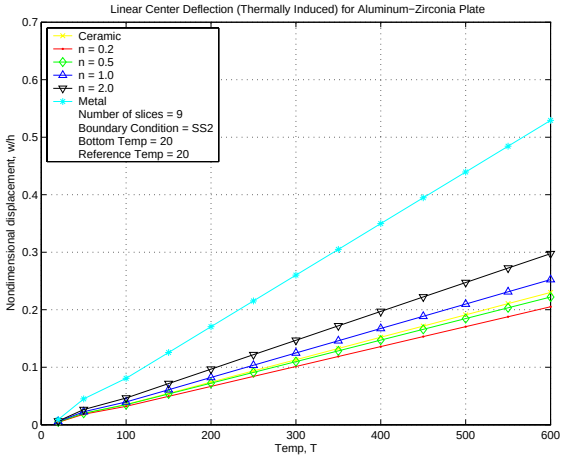

Figure 26. Plate-Thermally Induced Deflection for SS2 (Linear)

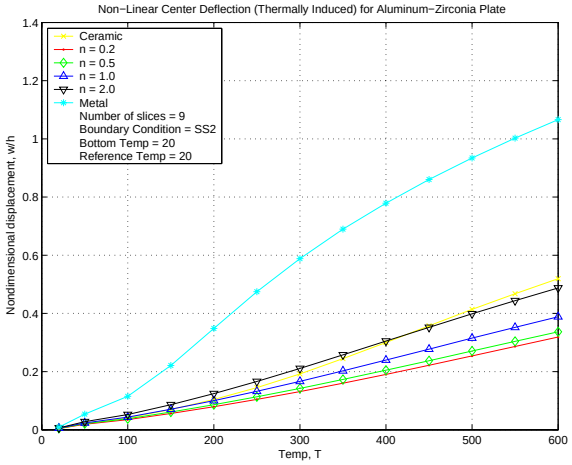

Figure 27. Plate-Thermally Induced Deflection for SS2 (Non-Linear)

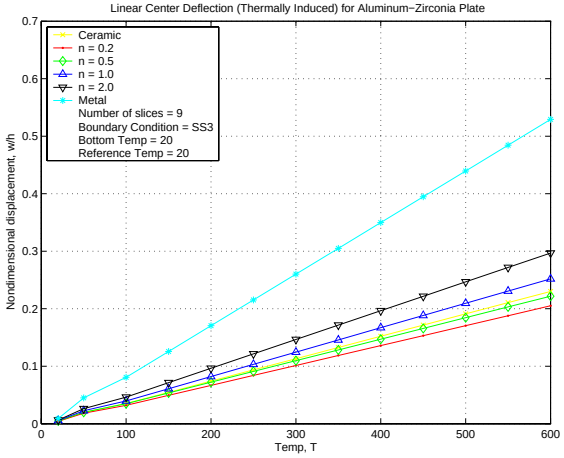

Figure 28. Plate-Thermally Induced Deflection for SS3 (Linear)

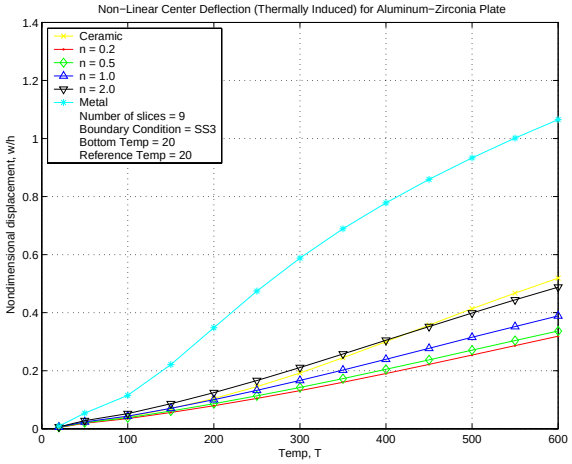

Figure 29. Plate-Thermally Induced Deflection for SS3 (Non-Linear)

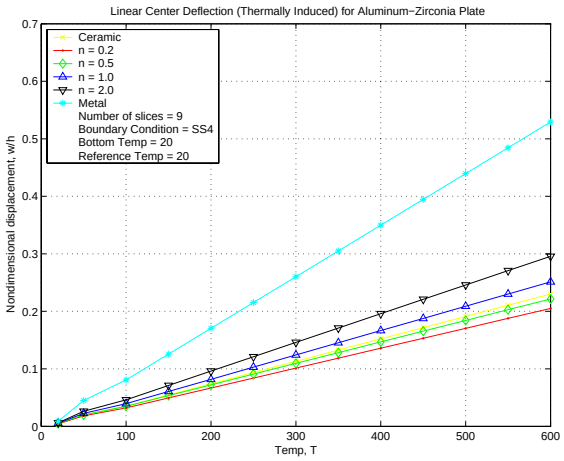

Figure 30. Plate-Thermally Induced Deflection for SS4 (Linear)

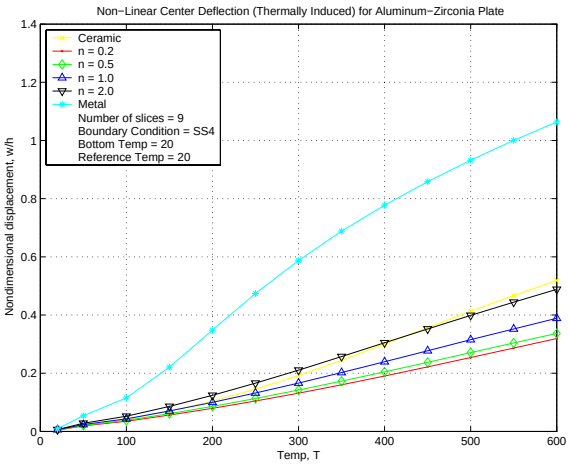

Figure 31. Plate-Thermally Induced Deflection for SS4 (Non-Linear)

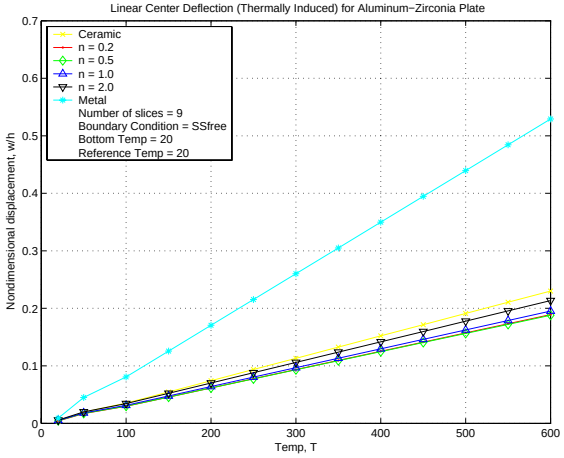

Figure 32. Plate-Thermally Induced Deflection for SSFree (Linear)

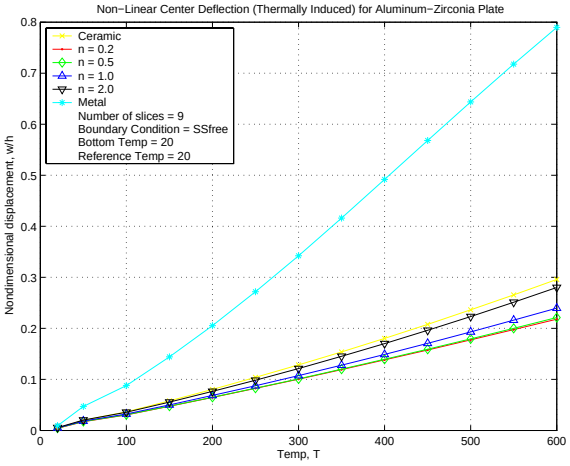

Figure 33. Plate-Thermally Induced Deflection for SSFree (Non-Linear)

It is noted that SS1 and SS-Free boundary conditions produce the lowest deflections. SS-Free and SS1 are the least restrictive boundary condition while SS4 is the most restrictive boundary condition. Consequently, deflections are lowest and nearly identical in SS-Free and SS1 (approx. 0.8) while deflection is highest with SS4 (approximately 1.08 or 35% higher than SS1).

SS2, SS3, and SS4 boundary conditions provided nearly identical deflections while were 35% more than SS1. In effect, adding a shear boundary condition found in SS2, SS3, and SS4 causes the deflection to increase. (SS1 only has a normal boundary condition).

Metal and ceramic plates provide the highest deflection with metal having over twice the magnitude of the FGM plate deflections. At n=0.2, deflection is minimized and is approximately 4 times less than the metal plate. Of special importance is the effect of lowering "n" tending to lower the deflection of the plate. This is effect is consistent within the FGM plates, however does not apply to the limits of "n" (n=0 or n=∞). At these limits, the material is homogeneous. Finally, it is noted that all FGM plates have deflections of similar magnitude. This is likely explained by the very similar FGM temperature profiles.

It is also noted that non-linear analysis provides higher deflections than a linear analysis. This is opposite what one might expect – usually a non-linear analysis provides lower displacements because of stress stiffening of the structure. However, the thermally loaded plate experiences stress softening because of the compression in the plate caused by the thermal expansion, which is resisted by the boundary condition. Additionally, the temperature profile through-the-thickness shown in Figure 23 causes moments to be produced through-the-thickness. These moments are caused by the expansion of the material, which is product of the coefficient of thermal expansion and the temperature change. A moment is created if the top side of the plate is expanding more than the bottom side of the plate, or vice-a-versa. This moment does not affect a

linear solution because the stiffness matrix isn't updated after every iteration and checked for continuity with internal forces and displacements. However, this moment is found to have a significant impact on the non-linear solution because the stiffness matrix is updated after every iteration.

This effect of thermal moments also explains why the effect of lowering "n" tends to lower displacements. Lowering "n" creates plates that have much more ceramic that extends deeper into the thickness. This ceramic portion has the lowest thermal expansion coefficient, however it is exposed to the highest temperatures. The metal found in the bottom of the plate has the highest coefficient of thermal expansion but is exposed to the lowest temperature. It is apparent that a low "n" value provides a combination of $\alpha \cdot \Delta T$ that is nearly constant through-the-thickness.

Stress in SS-Free plates are of importance because the exhaust wash deck is modeled as a SS-Free structure. Also, the stress values for flat plates are compared to curved panels (in following sections) in order to study effect of curvature. Figure 34 through Figure 45 show mid-plane stress for all six "n" values studied and for both linear and non-linear analysis. Note: these stress graphs are at a top surface temperature of 600°C.

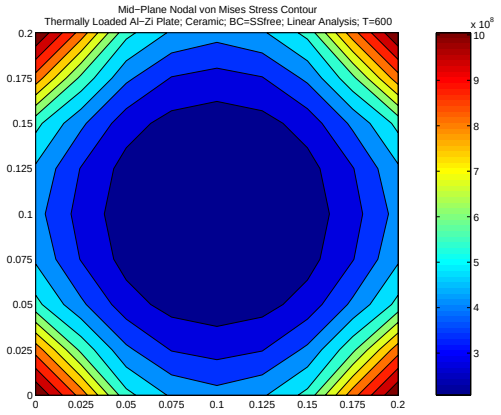

Figure 34. Plate-Thermally Induced Stress for n=Ceramic (Linear)

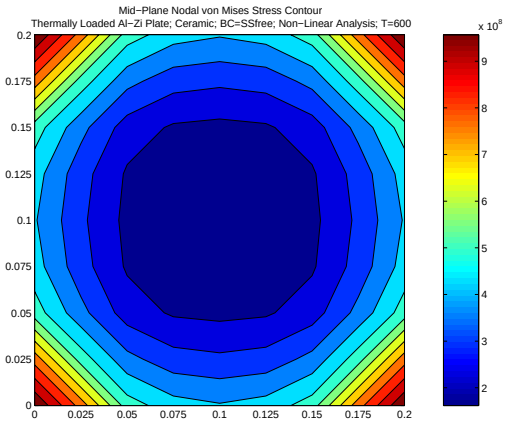

Figure 35. Plate-Thermally Induced Stress for n=Ceramic (Non-Linear)

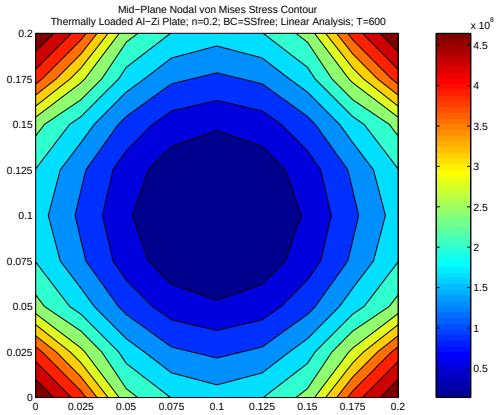

Figure 36. Plate-Thermally Induced Stress for n=0.2 (Linear)

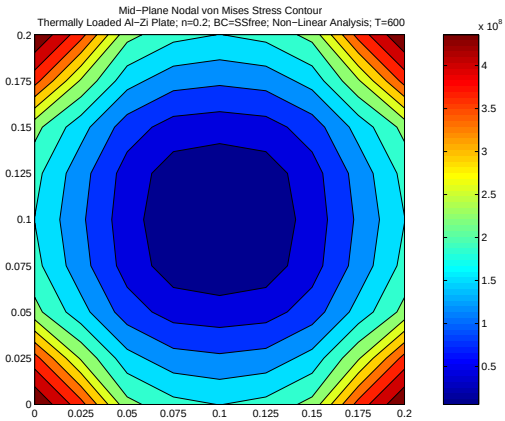

Figure 37. Plate-Thermally Induced Stress for n=0.2 (Non-Linear)

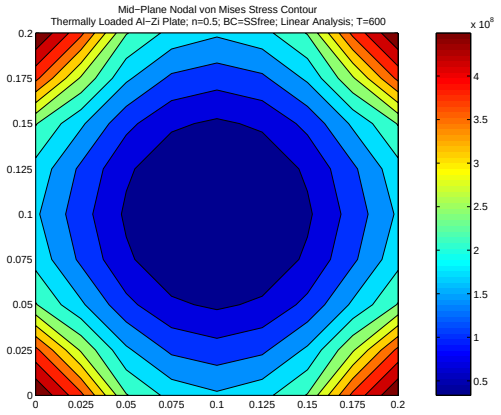

Figure 38. Plate-Thermally Induced Stress for n=0.5 (Linear)

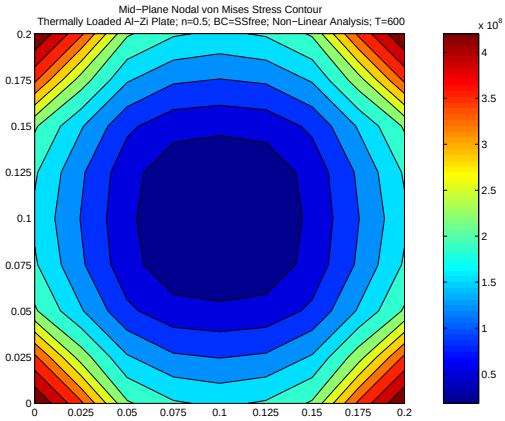

Figure 39. Plate-Thermally Induced Stress for n=0.5 (Non-Linear)

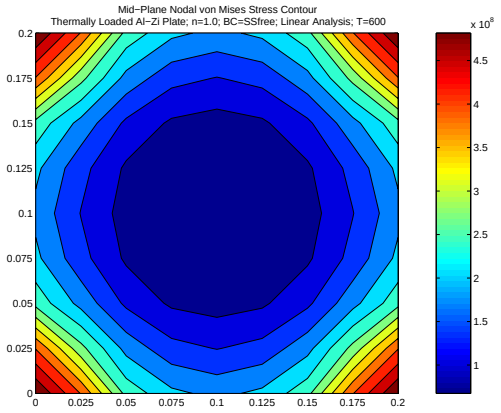

Figure 40. Plate-Thermally Induced Stress for n=1.0 (Linear)

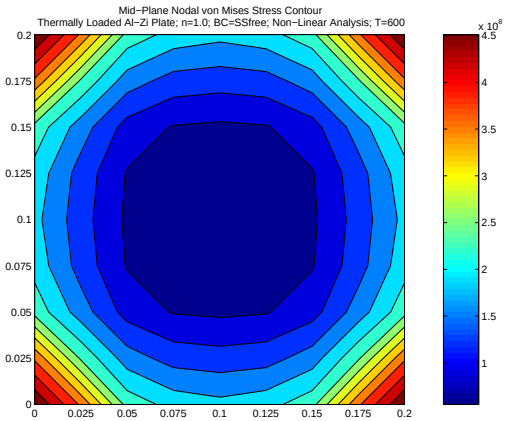

Figure 41. Plate-Thermally Induced Stress for n=1.0 (Non-Linear)

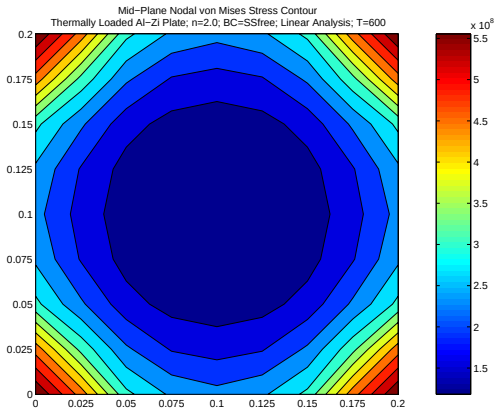

Figure 42. Plate-Thermally Induced Stress for n=2.0 (Linear)

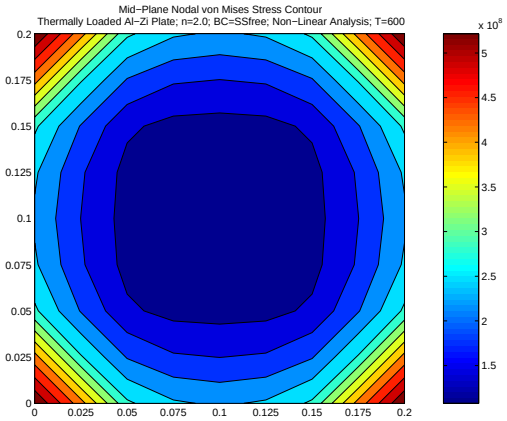

Figure 43. Plate-Thermally Induced Stress for n=2.0 (Non-Linear)

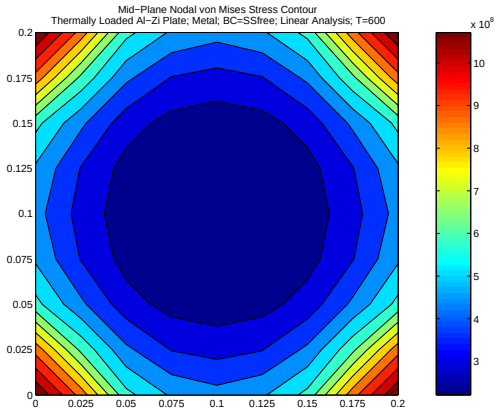

Figure 44. Plate-Thermally Induced Stress for n=Metal (Linear)

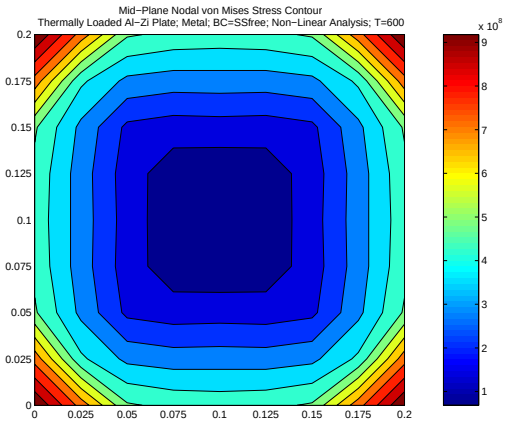

Figure 45. Plate-Thermally Induced Stress for n=Metal (Non-Linear)

It is noted that a value of n=∞ (metal) provides the highest mid-plane stress, while n=0.5 provides the lowest mid-plane stress (non-linear analysis) and is 54% lower than a metal plate. Also, the effect of raising the "n" value tends to raise the mid-plane stress values. Also, it is noted that the linear analysis provides lower stress values than a non-linear analysis. This is due to the non-linear stress stiffening being negated by the non-linear thermal moments as discussed in the deflection analysis.

In summary, lowering "n" tends to lower the deflection in flat plates under thermal loads with n=0.2 providing the lowest deflection. Also, non-linear analysis must be used in a thermal FGM shell analysis, because thermal moments play an important part in the stress stiffening of the structure. These thermal moments are caused by the drastic difference in through-the-thickness temperatures and by the material property variation found in an FGM. Also, SS-Free provides displacement that is nearly identical to SS1 (which has a "normal" boundary condition). Finally, n=0.5 provided the lowest mid-plane stress even through n=0.2 provided the lowest displacement. However, n=0.2 provides only 2.4% higher mid-plane stress than n=0.5. It can be concluded that a non-linear analysis with a range of "n" from 0.2 to 0.5 provides the optimum solution to this exercise.

Flat Plate under Distributed Pressure Loading

The goal of analyzing flat plates under distributed pressure loading is to characterize the effect "n" has on the structural response to mechanical loading. Again following work published by J.N. Reddy [3], the same flat plate previously analyzed was exposed to a distributed pressure load applied to the elements and in the –z direction. A

2D shell analysis with a 8x8 mesh and 9 slices is again used to solve the problem. Analysis was performed for both linear and non-linear geometries and for all studied boundary conditions. Linear and non-linear plots of non-dimensionalized deflections (w/h) vs. load parameter (q_0a^4/ E_bh^4) are shown in Figure 46 through Figure 53.

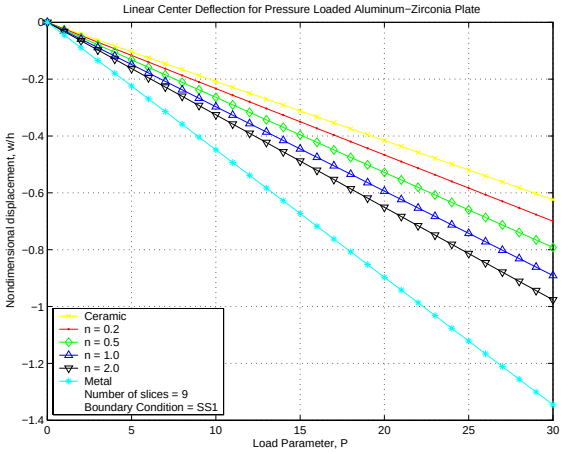

Figure 46. Plate-Pressure Induced Deflection for SS1 (Linear)

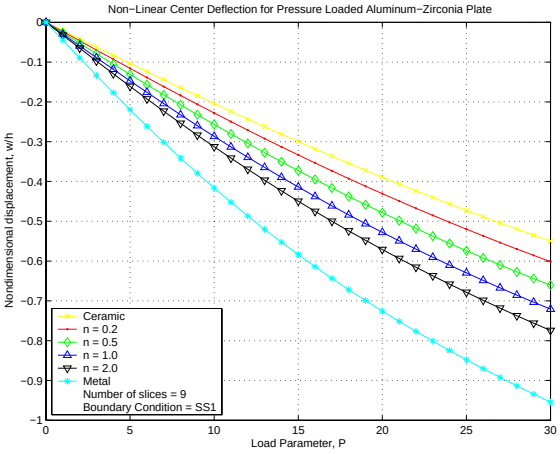

Figure 47. Plate-Pressure Induced Deflection for SS1 (Non-Linear)

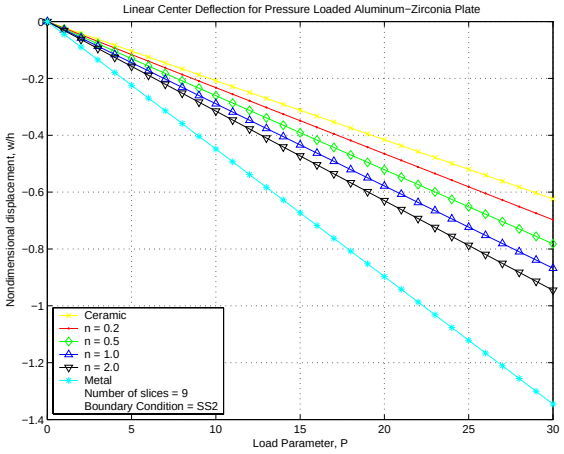

Figure 48. Plate-Pressure Induced Deflection for SS2 (Linear)

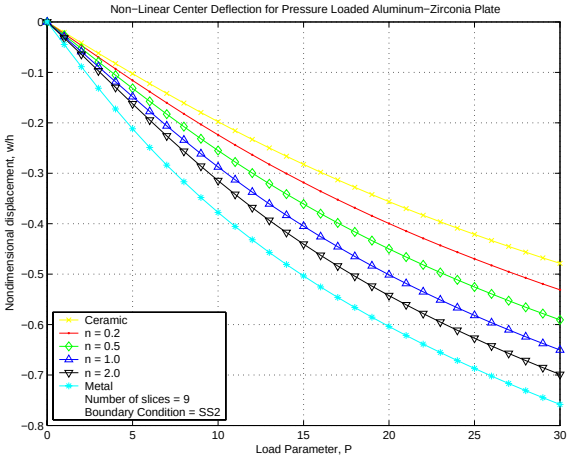

Figure 49. Plate-Pressure Induced Deflection for SS2 (Non-Linear)

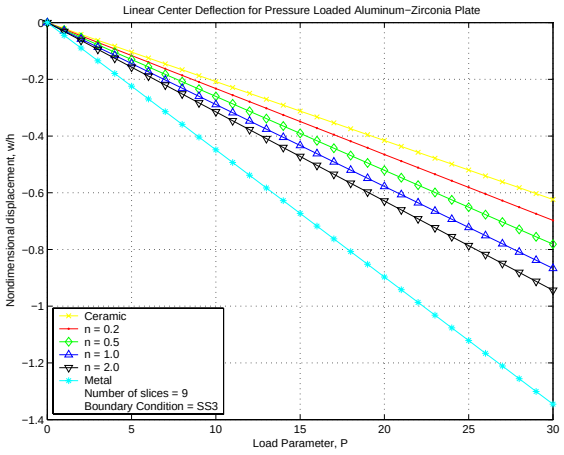

Figure 50. Plate-Pressure Induced Deflection for SS3 (Linear)

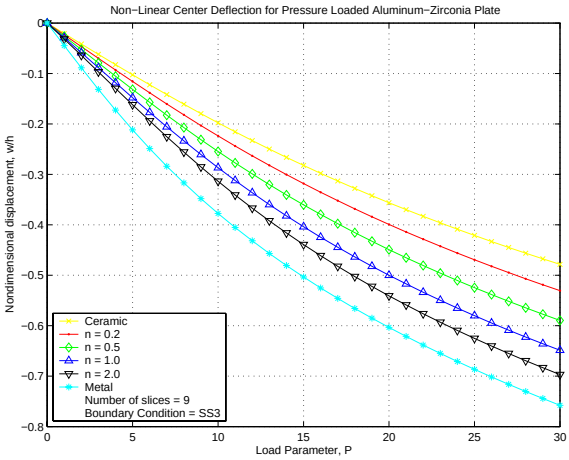

Figure 51. Plate-Pressure Induced Deflection for SS3 (Non-Linear)

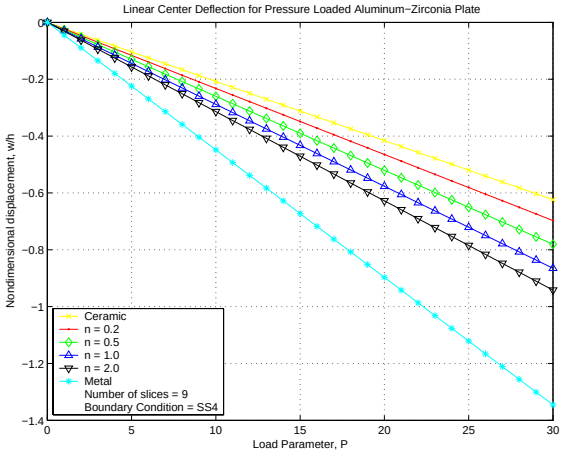

Figure 52. Plate-Pressure Induced Deflection for SS4 (Linear)

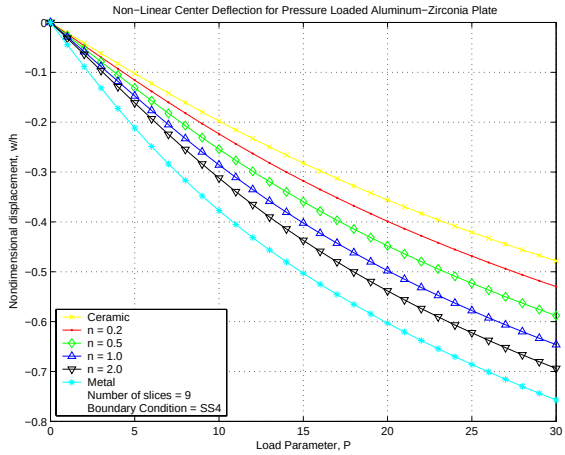

Figure 53. Plate-Pressure Induced Deflection for SS4 (Non-Linear)

It is noted that SS1 and SS-Free provide the highest displacement while SS2, SS3, and SS4 provide the lowest displacements. Metal displacements in boundary conditions SS2, SS3, and SS4 are approximately 0.95. Metal displacements in SS1 and SS-Free boundary conditions are 0.75, or 27% lower than other SS2, etc. This trend is opposite to the displacement trend in thermally loaded flat plates where SS1 has 35% lower

deflections than SS2, etc. As one would predict, adding more restraints at the boundary tends to decrease the deflection in pressure loaded plates.

Ceramic provides the lowest deflection because it is the stiffest material while aluminum provides the highest deflection because it is the softest material. FGM plate deflections fall in the middles with n=0.2 providing the minimum deflection. Lowering "n" tends to lower the center deflection. Of particular importance is the drastic reduction of deflections by functionally graded materials. For all "n" values, FGMs reduced deflections by approximately 50% over a metal plate. The trend of lowering "n" to lower deflection follows the same trend found in thermally loaded plates. In addition, n=0.2 provides the lowest deflection on both thermally loaded plates and pressure loaded plates.

It is noted that a non-linear analysis provides lower displacements than a linear analysis. This is due to the geometric stiffening effect provided by a non-linear analysis and as discussed in the previous section. It is important to note that a linear analysis provides non-dimensional displacements greater than 0.5, which is the general cutoff for deciding between a linear and non-linear analysis. Finally, it is noted that FGMs exhibit non-linearity much earlier than homogeneous materials.

Figure 56 through Figure 65 show mid-plane stress for all six "n" values studied, for both linear and non-linear analysis, at a load parameter of 30.

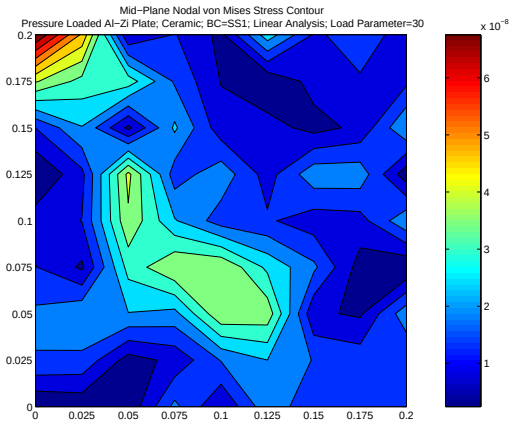

Figure 54. Plate-Pressure Induced Stress for n=Metal (Linear)

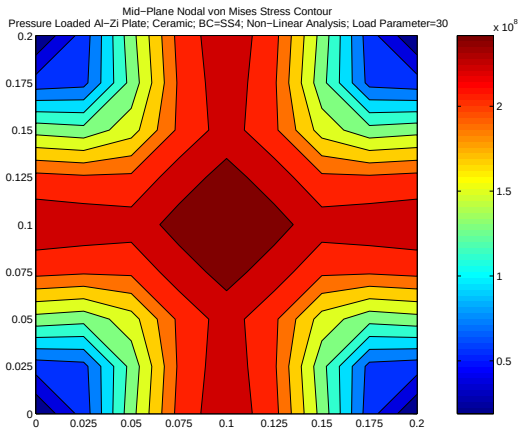

Figure 55. Plate-Pressure Induced Stress for n=Metal (Non-Linear)

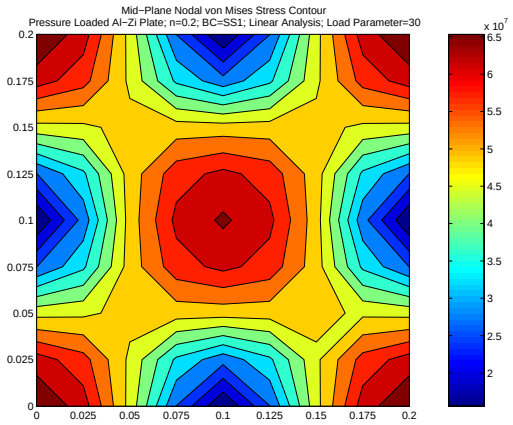

Figure 56. Plate-Pressure Induced Stress for n=0.2 (Linear)

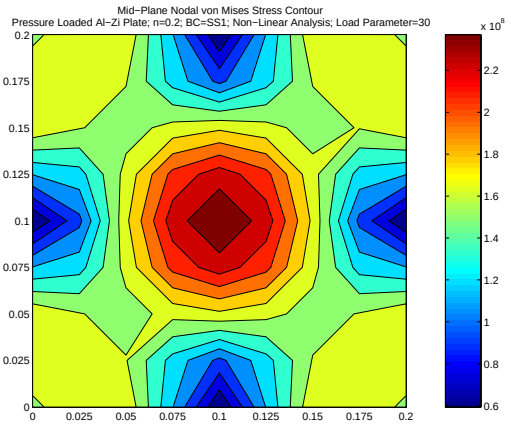

Figure 57. Plate-Pressure Induced Stress for n=0.2 (Non-Linear)

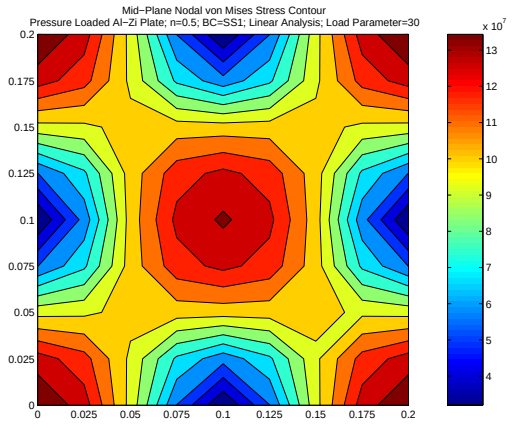

Figure 58. Plate-Pressure Induced Stress for n=0.5 (Linear)

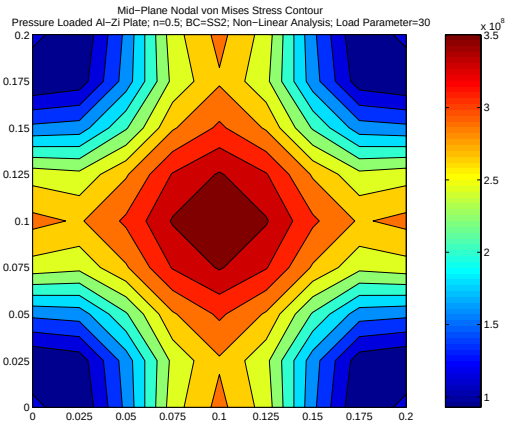

Figure 59. Plate-Pressure Induced Stress for n=0.5 (Non-Linear)

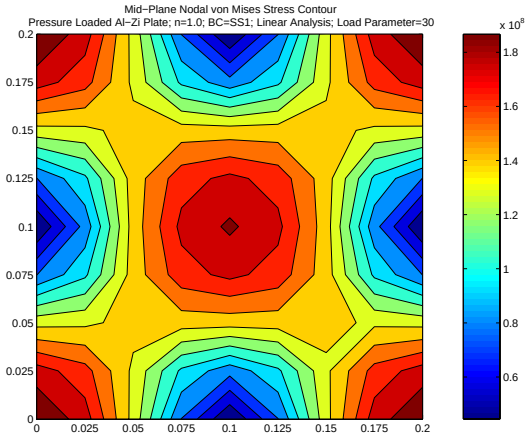

Figure 60. Plate-Pressure Induced Stress for n=1.0 (Linear)

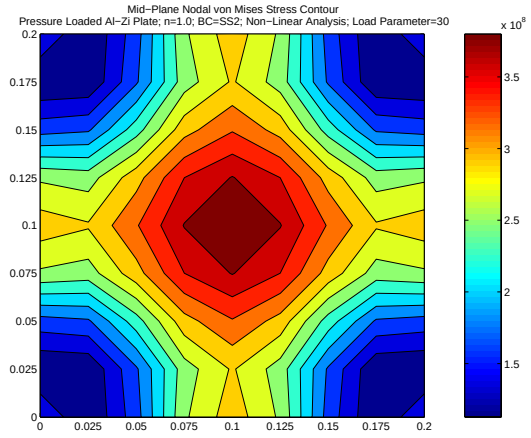

Figure 61. Plate-Pressure Induced Stress for n=1.0 (Non-Linear)

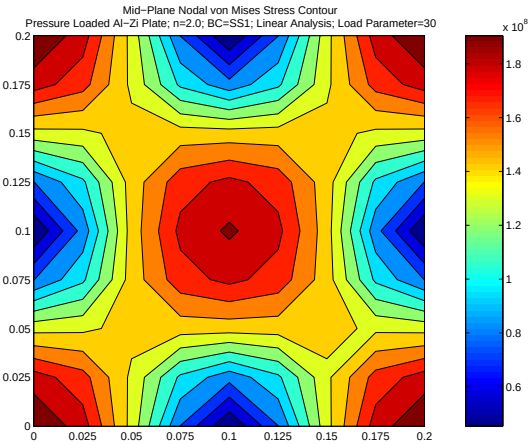

Figure 62. Plate-Pressure Induced Stress for n=2.0 (Linear)

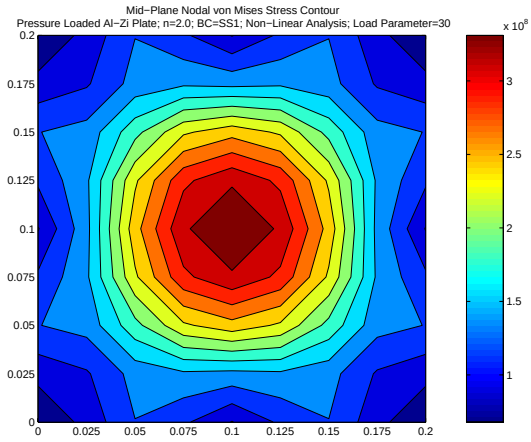

Figure 63. Plate-Pressure Induced Stress for n=2.0 (Non-Linear)

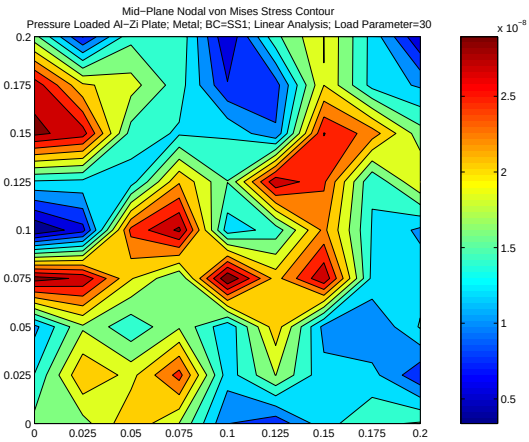

Figure 64. Plate-Pressure Induced Stress for n=Ceramic (Linear)

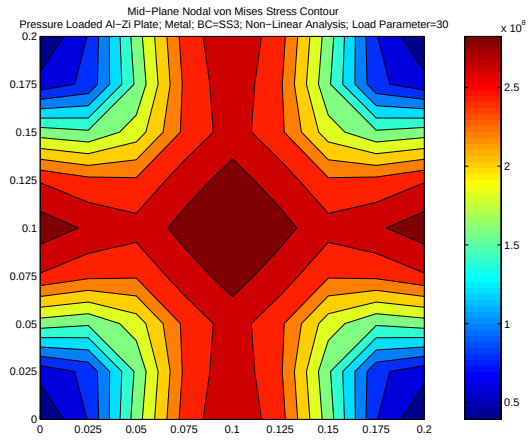

Figure 65. Plate-Pressure Induced Stress for n=Ceramic (Non-Linear)

It is noted that among the FGMs, increasing "n" tends to raise the stress. n=0.2 provides the overall lowest stress and 4% lower than a metal plate. The highest mid-plane stress is found at n=1.0 and is 27% higher than metal's mid-plane stress. These mid-plane stress values are a good representation of the bend-stretch coupling found in the FGMs. Bend-stretch coupling is found in materials that are not symmetric about their mid-plane. That is, a material that has non-symmetric E values about it's mid-plane therefore as the material is stretched it undergoes non-uniform strain. This unsymmetrical strain creates a bending moment inside the material. This explains why metal, a homogenous material, has a very low mid-plane stress as it exhibits no bend-stretch coupling; the material is symmetric about its mid-plane. In addition, n=1.0 is the most unsymmetrical layup of the FGMs, because it has a linear material distribution from ceramic on the top surface to metal on the bottom surface. Consequently, it has the highest bend-stretch coupling as evident by the high mid-plane stresses.

Non-linear analysis plays an important role in the stress analysis of mechanical loaded plates. Of particular importance is the lack of mid-plane stress in homogeneous plates with a linear analysis. Because the stiffness matrix is never updated in a linear analysis, the plate does not "stretch" and exhibit stress at the mid-plane; the plate is under pure bending. In addition, linear mid-plane stress values found in FGMs vary drastically from non-linear stress values. This is again due to the lack of stress stiffening in a linear analysis. It is concluded that non-linear analysis is required for analyzing FGMs plates under both thermal and mechanical loading.

In summary, lowering the "n" value tends to lower both deflection and mid-plane stress in FGM plates under pressure loading. At n=0.2 both deflection and stress are minimized among the FGM plates; n=0 (ceramic) provides the lowest overall deflection and n=0.2 provides the overall lowest stress. Finally, it is concluded that non-linear analysis is required to accurately model FGMs, because they exhibit bend-stretch coupling.

Curved Panel under Concentrated Force Loading

The goal of analyzing a curved panel under concentrated force loading is to verify ABAQUS' ability to handle localized buckling. While this may seem trivial, it is important to gain an understanding of local buckling of panels as it will likely be encountered in the exhaust wash structure. The goal is to verify ABAQUS' ability to handle local buckling of a panel and provide accurate results.

Following work published by A. Palazotto and S. Dennis [5] a hinged-free curved panel is exposed a concentrated force at the center of the panel. The homogeneous panel is 0.508 m (20 in) long, 0.508 m (20 in) wide, 25.4 mm (1.0 in) thick and has a radius of curvature of 2.54 m (100 in). The modulus of elasticity E=3.109 GPa (450 ksi) and Poisson's Ratio ν=0.3.

A 2D shell analysis with a 8x8 mesh and 9 slices is used to solve the problem. A concentrated force of 21.35 kN (4800 lbs) is applied to the center of the panel. Figure 66 shows the panel center deflection vs. applied center load.

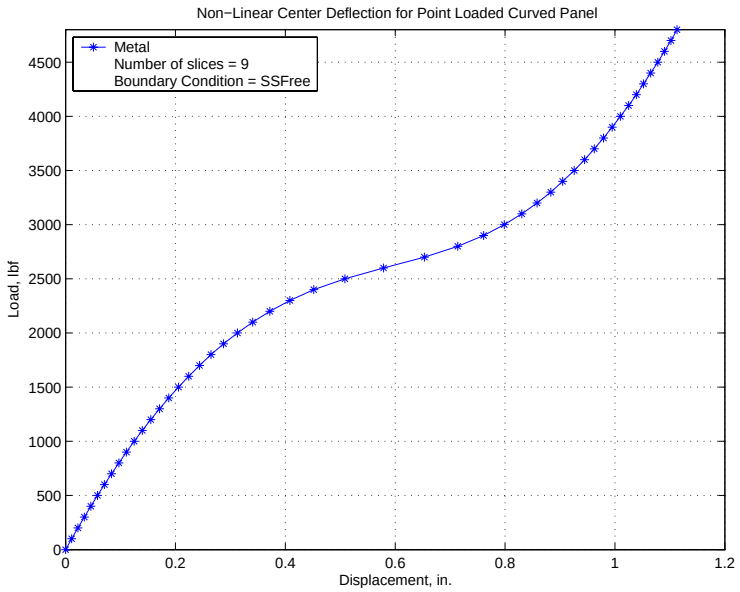

Figure 66. Panel-Concentrated Force Induced Deflection for SSFree (Non-Linear)

Because the panel is hinged (rotations are allowed) it is subject to snap through buckling, however the panel is sufficiently thick and does not snap through. Local buckling of the panel is apparent at a load of 2.67 kN (600 lbs), however, the panel does not experience snap through bucking because of its 25.4 mm (1.0 in) thickness.

Figure 66 matches work published by A. Palazotto and S. Dennis [5]. It is apparent that ABAQUS can handle local buckling without any special analysis techniques. This is important as it provides confidence in the accuracy of modeling shells that can experience localized buckling. The exhaust wash structure is subject to local buckling because of its clamped boundary condition resisting thermal expansion of the shell. In summary, ABAQUS has the ability to analyze panel structures past localized buckling without implementing special analysis techniques.

Curved Panel under Thermal Loading

The goal of analyzing curved panels under thermal loading is to characterize the effect "n" has on shell structural response to thermal loading and to explore the effects curvature has on structural response. A panel is created out of the flat plate by adding a 5.08 m (200 in) radius of curvature. The same materials, properties, and geometry still apply to the panel. A 2D shell analysis with a 8x8 mesh and 9 slices is again used to solve the problem. The top surface is exposed to temperatures ranging from T_t=20°C to T_t=600°C while the bottom surface is held at T_b=20°C. Displacement is fixed along the circumferential edges while the remaining edges free (SS-Free). Figure 67 and Figure 68 show the non-dimensional displacement vs. top temperature.

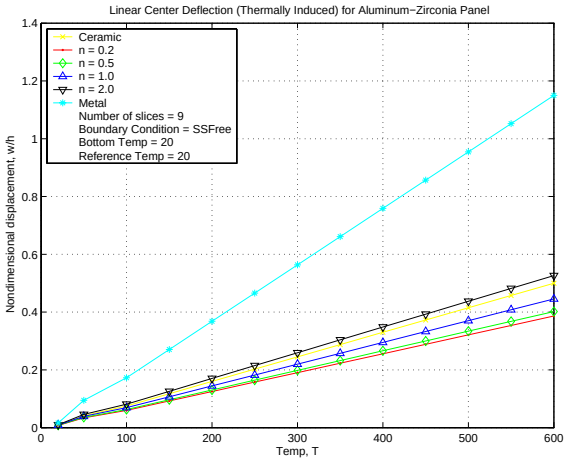

Figure 67. Panel-Thermally Induced Deflection for SSFree (Linear)

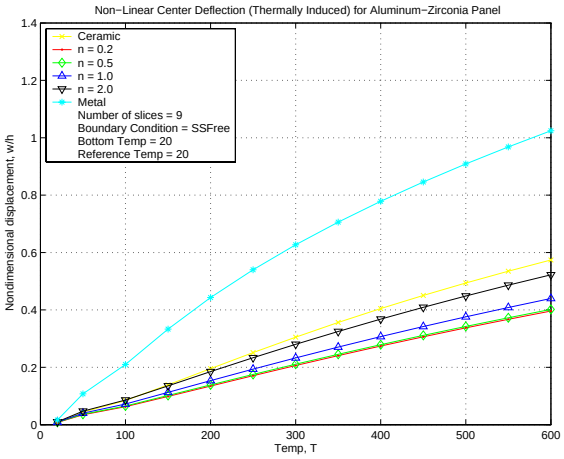

Figure 68. Panel-Thermally Induced Deflection for SSFree (Non-Linear)

It is important to note that a curved panel at Tt=600°C with has 31% higher center deflections than a flat plate in both linear and non-linear analysis (reference Figure 32 and Figure 33). The effect of adding curvatures tends in to increase deflection in a curved shell panel.

Decreasing “n” tends to lower the deflection with n=0.2 providing the overall lowest deflections (62% less deflection than metal). Of particular importance, the performance of each “n” is proportional to its flat plate counterpart. It appears that the addition of curvature increases the deflections due to thermal loading, but does not change the relative performance of an FGM.

Again, stress in SS-Free plates are of importance because the exhaust wash deck is modeled as a SS-Free structure. Figure 56 through Figure 65 show mid-plane stress for all six “n” values studied and for both linear and non-linear analysis. Note: these stress graphs are for a top surface temperature of 600°C.

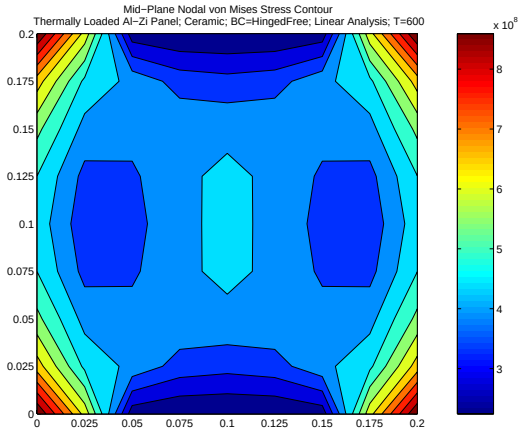

Figure 69. Panel-Thermally Induced Stress for n=Ceramic (Linear)

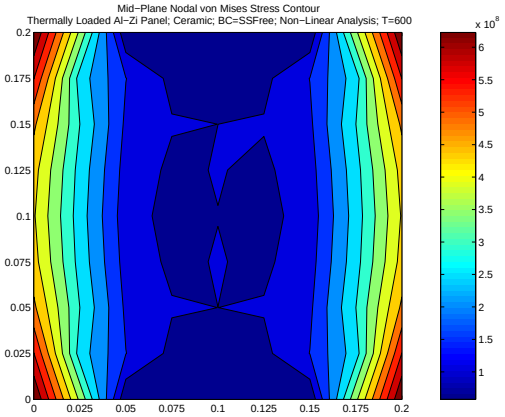

Figure 70. Panel-Thermally Induced Stress for n=Ceramic (Non-Linear)

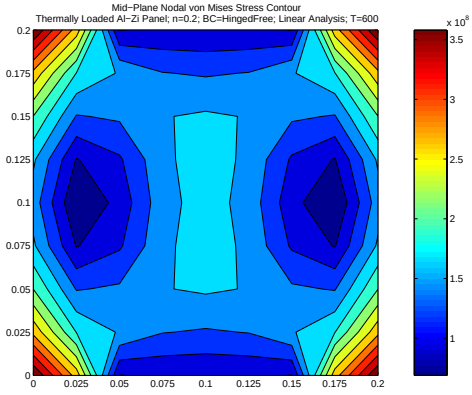

Figure 71. Panel-Thermally Induced Stress for n=0.2 (Linear)

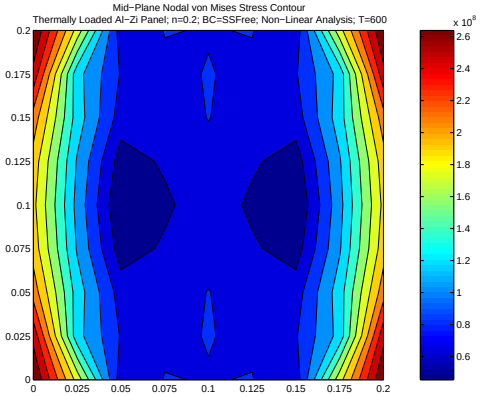

Figure 72. Panel-Thermally Induced Stress for n=0.2 (Non-Linear)

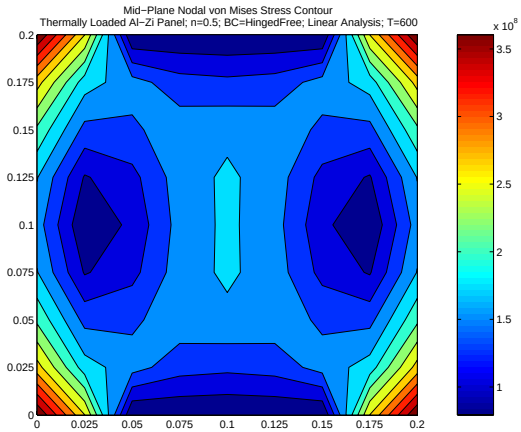

Figure 73. Panel-Thermally Induced Stress for n=0.5 (Linear)

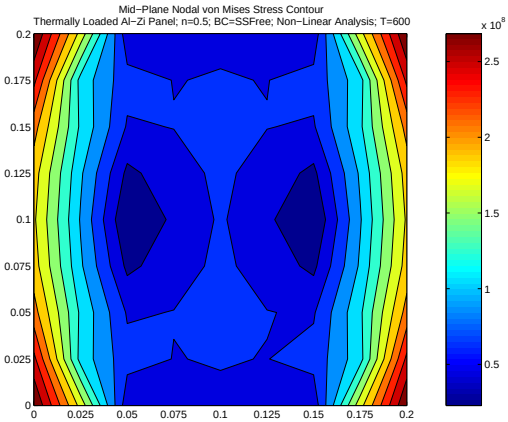

Figure 74. Panel-Thermally Induced Stress for n=0.5 (Non-Linear)

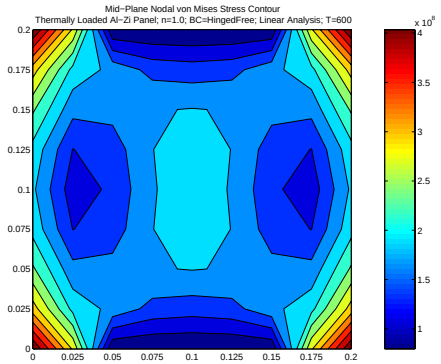

Figure 75. Panel-Thermally Induced Stress for n=1.0 (Linear)

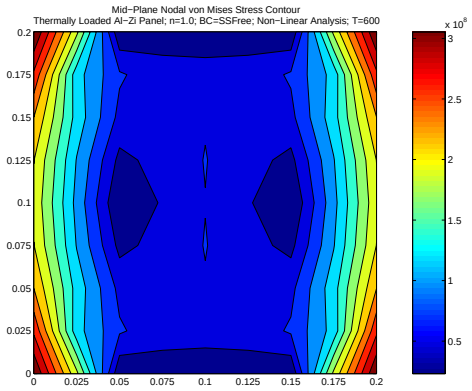

Figure 76. Panel-Thermally Induced Stress for n=1.0 (Non-Linear)

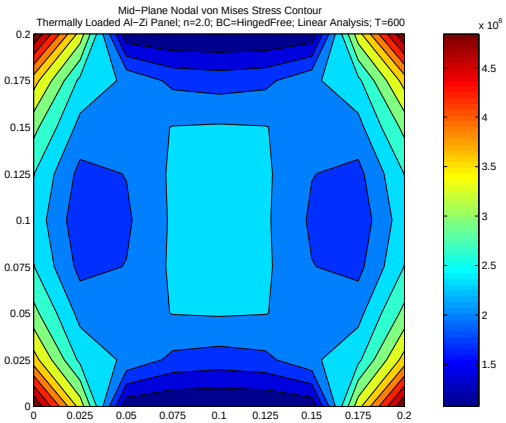

Figure 77. Panel-Thermally Induced Stress for n=2.0 (Linear)

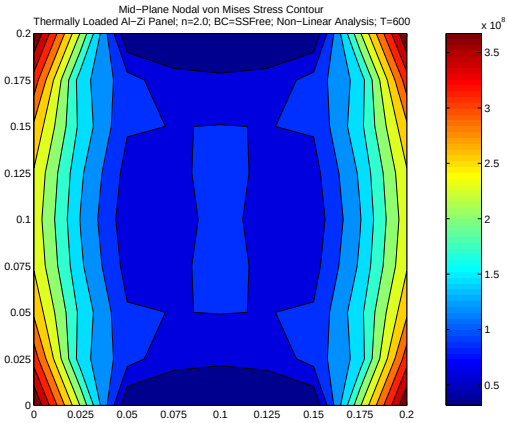

Figure 78. Panel-Thermally Induced Stress for n=2.0 (Non-Linear)

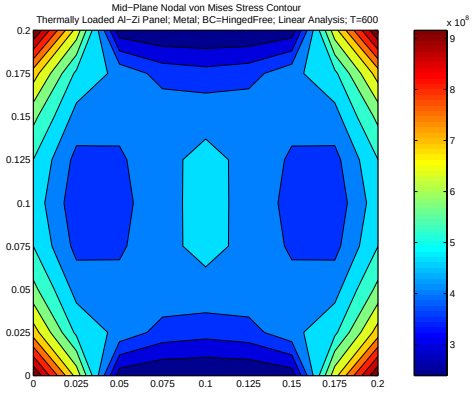

Figure 79. Panel-Thermally Induced Stress for n=Metal (Linear)

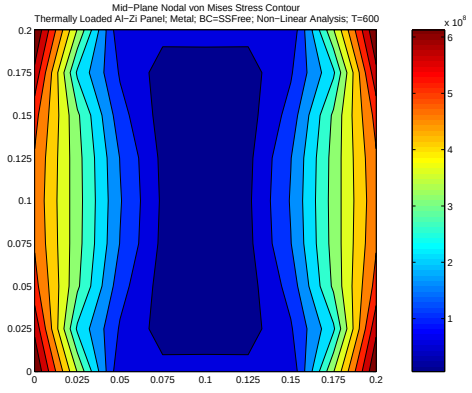

Figure 80. Panel-Thermally Induced Stress for n=Metal (Non-Linear)

It is noted that lowering "n" lowers mid-plane stress with n=0.2 providing the lowest stress (57% less stress than a metal plate). Also, a curved panel has 41% less stress than a flat plate (n=0.2, non-linear, SS-Free). In addition, a curved panel stress field has stresses concentrated throughout the boundary edge while a flat plate has stress concentrated at the corners. The shape of the stress field also changes to one which is aligned with the boundary edges in a curved panel vice a symmetric stress field in a flat plate. These changes are caused by the curved panels already having out-of-plane geometry and, therefore, an avenue for the panel expansion to deform out of plane.

In summary, decreasing "n" tends to lower the deflection in a curved shell under thermal loading with n=0.2 providing the lowest deflection and stress. Increasing "n" increases stress levels with the lowest mid-plane stress levels at n=0.2. Finally, stress levels in a curved panel are generally lower than a flat plate.

It is important to note that n=0.2 to n=0.5 consistently provided the lowest deflection and lowest stress in both flat plates and curved panels, under both mechanical and thermal loading throughout the characterization of FGMs. An FGM can significantly outperform a homogenous plate and the "n" value of the FGM can be tailored to minimize desired parameters (stress, deflection, etc). It was shown that FGM panels and shells can reduce deflections by approximately 30% to 100%.

Exhaust Wash Structure under Thermal Loading (Structure Only)

The goal of analyzing the exhaust wash structure is to provide a baseline stress and displacement field which can be used to evaluate the effectiveness of any patch applied to the structure.

A clamped-free curved panel representing the exhaust wash structure is exposed to gases on the top and bottom surfaces. The top surface gas temperature ranges from T_t=260°C (500°F) to 538°C (1000°F) and has a convective heat transfer film coefficient of h_t= 283.9 W/m^2·°C (50.0 BTU/hr·ft^2·°F) The bottom surface gas temperature is a constant T_b= 15.6°C (60°F) and has a convective heat transfer film coefficient of h_b= 5.678 W/m^2·°C (1.00 BTU/hr·ft^2·°F). The panel is 0.9144 m (36 in) long, 0.3048 m (12 in) wide at the mid-plane, 0.004064 m (0.160 in) thick and has a radius of curvature of 5.08 m (200 in).

The structure is made from Ti-6-2-4-2 and has material properties listed below [7 and 8]:

Ti-6-2-4-2 at 80°C

E = 113.8 GPa; ν = 0.32; ρ = 4540 Kg/m^3; α = 7.7μm/m·ºC; k = 6.9 W/m·K

E = 16,505 ksi; ν = 0.32; ρ = 283.4 lbm/ft^3; α = 4.28 μin/in·ºF; k = 4.0 BTU·ft/hr·ft^2·°F

Up to 80°C (176°F), materials properties of Ti-6-2-4-2 are unaffected by temperature. However, at 538°C (1000°F) Ti-6-2-4-2 shows significant reductions in E, F_{tu}, and F_{ty} while α and K increase in value. Table 2 lists temperature dependent material properties at 80°C and 538°C.

Table 2. Ti-6-2-4-2 Material Properties at 80°C and 538°C

	80°C 176°F	538°C 1000°F
E	113.8 GPa 16,505 ksi	83.1 GPa 12,045 ksi
α	7.7 µm/m-°C 4.28 µin/in-°F	8.1µm/m·ºC 4.5 µin/in·ºF
k	6.9 W/m·K 4.0 BTU·ft/hr·ft^2·°F	13.2 W/m·K 7.7 BTU·ft/hr·ft^2·°F
F_{cy}	1070 MPa 155 ksi	577.8 MPa 83.7 ksi
F_{ty}	860 MPa 125 ksi	482.6 MPa 76.1 ksi
F_{tu}	940 MPa 136 ksi	618.9 MPa 89.8 ksi

A simple convective heat transfer analysis is performed to obtain the surface temperatures of the exhaust wash panel, as discussed in the heat transfer methodology section. Knowing that a steady state heat flux is uniform throughout all heat transfer regions of the panel, simultaneous equations are solved in order to find the heat flux and panel surface temperatures, outlined below. (Reference Figure 14. Convective Heat Transfer Diagram, page 22 for a diagram of convective heat transfer)

$$q = h_{HotGas}\left(T_{HotGas} - T_{TopSurface}\right)$$ Convection from the hot gas to the top surface of the exhaust wash panel (18)

$$q = \frac{K_{structure}}{t_{structure}}\left(T_{TopSurface} - T_{BottomSurface}\right)$$ Conduction from the top surface of the exhaust wash panel to the bottom surface (19)

$$q = h_{ColdGas}\left(T_{BottomSurface} - T_{ColdGas}\right)$$ Convection from the bottom surface of the exhaust wash panel to the cold gas (20)

The steady state heat transfer analysis indicated that the panel is at a uniform temperature equal to the hot gas temperature. Because the material is homogenous with the top surface having a higher heat transfer film coefficient than the bottom surface, the material heats to a steady state temperature equal to the top gas sink temperature 538°C (538°F). There is no temperature variation through-the-thickness and all nodes are at the same temperature. As such, the structural analysis uses material properties for Ti-6-2-4-2 at 538°C.

The nodal temperatures obtained in the previous analysis are applied to a structural analysis with hinged-free boundary conditions. This difference in the applied temperature and the stress free reference temperature cause the center of the panel to deform 0.01208 m (0.4757 in) or three times the panel thickness. Contour plots of the stress field are shown in Figure 81 through Figure 86.

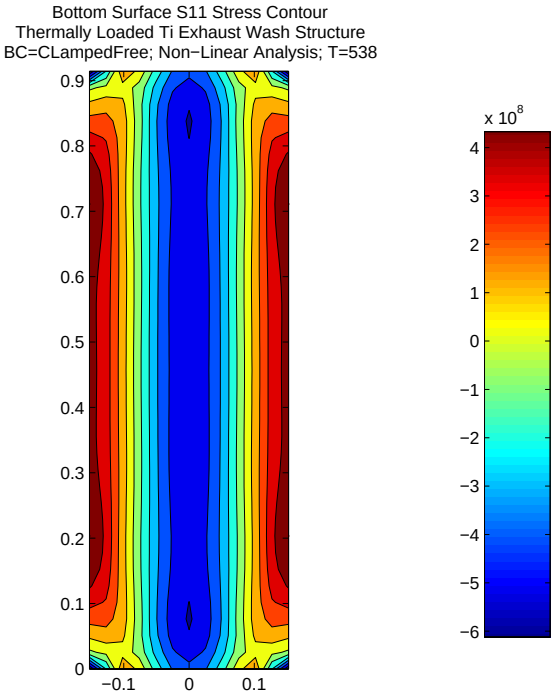

Figure 81. Bottom Surface S11 Stress Contour

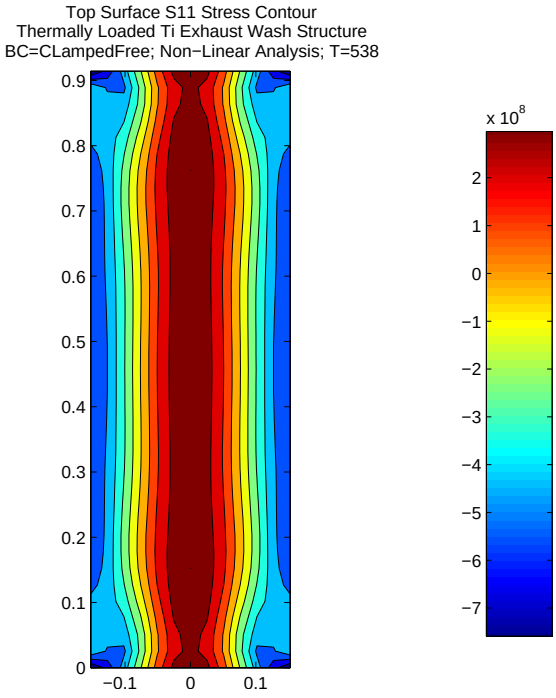

Figure 82. Top Surface S11 Stress Contour

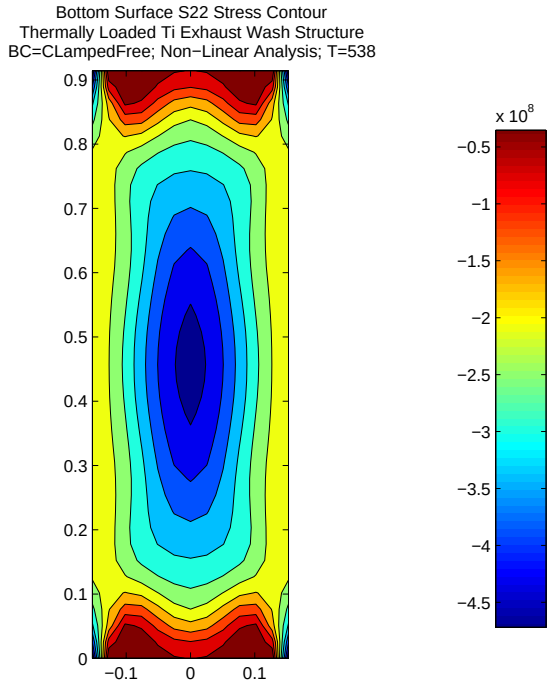

Figure 83. Bottom Surface S22 Stress Contour

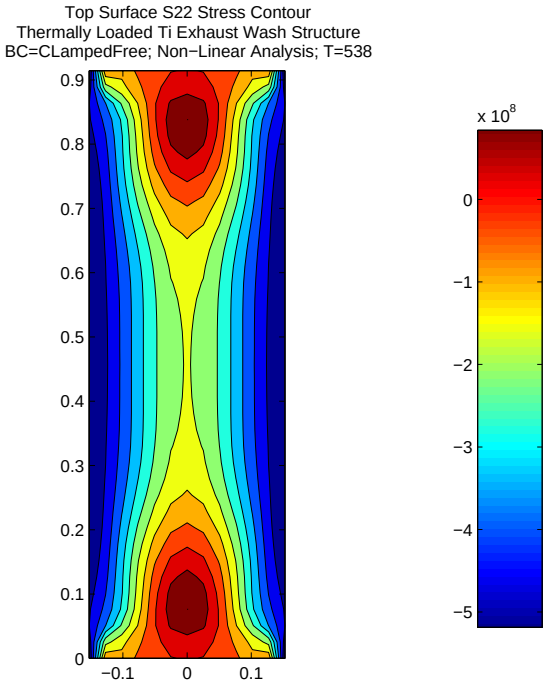

Figure 84. Top Surface S22 Stress Contour

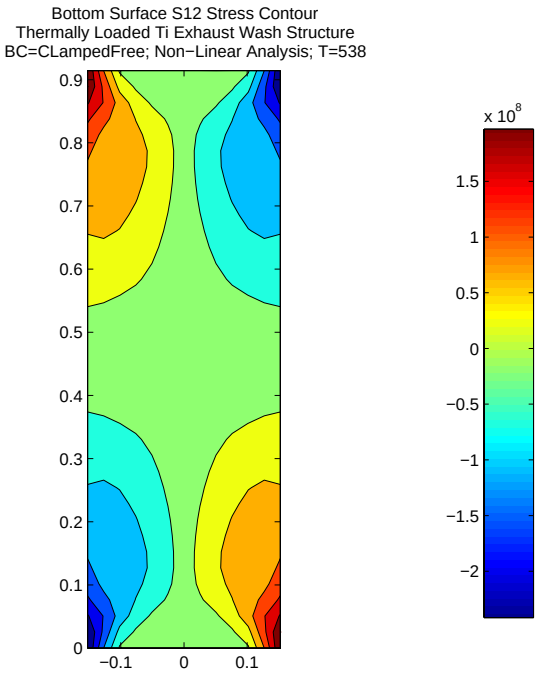

Figure 85. Bottom Surface S12 Stress Contour

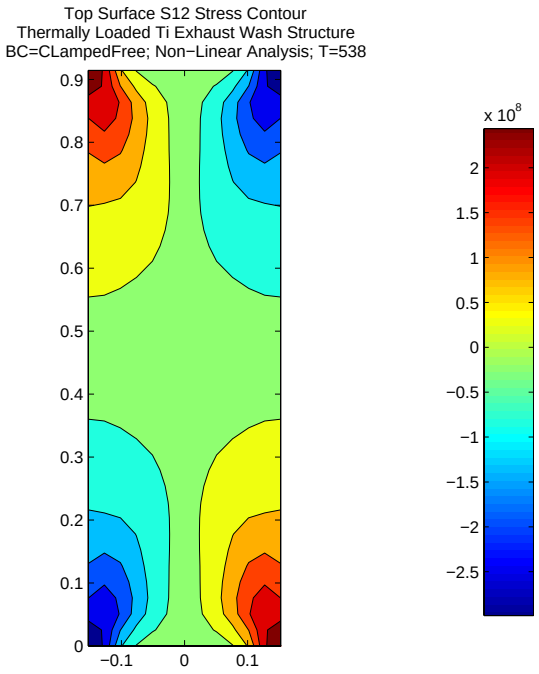

Figure 86. Top Surface S12 Stress Contour

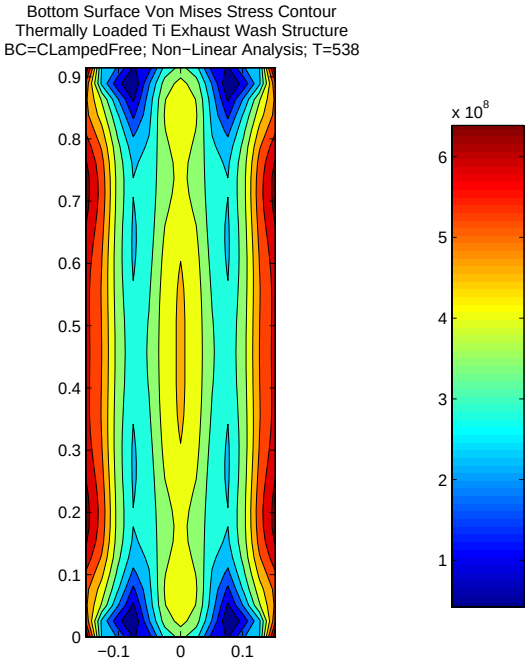

Figure 87. Bottom Surface von Mises Stress Contour

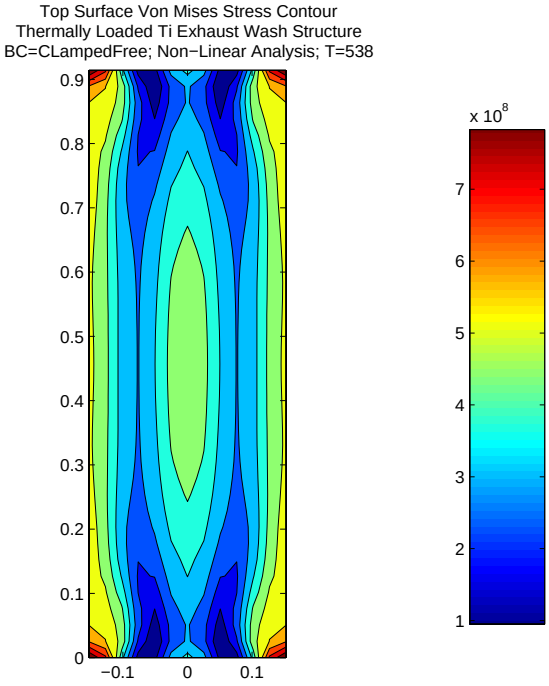

Figure 88. Top Surface von Mises Stress Contour

It is noted that the highest stresses, both compressive and tensile, are located at the edges where the material is clamped. Cracking is caused by thermally induced deflections resisted by stiffeners at the panel's edges. These stiffeners are modeled as a clamped boundary but, in reality, the stiffeners allow minimal deflection and some rotations. A clamped boundary was chosen in order to model the "worst case" scenario.

As the panel is heated it elongates and moves in the +z direction. However, its rotation at the clamped edge is restricted and therefore a large bending stress develops at the clamped edge. This bending is noted by the high tensile stress at the edges in Figure 81 and the large compressive stress at the edges in Figure 82.

ABAQUS models indicate the highest von Mises stress is 858 MPa and is located at the four corners of the top surface of the panel. The highest x direction tensile stress 547 MPa and is located at the left and right clamped edges at a distance of b/4 from the top and bottom faces. The highest x direction compressive stress is -767 MPa and is located at the four corners of the top surface of the panel. At 538°C (1000°F), Table 2 indicates F_{cy}=577.8 MPa, F_{ty}=482.6 MPa, and F_{tu}=618.9 MPa. It is clear that both compressive and tensile yield strengths have been exceeded at the clamped panel supports. Additionally, the von Mises stress is above ultimate stresses. It is reported that original versions of exhaust wash structure cracked in less than 100 hours of service and that the current version last up to 1,500 hours in service (the original version was thinner than existing version)

In order to quickly measure the effectiveness of any patch applied to the exhaust wash structure, the number of nodes that are above yield stress and above ultimate stress

can be compared to the baseline exhaust wash structure failed nodal count. This, in essence, provides a generalized number that can be compared from patch to patch to measure the effectiveness of reducing exhaust wash panel stress. A patch that has a high nodal yield count is obviously inferior to a patch with a low nodal yield count. The nodal count is the sum of the top AND bottom surface von Mises nodes that are above the structural yield or structural ultimate stresses of Ti-6-2-4-2 at 538°C. The baseline nodal yield and nodal ultimate count is 74 and 40, respectively. In other words, the top and bottom surfaces have 74 nodes that are above yield stress. Of those 74 nodes, 40 are above ultimate stress.

In summary, the exhaust wash structure fails at the edges due to thermally induced bending. As the panel expands 0.01208 m in the +z direction, it is resisted by the rigid boundary condition and causes very high x direction stress at the boundary edges. The highest von Mises stress is 858 MPa, the highest x direction stress is 547 MPa and the lowest x direction stress is -767 MPa.

Exhaust Wash Structure under Thermal Loading (Structure and Patch)

The goal of this section is to use conclusions from aforementioned research to develop a patch for the exhaust wash structure. This patch should limit thermally induced deflections and stresses found in the baseline exhaust wash structure solution, while hindering further crack growth.

Having established a baseline for structural deflection and stress levels, it is desirable to develop an FGM patch that limits the structural deflection which will reduce the large bending stresses at the clamped boundary. Also, because aerodynamic flow of

the exhaust wash is to be unchanged, this patch may only be applied to the underside of the structure. Finally, it is desirable to have a patch which does not translate reduced deflection into increased compression at the boundary condition. Note: all model results are summarized in Appendix D where maximum and minimum stress, and center deflections are listed for all patches studies (in SI units).

It has been established that the exhaust wash structures deflects in the +z direction under thermal loading. Therefore, it is desired to develop an FGM patch which deforms in the –z direction under thermal loading. Figure 68 shows that a SS-Free Zirconium-Aluminum FGM panel (with ceramic on the top surface) deflects in the +z direction under thermal loading. Therefore, it is hypothesized that an FGM patch should have the material with the lower coefficient of thermal expansion on the bottom surface; however, FGM patches are examined in both orientations in order to verify this hypothesis. Two FGM patches with Ti-6-2-4-2 are examined. The first is Ti-6-2-4-2 / Zirconia in which Ti has the highest coefficient of thermal expansion of the two materials; the second is Ti-6-2-4-2 / A-286 in which Ti has the lowest coefficient of thermal expansion of the two materials. Material properties for Ti-6-2-4-2 and A286 are summarized in Table 5. Material properties for Zirconia are the same as used in previous FGM analysis and are summarized below:

Zirconia

$E = 151$ GPa; $\nu = 0.3$; $\rho = 3{,}000$ Kg/m^3; $\alpha = 10$ μm/m·ºC ; $k = 2.09$ W/m·K

It is important to note that the "n" value of an FGM is relative to the top and bottom materials and can change with material orientation. In previous analysis, an

Aluminum-Zirconian FGM was analyzed with Zirconia composing the top surface material. The significance of "n" was discussed in detail with respect to FGMs with ceramic on the top surface and metal on the bottom surface. It was shown that at n=0 the FGM is wholly ceramic and at n=∞ the FGM is wholly metal. In reality, at n=0 the FGM is wholly composed of the *top* surface material and at n=∞ the FGM is wholly composed of the *bottom* surface material. The simplification of "n" was used in order to establish and develop the basis of FGM theory without adding confusion to the reader. It is important to understand the meaning of "n" with respect to top and bottom surfaces because this section will analyze FGMs in both orientations. For example, a Ti-6-2-4-2 / Zirconia FGM with n=0.5 is not the same as a Zirconia / Ti-6-2-4-2 FGM with n=2.0. In order to simplify which material is on the top surface and which is on the bottom surface, FGMs in this section will be listed as top material / bottom material, i.e. Zi-Ti has Zi on the top surface.

The exhaust wash structure with FGM patch is modeled in a 3D shell analysis with a 12x36 mesh and one through-the-thickness "slice" for the exhaust wash structure and eight "slices" for the FGM patch. Previous discussion outlined the 20 thermal degrees-of-freedom limitation (nine "slices" total) in ABAQUS using shell elements. Additionally, previous analysis was completed with nine "slices," however the FGM patch is modeled with eight "slices" in this section to allow one "slice" for the structure.

An installed exhaust wash structure has stringers and stiffeners around the edges; therefore, an FGM patch can not extend all the way to the edges. As such, the patch is

modeled to extend 90% of the length and width of the exhaust wash structure, as shown in Figure 89.

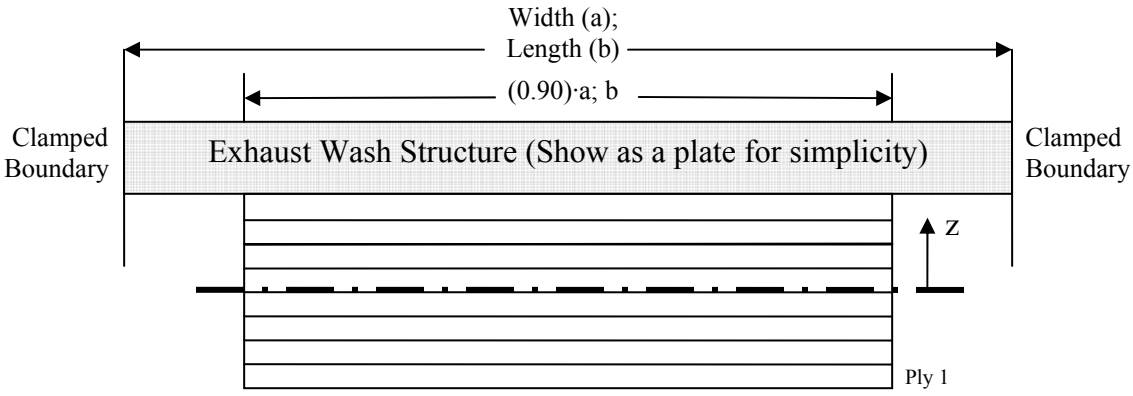

Figure 89. Diagram of FGM Patch Attached to Exhaust Wash Structure

Because ABAQUS does not have provisions for convection using shell elements, a manual calculation of the convective heat transfer is performed to obtain surface temperatures, as outlined in the background section. However, it was found that the difference between bottom and top surface temperatures was less than 9°C (approximately) for the majority of patches studied. The hot, high speed gas flow on the top surface of the exhaust panel has a very high heat transfer coefficient. The cold, stagnant air on the underside of the exhaust wash structure has a very low heat transfer coefficient. Therefore, at steady state conditions the entire patch and exhaust wash structure are heat soaked by the engine exhaust. Zi-Ti patches will have the greatest effect of the temperature profile and provide the highest difference between top and bottom surface temperatures, as shown in Table 3

Table 3. Surface Temperatures with a Zi-Ti Patch

Patch	n	Top Surface Temp (°C)	Bottom Surface Temp (°C)
0.5” Ti	N/A	527.8	556.8
0.2” Zi-Ti	0.0	527.9	520.1
	0.2	527.9	522.7
	0.5	527.8	523.8
	1.0	527.8	524.5
0.5” Zi-Ti	0.0	528.1	510.2
	0.2	528.0	516.6
	0.5	527.9	519.3
	1.0	527.9	521.0

Only 0.5” Zi-Ti patches with “n” values of 0.0 and 0.2 exceed a 9°C temperature difference between the upper and lower surfaces. Therefore, all patch models are entered as having top and bottom surface temperatures equal to the hot, top surface gas temperature, 538°C (1000°F). As such, the structural analysis uses material properties at 538°C. In order to check the accuracy of this assumption, a 0.5” Zi-Ti patch with n=0.2 and assumed surface temperatures was compared the same patch with the actual surface temperatures. Results are shown in Table 4.

Table 4. Summary of Assumed Temperature Profile Error

0.5” Zi-Ti	Field	Assumed Temperature Profile	Actual Temperature Profile	% Difference
n=0.0	Stress (Pa)	1.6816E+09	1.6751E+09	0.39
	Displacement (m)	0.012451	0.012387	0.52
n=0.2	Stress (Pa)	1.2988E+09	1.2954E+09	0.26
	Displacement (m)	0.012217	0.012175	0.35

The upper bound of error in an assumed temperature profile is 0.52% in displacement and 0.39% in stress. These errors are well within acceptable limits given.

Even though a uniform temperature profile is assumed, an ABAQUS steady state heat transfer analysis is performed in order to generate a nodal temperature file. The nodal temperatures are then applied to a second structural analysis to obtain displacements and stresses.

Ti-Zi FGM patches are first analyzed in thicknesses of 0.1", 0.2", and 0.5". Note: the first material listed corresponds to the top surface (Ti is on the top surface). Figure 90 through Figure 92 show the deflection of the structure and patch for n=[0.0, 0.2, 0.5, 0.8, 0.9, 1.0, 1.1, 1.2, 1.3, 1.4, 1.5, and 2.0]. Numerous values of "n" were studied in order to establish the best "n" for this problem.

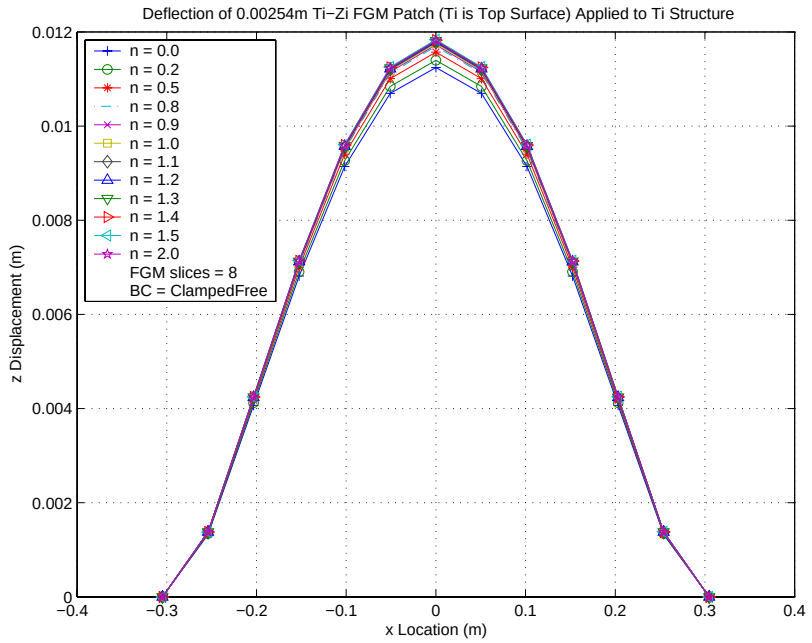

Figure 90. Exhaust Wash Deflection with 0.1" Ti-Zi FGM Patch

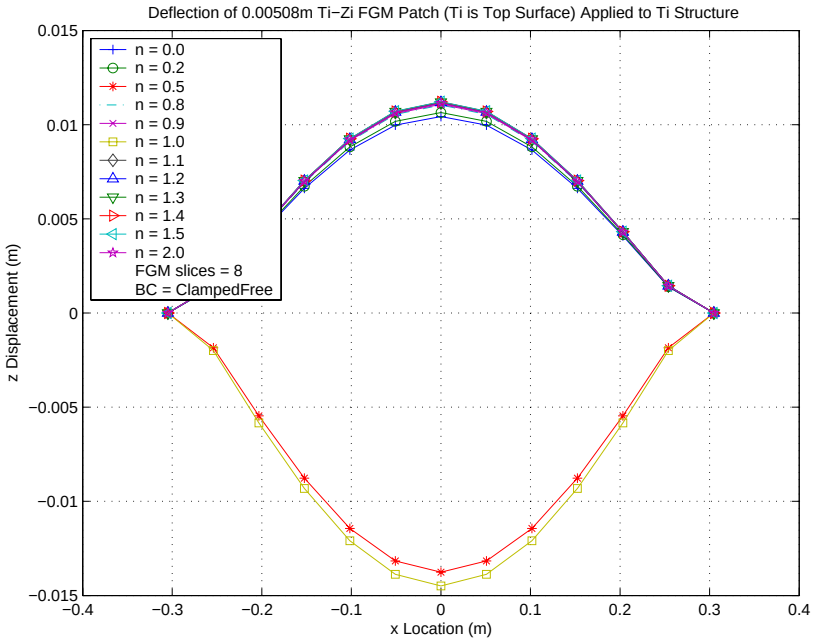

Figure 91. Exhaust Wash Deflection with 0.2" Ti-Zi FGM Patch

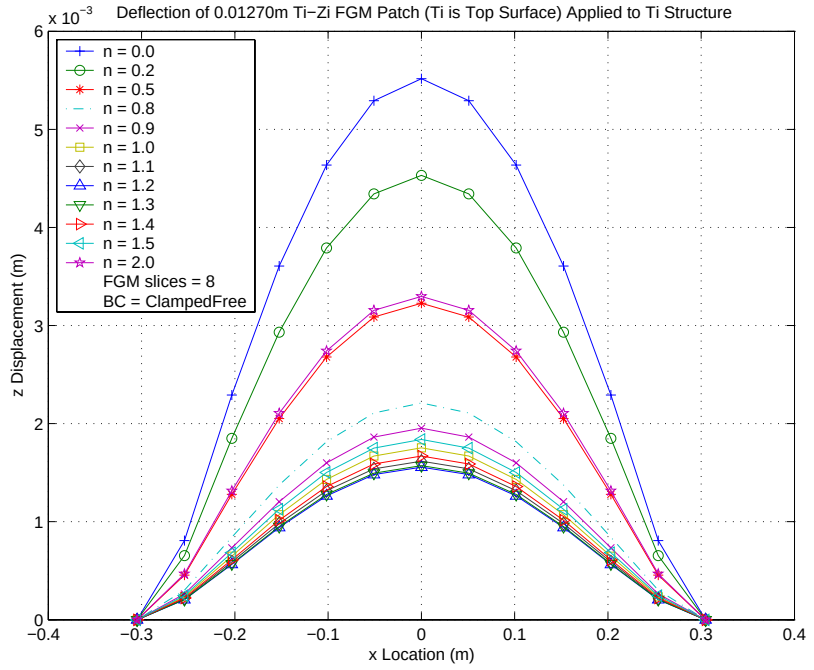

Figure 92. Exhaust Wash Deflection with 0.5" Ti-Zi FGM Patch

For the 0.1”, 0.2”, and 0.5” Ti-Zi patches, the lowest center deflection is found with n=0.0 (Ti), n=0.2, and n=1.2, respectively, and provide a 7%, 87%, and 214% reduction in deflection, respectively; the nodal yield/nodal ultimate count is 160/156, 165/156, and 172/168, respectively. A 0.2” panel with n=0.5 or n=1.0 causes the exhaust wash structure to buckle into an inverted position and is not considered to be effective.

While it may seem a 0.5” Ti-Zi patch with n=1.2 will provide a solution to the exhaust wash problem, additional consideration is required when the stresses are examined. Figure 93 and Figure 94 show the von Mises stress contour of the bottom and top surface of the exhaust wash structure with a 0.5” Ti-Zi patch with n=1.2. The highest von Mises stress is 2,000 MPa and is much higher than the structural F_{tu}=618.9 MPa at 538°C (1000°F) as shown in Table 2.

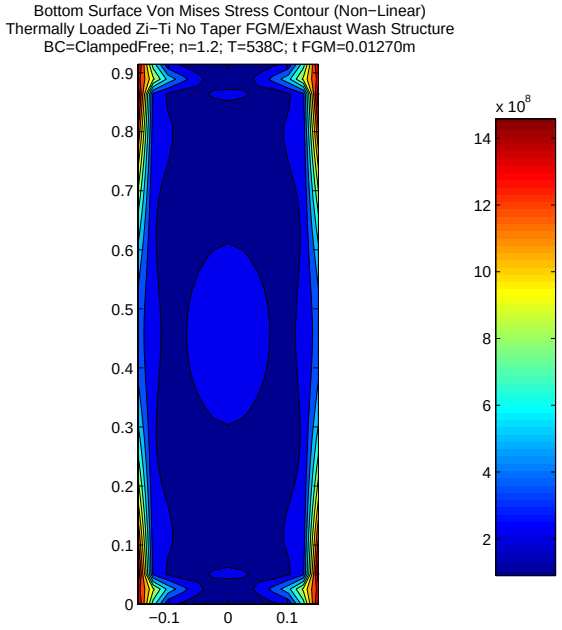

Figure 93. Exhaust Wash Bottom von Mises Stress: 0.5" Ti-Zi patch with n=1.2

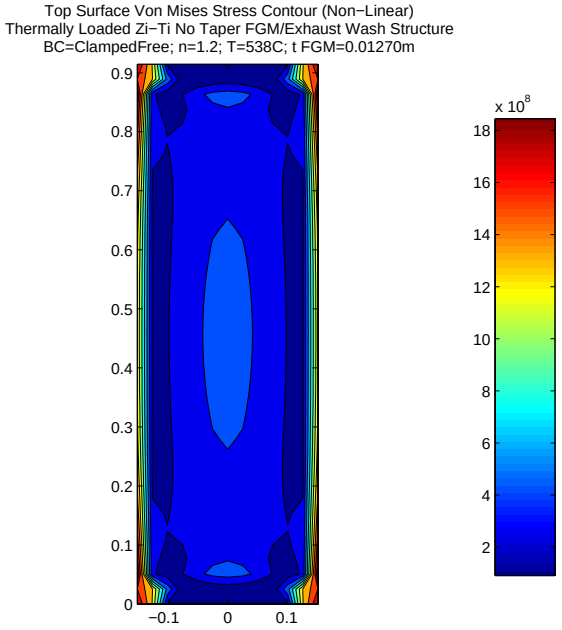

Figure 94. Exhaust Wash Top von Mises Stress: 0.5" Ti-Zi patch with n=1.2

It is noted that the patch shown in Figure 93 successfully reduced center deflection by over 87%, however it raised the exhaust wash panel von Mises stress at the boundary condition by 133% (well beyond compressive yielding). In fact, all Ti-Zi FGM panels studied showed a significant increase in exhaust wash panel von Mises stress (All model output data is listed in Appendix D). The critical areas of the exhaust wash panel are at the intersection of the clamped boundary condition and the free surface (the corners). The free edge is a stress free edge, however the clamped boundary experiences high compression. Therefore, this is the most critical location for stress. Finally, even adding 0.1" Ti patch increased the exhaust wash panel von Mises stress by 25% while decreasing deflection by only 7%.

Raising the "n" value on Ti-Zi patches tends to raise both stresses and displacements in the 0.1" and 0.5" patch. In other words, patches tending toward Ti perform best in the Ti-Zi series of patches. The 0.2" patch doesn't show a strong correlation because several FGMs patches experienced snap through buckling.

In order to evaluate the hypothesis that the highest coefficient of thermal expansion must be on the top surface of the FGM patch in order to cause deflection in the –z direction, Zi-Ti patches are analyzed in thicknesses of 0.1", 0.2", and 0.5". Note: the first material listed corresponds to the top surface (Zi is on the top surface). Figure 95 through Figure 97 show the deflection of the exhaust wash structure with FGM patch.

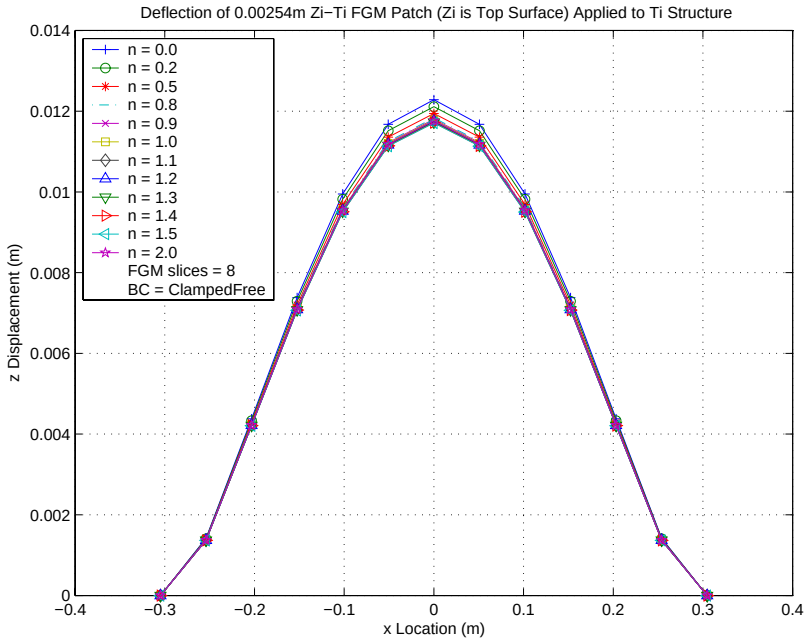

Figure 95. Exhaust Wash Deflection with 0.1" Zi-Ti FGM Patch

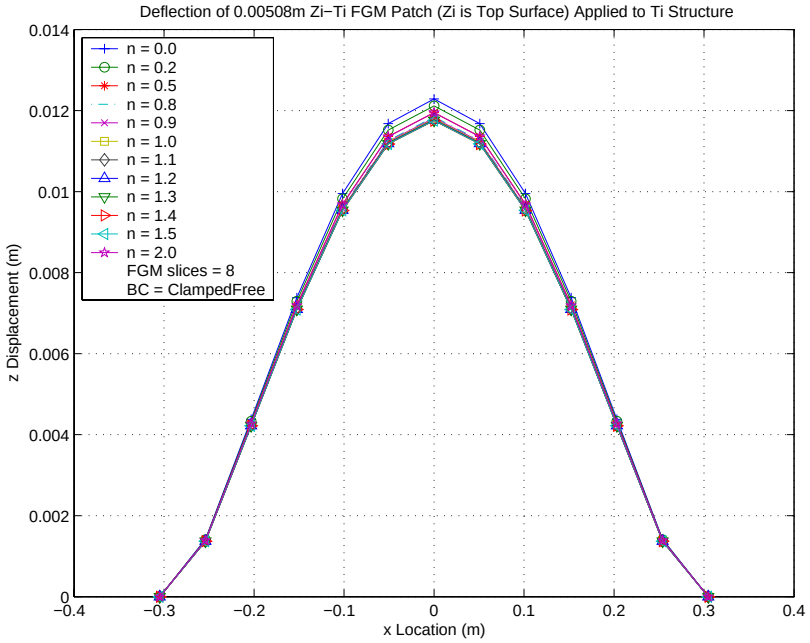

Figure 96. Exhaust Wash Deflection with 0.2" Zi-Ti FGM Patch

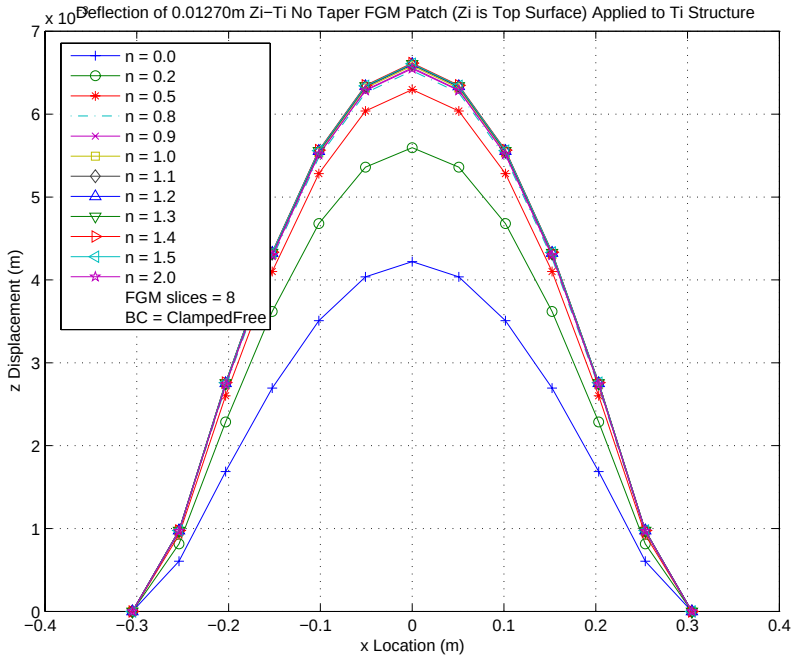

Figure 97. Exhaust Wash Deflection with 0.5" Zi-Ti FGM Patch

For the 0.1”, 0.2”, and 0.5” Zi-Ti patches, it is noted that n=1.5, n=1.4, and n=0.0 (Zi) provide the lowest deflection, respectively, with 3.0%, 2.7%, 186% reductions in center deflection, respectively; exhaust wash panel von Mises stress was increased by 31.8%, 58.3%, and 197%, respectively; the nodal yield/nodal ultimate count is 160/160, 199/165, 172/172. Top and bottom exhaust wash surface von Mises stress are shown for a 0.5” Zi-Ti patch Figure 98 and Figure 99.

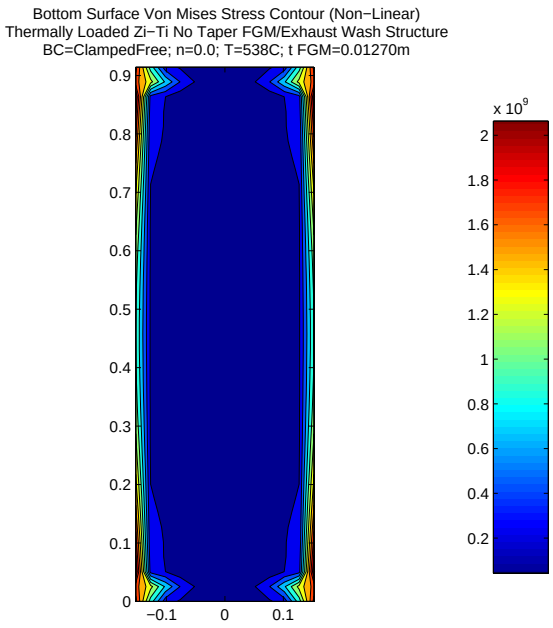

Figure 98. Exhaust Wash Bottom von Mises Stress: 0.5" Zi-Ti Patch with n=0.0

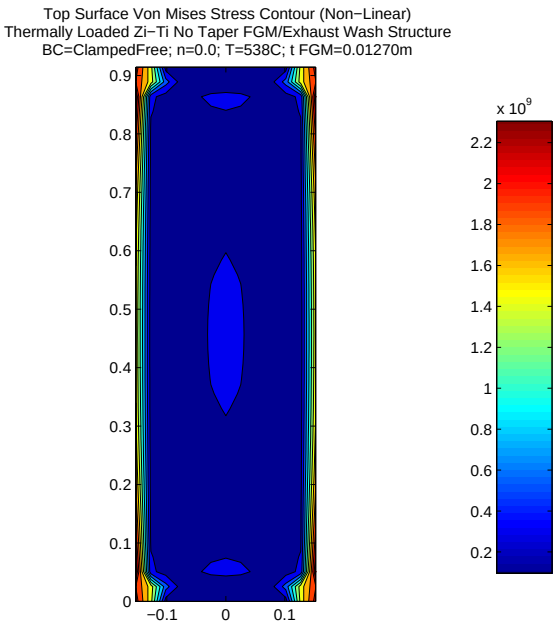

Figure 99. Exhaust Wash Top von Mises Stress: 0.5" Zi-Ti Patch with n=0.0

It is noted that the corners are again the critical location for stresses in both the top and bottom surface of the exhaust wash structure. Also, raising "n" lowered both stresses and deflection in all thickness in the Zi-Ti series of patches. In other words, patches tending toward Ti performed best.

A *Ti*-Zi patch reduces deflection by 3.0%, 2.7%, 186% for patch thicknesses of 0.1", 0.2", and 0.5". Additionally, the nodal yield count is 160/156, 165/156, and 172/168. A *Zi*-Ti patch reduces deflection by 7%, 87%, and 214% for the same patch thicknesses. Additionally, the nodal yield count is 160/160, 199/165, 172/172. It is not conclusive as to which patch is best. The Ti-Zi series patch provides the lowest stresses but also provides a smaller decrease in deflection. However, it is conclusive that patches tending toward Ti perform best.

It is clear that both Ti-Zi and Zi-Ti FGM patches extending 90% of the exhaust wash panel width and length are not effective in reducing stress and center deflection. It is hypothesized that an FGM with Ti having the lowest coefficient of thermal expansion could possibly provide better results. An A-286 / Ti-2-6-4-2 FGM is considered because A-286 provides a high coefficient of thermal expansion and with a very tough material. Material properties of A-286 and Ti-2-6-4-2 are shown in Table 5 at 80°C and 538°C.

Table 5. Material Properties of A-286 and Ti-6-2-4-2 at 80°C and 538°C

	A-286		Ti-6-2-4-2	
	80°C 176°F	538°C 1000°F	80°C 176°F	538°C 1000°F
E	200.6 GPa 29,100 ksi	162.5 GPa 23,571 ksi	113.8 GPa 16,505 ksi	83.1 GPa 12,045 ksi
α	16.2 µm/m-°C 9.0 µin/in-°F	17.6 µm/m·ºC 9.8 µin/in·ºF	7.7 µm/m-°C 4.28 µin/in-°F	8.1µm/m·ºC 4.5 µin/in·ºF
k	12.6 W/m·K 7.3 BTU·ft/hr·ft^2·°F	22.5 W/m·K 13.0 BTU·ft/hr·ft^2·°F	6.9 W/m·K 4.0 BTU·ft/hr·ft^2·°F	13.2 W/m·K 7.7 BTU·ft/hr·ft^2·°F
F_{cy}	655.0 MPa 95 ksi	unknown	1070 MPa 155 ksi	577.8 MPa 83.7 ksi
F_{ty}	655.0 MPa 95 ksi	563.3 MPa 81.7 ksi	860 MPa 125 ksi	482.6 MPa 76.1 ksi
F_{tu}	965.3 MPa 140 ksi	801.2 MPa 116.2 ksi	940 MPa 136 ksi	618.9 MPa 89.8 ksi
ρ	7944 kg/m^3 0.284 lbm/in^3	unknown	4540 Kg/m^3 0.164 lbm/in^3	unknown
ν	0.306	0.328	0.32	unknown

An ABAQUS steady state heat transfer analysis is performed in order to generate a nodal temperature file (the temperature profile is known to be uniform, however, the binary input file is required for a structural analysis). The nodal temperatures are then applied to a second structural analysis to obtain displacements and stresses. Figure 100 through Figure 102 show the center displacement for a 0.1", 0.2", and 0.5" A286/Ti-2-6-4-2 patches

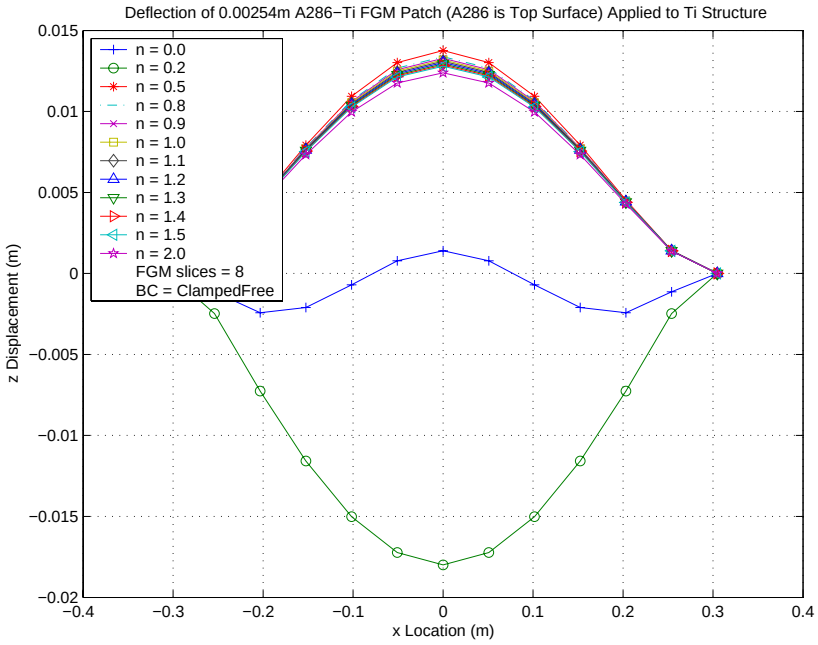

Figure 100. Exhaust Wash Deflection with 0.1" A-286/Ti FGM Patch

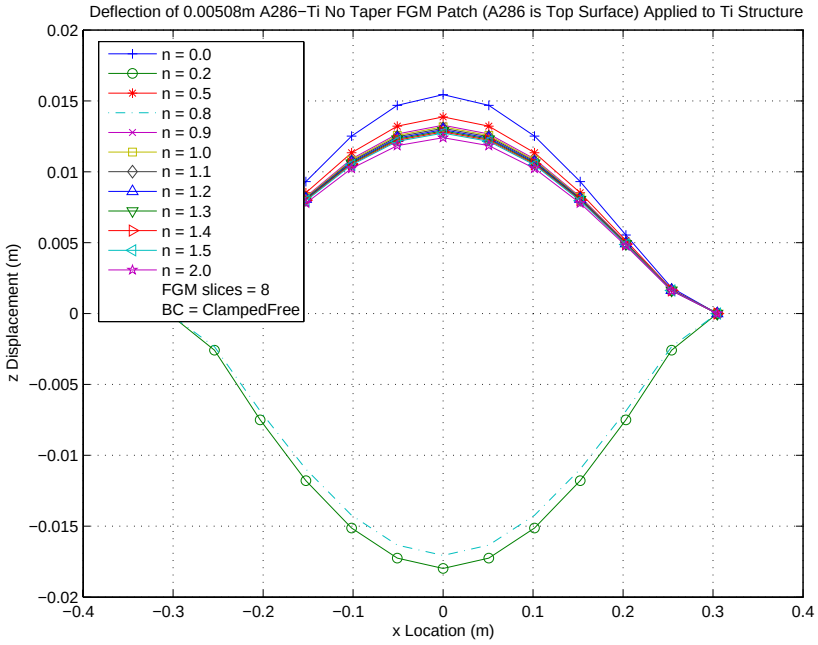

Figure 101. Exhaust Wash Deflection with 0.2" A-286/Ti FGM Patch

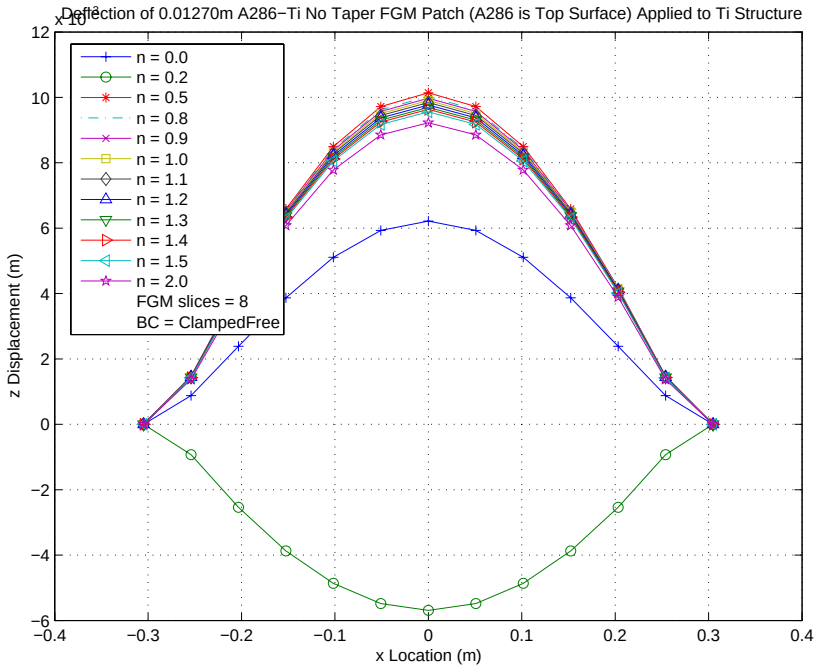

Figure 102. Exhaust Wash Deflection with 0.5" A-286/Ti FGM Patch

For the 0.1”, 0.2”, and 0.5” A286/Ti patches, it is noted that n=0.0 (A286), n=2.0, and n=0.0 (A286) provide the lowest deflection, respectively, with 91.5%, 2.6%, 94.3% reductions in center deflection, respectively; exhaust wash panel von Mises stress was increased by 81.2%, 71.1%, and 383%, respectively; the nodal yield/nodal ultimate count is 373/349, 285/255, and 223/211, respectively. It is noted that a weak correlation of raising “n” to lower stresses and displacements exists. Several of the A286/Ti patches experience snap through buckling so a strong correlation does not exist. However, patches tending toward Ti performed best in general. Top and bottom exhaust wash surface von Mises stress are shown for a 0.5” A286-Ti with patch n=0.0 (A286) in Figure 103 and Figure 104.

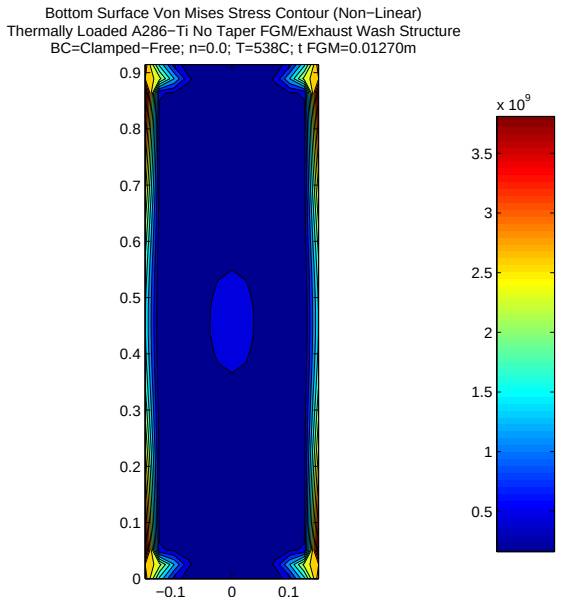

Figure 103. Exhaust Wash Bottom von Mises Stress: 0.5" A286-Ti Patch with n=0.0

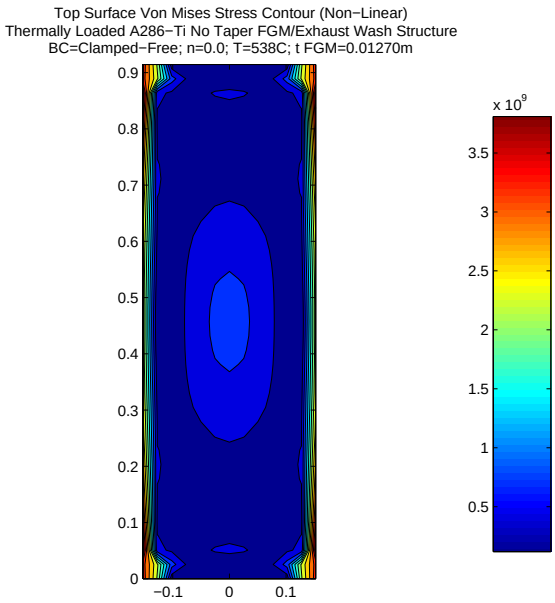

Figure 104. Exhaust Wash Top von Mises Stress: 0.5" A286-Ti Patch with n=0.0

It was previously show that the material with the highest coefficient of thermal expansion had to be examined on both the top and the bottom surface because of mixed results. Therefore, Ti/A286 are now examined in 0.1", 0.2", and 0.5" thicknesses. Center displacements are shown in Figure 105 through Figure 107.

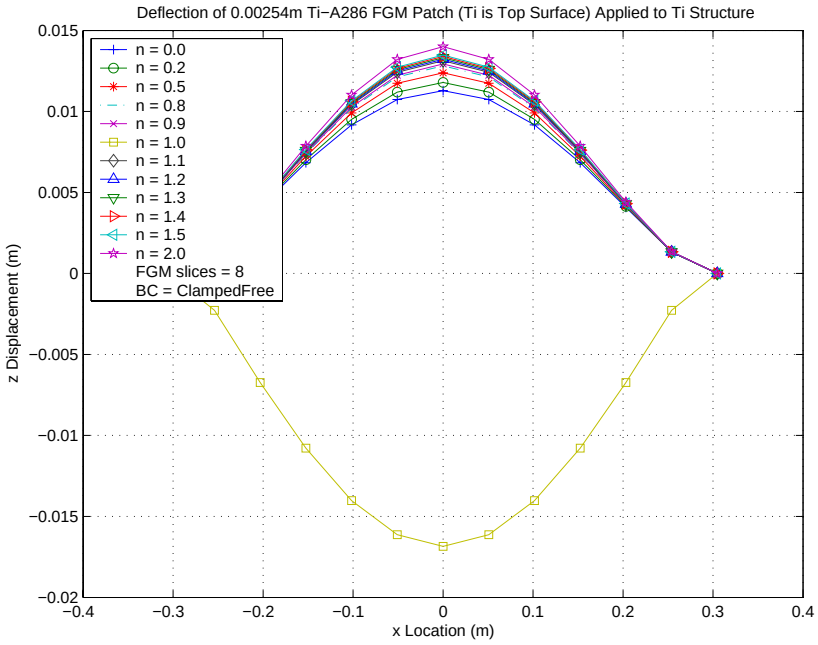

Figure 105. Exhaust Wash Deflection with 0.1" Ti-A286 FGM Patch

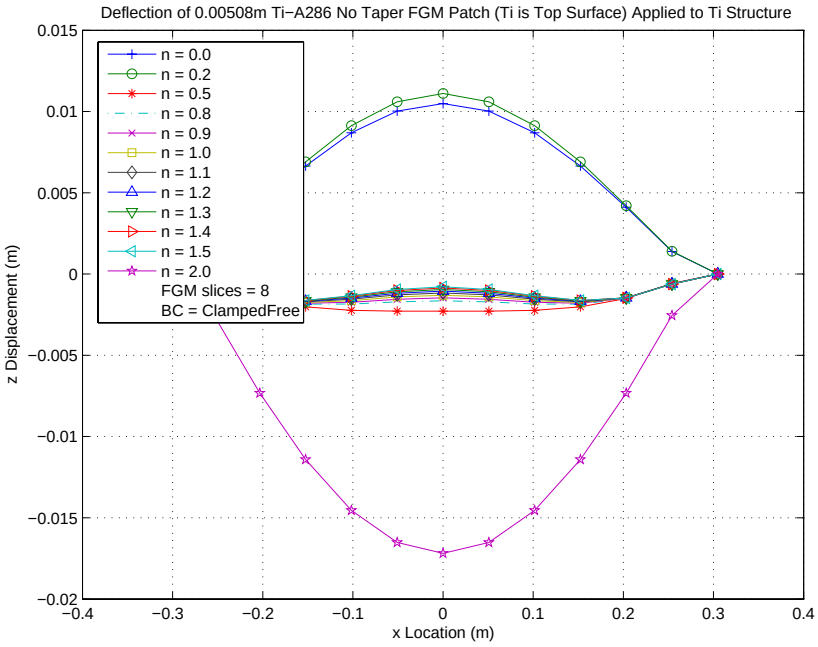

Figure 106. Exhaust Wash Deflection with 0.2" Ti-A286 FGM Patch

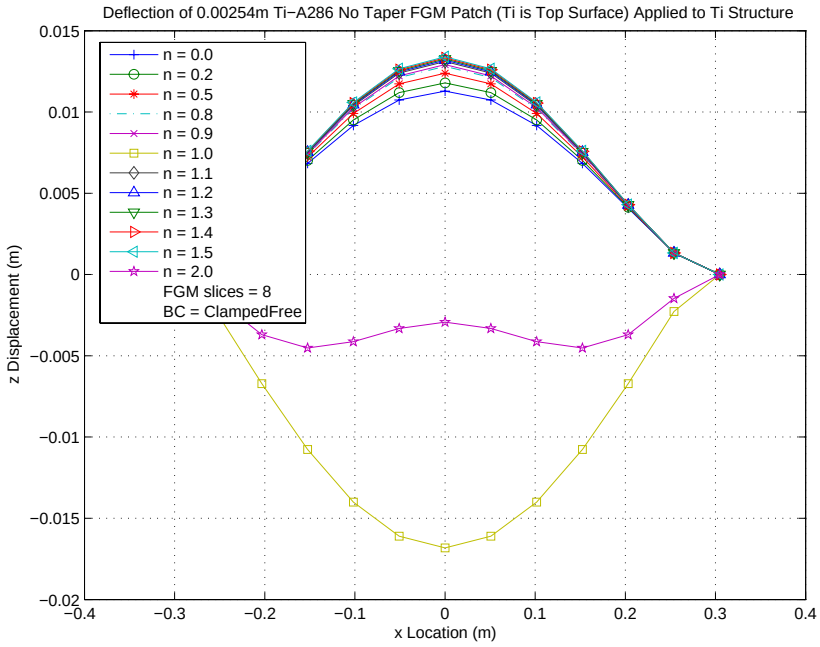

Figure 107. Exhaust Wash Deflection with 0.5" Ti-A286 FGM Patch

For the 0.1”, 0.2”, and 0.5” Ti /A286 patches, it is noted that n=0.0 (Ti), n=0.5, and n=2.0 provide the least deflection, respectively, with 6.6%, -118.9%, and -208% reductions in center deflection, respectively; exhaust wash panel von Mises stress was increased by 24.7%, 131%, and 283%, respectively; the nodal yield/nodal ultimate count is 160/156, 231/192, and 393/385. Also, 0.2” Ti/A286 patches provided near zero displacement. A moderate correlation between lowering “n” to lower stress and displacement exits. In other words, patches tending to Ti perform best. Top and bottom exhaust wash surface von Mises stresses are shown for a 0.5” Ti/A286 patch with n=2.0 in Figure 108 and Figure 109.

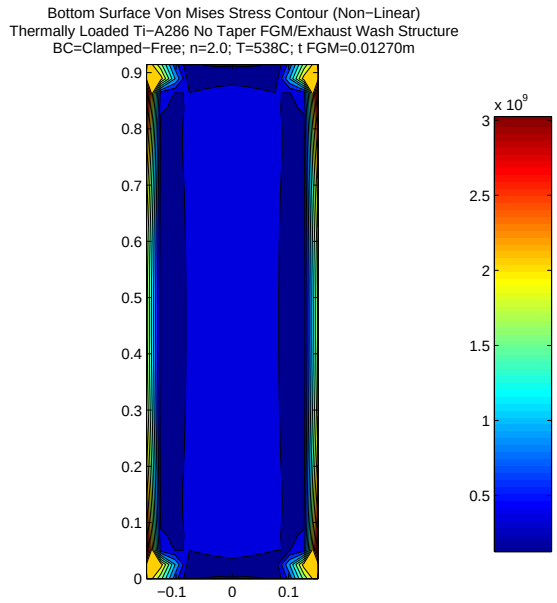

Figure 108. Exhaust Wash Bottom von Mises Stress: 0.5" Ti-A286 Patch with n=2.0

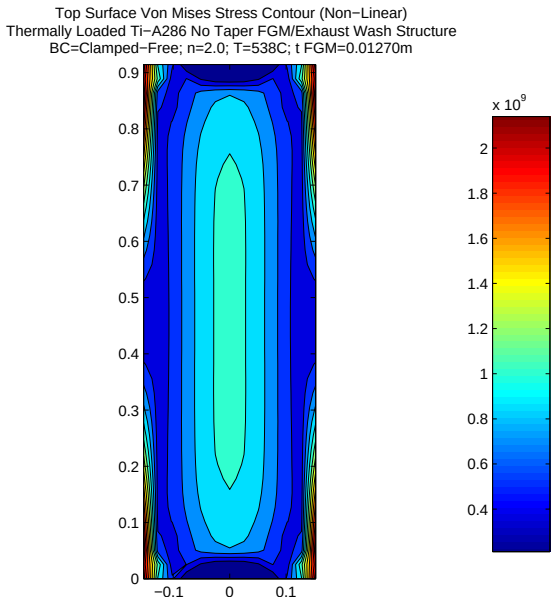

Figure 109. Exhaust Wash Top von Mises Stress: 0.5" Ti-A286 Patch with n=2.0

Of all patch configurations considered in this section, patches tending to Ti perform best. A 0.5” Ti-Zi patch with n=1.2 patch provides the lowest *deflection* (214% reduction in deflection) while a 0.5” Ti patch provides the lowest change in *stress* (86.5% / 235% increase in nodes above yield / ultimate stress). The 0.5” Ti patch actually increased the stress in the top and bottom surface of the exhaust wash panel, as shown in Figure 110 and Figure 111.

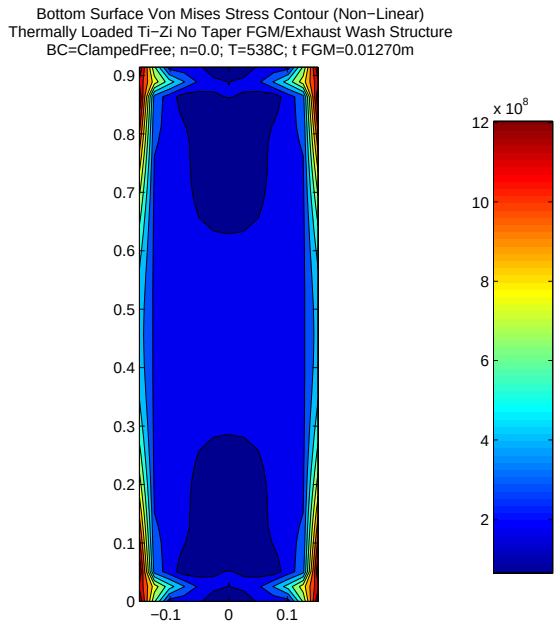

Figure 110. Exhaust Wash Bottom von Mises Stress with 0.5" Ti Patch

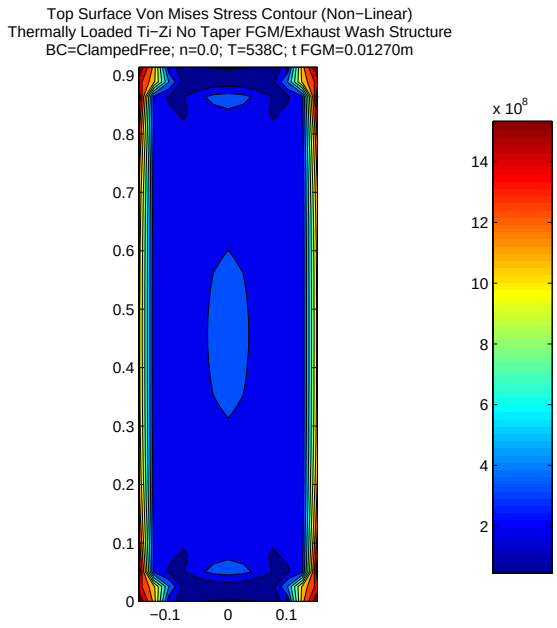

Figure 111. Exhaust Wash Top von Mises Stress with 0.5" Ti Patch

It is clear that all attempts to reduce center deflection using a 90% width and 90% length patch will fail. The patch must be redesigned to allow for better stress flow and reduce the stress concentration found between the transition of the patch to the exhaust wash structure as shown in Figure 89. This transition is required because the FGM patch can not extend the full length and width of the exhaust wash panel due to installation requirements. However, the patch could be tapered to allow for a gradual transition of stress in the FGM to the exhaust wash structure. Figure 112 shows the tapered patch as it would be fabricated and the equivalent rectangular patch as modeled.

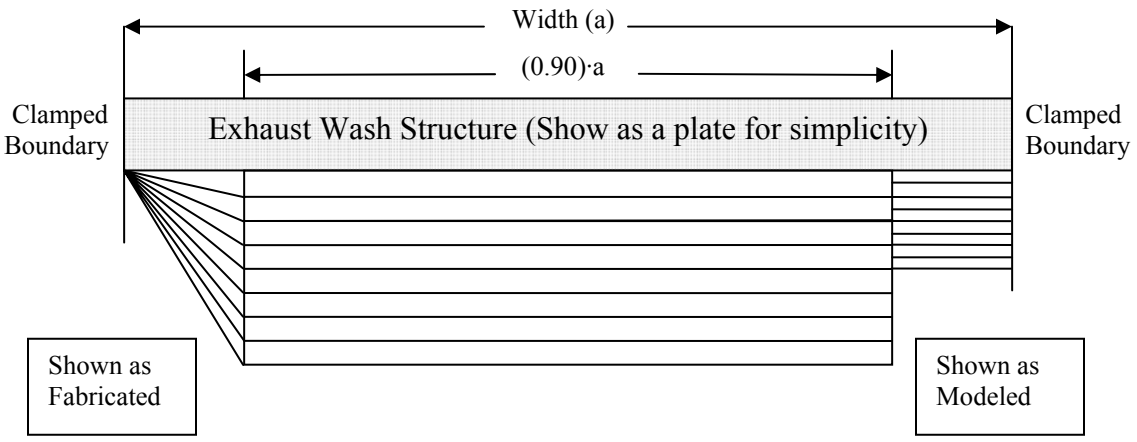

Figure 112. Diagram of Tapered FGM Patch Attached to Exhaust Wash Structure

In order to simplify modeling a tapered triangular section, the taper is modeled as a rectangular section equal to half the FGM thickness. Inherent problems with this technique include stress concentrations at the FGM / taper sections and the patch being included in the rigid boundary condition. However, it is important to explore the effect of tapering the edges and it is assumed that these limitations will have a minimal impact on model accuracy.

Tapered sections will be studied for a patch that extends 90% of the length and 100% of the width (including the taper), and for a patch that extends 100% of the length (including the taper) and 100% of the width (including the taper). They are named partial taper and full taper, respectively.

Once again, Ti & Zi and A286 & Ti patches in 0.1", 0.2", and 0.5" are analyzed beginning with a Ti-Zi series partial taper patch shown in Figure 113 through Figure 115.

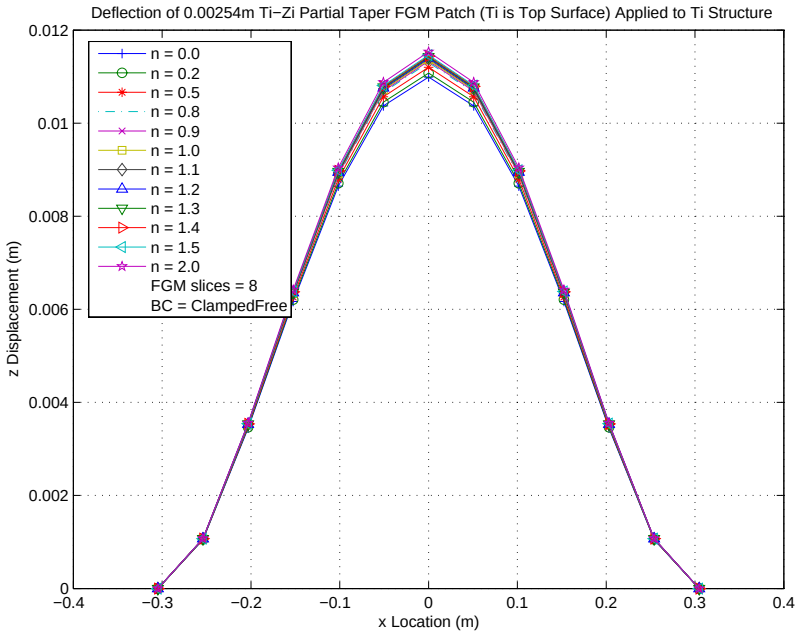

Figure 113. Exhaust Wash Deflection with 0.1” Ti-Zi FGM Partial Taper Patch

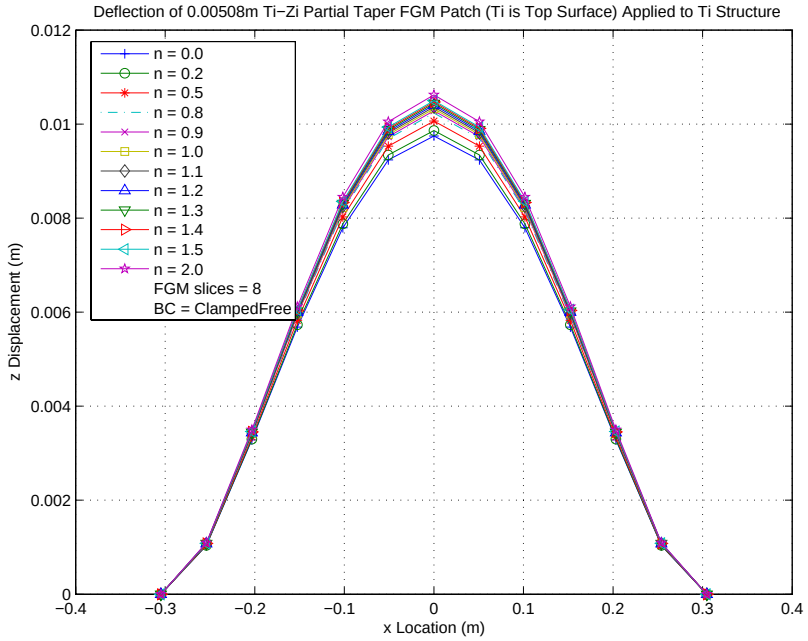

Figure 114. Exhaust Wash Deflection with 0.2" Ti-Zi FGM Partial Taper Patch

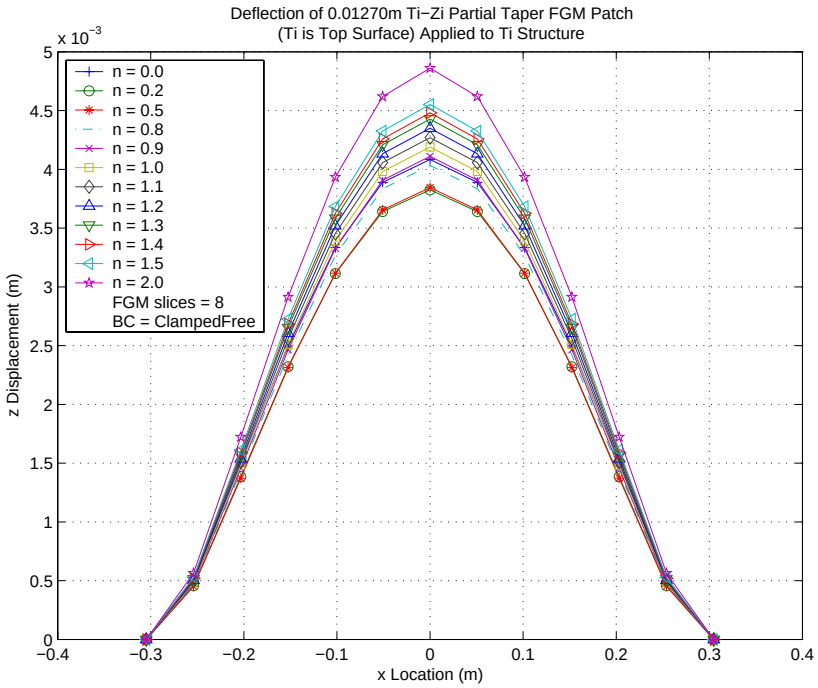

Figure 115. Exhaust Wash Deflection with 0.5" Ti-Zi FGM Partial Taper Patch

For the 0.1”, 0.2”, and 0.5” Ti-Zi partial taper patches, the lowest center deflection is found with n=0.0 (Ti), n=0.0, and n=0.2, respectively, and provide a 9%, 19.3%, and 68.3% reduction in deflection, respectively; the von Mises stress in the exhaust wash panel is increased by 20.1%, 39.2%, and 84.7%, respectively; the nodal yield/nodal ultimate count is 94/94, 102/94, and 172/164, respectively. Figure 116 and Figure 117 show the von Mises stress contour of the bottom and top surface of the exhaust wash structure with a 0.5” Ti-Zi partial taper patch with n=0.2.

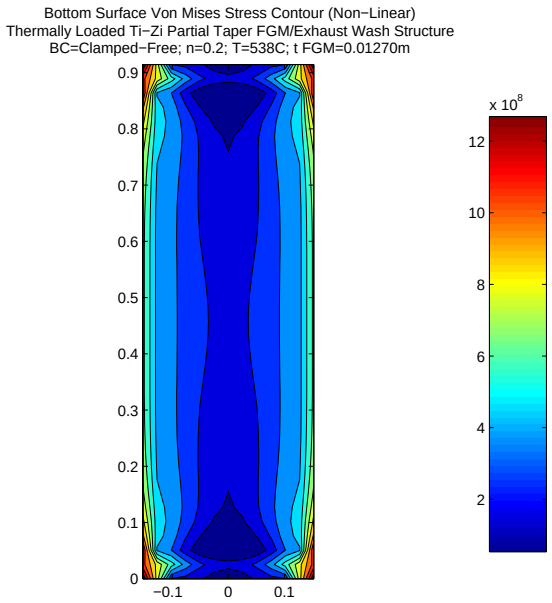

Figure 116. Exhaust Wash Bottom von Mises Stress: 0.5" Ti-Zi Partial Taper Patch with n=0.2

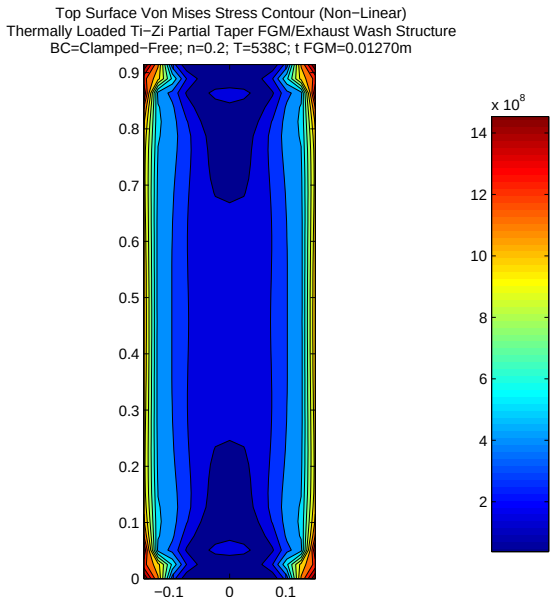

Figure 117. Exhaust Wash Top von Mises Stress: 0.5" Ti-Zi Partial Taper Patch with n=0.2

The critical areas of the exhaust wash panel are at the intersection of the clamped boundary condition and the free surface (the corners). The free edge is a stress free edge; however the clamped boundary experiences high compression. Therefore, this is the most critical location for stress.

Raising the "n" value on Ti-Zi partial taper patches tends to raise stresses in all thicknesses studied and raises displacements in the 0.1" and 0.2" patches. A 0.5" partial taper patch does not have a strong correlation between displacement and "n", however, values of n<1 provided the lowest displacements. In other words, patches tending toward Ti perform best in the Ti-Zi series of partial taper patches.

Zi-Ti partial taper patches are analyzed next in thicknesses of 0.1", 0.2", and 0.5". Figure 118 through Figure 120 show the deflection of the exhaust wash structure with Zi-Ti FGM partial taper patch.

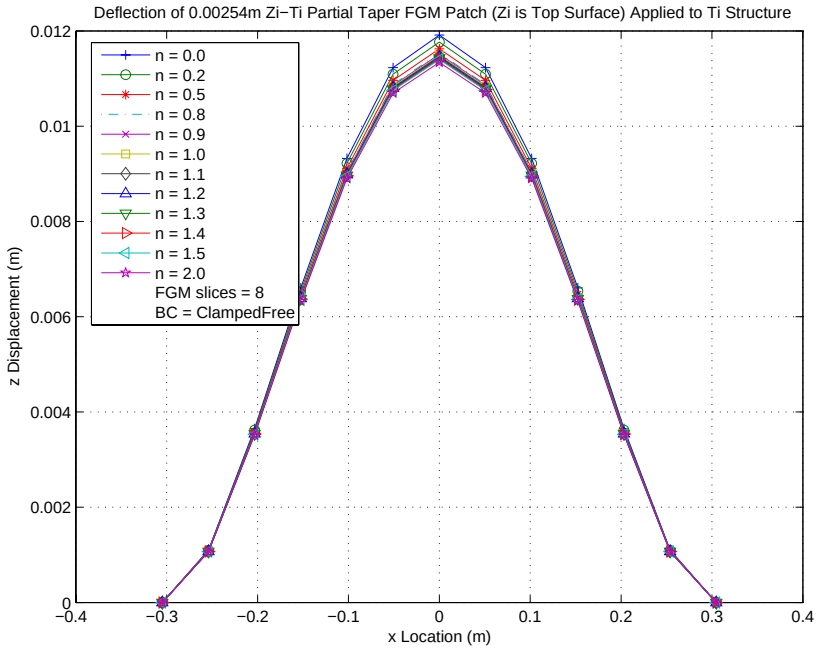

Figure 118. Exhaust Wash Deflection with 0.1" Zi-Ti FGM Partial Taper Patch

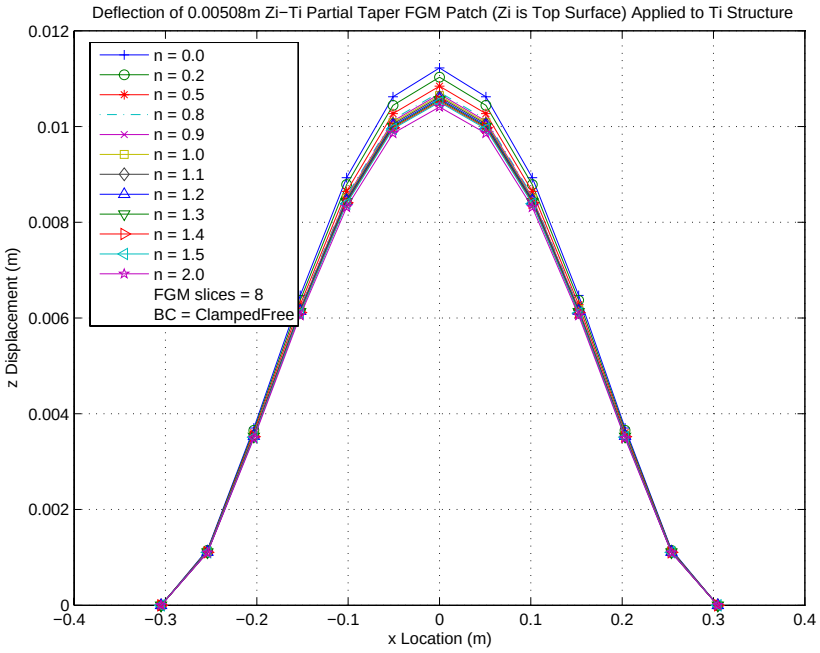

Figure 119. Exhaust Wash Deflection with 0.2" Zi-Ti FGM Partial Taper Patch

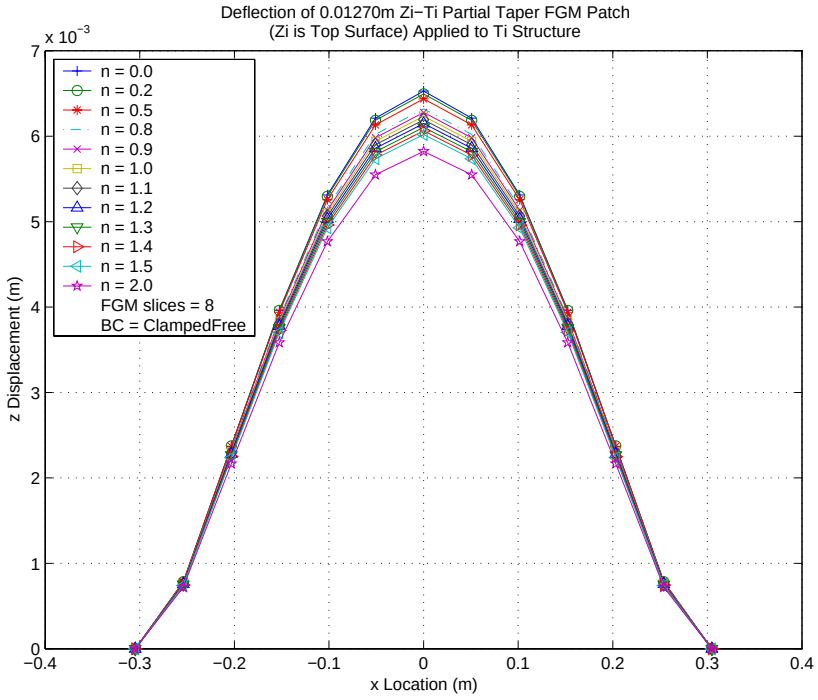

Figure 120. Exhaust Wash Deflection with 0.5" Zi-Ti FGM Partial Taper Patch

For the 0.1”, 0.2”, and 0.5” Zi-Ti partial taper patches, it is noted that n=2.0, n=2.0, and n=0.0 (Zi) provide the lowest deflection, respectively, with 6.1%, 13.9%, 51.8% reductions in center deflection, respectively; exhaust wash panel von Mises stress was increased by 24.7%, 44.1%, and 93.9%, respectively; the nodal yield/nodal ultimate count is 113/94, 141/113, 168/168. Top and bottom exhaust wash surface von Mises stresses are shown for a 0.5” Zi-Ti partial taper patch with n=0.0 in Figure 121 and Figure 122.

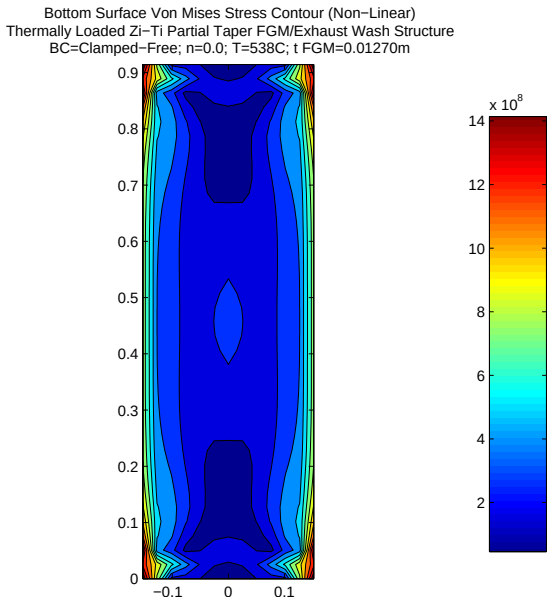

Figure 121. Exhaust Wash Bottom von Mises Stress: 0.5" Zi-Ti Partial Taper Patch with n=0.0

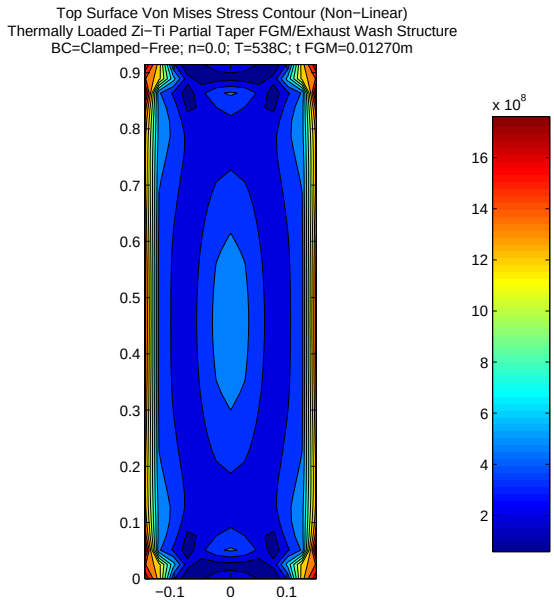

Figure 122. Exhaust Wash Top von Mises Stress: 0.5" Zi-Ti Partial Taper Patch with n=0.0

It is noted that the corners and edges are again the critical location for stresses in both the top and bottom surface of the exhaust wash structure. Also, raising "n" lowered both stresses and deflection in all thickness in the Zi-Ti series of partial taper patches. In other words, patches tending toward Ti performed best.

Next, A-286/Ti partial taper patches are examined. Figure 123 through Figure 125 show the center displacement for 0.1", 0.2", and 0.5" A286/Ti-2-6-4-2 partial taper patches.

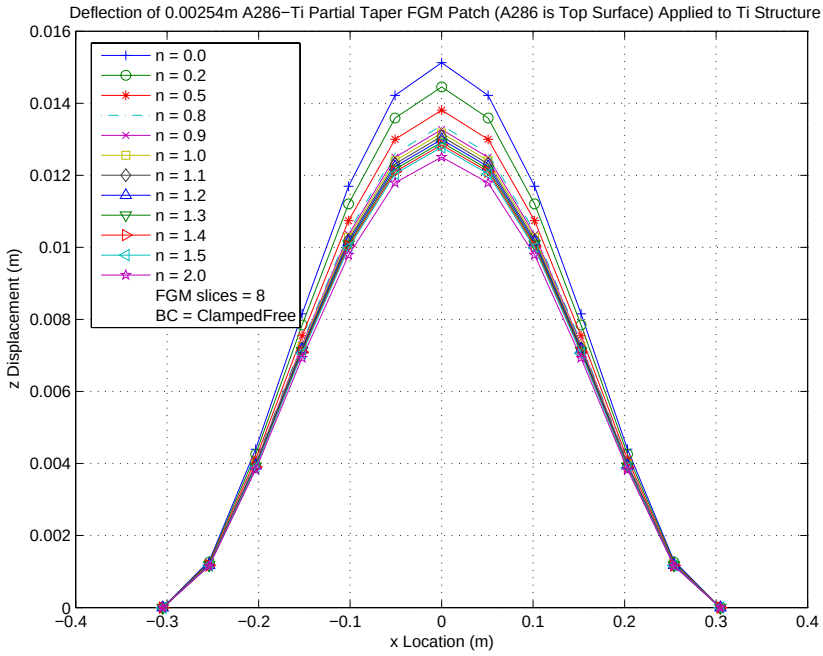

Figure 123. Exhaust Wash Deflection with 0.1" A-286/Ti FGM Partial Taper Patch

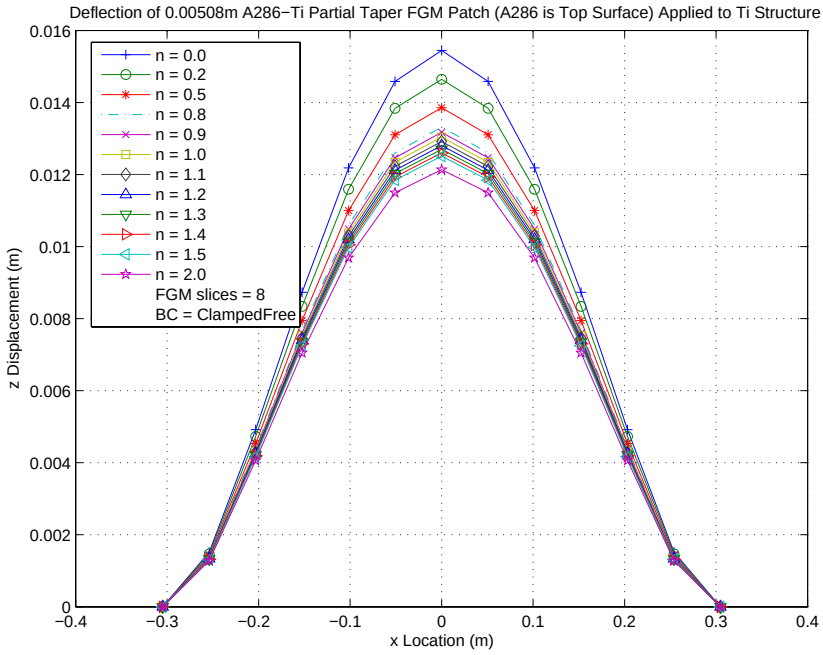

Figure 124. Exhaust Wash Deflection with 0.2" A-286/Ti FGM Partial Taper Patch

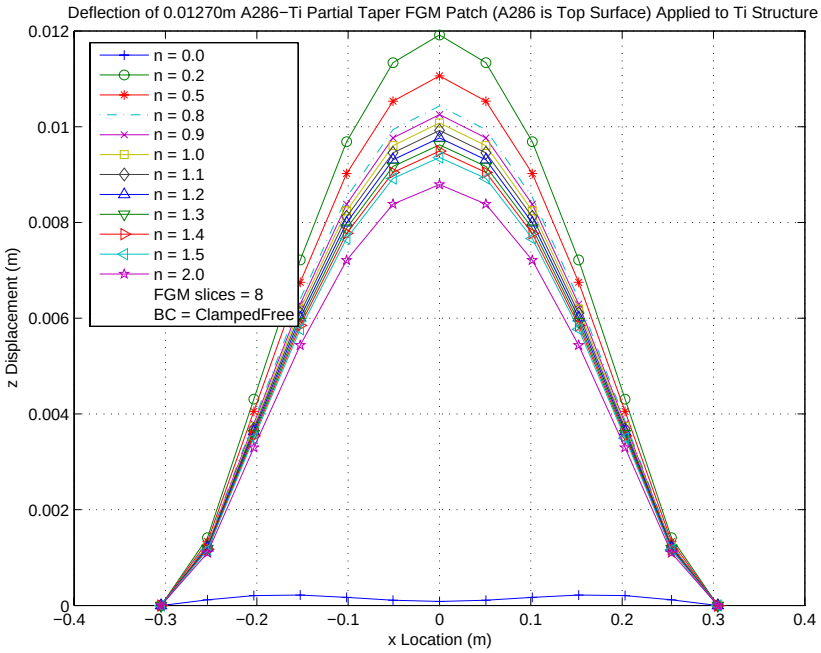

Figure 125. Exhaust Wash Deflection with 0.5" A-286/Ti FGM Partial Taper Patch

For the 0.1”, 0.2”, and 0.5” A286/Ti partial taper patches, it is noted that n=2.0, n=2.0, and n=0.0 (A286) provide the lowest deflection, respectively, with a 3.5% increase, 0.4% increase, and 99.3% decrease in center deflection, respectively; exhaust wash panel von Mises stress was increased by 36%, 57.1%, and 165.6%, respectively; the nodal yield/nodal ultimate count is 209/167, 235/189, and 627/583, respectively.

It is noted that a strong correlation of raising “n” to lower stresses and displacements exists with the exception when n=0.0 in the 0.5” patch. In general, partial taper patches tending toward Ti performed best. At 0.5”, a partial taper patch with n=0.0 provides near zero deflection of the structure. Top and bottom exhaust wash surface von Mises stress are shown for a 0.5” A286-Ti partial taper patch with n=0.0 in Figure 126 and Figure 127.

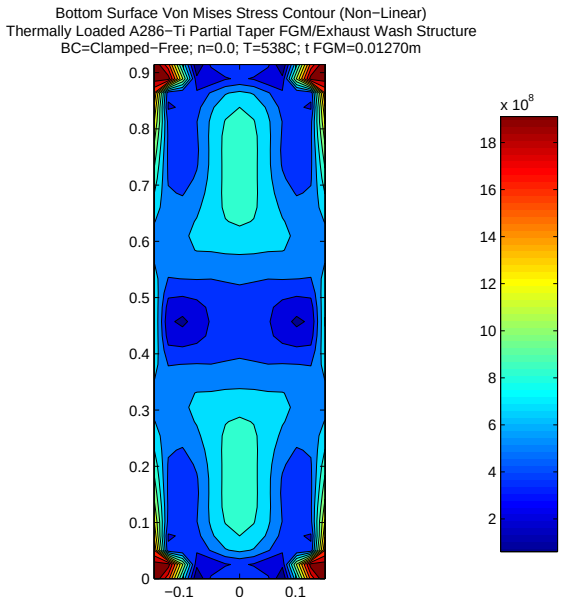

Figure 126. Exhaust Wash Bottom von Mises Stress: 0.5" A286-Ti Partial Taper Patch with n=0.0

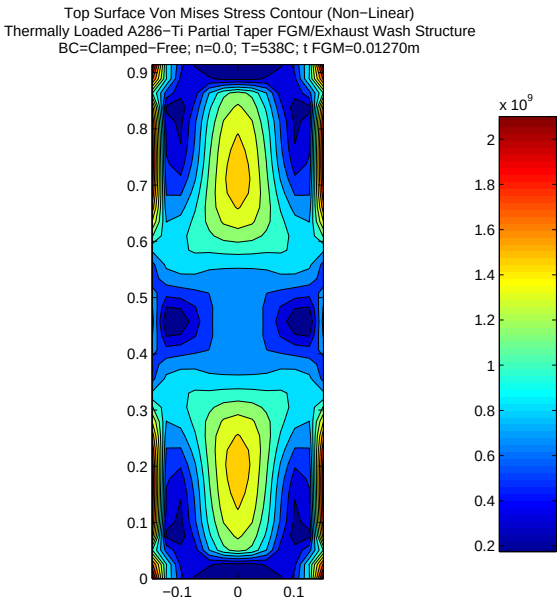

Figure 127. Exhaust Wash Top von Mises Stress: 0.5" A286-Ti Partial Taper Patch with n=0.0

In order to fully evaluate a FGM patch, both material orientations must be explored. Therefore, Ti/A286 partial taper patches are evaluated in 0.1", 0.2", and 0.5" thicknesses. Center displacements are listed in Figure 128 through Figure 130.

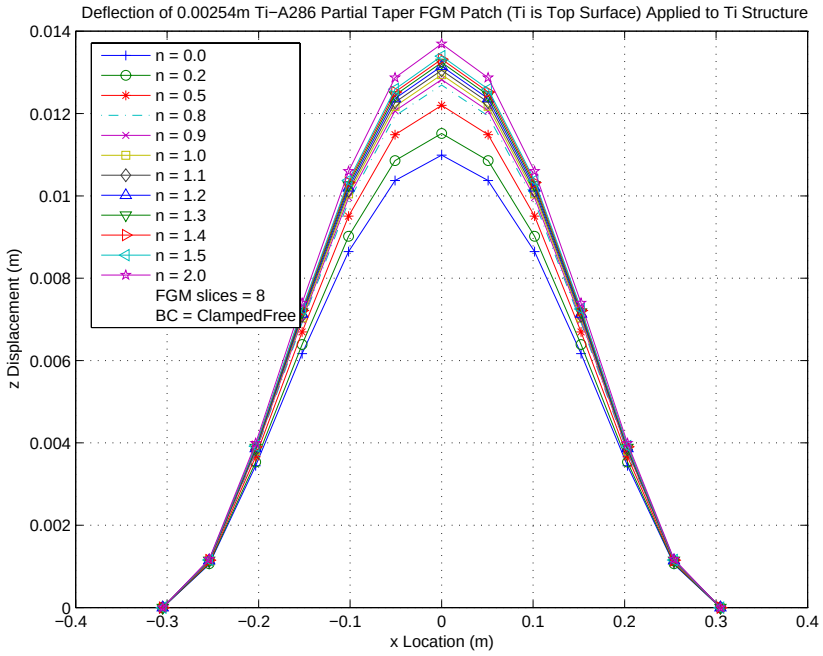

Figure 128. Exhaust Wash Deflection with 0.1" Ti-A286 FGM Partial Taper Patch

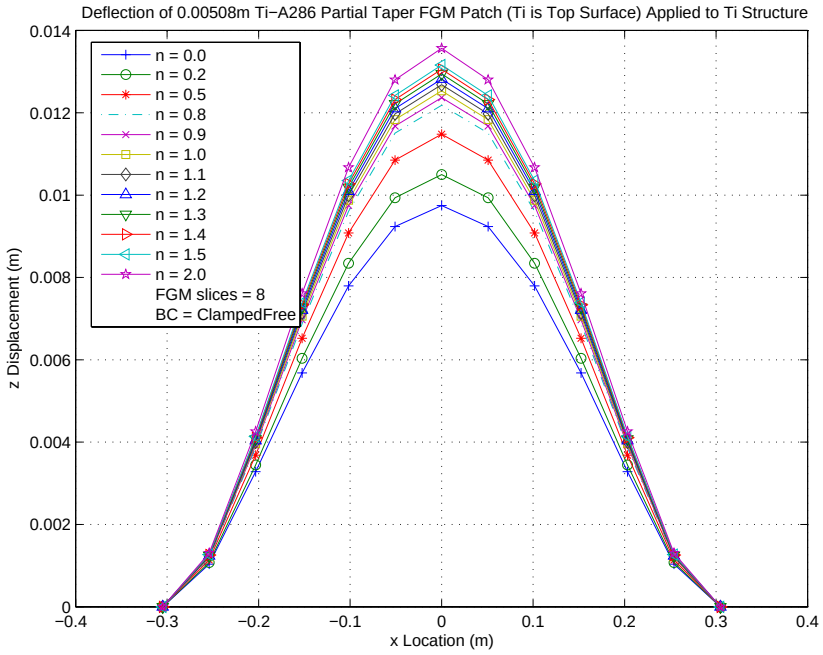

Figure 129. Exhaust Wash Deflection with 0.2" Ti-A286 FGM Partial Taper Patch

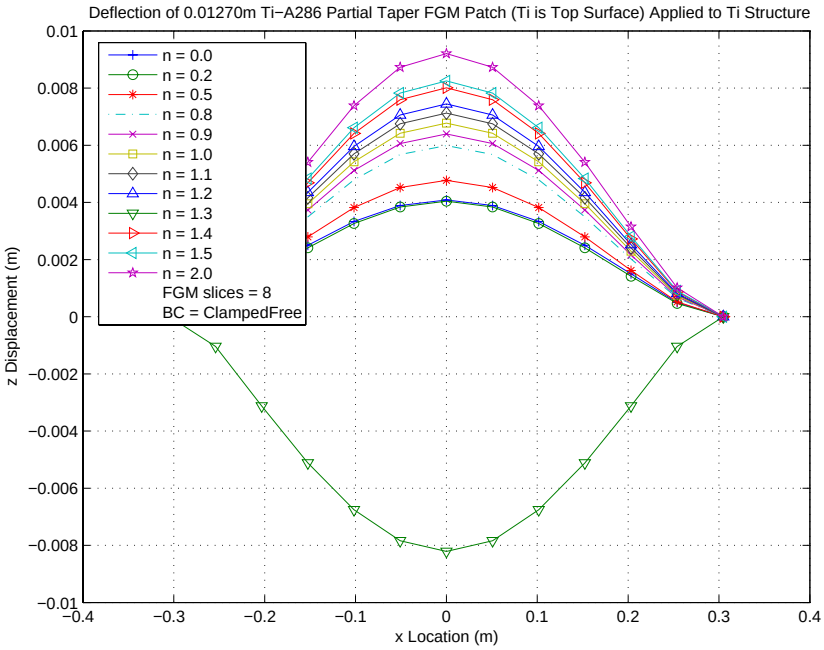

Figure 130. Exhaust Wash Deflection with 0.5" Ti-A286 FGM Partial Taper Patch

For the 0.1”, 0.2”, and 0.5” Ti /A286 partial taper patches, it is noted that n=0.0 (Ti), n=0.0, and n=0.2 provide the least deflection, respectively, with 9.0%, 19.3%, and 66.6% reductions in center deflection, respectively; exhaust wash panel von Mises stress was increased by 20.1%, 98.1%, and 102.9%, respectively; the nodal yield/nodal ultimate count is 94/94, 102/94, and 172/168.

A strong correlation between lowering “n” to lower *stress* exists in all Ti-A286 partial taper patches. 0.1” and 0.2” patches exhibit a strong correlation between lowering “n” to lower *deflection*, however 0.5” has no correlation as some patches have experienced snap through buckling. In other words, patches tending to Ti perform best. Top and bottom exhaust wash surface von Mises stresses are shown for a 0.5” Ti/A286 partial taper patch with n=0.2 in Figure 131 and Figure 132.

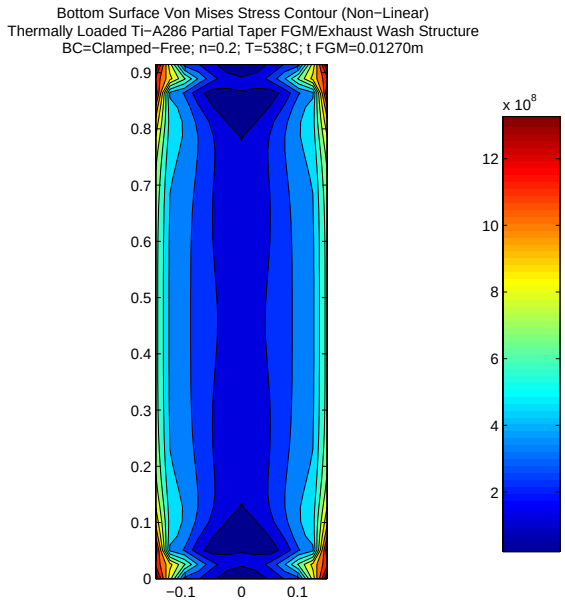

Figure 131. Exhaust Wash Bottom von Mises Stress: 0.5" Ti-A286-Ti Partial Taper Patch with n=0.2

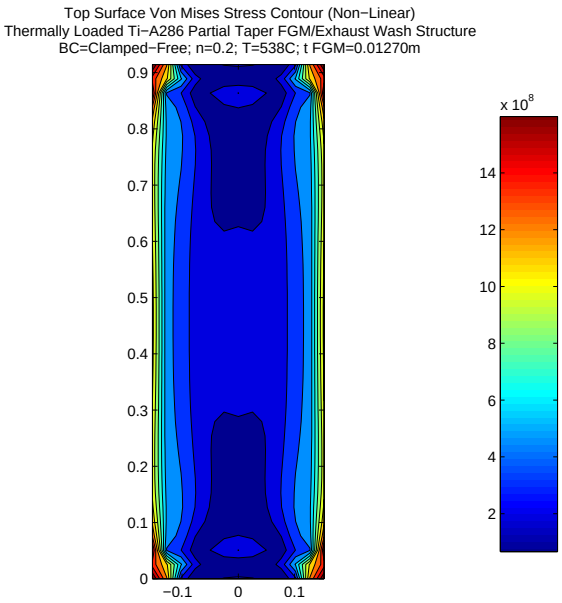

Figure 132. Exhaust Wash Top von Mises Stress: 0.5" Ti-A286-Ti Partial Taper Patch with n=0.2

Of all patch configurations considered, patches tending to Ti perform best. Additionally, a 0.5” A286 partial taper patch provided the lowest *displacement* (99.3% reduction in deflection). A 0.1” Ti partial taper patch provides the lowest change in *stress* with a nodal yield and nodal ultimate count (94/94, or a 27.0% / 135% increase). Contour plots for the von Mises stress in the top and bottom surface of the exhaust wash structure with a 0.1” Ti partial taper patch are shown in Figure 133 and Figure 134.

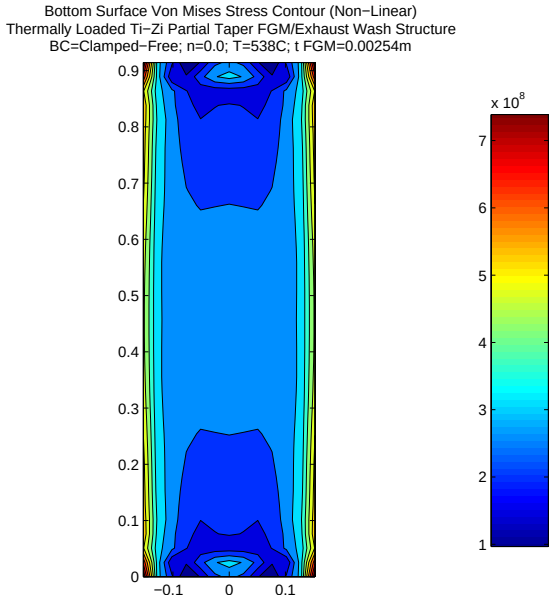

Figure 133. Exhaust Wash Bottom von Mises Stress with 0.1" Ti Partial Taper Patch

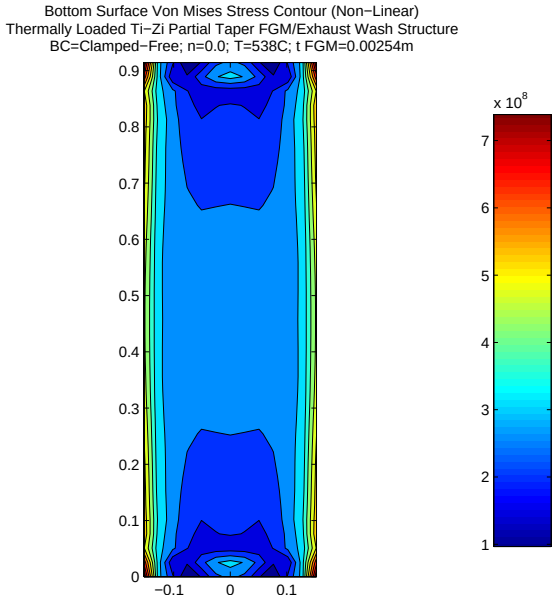

Figure 134. Exhaust Wash Top von Mises Stress with 0.1" Ti Partial Taper Patch

It is clear that all attempts to reduce center deflection using a 100% width and 90% length patch will fail because stress is increased rather than decreased. Next, 100% width and 100% length full taper patches are examined. Once again, Ti & Zi and A286 & Ti patches in 0.1", 0.2", and 0.5" are analyzed beginning with a Ti-Zi series full taper patch shown in Figure 135 through Figure 137.

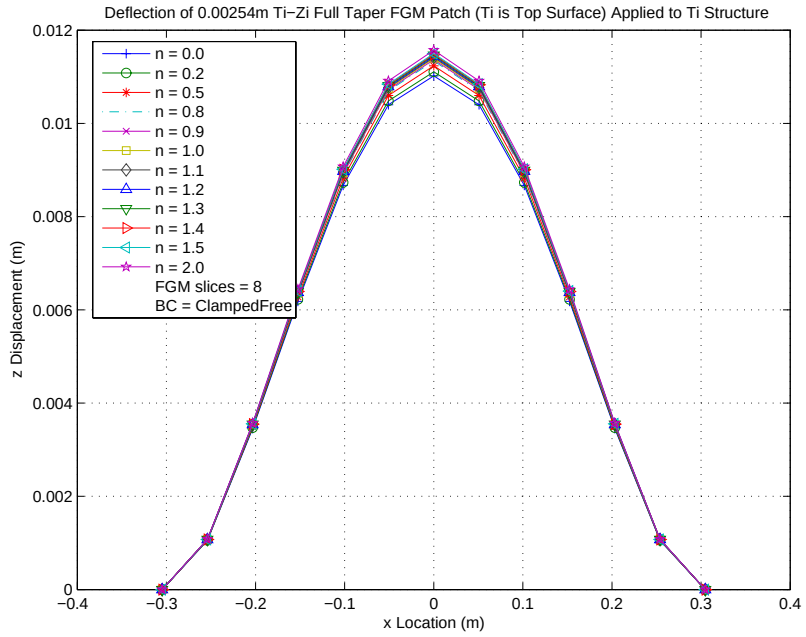

Figure 135. Exhaust Wash Deflection with 0.1” Ti-Zi FGM Full Taper Patch

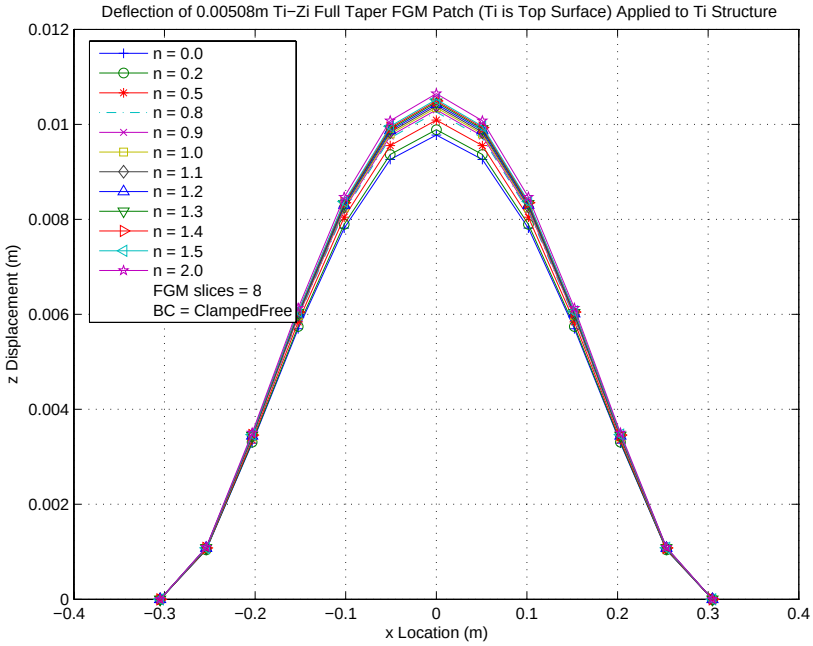

Figure 136. Exhaust Wash Deflection with 0.2" Ti-Zi FGM Full Taper Patch

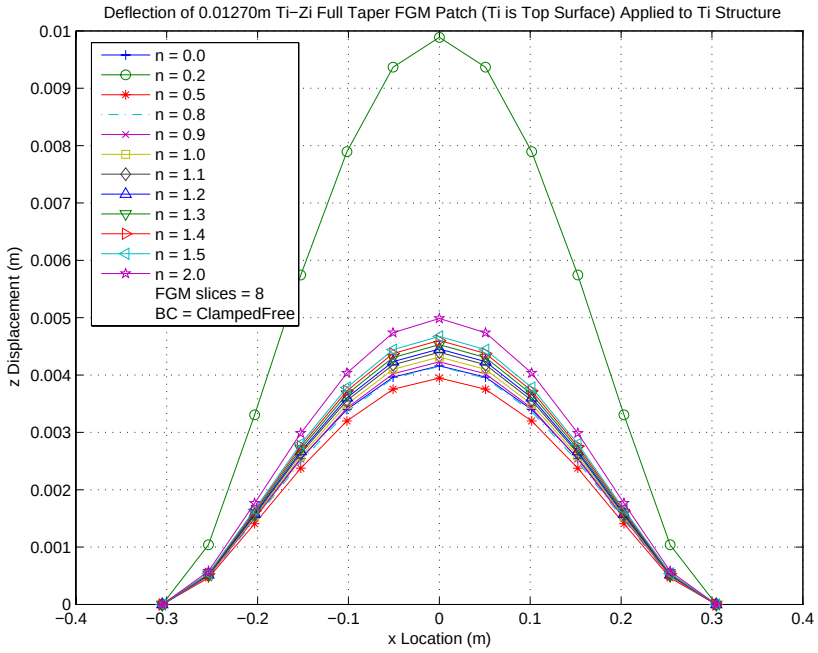

Figure 137. Exhaust Wash Deflection with 0.5" Ti-Zi FGM Full Taper Patch

For the 0.1”, 0.2”, and 0.5” Ti-Zi full taper patches, the lowest center deflection is found with n=0.0 (Ti), n=0.0, and n=0.5, respectively, and provide a 8.8%, 19.1%, and 67.3% reduction in deflection, respectively; the von Mises stress in the exhaust wash panel is *decreased* by 4.7%, not changed, and *increased* by 114%, respectively; the nodal yield/nodal ultimate count is 152/152, 152/152, and 214/204, respectively. Figure 138 and Figure 139 show the von Mises stress contour of the bottom and top surface of the exhaust wash structure with a 0.5” Ti-Zi full taper patch with n=0.5.

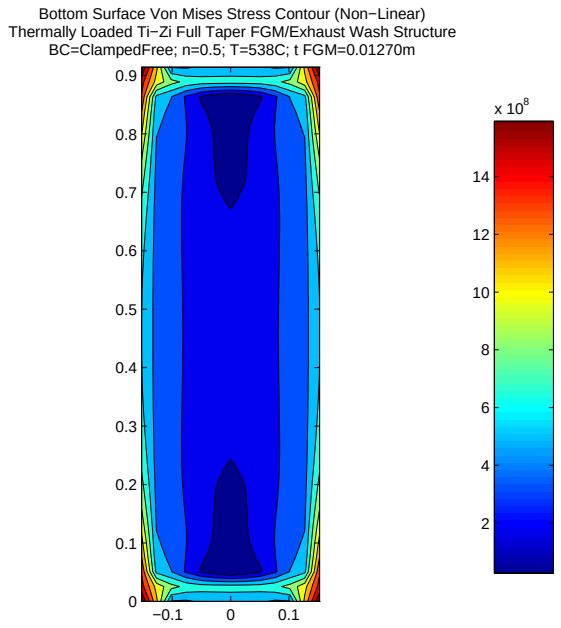

Figure 138. Exhaust Wash Bottom von Mises Stress: 0.5" Ti-Zi Full Taper Patch with n=0.5

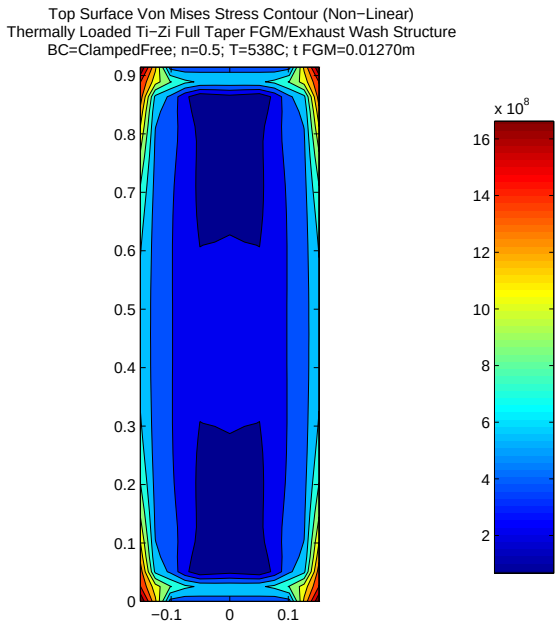

Figure 139. Exhaust Wash Top von Mises Stress: 0.5" Ti-Zi Full Taper Patch with n=0.5

As with all other patches considered, the critical areas of the exhaust wash panel are at the intersection of the clamped boundary condition and the free surface (the corners). Raising the "n" value on Ti-Zi full taper patches tends to raise stresses and displacement in 0.1" and 0.2" full taper patch. A 0.5" full taper patch does not have a strong correlation between displacement, stress, and "n", however, values of n<1 provided the lowest displacements and stresses. In other words, patches tending toward Ti perform best in the Ti-Zi series of full taper patches.

Flipping the material orientation, Zi-Ti full taper patches are analyzed next in thicknesses of 0.1", 0.2", and 0.5". Figure 140 through Figure 142 show the deflection of the exhaust wash structure with Zi-Ti FGM full taper patch.

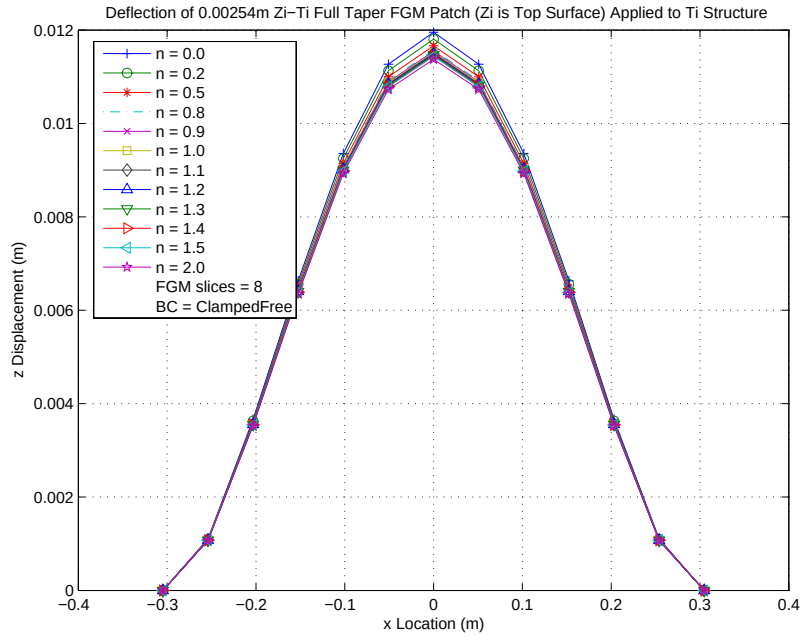

Figure 140. Exhaust Wash Deflection with 0.1" Zi-Ti FGM Full Taper Patch

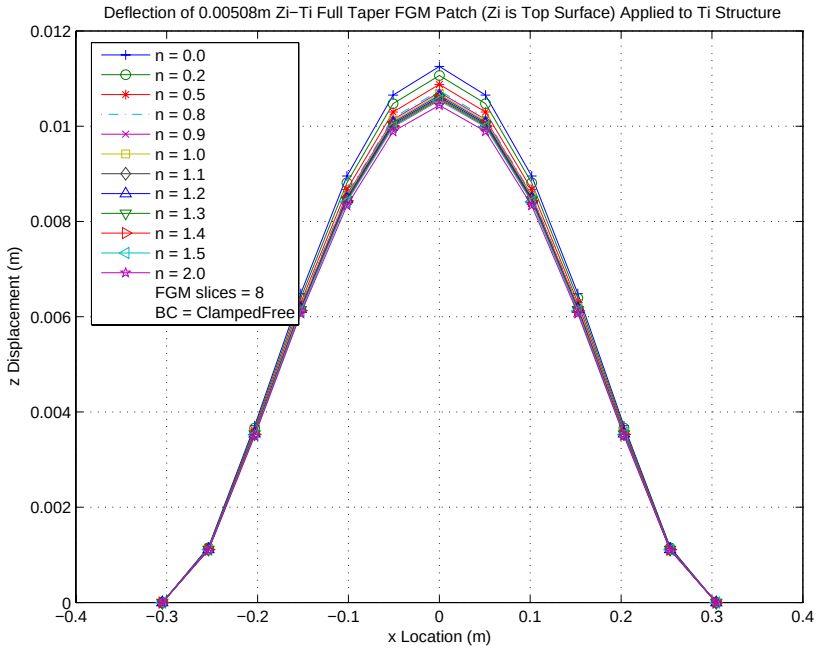

Figure 141. Exhaust Wash Deflection with 0.2" Zi-Ti FGM Full Taper Patch

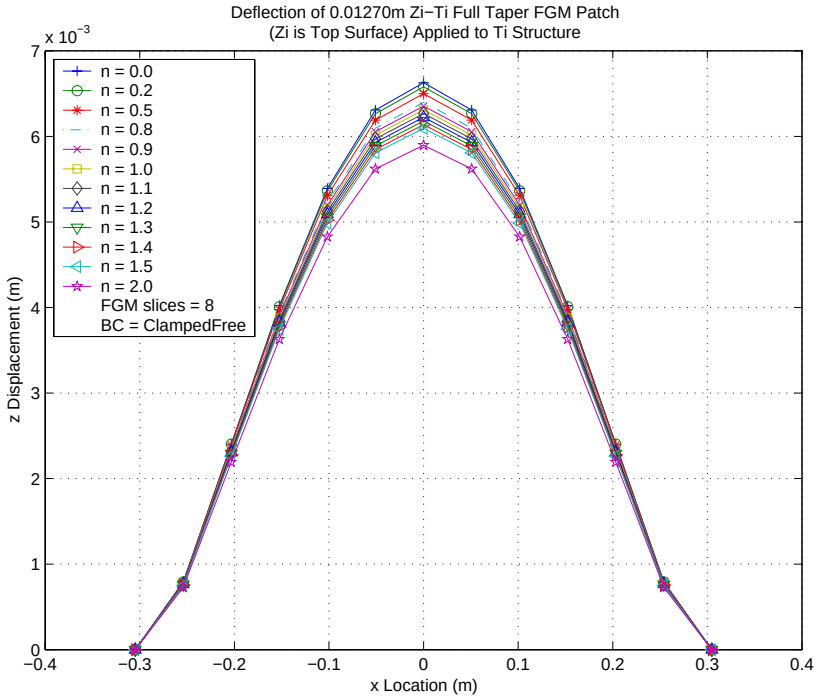

Figure 142. Exhaust Wash Deflection with 0.5" Zi-Ti FGM Full Taper Patch

For the 0.1”, 0.2”, and 0.5” Zi-Ti full taper patches, it is noted that n=2.0, n=2.0, and n=2.0 provide the lowest deflection, respectively, with 5.9%, 13.6%, 51.2% reductions in center deflection, respectively; exhaust wash panel von Mises stress was *decreased* by 3.9%, *increased* by 6.8%, and *increased* by 9.4%, respectively; the nodal yield/nodal ultimate count is 169/152, 197/165, 122/110. Top and bottom exhaust wash panel von Mises stress are shown for a 0.5” Zi-Ti full taper patch with n=2.0 in Figure 143 and Figure 144.

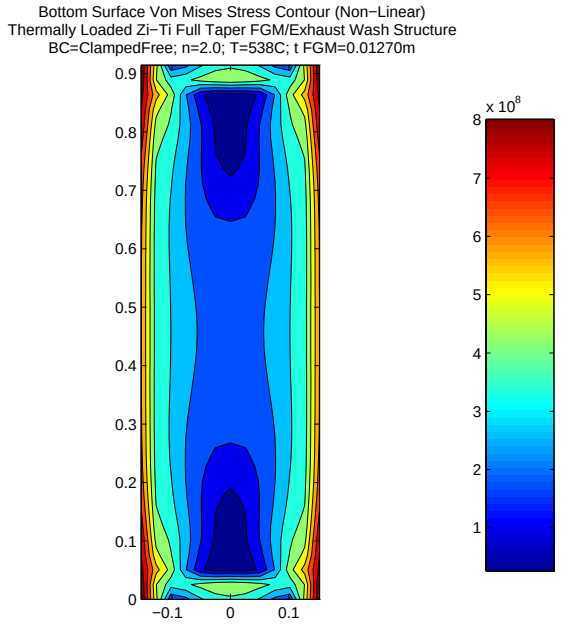

Figure 143. Exhaust Wash Bottom von Mises Stress: 0.5" Zi-Ti Full Taper Patch with n=2.0

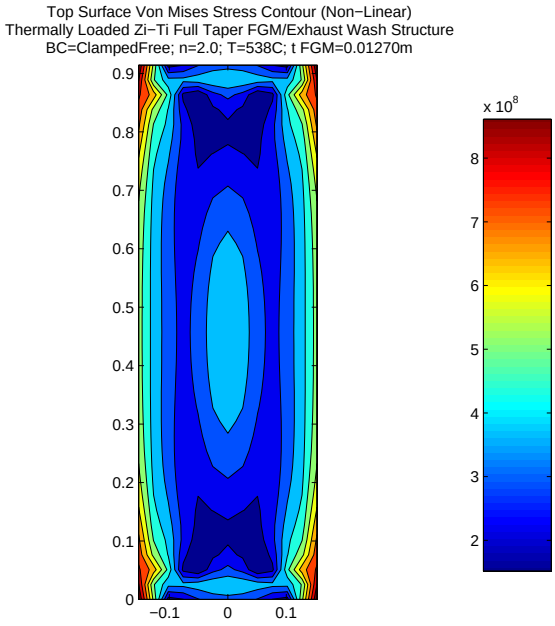

Figure 144. Exhaust Wash Top von Mises Stress: 0.5" Zi-Ti Full Taper Patch with n=2.0

It is noted that the corners and edges are again the critical location for stresses in both the top and bottom surface of the exhaust wash structure. Also, raising "n" lowered both stresses and deflection in all thickness in the Zi-Ti series of full taper patches. In other words, patches tending toward Ti performed best.

Now A286 and Ti full taper series patches are examined. Figure 145 through Figure 147 show the center displacement for 0.1", 0.2", and 0.5" A286/Ti-2-6-4-2 full taper patches.

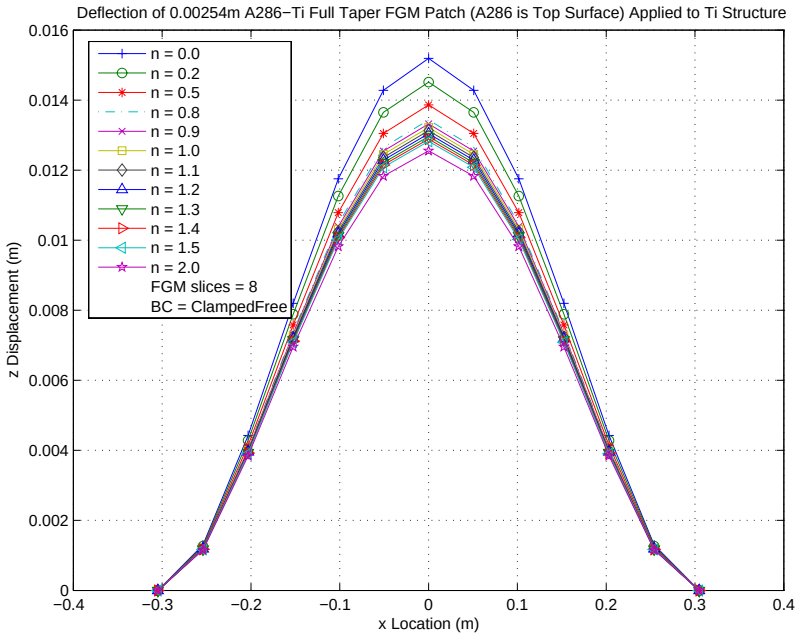

Figure 145. Exhaust Wash Deflection with 0.1" A-286/Ti FGM Full Taper Patch

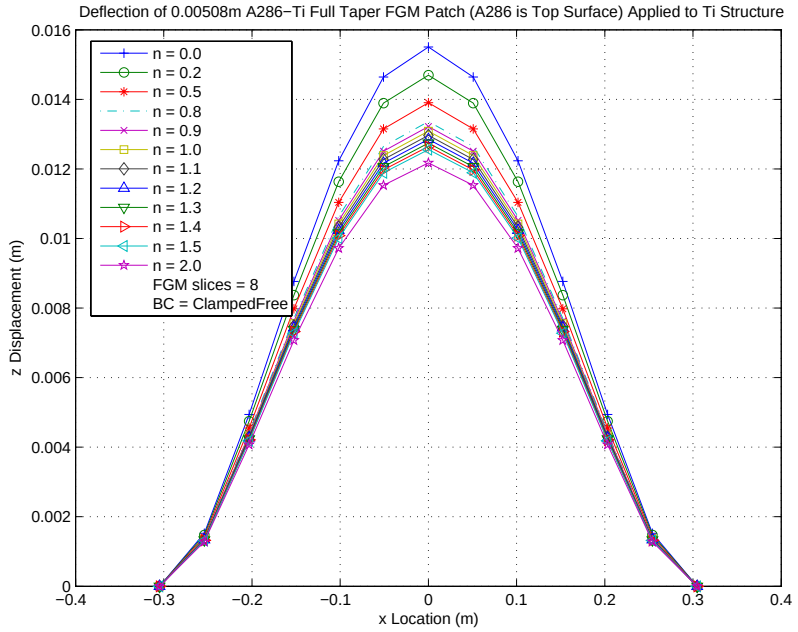

Figure 146. Exhaust Wash Deflection with 0.2" A-286/Ti FGM Full Taper Patch

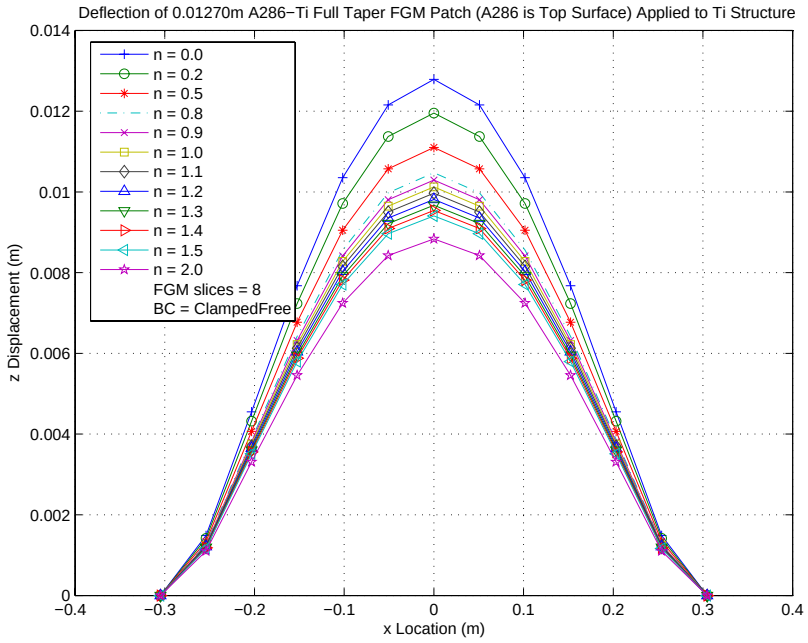

Figure 147. Exhaust Wash Deflection with 0.5" A-286/Ti FGM Full Taper Patch

For the 0.1", 0.2", and 0.5" A286/Ti full taper patches, it is noted that n=2.0, n=2.0, and n=2.0 provide the lowest deflection, respectively, with a 3.9% increase, 0.8% increase, and 26.9% decrease in center deflection, respectively; exhaust wash panel von Mises stress was increased by 8.2%, 33.0%, and 40.5%, respectively; the nodal yield/nodal ultimate count is 229/219, 277/237, and 255/221, respectively.

It is noted that a strong correlation of raising "n" to lower stresses and displacements exists. Top and bottom surface von Mises stresses for the exhaust wash panel with a 0.5" A286-Ti full taper patch with n=2.0 are shown in Figure 148 and Figure 149.

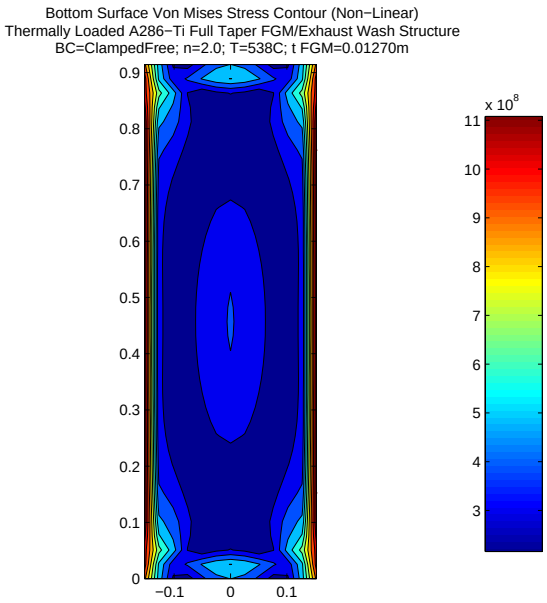

Figure 148. Exhaust Wash Bottom von Mises Stress: 0.5" A286-Ti Full Taper Patch with n=2.0

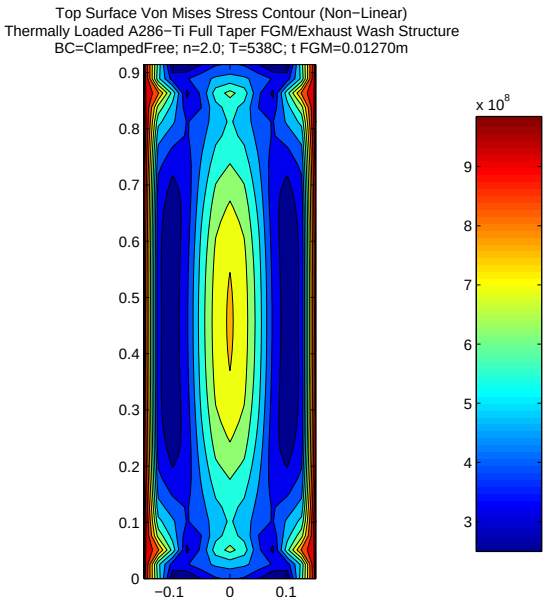

Figure 149. Exhaust Wash Top von Mises Stress: 0.5" A286-Ti Full Taper Patch with n=2.0

Flipping the material orientation, Ti/A286 full taper patches are evaluated in 0.1", 0.2", and 0.5" thicknesses. Center displacements are listed in Figure 150 through Figure 152.

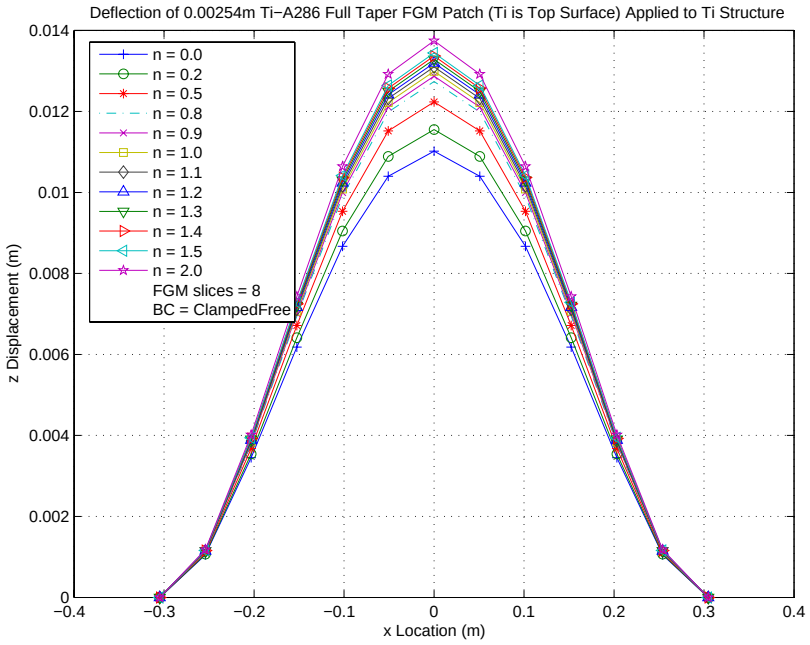

Figure 150. Exhaust Wash Deflection with 0.1" Ti-A286 FGM Full Taper Patch

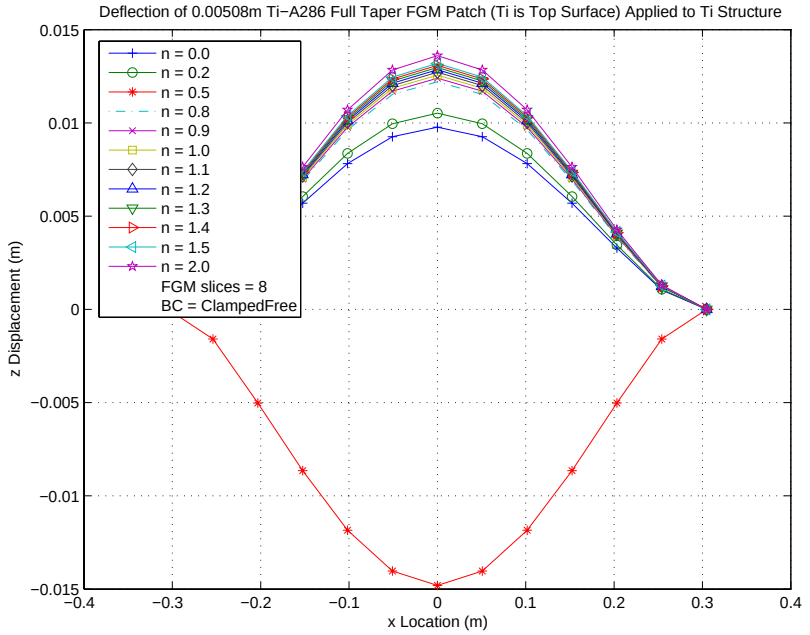

Figure 151. Exhaust Wash Deflection with 0.2" Ti-A286 FGM Full Taper Patch

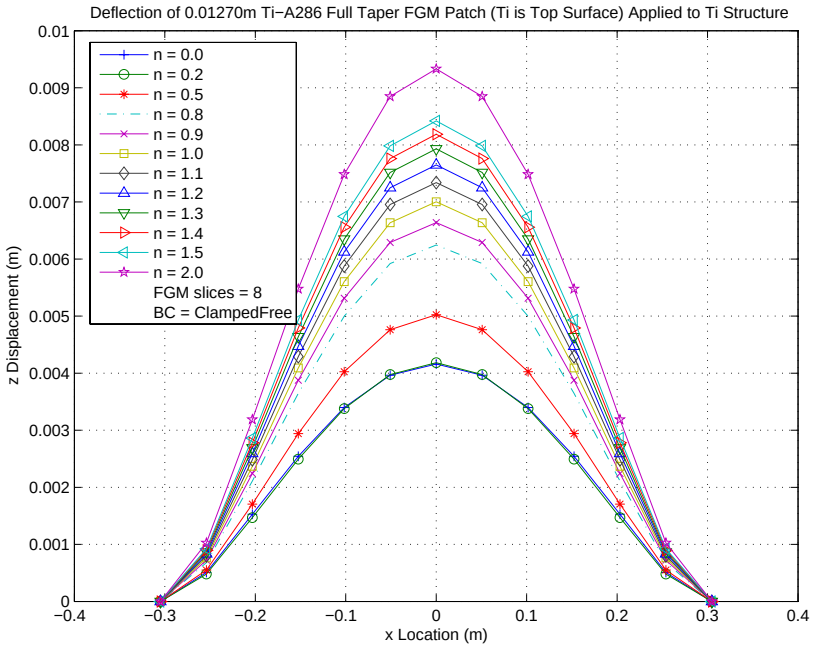

Figure 152. Exhaust Wash Deflection with 0.5" Ti-A286 FGM Full Taper Patch

For the 0.1”, 0.2”, and 0.5” Ti /A286 full taper patches, it is noted that n=0.0 (Ti) provides the least deflection, respectively, with 8.8%, 19.1%, and 65.6% reductions in center deflection, respectively; exhaust wash panel von Mises stress was *decreased* by 4.7%, unchanged, and in*creased* by 9.4%, respectively; the nodal yield/nodal ultimate count is 152/152, 102/94, and 64/48.

A strong correlation between lowering “n” to lower stress and displacement exists in all Ti-A286 full taper patches (patches tending to Ti performing best). Top and bottom exhaust wash surface von Mises stresses are shown for a 0.5” Ti/A286 patch with n=0.0 (Ti) in Figure 153 and Figure 154.

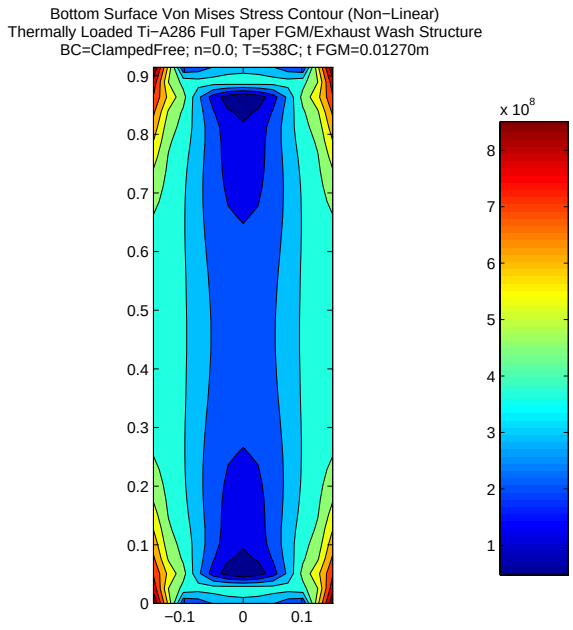

Figure 153. Exhaust Wash Bottom von Mises Stress: 0.5" Ti-A286-Ti Full Taper Patch with n=0.0

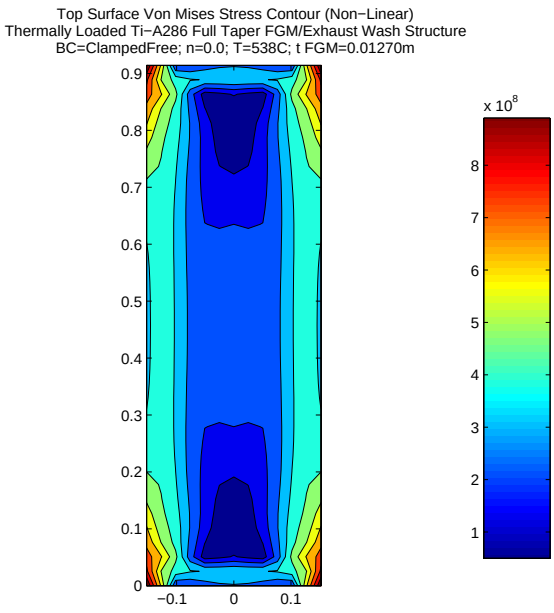

Figure 154. Exhaust Wash Top von Mises Stress: 0.5" Ti-A286-Ti Full Taper Patch with n=0.0

In summary, of all patch configurations considered (no taper, partial taper, and full taper), patches tending to Ti perform best. A 0.5" Ti full taper patch provides *near lowest* displacement and the *lowest* stress (65.6% reduction in deflection, and -13.5% / +20.0% change in nodal yield / ultimate counts). It is apparent that FGM patches are not feasible to retrofit the studied exhaust wash panel and that Ti patches perform best. Of all patches studied, the only patch to actually lower stress was 0.5" of Ti. The contour plots of the stress in the top and bottom surface of the exhaust wash structure are shown in Figure 153 and Figure 154, above, for a 0.5" Ti patch.

Exhaust Wash Panel made of Zi-Ti FGM

It was shown that FGM patches can not be used to retrofit an exhaust wash panel. However, in order to answer the question, "What if the exhaust wash panel was made of

an FGM?," a basic study of the structural performance of a 0.160" Zi-Ti FGM was performed (other geometry and FEA details remain the same as the structure/patch). Results are summarized in Table 6, below.

Table 6. Performance of a Zi-Ti FGM Exhaust Wash Structure

0.160" Zi-Ti FGM Exhaust Wash Structure

n	x11 Top (max)	x11 Top (min)	x22 Top (max)	x22 Top (min)	x12 Top (max)	x12 Top (min)	Top Mises (max)
0	1.98E+08	-4.34E+08	2.05E+08	-8.75E+08	2.79E+08	-2.79E+08	8.96E+08
0.2	1.78E+08	-3.90E+08	1.80E+08	-8.02E+08	2.55E+08	-2.55E+08	8.22E+08
0.5	1.64E+08	-3.39E+08	1.60E+08	-7.14E+08	2.27E+08	-2.27E+08	7.34E+08
0.8	1.56E+08	-3.00E+08	1.49E+08	-6.46E+08	2.06E+08	-2.06E+08	6.67E+08
0.9	1.54E+08	-2.89E+08	1.47E+08	-6.26E+08	2.01E+08	-2.01E+08	6.48E+08
1	1.52E+08	-2.79E+08	1.44E+08	-6.08E+08	1.96E+08	-1.96E+08	6.31E+08
1.1	1.50E+08	-2.70E+08	1.42E+08	-5.92E+08	1.91E+08	-1.91E+08	6.15E+08
1.2	1.49E+08	-2.62E+08	1.41E+08	-5.77E+08	1.86E+08	-1.86E+08	6.00E+08
1.3	1.47E+08	-2.55E+08	1.39E+08	-5.63E+08	1.82E+08	-1.82E+08	5.87E+08
1.4	1.46E+08	-2.48E+08	1.37E+08	-5.50E+08	1.79E+08	-1.79E+08	5.74E+08
1.5	1.45E+08	-2.42E+08	1.36E+08	-5.38E+08	1.75E+08	-1.75E+08	5.62E+08
2	1.39E+08	-2.17E+08	1.31E+08	-4.90E+08	1.61E+08	-1.61E+08	5.16E+08

n	x11 Bottom (max)	x11 Bottom (min)	x22 Bottom (max)	x22 Bottom (min)	x12 Bottom (max)	x12 Bottom (min)	Bottom Mises (max)	Center Deflection
0	3.24E+08	-2.10E+08	2.06E+08	-8.01E+08	2.77E+08	-2.77E+08	9.47E+08	0.028444
0.2	3.16E+08	-1.32E+08	1.67E+08	-5.79E+08	2.11E+08	-2.11E+08	7.26E+08	0.027892
0.5	2.89E+08	-1.05E+08	1.29E+08	-4.36E+08	1.64E+08	-1.64E+08	5.73E+08	0.027357
0.8	2.69E+08	-1.01E+08	1.06E+08	-3.83E+08	1.44E+08	-1.44E+08	5.08E+08	0.026992
0.9	2.64E+08	-1.01E+08	1.00E+08	-3.73E+08	1.40E+08	-1.40E+08	4.96E+08	0.026893
1	2.60E+08	-1.01E+08	9.57E+07	-3.67E+08	1.37E+08	-1.37E+08	4.87E+08	0.026803
1.1	2.56E+08	-1.02E+08	9.16E+07	-3.62E+08	1.35E+08	-1.35E+08	4.79E+08	0.026719
1.2	2.53E+08	-1.03E+08	8.81E+07	-3.59E+08	1.33E+08	-1.33E+08	4.74E+08	0.026642
1.3	2.50E+08	-1.04E+08	8.50E+07	-3.56E+08	1.31E+08	-1.31E+08	4.69E+08	0.026571
1.4	2.47E+08	-1.06E+08	8.24E+07	-3.54E+08	1.30E+08	-1.30E+08	4.65E+08	0.026504
1.5	2.45E+08	-1.07E+08	8.01E+07	-3.53E+08	1.29E+08	-1.29E+08	4.62E+08	0.026442
2	2.35E+08	-1.11E+08	7.21E+07	-3.51E+08	1.26E+08	-1.26E+08	4.53E+08	0.026181

It is noted that materials tending toward Ti perform best with n=2.0 giving the lowest deflection and lowest stress. The highest compressive stress in the *Zi* (top) portion of the panel is -217 MPa while the highest tensile stress is 139 MPa. These stresses are well within the compressive yield stress (-2500 MPa) and tensile yield stress (250 MPa)

of Zi. [10] The highest compressive stress in the *Ti* (bottom) portion of the panel is -351 MPa while the highest tensile stress is 235 MPa. These stresses are well within the compressive yield stress (-577.6 MPa) and tensile yield stress (482.6 MPa) of 500° C Ti-6-2-4-2.

It can be concluded from this basic research that FGM exhaust wash panels can perform better than pure metal exhaust wash panels and warrant consideration for new exhaust wash panel design. A detailed study into FGM exhaust wash panels can likely provide a suitable FGM that has vastly improved performance with deflections that similar to a Ti-6-2-4-2 panel.

Summary

Numerous patches were study and the volume of results is overwhelming. Table 7 summarizes the results for the best performing patches in each of the studied tapers.

Table 7. Summary of Best Performing Exhaust Wash Panel Patches

		% Change in Nodal Yield / Nodal Ultimate Counts over Baseline	% Change in Center Deflection over Baseline
No Taper	Lowest Deflection 0.5” Ti-Zi n=1.2	+132% / +320%	-214%
	Lowest Change in Stress 0.5” Ti	+86.5% / +235%	-54.4%
Partial Taper	Lowest Deflection 0.5” A286	+747% / +1,356%	-99.3%
	Lowest Change in Stress 0.1” Ti	+27% / +135%	-9.0%
Full Taper	Lowest Deflection 0.5” Ti-Zi n=0.5	+186% / +410%	-67.3%
	Lowest Change in Stress 0.5” Ti	-13.5% / +20.0%	-65.6%

Ti patches generally provide the lowest deflection and lowest stresses. There is a coupling of lowered deflection translating into increased stresses apparent in every patch studied. However, the degree of this coupling is least significant in a Ti patch with a 0.5" full taper Ti patch which provides the best all around results.

Because the temperature in the top surface gas (engine exhaust) is so high and has an extremely large heat transfer coefficient, the temperature through-the-thickness of the exhaust wash structure / patch was nearly uniform. This uniform temperature distribution through-the-thickness severely diminishes any benefits FGMs can offer (tailoring $\alpha \cdot \Delta T$ to be linear through-the-thickness). It has been consistently shown that patches tending toward Ti-6-2-4-2 provide the best results with a full taper 0.5" Ti-6-2-4-2 patch giving the lowest stress. This is likely because the Ti-6-2-4-2 matches the material properties of the exhaust wash panel. In other words, the thermal expansion through-the-thickness is uniform when the patch material matches the exhaust wash structure material. Thermal expansion through-the-thickness of an FGM patch is not uniform because the material properties change through-the thickness, namely the coefficient of thermal expansion. Figure 155 shoes through-the-thickness expansion for various n values studied.

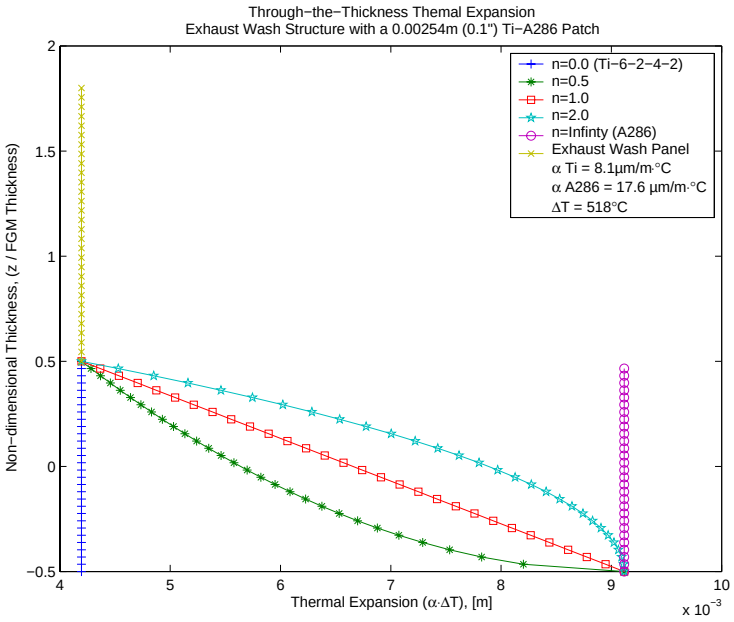

Figure 155. Thermal Expansion Exhaust Wash Structure with a 0.1" Ti-Zi Patch

Because the FGM patch expands at a different rate than the exhaust wash structure it, in essence, creates a stress concentration at the interface of the patch and structure. In addition, thermal moments are produced because of the difference in expansion. These moments exacerbate the high stresses found at the corners and along the edge of the exhaust wash panel.

Initial studies into Zi-Ti FGM exhaust wash panels showed that FGM exhaust wash panels perform better than Ti-6-2-4-2 panels. This is likely due to the gradual change of material properties through the thickness. The top surface is Zi, a material that handles compression well while the bottom surface is Ti, a material that handles tension well. Tailoring the material to the stresses encountered allows for the design of an exhaust wash panel that can handle the extreme temperatures without cracking at the boundary condition.

IV. Conclusions and Recommendations

Chapter Overview

This section will use conclusions from the research to provide recommendations and suggestions for further research.

Conclusions of FGM Plate and Shell Research

It has been consistently shown that FGMs offer lower deflection and lower stresses than metal in thermally loaded shell panels, thermally loaded shell plates, and pressure loaded plates studied in this thesis, all while adding thermal protection to the underlying metal. These results are especially useful for future aircraft and spacecraft design which require significant heat shielding as Mach numbers exceed Mach 3. An FGM can provide that thermal protection to extreme heat encountered at high speed while providing better structural performance than a metal alone.

For rectangular Zi-Al FGM *flat plates* with a temperature gradient of 580°C it was found that a plate with n=0.2 provides the lowest deflection and n=0.5 provides the lowest mid-plane stress (only 2.4% lower than mid-plane stress for n=0.2). These displacements and stresses are 68% and 54%, respectively, lower than a metal plate. It can be concluded that a non-linear analysis with a range of "n" from 0.2 to 0.5 provides the optimum solution to thermally loaded plates studied in this thesis (n=0.2 corresponds to a plate that is 83.3% by volume Zi).

For rectangular Zi-Al FGM *flat plates* under a non-dimensional pressure loading of 30 it was found that a plate with n=0.2 provides the lowest deflection and lowest mid-plane stress; the displacements and stresses are 50% and 4%, respectively, lower than a

metal plate. It can be concluded that a non-linear analysis with n=0.2 provides the optimum solution to pressure loaded plates studied in this thesis.

For rectangular Zi-Al FGM *curved panels* with a temperature gradient of 580°C it was found that a panel with n=0.2 provides the lowest deflection and stress (57% and 62% less than metal, respectively). The addition of a 200" (5.08 m) curvature raised the displacements by 31% but did not change the plot shape. In other words, the curvature simply shifted the displacements higher than a flat plate and did not affect the relative displacement profile. It can be concluded that a non-linear analysis with n=0.2 provides the optimum solution to thermally loaded shell panels studied in this thesis.

It is important to note that n=0.2 performed best in nearly every FGM plate and panel analyzed in this thesis, both under pressure and thermal loading.

Conclusions of Exhaust Wash Panel Research

The exhaust wash structure fails at the edges due to thermally induced bending. As the panel expands 0.01208 m in the +z direction, it is resisted by the rigid boundary condition and causes very high x direction stress at the boundary edges. The highest von Mises stress is 858 MPa, the highest x direction stress is 547 MPa and the lowest x direction stress is -767 MPa, all of which are well above yield and ultimate stresses. Critical stress locations are along the bottom surface edges and at the top surface corners.

Conclusions of Exhaust Wash Panel with FGM Patch Research

It can be concluded that patches applied to the exhaust wash structure perform best when they are tapered. A 0.5" patch with no taper increases the nodal yield and ultimate count by 86.5% / 235% while the same thickness patch that is fully tapered

changes the nodal yield and ultimate count by only -13.5% / 20%. The non-tapered patch provides a 54% reduction in center deflection while a fully tapered patch provides a 66% reduction in center deflection. Essentially, the taper helps to lower stress values at the critical location (edges and corners) while having a lesser impact on the center deflection.

Because of the uniform temperature profile through-the-thickness, FGMs are not an acceptable solution to cracking of the exhaust wash panel. However, FGMs can limit aeroelastic deformation, but at the cost of increasing stress. It appears that any reduction of center deflection is translated into increased compression at the boundary condition. FGMs do have the effect of creating compression at the boundary condition and could be used to essentially "close" the existing crack growth. However, it is likely that the panel will exhibit cracking in a different location due to the increased compression at the boundary.

Of all patches studied, a fully tapered 0.5" Ti-6-2-4-2 patch provides the smallest change in stress levels over the baseline exhaust wash structure (-13.5% reduction in nodes that are above yielding and a 20% increase in nodes that are above yielding.

Recommendations for Action

It is recommended that physical testing of FGM materials be compared to analytical results in order to better understand the effect grading the material has under thermal environments. In addition, it is recommended that a composite patch be considered because its thermal expansion can be controlled by orienting the composite.

Recommendations for Future Research

It is recommended that the aircraft exhaust wash deck be analyzed in 3D using continuum shells elements. ABAQUS CAE Version 6.5 now supports the use of continuum shells; ABAQUS CAE Version 6.4 (latest version at start of this thesis) does not.

A 3D *heat transfer* analysis will provide more accurate nodal temperatures because the third dimension allows the *sides* of the FGM patch to be exposed to the cooler lower gas thus creating a 3D temperature field through the patch. This exposed edge of the FGM will affect the nodal temperatures because extra cooling is essentially added to the patch. In addition, a 3D analysis allows for convection to be applied to the model and eliminates the need to manually calculate surface temperatures.

A 3D *stress* analysis will provide more accurate results at the corner of the exhaust wash deck where stress is concentrated by the intersection of a clamped boundary condition and a free edge. In addition, a 3D stress analysis allows for accurate modeling of the edge taper. In a 2D analysis, the taper was modeled as a rectangular section equal to half the thickness of the patch because a 2D analysis does not provide provisions for a tapered element. However, a 3D analysis allows elements to be tapered and can more accurately model the effect of a taper. A taper was shown to be effective in allowing for better transitions of stress from the FGM patch to the structure, as outline in Table 7.

It is also recommended that FGMs be modeled using a Python script instead of breaking the FGM into "slices," manually calculating the material properties using a

power-law, and entering the "slices" into ABAQUS (this process was automated using Matlab scripts). ABAQUS uses the Python object-oriented programming language to interface with the ABAQUS kernel (program) and allows for scripting that is integral to the ABAQUS environment. In other words, the ABAQUS Scripting Interface allows you to bypass the ABAQUS/CAE GUI and communicate directly with the kernel. This important feature allows for the following:

1) To automate repetitive tasks
2) Perform a parametric study
3) Create and modify the model databases and models that are created interactively when you work with ABAQUS/CAE
4) Access the data in an output database in order to customize postprocessing of analysis results
5) Provide a means for the exact modeling of FGMs by allowing ABAQUS to query material properties at Gaussian integration points.

The advantages of a Python script are greatly improved material property accuracy, automation of material property calculation using the power law, and the ability to add material properties with their dependency on temperature.

In addition to the aforementioned advantages of a Python script, more accurate modeling of the heat transfer can be accomplished by using a coupled thermal-displacement analysis in order to capture the mechanical properties change due to temperature. When breaking the FGM into "slices," material properties are calculated for each slice. This method requires knowledge of the temperature at the particular "slice"

and, therefore, becomes and iterative process to accurately enter material properties accurately. A heat transfer analysis is first performed to get the temperature of each slice. Material properties must then be updated to reflect the "slice" temperature then another heat transfer analysis is performed. This iterative process is time consuming and can be avoided with an advanced Python script which allows ABAQUS to query the Python script for material properties at the Gaussian points for the given "n" value and temperature.

Finally, it is recommended that a study of the suitability of FGMs in new exhaust wash structure design be performed. It was briefly shown in this thesis that FGMs have application in exhaust wash panels and can provide acceptable stress levels. A full study of various FGM materials, thicknesses, and "n" values is recommended.

Summary

FGMs provide designers the ability to customize material response to meet their design objectives. In addition, FGMs provide thermal protection and load carrying capability, all while alleviating the stress concentrations found in thermal protection systems. FGMs will play an important part in future aircraft design, however they are not suitable as retrofits to exhaust wash panels which have a uniform temperature.

Appendix A. Flow Chart of Matlab & ABAQUS Coupling

Discussion of this flowchart is provided in the Pre-processing and Post-processing subsections of the Methodology section.

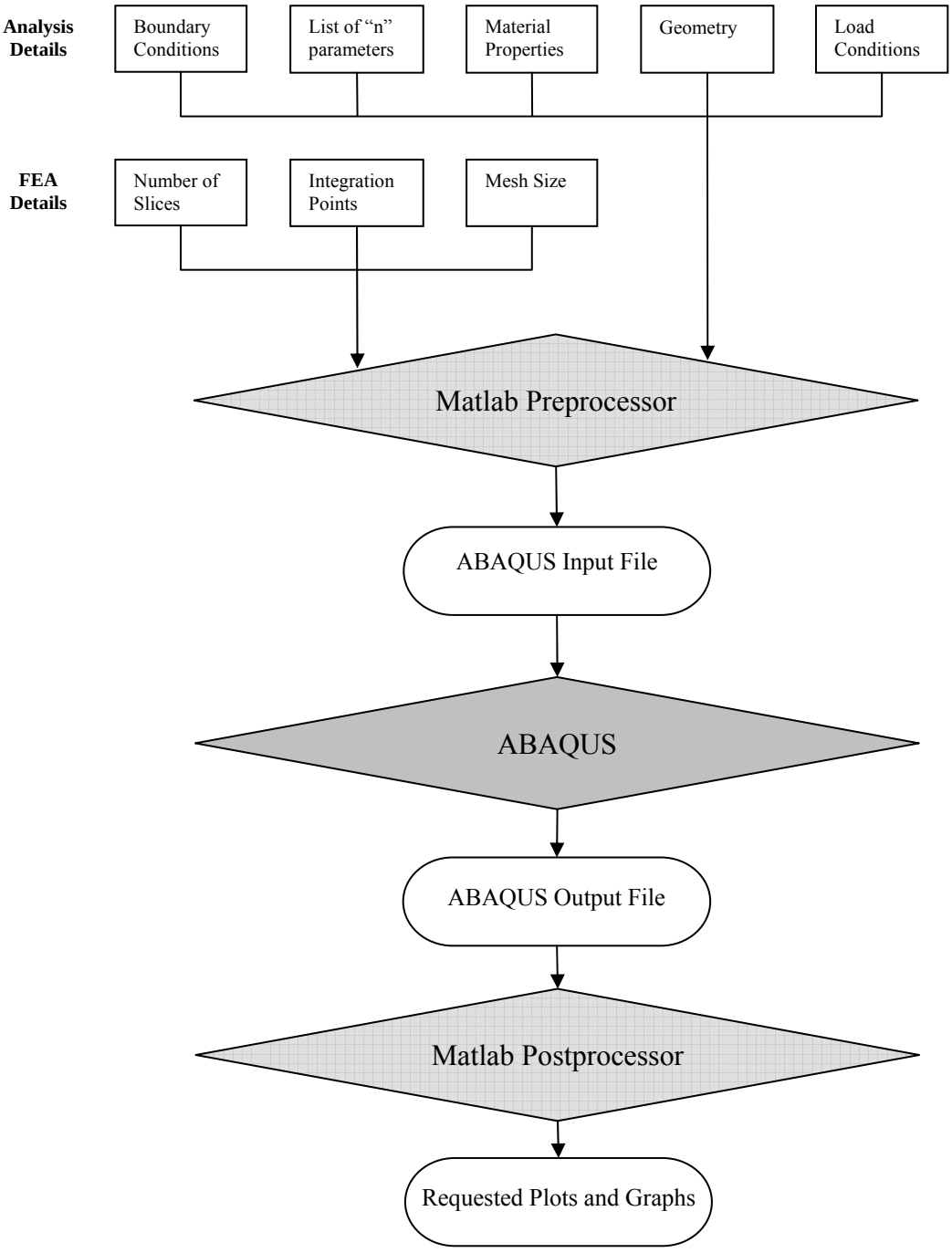

Appendix B. Sample ABAQUS Input File (Thermal Analysis)

This example is for a flat plate under thermal loading, however, this example file is applicable to both flat plates and curved panels. Note: Long lists are places in columns to save space in this thesis; in ABAQUS they are listed one per line)

```
*HEADING
FGM Plate
Written by Capt W. Glenn Cooley
**
*NODE
```

1, 0.000, 0.000, 0.	28, 0.000, 0.075, 0.	55, 0.000, 0.150, 0.
2, 0.025, 0.000, 0.	29, 0.025, 0.075, 0.	56, 0.025, 0.150, 0.
3, 0.050, 0.000, 0.	30, 0.050, 0.075, 0.	57, 0.050, 0.150, 0.
4, 0.075, 0.000, 0.	31, 0.075, 0.075, 0.	58, 0.075, 0.150, 0.
5, 0.100, 0.000, 0.	32, 0.100, 0.075, 0.	59, 0.100, 0.150, 0.
6, 0.125, 0.000, 0.	33, 0.125, 0.075, 0.	60, 0.125, 0.150, 0.
7, 0.150, 0.000, 0.	34, 0.150, 0.075, 0.	61, 0.150, 0.150, 0.
8, 0.175, 0.000, 0.	35, 0.175, 0.075, 0.	62, 0.175, 0.150, 0.
9, 0.200, 0.000, 0.	36, 0.200, 0.075, 0.	63, 0.200, 0.150, 0.
10, 0.000, 0.025, 0.	37, 0.000, 0.100, 0.	64, 0.000, 0.175, 0.
11, 0.025, 0.025, 0.	38, 0.025, 0.100, 0.	65, 0.025, 0.175, 0.
12, 0.050, 0.025, 0.	39, 0.050, 0.100, 0.	66, 0.050, 0.175, 0.
13, 0.075, 0.025, 0.	40, 0.075, 0.100, 0.	67, 0.075, 0.175, 0.
14, 0.100, 0.025, 0.	41, 0.100, 0.100, 0.	68, 0.100, 0.175, 0.
15, 0.125, 0.025, 0.	42, 0.125, 0.100, 0.	69, 0.125, 0.175, 0.
16, 0.150, 0.025, 0.	43, 0.150, 0.100, 0.	70, 0.150, 0.175, 0.
17, 0.175, 0.025, 0.	44, 0.175, 0.100, 0.	71, 0.175, 0.175, 0.
18, 0.200, 0.025, 0.	45, 0.200, 0.100, 0.	72, 0.200, 0.175, 0.
19, 0.000, 0.050, 0.	46, 0.000, 0.125, 0.	73, 0.000, 0.200, 0.
20, 0.025, 0.050, 0.	47, 0.025, 0.125, 0.	74, 0.025, 0.200, 0.
21, 0.050, 0.050, 0.	48, 0.050, 0.125, 0.	75, 0.050, 0.200, 0.
22, 0.075, 0.050, 0.	49, 0.075, 0.125, 0.	76, 0.075, 0.200, 0.
23, 0.100, 0.050, 0.	50, 0.100, 0.125, 0.	77, 0.100, 0.200, 0.
24, 0.125, 0.050, 0.	51, 0.125, 0.125, 0.	78, 0.125, 0.200, 0.
25, 0.150, 0.050, 0.	52, 0.150, 0.125, 0.	79, 0.150, 0.200, 0.
26, 0.175, 0.050, 0.	53, 0.175, 0.125, 0.	80, 0.175, 0.200, 0.
27, 0.200, 0.050, 0.	54, 0.200, 0.125, 0.	81, 0.200, 0.200, 0.

```
**
*ELEMENT, TYPE = DS4
```

1, 1, 2, 11, 10	23, 25, 26, 35, 34	45, 50, 51, 60, 59
2, 2, 3, 12, 11	24, 26, 27, 36, 35	46, 51, 52, 61, 60
3, 3, 4, 13, 12	25, 28, 29, 38, 37	47, 52, 53, 62, 61
4, 4, 5, 14, 13	26, 29, 30, 39, 38	48, 53, 54, 63, 62
5, 5, 6, 15, 14	27, 30, 31, 40, 39	49, 55, 56, 65, 64
6, 6, 7, 16, 15	28, 31, 32, 41, 40	50, 56, 57, 66, 65
7, 7, 8, 17, 16	29, 32, 33, 42, 41	51, 57, 58, 67, 66
8, 8, 9, 18, 17	30, 33, 34, 43, 42	52, 58, 59, 68, 67
9, 10, 11, 20, 19	31, 34, 35, 44, 43	53, 59, 60, 69, 68
10, 11, 12, 21, 20	32, 35, 36, 45, 44	54, 60, 61, 70, 69

11, 12, 13, 22, 21	33, 37, 38, 47, 46	55, 61, 62, 71, 70
12, 13, 14, 23, 22	34, 38, 39, 48, 47	56, 62, 63, 72, 71
13, 14, 15, 24, 23	35, 39, 40, 49, 48	57, 64, 65, 74, 73
14, 15, 16, 25, 24	36, 40, 41, 50, 49	58, 65, 66, 75, 74
15, 16, 17, 26, 25	37, 41, 42, 51, 50	59, 66, 67, 76, 75
16, 17, 18, 27, 26	38, 42, 43, 52, 51	60, 67, 68, 77, 76
17, 19, 20, 29, 28	39, 43, 44, 53, 52	61, 68, 69, 78, 77
18, 20, 21, 30, 29	40, 44, 45, 54, 53	62, 69, 70, 79, 78
19, 21, 22, 31, 30	41, 46, 47, 56, 55	63, 70, 71, 80, 79
20, 22, 23, 32, 31	42, 47, 48, 57, 56	64, 71, 72, 81, 80
21, 23, 24, 33, 32	43, 48, 49, 58, 57	
22, 24, 25, 34, 33	44, 49, 50, 59, 58	

```
**
*ELSET, ELSET=allElements, GENERATE
1, 64, 1
*NSET, NSET = allNodes, GENERATE
1, 81, 1
*NSET, NSET = centerNode
41
**
*SHELL SECTION, ELSET=allElements, TEMPERATURE = 3, COMPOSITE
0.00111, 3, PLY1, 0.
0.00111, 3, PLY2, 0.
0.00111, 3, PLY3, 0.
0.00111, 3, PLY4, 0.
0.00111, 3, PLY5, 0.
0.00111, 3, PLY6, 0.
0.00111, 3, PLY7, 0.
0.00111, 3, PLY8, 0.
0.00111, 3, PLY9, 0.
**
*MATERIAL, NAME=PLY9
*CONDUCTIVITY
 4.385
*DENSITY
2996.670
*MATERIAL, NAME=PLY8
*CONDUCTIVITY
 9.320
*DENSITY
2989.508
*MATERIAL, NAME=PLY7
*CONDUCTIVITY
14.813
*DENSITY
2981.538
*MATERIAL, NAME=PLY6
*CONDUCTIVITY
21.029
*DENSITY
2972.517
*MATERIAL, NAME=PLY5
*CONDUCTIVITY
28.227
```

```
*DENSITY
2962.071
*MATERIAL, NAME=PLY4
*CONDUCTIVITY
36.844
*DENSITY
2949.568
*MATERIAL, NAME=PLY3
*CONDUCTIVITY
47.722
*DENSITY
2933.781
*MATERIAL, NAME=PLY2
*CONDUCTIVITY
62.900
*DENSITY
2911.756
*MATERIAL, NAME=PLY1
*CONDUCTIVITY
90.733
*DENSITY
2871.366
**
*STEP
**
*HEAT TRANSFER, STEADY STATE
**
*BOUNDARY, OP=NEW
allNodes, 29, 29, 100.0
allNodes, 11, 11, 20.0
**
**
*NODE PRINT, NSET = allNodes
NT
*NODE FILE, NSET = allNodes
NT
**
*END STEP
```

Appendix C. Sample ABAQUS Input File (Structural Analysis)

This example is for a flat plate under thermal loading, however, this example file is applicable to both flat plates and curved panels. Note: Long lists are places in columns to save space in this thesis; in ABAQUS they are listed one per line)

```
*HEADING
FGM Plate
Written by Capt W. Glenn Cooley
**
*NODE
```

1, 0.000, 0.000, 0.	28, 0.000, 0.075, 0.	55, 0.000, 0.150, 0.
2, 0.025, 0.000, 0.	29, 0.025, 0.075, 0.	56, 0.025, 0.150, 0.
3, 0.050, 0.000, 0.	30, 0.050, 0.075, 0.	57, 0.050, 0.150, 0.
4, 0.075, 0.000, 0.	31, 0.075, 0.075, 0.	58, 0.075, 0.150, 0.
5, 0.100, 0.000, 0.	32, 0.100, 0.075, 0.	59, 0.100, 0.150, 0.
6, 0.125, 0.000, 0.	33, 0.125, 0.075, 0.	60, 0.125, 0.150, 0.
7, 0.150, 0.000, 0.	34, 0.150, 0.075, 0.	61, 0.150, 0.150, 0.
8, 0.175, 0.000, 0.	35, 0.175, 0.075, 0.	62, 0.175, 0.150, 0.
9, 0.200, 0.000, 0.	36, 0.200, 0.075, 0.	63, 0.200, 0.150, 0.
10, 0.000, 0.025, 0.	37, 0.000, 0.100, 0.	64, 0.000, 0.175, 0.
11, 0.025, 0.025, 0.	38, 0.025, 0.100, 0.	65, 0.025, 0.175, 0.
12, 0.050, 0.025, 0.	39, 0.050, 0.100, 0.	66, 0.050, 0.175, 0.
13, 0.075, 0.025, 0.	40, 0.075, 0.100, 0.	67, 0.075, 0.175, 0.
14, 0.100, 0.025, 0.	41, 0.100, 0.100, 0.	68, 0.100, 0.175, 0.
15, 0.125, 0.025, 0.	42, 0.125, 0.100, 0.	69, 0.125, 0.175, 0.
16, 0.150, 0.025, 0.	43, 0.150, 0.100, 0.	70, 0.150, 0.175, 0.
17, 0.175, 0.025, 0.	44, 0.175, 0.100, 0.	71, 0.175, 0.175, 0.
18, 0.200, 0.025, 0.	45, 0.200, 0.100, 0.	72, 0.200, 0.175, 0.
19, 0.000, 0.050, 0.	46, 0.000, 0.125, 0.	73, 0.000, 0.200, 0.
20, 0.025, 0.050, 0.	47, 0.025, 0.125, 0.	74, 0.025, 0.200, 0.
21, 0.050, 0.050, 0.	48, 0.050, 0.125, 0.	75, 0.050, 0.200, 0.
22, 0.075, 0.050, 0.	49, 0.075, 0.125, 0.	76, 0.075, 0.200, 0.
23, 0.100, 0.050, 0.	50, 0.100, 0.125, 0.	77, 0.100, 0.200, 0.
24, 0.125, 0.050, 0.	51, 0.125, 0.125, 0.	78, 0.125, 0.200, 0.
25, 0.150, 0.050, 0.	52, 0.150, 0.125, 0.	79, 0.150, 0.200, 0.
26, 0.175, 0.050, 0.	53, 0.175, 0.125, 0.	80, 0.175, 0.200, 0.
27, 0.200, 0.050, 0.	54, 0.200, 0.125, 0.	81, 0.200, 0.200, 0.

```
**
*ELEMENT, TYPE = S4
```

1, 1, 2, 11, 10	23, 25, 26, 35, 34	45, 50, 51, 60, 59
2, 2, 3, 12, 11	24, 26, 27, 36, 35	46, 51, 52, 61, 60
3, 3, 4, 13, 12	25, 28, 29, 38, 37	47, 52, 53, 62, 61
4, 4, 5, 14, 13	26, 29, 30, 39, 38	48, 53, 54, 63, 62
5, 5, 6, 15, 14	27, 30, 31, 40, 39	49, 55, 56, 65, 64
6, 6, 7, 16, 15	28, 31, 32, 41, 40	50, 56, 57, 66, 65
7, 7, 8, 17, 16	29, 32, 33, 42, 41	51, 57, 58, 67, 66
8, 8, 9, 18, 17	30, 33, 34, 43, 42	52, 58, 59, 68, 67
9, 10, 11, 20, 19	31, 34, 35, 44, 43	53, 59, 60, 69, 68
10, 11, 12, 21, 20	32, 35, 36, 45, 44	54, 60, 61, 70, 69

11, 12, 13, 22, 21	33, 37, 38, 47, 46	55, 61, 62, 71, 70
12, 13, 14, 23, 22	34, 38, 39, 48, 47	56, 62, 63, 72, 71
13, 14, 15, 24, 23	35, 39, 40, 49, 48	57, 64, 65, 74, 73
14, 15, 16, 25, 24	36, 40, 41, 50, 49	58, 65, 66, 75, 74
15, 16, 17, 26, 25	37, 41, 42, 51, 50	59, 66, 67, 76, 75
16, 17, 18, 27, 26	38, 42, 43, 52, 51	60, 67, 68, 77, 76
17, 19, 20, 29, 28	39, 43, 44, 53, 52	61, 68, 69, 78, 77
18, 20, 21, 30, 29	40, 44, 45, 54, 53	62, 69, 70, 79, 78
19, 21, 22, 31, 30	41, 46, 47, 56, 55	63, 70, 71, 80, 79
20, 22, 23, 32, 31	42, 47, 48, 57, 56	64, 71, 72, 81, 80
21, 23, 24, 33, 32	43, 48, 49, 58, 57	
22, 24, 25, 34, 33	44, 49, 50, 59, 58	

```
**
*ELSET, ELSET=allElements, GENERATE
1, 64, 1
*NSET, NSET = allNodes, GENERATE
1, 81, 1
*NSET, NSET = centerNode
41
**
*SHELL SECTION, ELSET=allElements, TEMPERATURE = 3, COMPOSITE
0.00111, 3, PLY1, 0.
0.00111, 3, PLY2, 0.
0.00111, 3, PLY3, 0.
0.00111, 3, PLY4, 0.
0.00111, 3, PLY5, 0.
0.00111, 3, PLY6, 0.
0.00111, 3, PLY7, 0.
0.00111, 3, PLY8, 0.
0.00111, 3, PLY9, 0.
**
*MATERIAL, NAME=PLY9
*ELASTIC, TYPE=LAMINA
1.4650e+011, 1.4650e+011, 0.3, 5.6346e+010, 5.6346e+010, 5.6346e+010
*CONDUCTIVITY
13.307
*DENSITY
2983.722
*EXPANSION
1.0722e-005
*MATERIAL, NAME=PLY8
*ELASTIC, TYPE=LAMINA
1.3750e+011, 1.3750e+011, 0.3, 5.2885e+010, 5.2885e+010, 5.2885e+010
*CONDUCTIVITY
35.742
*DENSITY
2951.167
*EXPANSION
1.2167e-005
*MATERIAL, NAME=PLY7
*ELASTIC, TYPE=LAMINA
1.2850e+011, 1.2850e+011, 0.3, 4.9423e+010, 4.9423e+010, 4.9423e+010
*CONDUCTIVITY
58.176
```

```
*DENSITY
2918.611
*EXPANSION
1.3611e-005
*MATERIAL, NAME=PLY6
*ELASTIC, TYPE=LAMINA
1.1950e+011, 1.1950e+011, 0.3, 4.5962e+010, 4.5962e+010, 4.5962e+010
*CONDUCTIVITY
80.611
*DENSITY
2886.056
*EXPANSION
1.5056e-005
*MATERIAL, NAME=PLY5
*ELASTIC, TYPE=LAMINA
1.1050e+011, 1.1050e+011, 0.3, 4.2500e+010, 4.2500e+010, 4.2500e+010
*CONDUCTIVITY
103.045
*DENSITY
2853.500
*EXPANSION
1.6500e-005
*MATERIAL, NAME=PLY4
*ELASTIC, TYPE=LAMINA
1.0150e+011, 1.0150e+011, 0.3, 3.9038e+010, 3.9038e+010, 3.9038e+010
*CONDUCTIVITY
125.479
*DENSITY
2820.944
*EXPANSION
1.7944e-005
*MATERIAL, NAME=PLY3
*ELASTIC, TYPE=LAMINA
9.2500e+010, 9.2500e+010, 0.3, 3.5577e+010, 3.5577e+010, 3.5577e+010
*CONDUCTIVITY
147.914
*DENSITY
2788.389
*EXPANSION
1.9389e-005
*MATERIAL, NAME=PLY2
*ELASTIC, TYPE=LAMINA
8.3500e+010, 8.3500e+010, 0.3, 3.2115e+010, 3.2115e+010, 3.2115e+010
*CONDUCTIVITY
170.348
*DENSITY
2755.833
*EXPANSION
2.0833e-005
*MATERIAL, NAME=PLY1
*ELASTIC, TYPE=LAMINA
7.4500e+010, 7.4500e+010, 0.3, 2.8654e+010, 2.8654e+010, 2.8654e+010
*CONDUCTIVITY
192.783
```

```
*DENSITY
2723.278
*EXPANSION
2.2278e-005
**
*INITIAL CONDITIONS, type=TEMPERATURE
allNodes, 20,20,20,20,20,20,20,
20,20,20,20,20,20,20,20,
20,20,20,20
**
*STEP, NLGEOM = YES
**
*STATIC
**
*BOUNDARY
```

1, 1	10, 1	19, 1	28, 1	37, 1	46, 1	55, 1	64, 1	73, 1
1, 2	10, 2	19, 2	28, 2	37, 2	46, 2	55, 2	64, 2	73, 2
1, 3	10, 3	19, 3	28, 3	37, 3	46, 3	55, 3	64, 3	73, 3
1, 4	10, 4	19, 4	28, 4	37, 4	46, 4	55, 4	64, 4	73, 4
1, 6	10, 6	19, 6	28, 6	37, 6	46, 6	55, 6	64, 6	73, 6
2, 6	11, 6	20, 6	29, 6	38, 6	47, 6	56, 6	65, 6	74, 6
3, 6	12, 6	21, 6	30, 6	39, 6	48, 6	57, 6	66, 6	75, 6
4, 6	13, 6	22, 6	31, 6	40, 6	49, 6	58, 6	67, 6	76, 6
5, 6	14, 6	23, 6	32, 6	41, 6	50, 6	59, 6	68, 6	77, 6
6, 6	15, 6	24, 6	33, 6	42, 6	51, 6	60, 6	69, 6	78, 6
7, 6	16, 6	25, 6	34, 6	43, 6	52, 6	61, 6	70, 6	79, 6
8, 6	17, 6	26, 6	35, 6	44, 6	53, 6	62, 6	71, 6	80, 6
9, 1	18, 1	27, 1	36, 1	45, 1	54, 1	63, 1	72, 1	81, 1
9, 2	18, 2	27, 2	36, 2	45, 2	54, 2	63, 2	72, 2	81, 2
9, 3	18, 3	27, 3	36, 3	45, 3	54, 3	63, 3	72, 3	81, 3
9, 4	18, 4	27, 4	36, 4	45, 4	54, 4	63, 4	72, 4	81, 4
9, 6	18, 6	27, 6	36, 6	45, 6	54, 6	63, 6	72, 6	81, 6

```
**
*TEMPERATURE, file=T100n1.0HT
**
*NODE PRINT, NSET=centerNode
U
*EL PRINT, ELSET=allElements, POSITION=AVERAGED AT NODES
14
MISES
*
*OUTPUT, FIELD
*ELEMENT OUTPUT
1,14,27
MISES
**
*END STEP
```

Appendix D. Summarized Exhaust Wash Model Data (Stress and Deflection)

0.10" Ti-Zi (No Taper)

n	x11 Top (max)	x11 Top (min)	x22 Top (max)	x22 Top (min)	x12 Top (max)	x12 Top (min)	Top Mises (max)
0	7.23E+08	-6.22E+08	1.49E+07	-4.77E+08	3.18E+08	-3.18E+08	8.21E+08
0.2	7.26E+08	-6.34E+08	9.07E+06	-4.79E+08	3.32E+08	-3.32E+08	8.25E+08
0.5	7.28E+08	-6.51E+08	2.94E+06	-4.83E+08	3.49E+08	-3.49E+08	8.29E+08
0.8	7.31E+08	-6.62E+08	2.57E+06	-4.85E+08	3.59E+08	-3.59E+08	8.33E+08
0.9	7.32E+08	-6.65E+08	2.48E+06	-4.85E+08	3.62E+08	-3.62E+08	8.34E+08
1	7.33E+08	-6.69E+08	2.38E+06	-4.86E+08	3.64E+08	-3.64E+08	8.35E+08
1.1	7.34E+08	-6.72E+08	2.28E+06	-4.87E+08	3.67E+08	-3.67E+08	8.36E+08
1.2	7.35E+08	-6.75E+08	2.18E+06	-4.88E+08	3.69E+08	-3.69E+08	8.40E+08
1.3	7.35E+08	-6.77E+08	2.08E+06	-4.88E+08	3.70E+08	-3.70E+08	8.43E+08
1.4	7.36E+08	-6.80E+08	2.02E+06	-4.89E+08	3.72E+08	-3.72E+08	8.46E+08
1.5	7.37E+08	-6.82E+08	1.88E+06	-4.89E+08	3.74E+08	-3.74E+08	8.49E+08
2	7.40E+08	-6.93E+08	7.03E+06	-4.92E+08	3.80E+08	-3.80E+08	8.62E+08

n	x11 Bottom (max)	x11 Bottom (min)	x22 Bottom (max)	x22 Bottom (min)	x12 Bottom (max)	x12 Bottom (min)	Bottom Mises (max)
0	4.55E+08	-9.71E+08	1.05E+08	-6.20E+08	3.78E+08	-3.78E+08	1.07E+09
0.2	4.89E+08	-1.01E+09	1.15E+08	-6.27E+08	3.92E+08	-3.92E+08	1.11E+09
0.5	5.26E+08	-1.04E+09	1.32E+08	-6.32E+08	4.06E+08	-4.06E+08	1.15E+09
0.8	5.53E+08	-1.06E+09	1.44E+08	-6.36E+08	4.17E+08	-4.17E+08	1.17E+09
0.9	5.59E+08	-1.06E+09	1.47E+08	-6.36E+08	4.19E+08	-4.19E+08	1.18E+09
1	5.65E+08	-1.07E+09	1.50E+08	-6.37E+08	4.22E+08	-4.22E+08	1.18E+09
1.1	5.71E+08	-1.07E+09	1.52E+08	-6.38E+08	4.24E+08	-4.24E+08	1.19E+09
1.2	5.76E+08	-1.08E+09	1.55E+08	-6.38E+08	4.25E+08	-4.25E+08	1.19E+09
1.3	5.80E+08	-1.08E+09	1.57E+08	-6.39E+08	4.27E+08	-4.27E+08	1.19E+09
1.4	5.84E+08	-1.08E+09	1.59E+08	-6.39E+08	4.28E+08	-4.28E+08	1.20E+09
1.5	5.88E+08	-1.08E+09	1.61E+08	-6.40E+08	4.30E+08	-4.30E+08	1.20E+09
2	6.02E+08	-1.09E+09	1.69E+08	-6.41E+08	4.36E+08	-4.36E+08	1.21E+09

n	Center Deflection	Top Yield Count	Top Ultimate Count	Bottom Yield Count	Bottom Ultimate Count	Total Yield Count	Total Ultimate Count
0	0.011286	74	74	86	82	160	156
0.2	0.011443	74	74	86	82	160	156
0.5	0.011626	74	74	86	82	160	156
0.8	0.011752	74	74	93	82	167	156
0.9	0.011786	74	74	95	82	169	156
1	0.011816	74	74	97	82	171	156
1.1	0.011843	74	74	97	82	171	156
1.2	0.011868	74	74	99	82	173	156
1.3	0.011892	74	74	99	82	173	156
1.4	0.011914	74	74	101	86	175	160
1.5	0.01193	74	74	101	86	175	160
2	0.012006	74	74	113	86	187	160

0.20" Ti-Zi (No Taper)

n	x11 Top (max)	x11 Top (min)	x22 Top (max)	x22 Top (min)	x12 Top (max)	x12 Top (min)	Top Mises (max)
0	6.40E+08	-6.35E+08	6.27E+06	-4.74E+08	3.93E+08	-3.93E+08	8.37E+08
0.2	6.18E+08	-6.58E+08	-4.80E+06	-4.79E+08	4.34E+08	-4.34E+08	8.74E+08
0.5	4.65E+08	-1.36E+09	1.04E+08	-7.83E+08	5.36E+08	-5.36E+08	1.44E+09
0.8	5.98E+08	-7.06E+08	1.43E+07	-4.90E+08	5.06E+08	-5.06E+08	9.59E+08
0.9	5.97E+08	-7.11E+08	1.64E+07	-4.91E+08	5.13E+08	-5.13E+08	9.69E+08
1	5.97E+08	-7.16E+08	1.84E+07	-4.93E+08	5.19E+08	-5.19E+08	9.78E+08
1.1	5.97E+08	-7.21E+08	2.02E+07	-4.94E+08	5.25E+08	-5.25E+08	9.86E+08
1.2	5.97E+08	-7.25E+08	2.18E+07	-4.95E+08	5.30E+08	-5.30E+08	9.93E+08
1.3	5.97E+08	-7.29E+08	2.33E+07	-4.96E+08	5.34E+08	-5.34E+08	1.00E+09
1.4	5.98E+08	-7.33E+08	2.47E+07	-4.97E+08	5.38E+08	-5.38E+08	1.01E+09
1.5	5.99E+08	-7.37E+08	2.60E+07	-4.98E+08	5.42E+08	-5.42E+08	1.01E+09
2	4.58E+08	-1.39E+09	1.04E+08	-7.93E+08	6.02E+08	-6.02E+08	1.56E+09

n	x11 Bottom (max)	x11 Bottom (min)	x22 Bottom (max)	x22 Bottom (min)	x12 Bottom (max)	x12 Bottom (min)	Bottom Mises (max)
0	5.05E+08	-1.16E+09	8.35E+07	-6.61E+08	4.50E+08	-4.50E+08	1.27E+09
0.2	5.57E+08	-1.21E+09	9.79E+07	-6.72E+08	4.83E+08	-4.83E+08	1.32E+09
0.5	8.24E+08	-9.60E+08	7.32E+07	-5.40E+08	4.42E+08	-4.42E+08	9.66E+08
0.8	6.50E+08	-1.28E+09	1.35E+08	-6.90E+08	5.41E+08	-5.41E+08	1.42E+09
0.9	6.59E+08	-1.28E+09	1.39E+08	-6.92E+08	5.47E+08	-5.47E+08	1.43E+09
1	6.68E+08	-1.29E+09	1.43E+08	-6.93E+08	5.53E+08	-5.53E+08	1.43E+09
1.1	6.75E+08	-1.30E+09	1.47E+08	-6.94E+08	5.57E+08	-5.57E+08	1.44E+09
1.2	6.82E+08	-1.30E+09	1.50E+08	-6.95E+08	5.61E+08	-5.61E+08	1.45E+09
1.3	6.88E+08	-1.30E+09	1.53E+08	-6.96E+08	5.65E+08	-5.65E+08	1.45E+09
1.4	6.94E+08	-1.31E+09	1.56E+08	-6.97E+08	5.68E+08	-5.68E+08	1.46E+09
1.5	6.99E+08	-1.31E+09	1.59E+08	-6.98E+08	5.72E+08	-5.72E+08	1.46E+09
2	8.86E+08	-9.51E+08	9.13E+07	-5.26E+08	4.86E+08	-4.86E+08	1.05E+09

n	Center Deflection	Top Yield Count	Top Ultimate Count	Bottom Yield Count	Bottom Ultimate Count	Total Yield Count	Total Ultimate Count
0	0.01049	74	74	82	82	156	156
0.2	0.010708	74	74	91	82	165	156
0.5	-0.013853	86	82	239	235	325	317
0.8	0.011122	74	74	131	111	205	185
0.9	0.011167	74	74	135	115	209	189
1	0.011208	74	74	137	121	211	195
1.1	0.011245	74	74	137	125	211	199
1.2	0.011279	74	74	143	125	217	199
1.3	0.011309	74	74	143	127	217	201
1.4	0.011338	74	74	143	131	217	205
1.5	0.011363	74	74	143	131	217	205
2	-0.014072	86	82	239	235	325	317

0.50" Ti-Zi (No Taper)

n	x11 Top (max)	x11 Top (min)	x22 Top (max)	x22 Top (min)	x12 Top (max)	x12 Top (min)	Top Mises (max)
0	1.70E+08	-1.07E+09	-1.14E+07	-5.89E+08	7.21E+08	-7.21E+08	1.33E+09
0.2	1.44E+08	-1.19E+09	-1.14E+07	-6.24E+08	8.21E+08	-8.21E+08	1.55E+09
0.5	9.31E+07	-1.33E+09	-8.79E+06	-6.90E+08	9.20E+08	-9.20E+08	1.80E+09
0.8	3.84E+07	-1.42E+09	-1.88E+06	-7.68E+08	9.83E+08	-9.83E+08	1.97E+09
0.9	1.97E+07	-1.45E+09	1.61E+05	-7.89E+08	9.98E+08	-9.98E+08	2.02E+09
1	1.62E+06	-1.47E+09	2.36E+06	-8.08E+08	1.01E+09	-1.01E+09	2.07E+09
1.1	-1.88E+07	-1.50E+09	3.95E+06	-8.27E+08	1.02E+09	-1.02E+09	2.11E+09
1.2	-2.65E+07	-1.55E+09	5.59E+06	-8.44E+08	1.03E+09	-1.03E+09	2.15E+09
1.3	-2.05E+07	-1.60E+09	7.12E+06	-8.59E+08	1.04E+09	-1.04E+09	2.18E+09
1.4	-1.40E+07	-1.64E+09	1.04E+07	-8.73E+08	1.05E+09	-1.05E+09	2.22E+09
1.5	-7.49E+06	-1.68E+09	1.39E+07	-8.85E+08	1.06E+09	-1.06E+09	2.25E+09
2	1.92E+07	-1.79E+09	2.48E+07	-9.19E+08	1.09E+09	-1.09E+09	2.34E+09

n	x11 Bottom (max)	x11 Bottom (min)	x22 Bottom (max)	x22 Bottom (min)	x12 Bottom (max)	x12 Bottom (min)	Bottom Mises (max)
0	4.03E+08	-1.52E+09	5.68E+07	-7.70E+08	7.22E+08	-7.22E+08	1.70E+09
0.2	3.38E+08	-1.61E+09	6.00E+07	-8.07E+08	8.02E+08	-8.02E+08	1.86E+09
0.5	2.34E+08	-1.72E+09	5.74E+07	-8.32E+08	8.84E+08	-8.84E+08	2.01E+09
0.8	1.32E+08	-1.79E+09	5.07E+07	-8.37E+08	9.37E+08	-9.37E+08	2.09E+09
0.9	9.82E+07	-1.80E+09	4.80E+07	-8.35E+08	9.50E+08	-9.50E+08	2.11E+09
1	6.55E+07	-1.82E+09	4.53E+07	-8.33E+08	9.62E+08	-9.62E+08	2.13E+09
1.1	4.32E+07	-1.83E+09	4.19E+07	-8.28E+08	9.72E+08	-9.72E+08	2.14E+09
1.2	3.32E+07	-1.85E+09	3.85E+07	-8.23E+08	9.81E+08	-9.81E+08	2.14E+09
1.3	2.34E+07	-1.86E+09	3.49E+07	-8.20E+08	9.89E+08	-9.89E+08	2.15E+09
1.4	1.40E+07	-1.86E+09	3.14E+07	-8.22E+08	9.96E+08	-9.96E+08	2.15E+09
1.5	5.63E+06	-1.87E+09	2.81E+07	-8.23E+08	1.00E+09	-1.00E+09	2.15E+09
2	-1.58E+07	-1.89E+09	2.71E+07	-8.27E+08	1.03E+09	-1.03E+09	2.16E+09

n	Center Deflection	Top Yield Count	Top Ultimate Count	Bottom Yield Count	Bottom Ultimate Count	Total Yield Count	Total Ultimate Count
0	0.0055084	56	52	82	82	138	134
0.2	0.0044675	86	86	82	82	168	168
0.5	0.0030203	86	86	82	82	168	168
0.8	0.0017035	86	86	82	82	168	168
0.9	0.0012835	86	86	82	82	168	168
1	0.0008774	86	86	86	82	172	168
1.1	0.000451	86	86	86	82	172	168
1.2	3.532E-05	86	86	86	82	172	168
1.3	-0.0003715	86	86	86	82	172	168
1.4	-0.0007576	86	86	86	82	172	168
1.5	-0.0011048	86	86	86	82	172	168
2	-0.0021692	86	86	86	82	172	168

0.10" Zi-Ti (No Taper)

n	x11 Top (max)	x11 Top (min)	x22 Top (max)	x22 Top (min)	x12 Top (max)	x12 Top (min)	Top Mises (max)
0	7.65E+08	-7.49E+08	3.07E+07	-5.07E+08	4.16E+08	-4.16E+08	9.20E+08
0.2	7.63E+08	-7.30E+08	1.74E+07	-5.03E+08	3.91E+08	-3.91E+08	8.93E+08
0.5	7.58E+08	-7.11E+08	4.12E+06	-4.98E+08	3.75E+08	-3.75E+08	8.67E+08
0.8	7.54E+08	-6.98E+08	2.61E+06	-4.95E+08	3.65E+08	-3.65E+08	8.57E+08
0.9	7.53E+08	-6.95E+08	3.51E+06	-4.95E+08	3.62E+08	-3.62E+08	8.55E+08
1	7.52E+08	-6.91E+08	4.30E+06	-4.94E+08	3.60E+08	-3.60E+08	8.54E+08
1.1	7.52E+08	-6.89E+08	5.02E+06	-4.93E+08	3.58E+08	-3.58E+08	8.53E+08
1.2	7.51E+08	-6.86E+08	5.63E+06	-4.93E+08	3.56E+08	-3.56E+08	8.52E+08
1.3	7.50E+08	-6.84E+08	6.18E+06	-4.92E+08	3.54E+08	-3.54E+08	8.51E+08
1.4	7.49E+08	-6.82E+08	6.68E+06	-4.92E+08	3.53E+08	-3.53E+08	8.50E+08
1.5	7.48E+08	-6.79E+08	7.12E+06	-4.91E+08	3.51E+08	-3.51E+08	8.49E+08
2	7.45E+08	-6.71E+08	8.85E+06	-4.89E+08	3.45E+08	-3.45E+08	8.45E+08

n	x11 Bottom (max)	x11 Bottom (min)	x22 Bottom (max)	x22 Bottom (min)	x12 Bottom (max)	x12 Bottom (min)	Bottom Mises (max)
0	6.66E+08	-1.12E+09	2.11E+08	-6.47E+08	4.69E+08	-4.69E+08	1.26E+09
0.2	6.28E+08	-1.09E+09	1.94E+08	-6.42E+08	4.49E+08	-4.49E+08	1.22E+09
0.5	5.92E+08	-1.06E+09	1.77E+08	-6.37E+08	4.30E+08	-4.30E+08	1.18E+09
0.8	5.68E+08	-1.04E+09	1.66E+08	-6.34E+08	4.20E+08	-4.20E+08	1.16E+09
0.9	5.62E+08	-1.04E+09	1.63E+08	-6.33E+08	4.17E+08	-4.17E+08	1.16E+09
1	5.56E+08	-1.03E+09	1.60E+08	-6.32E+08	4.15E+08	-4.15E+08	1.15E+09
1.1	5.52E+08	-1.03E+09	1.58E+08	-6.32E+08	4.13E+08	-4.13E+08	1.15E+09
1.2	5.47E+08	-1.02E+09	1.55E+08	-6.31E+08	4.11E+08	-4.11E+08	1.14E+09
1.3	5.43E+08	-1.02E+09	1.53E+08	-6.31E+08	4.10E+08	-4.10E+08	1.14E+09
1.4	5.39E+08	-1.02E+09	1.51E+08	-6.30E+08	4.08E+08	-4.08E+08	1.13E+09
1.5	5.36E+08	-1.02E+09	1.50E+08	-6.30E+08	4.07E+08	-4.07E+08	1.13E+09
2	5.22E+08	-1.01E+09	1.42E+08	-6.28E+08	4.02E+08	-4.02E+08	1.12E+09

n	Center Deflection	Top Yield Count	Top Ultimate Count	Bottom Yield Count	Bottom Ultimate Count	Total Yield Count	Total Ultimate Count
0	0.012371	74	74	147	119	221	193
0.2	0.012198	74	74	131	97	205	171
0.5	0.012027	74	74	101	86	175	160
0.8	0.011905	74	74	97	86	171	160
0.9	0.011876	74	74	95	86	169	160
1	0.011849	74	74	93	86	167	160
1.1	0.01182	74	74	91	86	165	160
1.2	0.011799	74	74	89	86	163	160
1.3	0.011778	74	74	86	86	160	160
1.4	0.011759	74	74	86	86	160	160
1.5	0.011742	74	74	86	86	160	160
2	0.011669	74	74	86	86	160	160

0.20" Zi-Ti (No Taper)

n	x11 Top (max)	x11 Top (min)	x22 Top (max)	x22 Top (min)	x12 Top (max)	x12 Top (min)	Top Mises (max)
0	6.52E+08	-8.31E+08	6.08E+07	-5.22E+08	6.14E+08	-6.14E+08	1.12E+09
0.2	6.69E+08	-8.02E+08	5.05E+07	-5.16E+08	5.70E+08	-5.70E+08	1.05E+09
0.5	6.81E+08	-7.73E+08	3.94E+07	-5.09E+08	5.27E+08	-5.27E+08	1.00E+09
0.8	6.86E+08	-7.52E+08	3.14E+07	-5.03E+08	4.99E+08	-4.99E+08	9.71E+08
0.9	6.87E+08	-7.47E+08	2.92E+07	-5.02E+08	4.92E+08	-4.92E+08	9.63E+08
1	6.87E+08	-7.44E+08	2.73E+07	-5.02E+08	4.87E+08	-4.87E+08	9.60E+08
1.1	6.87E+08	-7.38E+08	2.54E+07	-5.00E+08	4.81E+08	-4.81E+08	9.51E+08
1.2	6.87E+08	-7.34E+08	2.37E+07	-4.99E+08	4.76E+08	-4.76E+08	9.45E+08
1.3	6.87E+08	-7.30E+08	2.21E+07	-4.98E+08	4.71E+08	-4.71E+08	9.40E+08
1.4	6.86E+08	-7.27E+08	2.07E+07	-4.97E+08	4.67E+08	-4.67E+08	9.36E+08
1.5	6.86E+08	-7.24E+08	1.93E+07	-4.97E+08	4.64E+08	-4.64E+08	9.32E+08
2	6.83E+08	-7.11E+08	1.38E+07	-4.93E+08	4.50E+08	-4.50E+08	9.15E+08

n	x11 Bottom (max)	x11 Bottom (min)	x22 Bottom (max)	x22 Bottom (min)	x12 Bottom (max)	x12 Bottom (min)	Bottom Mises (max)
0	7.90E+08	-1.36E+09	2.23E+08	-7.17E+08	6.35E+08	-6.35E+08	1.54E+09
0.2	7.39E+08	-1.31E+09	2.02E+08	-7.01E+08	5.99E+08	-5.99E+08	1.48E+09
0.5	6.90E+08	-1.27E+09	1.81E+08	-6.91E+08	5.64E+08	-5.64E+08	1.43E+09
0.8	6.57E+08	-1.24E+09	1.66E+08	-6.85E+08	5.43E+08	-5.43E+08	1.40E+09
0.9	6.49E+08	-1.24E+09	1.62E+08	-6.83E+08	5.38E+08	-5.38E+08	1.39E+09
1	6.41E+08	-1.23E+09	1.59E+08	-6.81E+08	5.32E+08	-5.32E+08	1.38E+09
1.1	6.34E+08	-1.23E+09	1.56E+08	-6.80E+08	5.28E+08	-5.28E+08	1.38E+09
1.2	6.28E+08	-1.22E+09	1.53E+08	-6.79E+08	5.24E+08	-5.24E+08	1.37E+09
1.3	6.22E+08	-1.22E+09	1.51E+08	-6.78E+08	5.20E+08	-5.20E+08	1.36E+09
1.4	6.17E+08	-1.21E+09	1.48E+08	-6.77E+08	5.17E+08	-5.17E+08	1.36E+09
1.5	6.12E+08	-1.21E+09	1.46E+08	-6.77E+08	5.14E+08	-5.14E+08	1.35E+09
2	5.93E+08	-1.20E+09	1.37E+08	-6.73E+08	5.02E+08	-5.02E+08	1.34E+09

n	Center Deflection	Top Yield Count	Top Ultimate Count	Bottom Yield Count	Bottom Ultimate Count	Total Yield Count	Total Ultimate Count
0	0.011928	78	78	195	149	273	227
0.2	0.011723	78	74	169	141	247	215
0.5	0.01151	74	74	145	131	219	205
0.8	0.01136	74	74	137	117	211	191
0.9	0.01132	74	74	135	107	209	181
1	0.011283	74	74	131	97	205	171
1.1	0.011248	74	74	131	95	205	169
1.2	0.011217	74	74	131	95	205	169
1.3	0.011188	74	74	125	93	199	167
1.4	0.011162	74	74	125	91	199	165
1.5	0.011137	74	74	125	91	199	165
2	0.011035	74	74	111	82	185	156

0.50" Zi-Ti (No Taper)

n	X11 Top (max)	x11 Top (min)	x22 Top (max)	x22 Top (min)	x12 Top (max)	x12 Top (min)	Top Mises (max)
0	2.28E+08	-1.55E+09	6.06E+07	-7.35E+08	1.18E+09	-1.18E+09	2.28E+09
0.2	2.78E+08	-1.42E+09	6.20E+07	-6.81E+08	1.08E+09	-1.08E+09	2.03E+09
0.5	2.90E+08	-1.32E+09	5.92E+07	-6.52E+08	9.84E+08	-9.84E+08	1.82E+09
0.8	2.85E+08	-1.25E+09	5.49E+07	-6.36E+08	9.27E+08	-9.27E+08	1.70E+09
0.9	2.82E+08	-1.24E+09	5.34E+07	-6.32E+08	9.12E+08	-9.12E+08	1.68E+09
1	2.80E+08	-1.23E+09	5.19E+07	-6.29E+08	9.00E+08	-9.00E+08	1.65E+09
1.1	2.77E+08	-1.22E+09	5.05E+07	-6.26E+08	8.89E+08	-8.89E+08	1.63E+09
1.2	2.74E+08	-1.21E+09	4.90E+07	-6.23E+08	8.79E+08	-8.79E+08	1.61E+09
1.3	2.71E+08	-1.20E+09	4.76E+07	-6.21E+08	8.70E+08	-8.70E+08	1.59E+09
1.4	2.69E+08	-1.19E+09	4.63E+07	-6.19E+08	8.62E+08	-8.62E+08	1.57E+09
1.5	2.66E+08	-1.18E+09	4.50E+07	-6.18E+08	8.54E+08	-8.54E+08	1.56E+09
2	2.54E+08	-1.16E+09	3.91E+07	-6.11E+08	8.27E+08	-8.27E+08	1.51E+09

n	x11 Bottom (max)	x11 Bottom (min)	x22 Bottom (max)	x22 Bottom (min)	x12 Bottom (max)	x12 Bottom (min)	Bottom Mises (max)
0	4.01E+08	-1.90E+09	7.58E+07	-9.41E+08	1.14E+09	-1.14E+09	2.55E+09
0.2	5.01E+08	-1.79E+09	8.44E+07	-9.04E+08	1.06E+09	-1.06E+09	2.39E+09
0.5	5.40E+08	-1.71E+09	9.37E+07	-8.66E+08	9.83E+08	-9.83E+08	2.23E+09
0.8	5.45E+08	-1.66E+09	9.29E+07	-8.42E+08	9.34E+08	-9.34E+08	2.13E+09
0.9	5.44E+08	-1.65E+09	9.18E+07	-8.36E+08	9.21E+08	-9.21E+08	2.10E+09
1	5.43E+08	-1.64E+09	9.06E+07	-8.31E+08	9.10E+08	-9.10E+08	2.08E+09
1.1	5.41E+08	-1.63E+09	8.91E+07	-8.27E+08	9.00E+08	-9.00E+08	2.06E+09
1.2	5.39E+08	-1.62E+09	8.77E+07	-8.23E+08	8.91E+08	-8.91E+08	2.04E+09
1.3	5.36E+08	-1.62E+09	8.61E+07	-8.19E+08	8.83E+08	-8.83E+08	2.02E+09
1.4	5.34E+08	-1.61E+09	8.47E+07	-8.16E+08	8.75E+08	-8.75E+08	2.00E+09
1.5	5.32E+08	-1.60E+09	8.30E+07	-8.14E+08	8.69E+08	-8.69E+08	1.99E+09
2	5.19E+08	-1.59E+09	7.53E+07	-8.04E+08	8.42E+08	-8.42E+08	1.94E+09

n	Center Deflection	Top Yield Count	Top Ultimate Count	Bottom Yield Count	Bottom Ultimate Count	Total Yield Count	Total Ultimate Count
0	0.0042201	86	86	86	86	172	172
0.2	0.0055952	86	86	86	82	172	168
0.5	0.0062969	80	76	82	82	162	158
0.8	0.0065237	72	64	82	82	154	146
0.9	0.0065597	68	60	82	82	150	142
1	0.0065834	68	60	82	82	150	142
1.1	0.0065979	68	60	82	82	150	142
1.2	0.0066052	64	60	82	82	146	142
1.3	0.0066071	64	60	82	82	146	142
1.4	0.0066161	64	56	82	82	146	138
1.5	0.0066085	60	56	82	82	142	138
2	0.0065491	60	56	82	82	142	138

0.10" A286-Ti (No Taper)

n	x11 Top (max)	x11 Top (min)	x22 Top (max)	x22 Top (min)	x12 Top (max)	x12 Top (min)	Top Mises (max)
0	7.20E+08	-1.78E+09	3.24E+08	-9.28E+08	5.30E+08	-5.30E+08	1.55E+09
0.2	4.76E+08	-1.49E+09	3.07E+08	-8.24E+08	6.29E+08	-6.29E+08	1.50E+09
0.5	7.86E+08	-9.07E+08	1.74E+08	-5.44E+08	5.18E+08	-5.18E+08	1.08E+09
0.8	7.83E+08	-8.57E+08	1.38E+08	-5.32E+08	4.72E+08	-4.72E+08	1.02E+09
0.9	7.81E+08	-8.45E+08	1.28E+08	-5.29E+08	4.60E+08	-4.60E+08	1.01E+09
1	7.80E+08	-8.34E+08	1.20E+08	-5.27E+08	4.50E+08	-4.50E+08	9.95E+08
1.1	7.79E+08	-8.25E+08	1.12E+08	-5.24E+08	4.41E+08	-4.41E+08	9.83E+08
1.2	7.78E+08	-8.17E+08	1.05E+08	-5.23E+08	4.34E+08	-4.34E+08	9.76E+08
1.3	7.76E+08	-8.09E+08	9.88E+07	-5.21E+08	4.27E+08	-4.27E+08	9.66E+08
1.4	7.75E+08	-8.01E+08	9.28E+07	-5.19E+08	4.20E+08	-4.20E+08	9.58E+08
1.5	7.74E+08	-7.93E+08	8.71E+07	-5.17E+08	4.13E+08	-4.13E+08	9.47E+08
2	7.69E+08	-7.66E+08	6.49E+07	-5.11E+08	3.96E+08	-3.96E+08	9.15E+08

n	x11 Bottom (max)	x11 Bottom (min)	x22 Bottom (max)	x22 Bottom (min)	x12 Bottom (max)	x12 Bottom (min)	Bottom Mises (max)
0	1.13E+09	-1.36E+09	1.49E+09	-1.20E+09	5.28E+08	-5.28E+08	1.41E+09
0.2	1.50E+09	-1.07E+09	1.57E+08	-6.14E+08	4.54E+08	-4.54E+08	1.52E+09
0.5	9.20E+08	-1.24E+09	3.82E+08	-6.52E+08	5.41E+08	-5.41E+08	1.40E+09
0.8	8.38E+08	-1.18E+09	3.38E+08	-6.44E+08	5.09E+08	-5.09E+08	1.33E+09
0.9	8.17E+08	-1.17E+09	3.26E+08	-6.43E+08	5.00E+08	-5.00E+08	1.32E+09
1	7.98E+08	-1.16E+09	3.15E+08	-6.42E+08	4.92E+08	-4.92E+08	1.30E+09
1.1	7.81E+08	-1.15E+09	3.05E+08	-6.41E+08	4.86E+08	-4.86E+08	1.29E+09
1.2	7.66E+08	-1.14E+09	2.97E+08	-6.41E+08	4.78E+08	-4.78E+08	1.28E+09
1.3	7.52E+08	-1.13E+09	2.89E+08	-6.40E+08	4.73E+08	-4.73E+08	1.27E+09
1.4	7.40E+08	-1.12E+09	2.81E+08	-6.39E+08	4.68E+08	-4.68E+08	1.26E+09
1.5	7.28E+08	-1.11E+09	2.74E+08	-6.39E+08	4.64E+08	-4.64E+08	1.25E+09
2	6.81E+08	-1.08E+09	2.47E+08	-6.36E+08	4.46E+08	-4.46E+08	1.21E+09

n	Center Deflection	Top Yield Count	Top Ultimate Count	Bottom Yield Count	Bottom Ultimate Count	Total Yield Count	Total Ultimate Count
0	0.00631	78	78	295	271	373	349
0.2	-0.018011	90	90	90	86	180	176
0.5	0.013781	78	74	231	211	309	285
0.8	0.01341	74	74	205	167	279	241
0.9	0.013311	74	74	189	163	263	237
1	0.013218	74	74	171	159	245	233
1.1	0.013133	74	74	167	159	241	233
1.2	0.013059	74	74	167	157	241	231
1.3	0.01299	74	74	167	153	241	227
1.4	0.012925	74	74	163	153	237	227
1.5	0.012868	74	74	163	147	237	221
2	0.012626	74	74	147	127	221	201

0.20" A286-Ti (No Taper)

n	x11 Top (max)	x11 Top (min)	x22 Top (max)	x22 Top (min)	x12 Top (max)	x12 Top (min)	Top Mises (max)
0	8.76E+08	-2.13E+09	4.46E+08	-1.00E+09	1.03E+09	-1.03E+09	2.56E+09
0.2	4.69E+08	-1.69E+09	2.49E+08	-9.03E+08	9.12E+08	-9.12E+08	2.10E+09
0.5	8.02E+08	-1.07E+09	2.41E+08	-5.82E+08	7.63E+08	-7.63E+08	1.36E+09
0.8	4.94E+08	-1.55E+09	1.74E+08	-8.44E+08	7.55E+08	-7.55E+08	1.80E+09
0.9	8.05E+08	-9.90E+08	1.97E+08	-5.62E+08	6.68E+08	-6.68E+08	1.23E+09
1	8.04E+08	-9.75E+08	1.88E+08	-5.59E+08	6.51E+08	-6.51E+08	1.21E+09
1.1	8.03E+08	-9.61E+08	1.80E+08	-5.55E+08	6.36E+08	-6.36E+08	1.19E+09
1.2	8.01E+08	-9.48E+08	1.72E+08	-5.52E+08	6.23E+08	-6.23E+08	1.17E+09
1.3	7.99E+08	-9.37E+08	1.65E+08	-5.50E+08	6.11E+08	-6.11E+08	1.16E+09
1.4	7.98E+08	-9.25E+08	1.59E+08	-5.47E+08	5.99E+08	-5.99E+08	1.14E+09
1.5	7.95E+08	-9.14E+08	1.53E+08	-5.44E+08	5.88E+08	-5.88E+08	1.13E+09
2	7.84E+08	-8.74E+08	1.28E+08	-5.34E+08	5.50E+08	-5.50E+08	1.08E+09

n	x11 Bottom (max)	x11 Bottom (min)	x22 Bottom (max)	x22 Bottom (min)	x12 Bottom (max)	x12 Bottom (min)	Bottom Mises (max)
0	1.51E+09	-1.48E+09	9.83E+08	-8.27E+08	9.58E+08	-9.58E+08	1.77E+09
0.2	1.48E+09	-1.27E+09	1.94E+08	-6.54E+08	6.83E+08	-6.83E+08	1.61E+09
0.5	1.11E+09	-1.49E+09	4.53E+08	-7.50E+08	7.76E+08	-7.76E+08	1.76E+09
0.8	1.25E+09	-1.06E+09	1.24E+08	-5.95E+08	5.82E+08	-5.82E+08	1.35E+09
0.9	9.81E+08	-1.39E+09	3.82E+08	-7.23E+08	7.02E+08	-7.02E+08	1.62E+09
1	9.57E+08	-1.38E+09	3.69E+08	-7.20E+08	6.88E+08	-6.88E+08	1.60E+09
1.1	9.35E+08	-1.36E+09	3.56E+08	-7.18E+08	6.76E+08	-6.76E+08	1.58E+09
1.2	9.16E+08	-1.35E+09	3.45E+08	-7.15E+08	6.65E+08	-6.65E+08	1.56E+09
1.3	8.98E+08	-1.34E+09	3.35E+08	-7.13E+08	6.55E+08	-6.55E+08	1.54E+09
1.4	8.81E+08	-1.33E+09	3.25E+08	-7.11E+08	6.46E+08	-6.46E+08	1.53E+09
1.5	8.65E+08	-1.32E+09	3.17E+08	-7.10E+08	6.39E+08	-6.39E+08	1.52E+09
2	8.05E+08	-1.28E+09	2.84E+08	-7.02E+08	6.06E+08	-6.06E+08	1.47E+09

n	Center Deflection	Top Yield Count	Top Ultimate Count	Bottom Yield Count	Bottom Ultimate Count	Total Yield Count	Total Ultimate Count
0	0.015446	94	86	333	325	427	411
0.2	-0.017982	90	90	177	177	267	267
0.5	0.01387	78	78	277	239	355	317
0.8	-0.017056	86	86	235	173	321	259
0.9	0.013286	78	78	239	231	317	309
1	0.013172	78	78	235	231	313	309
1.1	0.013068	78	78	235	227	313	305
1.2	0.012971	78	78	235	219	313	297
1.3	0.012882	78	78	231	219	309	297
1.4	0.012806	78	78	231	215	309	293
1.5	0.012723	78	74	227	209	305	283
2	0.012404	74	74	211	181	285	255

0.50" A286-Ti (No Taper)

n	x11 Top (max)	x11 Top (min)	x22 Top (max)	x22 Top (min)	x12 Top (max)	x12 Top (min)	Top Mises (max)
0	5.85E+08	-2.41E+09	3.35E+08	-1.18E+09	2.07E+09	-2.07E+09	4.15E+09
0.2	7.05E+08	-2.94E+09	3.98E+08	-1.29E+09	1.75E+09	-1.75E+09	3.24E+09
0.5	7.22E+08	-1.80E+09	3.40E+08	-7.85E+08	1.42E+09	-1.42E+09	2.57E+09
0.8	6.55E+08	-1.66E+09	3.13E+08	-7.39E+08	1.26E+09	-1.26E+09	2.28E+09
0.9	6.35E+08	-1.62E+09	3.04E+08	-7.30E+08	1.22E+09	-1.22E+09	2.21E+09
1	6.18E+08	-1.59E+09	2.97E+08	-7.22E+08	1.19E+09	-1.19E+09	2.14E+09
1.1	6.01E+08	-1.56E+09	2.89E+08	-7.15E+08	1.16E+09	-1.16E+09	2.09E+09
1.2	5.86E+08	-1.54E+09	2.82E+08	-7.08E+08	1.13E+09	-1.13E+09	2.04E+09
1.3	5.72E+08	-1.52E+09	2.75E+08	-7.02E+08	1.11E+09	-1.11E+09	2.00E+09
1.4	5.59E+08	-1.50E+09	2.68E+08	-6.98E+08	1.09E+09	-1.09E+09	1.96E+09
1.5	5.47E+08	-1.48E+09	2.61E+08	-6.93E+08	1.07E+09	-1.07E+09	1.93E+09
2	4.97E+08	-1.41E+09	2.32E+08	-6.74E+08	9.98E+08	-9.98E+08	1.79E+09

n	x11 Bottom (max)	x11 Bottom (min)	x22 Bottom (max)	x22 Bottom (min)	x12 Bottom (max)	x12 Bottom (min)	Bottom Mises (max)
0	9.40E+08	-2.90E+09	4.84E+08	-1.26E+09	1.95E+09	-1.95E+09	4.15E+09
0.2	9.92E+08	-2.57E+09	4.80E+08	-1.16E+09	1.68E+09	-1.68E+09	3.67E+09
0.5	1.15E+09	-2.21E+09	4.29E+08	-1.02E+09	1.43E+09	-1.43E+09	3.13E+09
0.8	1.07E+09	-2.03E+09	4.04E+08	-9.69E+08	1.30E+09	-1.30E+09	2.85E+09
0.9	1.04E+09	-1.99E+09	3.96E+08	-9.56E+08	1.27E+09	-1.27E+09	2.79E+09
1	1.02E+09	-1.95E+09	3.88E+08	-9.44E+08	1.24E+09	-1.24E+09	2.73E+09
1.1	9.98E+08	-1.92E+09	3.80E+08	-9.34E+08	1.21E+09	-1.21E+09	2.67E+09
1.2	9.77E+08	-1.89E+09	3.71E+08	-9.24E+08	1.19E+09	-1.19E+09	2.62E+09
1.3	9.58E+08	-1.86E+09	3.63E+08	-9.16E+08	1.16E+09	-1.16E+09	2.58E+09
1.4	9.41E+08	-1.83E+09	3.56E+08	-9.08E+08	1.14E+09	-1.14E+09	2.54E+09
1.5	9.23E+08	-1.81E+09	3.48E+08	-9.01E+08	1.13E+09	-1.13E+09	2.50E+09
2	8.51E+08	-1.72E+09	3.14E+08	-8.74E+08	1.06E+09	-1.06E+09	2.36E+09

n	Center Deflection	Top Yield Count	Top Ultimate Count	Bottom Yield Count	Bottom Ultimate Count	Total Yield Count	Total Ultimate Count
0	0.0062177	90	90	133	121	223	211
0.2	-0.0056904	96	86	117	104	213	190
0.5	0.010141	99	74	305	293	404	367
0.8	0.01003	68	68	305	285	373	353
0.9	0.009973	68	68	301	285	369	353
1	0.0099072	68	68	301	281	369	349
1.1	0.0098436	68	60	297	277	365	337
1.2	0.009767	68	60	293	269	361	329
1.3	0.0096949	68	60	289	257	357	317
1.4	0.0096324	68	60	285	239	353	299
1.5	0.0095572	64	60	281	239	345	299
2	0.0092226	60	60	239	215	299	275

0.10" Ti-A286 (No Taper)

n	x11 Top (max)	x11 Top (min)	x22 Top (max)	x22 Top (min)	x12 Top (max)	x12 Top (min)	Top Mises (max)
0	7.23E+08	-6.22E+08	1.49E+07	-4.77E+08	3.18E+08	-3.18E+08	8.21E+08
0.2	7.06E+08	-6.48E+08	4.31E+06	-4.79E+08	3.58E+08	-3.58E+08	8.13E+08
0.5	6.92E+08	-6.93E+08	6.32E+07	-4.87E+08	4.18E+08	-4.18E+08	8.84E+08
0.8	6.87E+08	-7.33E+08	1.02E+08	-4.96E+08	4.66E+08	-4.66E+08	9.39E+08
0.9	6.87E+08	-7.46E+08	1.12E+08	-4.98E+08	4.79E+08	-4.79E+08	9.54E+08
1	4.76E+08	-1.40E+09	1.93E+08	-7.96E+08	5.26E+08	-5.26E+08	1.33E+09
1.1	6.88E+08	-7.68E+08	1.29E+08	-5.04E+08	5.01E+08	-5.01E+08	9.81E+08
1.2	6.89E+08	-7.78E+08	1.37E+08	-5.06E+08	5.10E+08	-5.10E+08	9.93E+08
1.3	6.90E+08	-7.87E+08	1.43E+08	-5.08E+08	5.18E+08	-5.18E+08	1.00E+09
1.4	6.92E+08	-7.96E+08	1.49E+08	-5.10E+08	5.26E+08	-5.26E+08	1.01E+09
1.5	6.93E+08	-8.05E+08	1.55E+08	-5.12E+08	5.33E+08	-5.33E+08	1.02E+09
2	7.69E+08	-1.67E+09	2.07E+08	-8.89E+08	6.08E+08	-6.08E+08	1.45E+09

n	x11 Bottom (max)	x11 Bottom (min)	x22 Bottom (max)	x22 Bottom (min)	x12 Bottom (max)	x12 Bottom (min)	Bottom Mises (max)
0	4.55E+08	-9.71E+08	1.05E+08	-6.20E+08	3.78E+08	-3.78E+08	1.07E+09
0.2	5.60E+08	-1.07E+09	1.46E+08	-6.27E+08	4.13E+08	-4.13E+08	1.17E+09
0.5	6.86E+08	-1.18E+09	2.06E+08	-6.43E+08	4.56E+08	-4.56E+08	1.29E+09
0.8	7.77E+08	-1.24E+09	2.58E+08	-6.60E+08	4.92E+08	-4.92E+08	1.36E+09
0.9	8.01E+08	-1.26E+09	2.72E+08	-6.64E+08	5.01E+08	-5.01E+08	1.38E+09
1	1.33E+09	-9.19E+08	1.30E+08	-5.73E+08	3.86E+08	-3.86E+08	1.35E+09
1.1	8.42E+08	-1.29E+09	2.97E+08	-6.71E+08	5.17E+08	-5.17E+08	1.41E+09
1.2	8.59E+08	-1.30E+09	3.07E+08	-6.73E+08	5.24E+08	-5.24E+08	1.42E+09
1.3	8.75E+08	-1.31E+09	3.17E+08	-6.76E+08	5.31E+08	-5.31E+08	1.44E+09
1.4	8.90E+08	-1.32E+09	3.26E+08	-6.78E+08	5.36E+08	-5.36E+08	1.45E+09
1.5	9.03E+08	-1.32E+09	3.35E+08	-6.80E+08	5.41E+08	-5.41E+08	1.46E+09
2	7.20E+08	-1.41E+09	9.63E+08	-1.08E+09	5.61E+08	-5.61E+08	1.52E+09

n	Center Deflection	Top Yield Count	Top Ultimate Count	Bottom Yield Count	Bottom Ultimate Count	Total Yield Count	Total Ultimate Count
0	0.011286	74	74	86	82	160	156
0.2	0.011786	74	74	95	82	169	156
0.5	0.012385	74	74	147	127	221	201
0.8	0.012805	74	74	165	153	239	227
0.9	0.012916	74	74	169	157	243	231
1	-0.016827	90	86	123	84	213	170
1.1	0.013108	78	74	171	161	249	235
1.2	0.01319	78	74	201	165	279	239
1.3	0.013265	78	74	209	165	287	239
1.4	0.013334	78	74	219	169	297	243
1.5	0.013397	78	78	219	171	297	249
2	-0.0029289	78	78	241	231	319	309

0.20" Ti-A286 (No Taper)

n	x11 Top (max)	x11 Top (min)	x22 Top (max)	x22 Top (min)	x12 Top (max)	x12 Top (min)	Top Mises (max)
0	6.40E+08	-6.35E+08	6.27E+06	-4.74E+08	3.93E+08	-3.93E+08	8.37E+08
0.2	5.78E+08	-6.78E+08	2.90E+07	-4.80E+08	5.01E+08	-5.01E+08	9.58E+08
0.5	7.02E+07	-1.48E+09	4.98E+07	-8.22E+08	8.15E+08	-8.15E+08	1.58E+09
0.8	2.29E+08	-1.59E+09	8.67E+07	-8.57E+08	9.08E+08	-9.08E+08	1.69E+09
0.9	2.84E+08	-1.62E+09	9.77E+07	-8.66E+08	9.33E+08	-9.33E+08	1.72E+09
1	3.30E+08	-1.64E+09	1.08E+08	-8.74E+08	9.54E+08	-9.54E+08	1.75E+09
1.1	3.68E+08	-1.66E+09	1.17E+08	-8.81E+08	9.74E+08	-9.74E+08	1.78E+09
1.2	4.00E+08	-1.69E+09	1.26E+08	-8.88E+08	9.91E+08	-9.91E+08	1.80E+09
1.3	4.28E+08	-1.71E+09	1.34E+08	-8.94E+08	1.01E+09	-1.01E+09	1.82E+09
1.4	4.51E+08	-1.72E+09	1.42E+08	-9.00E+08	1.02E+09	-1.02E+09	1.84E+09
1.5	4.71E+08	-1.74E+09	1.49E+08	-9.05E+08	1.03E+09	-1.03E+09	1.86E+09
2	4.20E+08	-1.65E+09	1.64E+08	-8.87E+08	8.25E+08	-8.25E+08	1.96E+09

n	x11 Bottom (max)	x11 Bottom (min)	x22 Bottom (max)	x22 Bottom (min)	x12 Bottom (max)	x12 Bottom (min)	Bottom Mises (max)
0	5.05E+08	-1.16E+09	8.35E+07	-6.61E+08	4.50E+08	-4.50E+08	1.27E+09
0.2	6.49E+08	-1.30E+09	1.33E+08	-6.82E+08	5.33E+08	-5.33E+08	1.43E+09
0.5	3.08E+08	-1.94E+09	1.97E+08	-8.71E+08	6.98E+08	-6.98E+08	1.98E+09
0.8	4.66E+08	-2.00E+09	2.80E+08	-8.89E+08	7.78E+08	-7.78E+08	2.07E+09
0.9	5.03E+08	-2.00E+09	2.88E+08	-8.92E+08	8.00E+08	-8.00E+08	2.09E+09
1	5.34E+08	-2.01E+09	2.92E+08	-8.96E+08	8.19E+08	-8.19E+08	2.11E+09
1.1	5.59E+08	-2.02E+09	2.96E+08	-9.05E+08	8.36E+08	-8.36E+08	2.13E+09
1.2	5.80E+08	-2.02E+09	3.03E+08	-9.12E+08	8.51E+08	-8.51E+08	2.14E+09
1.3	5.98E+08	-2.02E+09	3.11E+08	-9.19E+08	8.65E+08	-8.65E+08	2.15E+09
1.4	6.13E+08	-2.03E+09	3.14E+08	-9.25E+08	8.78E+08	-8.78E+08	2.16E+09
1.5	6.26E+08	-2.03E+09	3.20E+08	-9.30E+08	8.89E+08	-8.89E+08	2.18E+09
2	1.46E+09	-1.19E+09	2.05E+08	-6.40E+08	6.09E+08	-6.09E+08	1.57E+09

n	Center Deflection	Top Yield Count	Top Ultimate Count	Bottom Yield Count	Bottom Ultimate Count	Total Yield Count	Total Ultimate Count
0	0.01049	74	74	82	82	156	156
0.2	0.011111	74	74	131	107	205	181
0.5	-0.0022839	86	86	145	106	231	192
0.8	-0.0016459	86	86	166	128	252	214
0.9	-0.001464	86	86	166	140	252	226
1	-0.0013034	86	86	166	140	252	226
1.1	-0.0011646	86	86	168	144	254	230
1.2	-0.0010467	86	86	176	144	262	230
1.3	-0.0009496	86	86	176	144	262	230
1.4	-0.0008558	86	86	180	148	266	234
1.5	-0.0007826	86	86	180	152	266	238
2	-0.017187	90	90	243	177	333	267

0.50" Ti-A286 (No Taper)

n	x11 Top (max)	x11 Top (min)	x22 Top (max)	x22 Top (min)	x12 Top (max)	x12 Top (min)	Top Mises (max)
0	1.70E+08	-1.07E+09	-1.14E+07	-5.89E+08	7.21E+08	-7.21E+08	1.33E+09
0.2	4.27E+07	-1.41E+09	-4.58E+06	-8.01E+08	9.86E+08	-9.86E+08	1.95E+09
0.5	2.80E+08	-2.04E+09	1.30E+08	-1.00E+09	1.13E+09	-1.13E+09	2.61E+09
0.8	3.25E+08	-2.15E+09	1.55E+08	-1.03E+09	1.24E+09	-1.24E+09	2.84E+09
0.9	3.34E+08	-2.18E+09	1.61E+08	-1.04E+09	1.27E+09	-1.27E+09	2.90E+09
1	3.42E+08	-2.21E+09	1.66E+08	-1.05E+09	1.29E+09	-1.29E+09	2.95E+09
1.1	3.49E+08	-2.24E+09	1.71E+08	-1.06E+09	1.32E+09	-1.32E+09	3.00E+09
1.2	3.55E+08	-2.27E+09	1.75E+08	-1.07E+09	1.34E+09	-1.34E+09	3.04E+09
1.3	3.60E+08	-2.29E+09	1.78E+08	-1.07E+09	1.36E+09	-1.36E+09	3.08E+09
1.4	3.65E+08	-2.31E+09	1.82E+08	-1.08E+09	1.38E+09	-1.38E+09	3.12E+09
1.5	3.70E+08	-2.33E+09	1.85E+08	-1.09E+09	1.40E+09	-1.40E+09	3.15E+09
2	3.88E+08	-2.41E+09	1.98E+08	-1.11E+09	1.47E+09	-1.47E+09	3.29E+09

n	x11 Bottom (max)	x11 Bottom (min)	x22 Bottom (max)	x22 Bottom (min)	x12 Bottom (max)	x12 Bottom (min)	Bottom Mises (max)
0	4.03E+08	-1.52E+09	5.68E+07	-7.70E+08	7.22E+08	-7.22E+08	1.70E+09
0.2	1.30E+08	-1.85E+09	6.32E+07	-8.22E+08	9.23E+08	-9.23E+08	2.07E+09
0.5	3.73E+08	-1.75E+09	1.30E+08	-7.90E+08	1.01E+09	-1.01E+09	1.95E+09
0.8	4.71E+08	-1.82E+09	1.69E+08	-8.06E+08	1.08E+09	-1.08E+09	2.03E+09
0.9	4.94E+08	-1.84E+09	1.79E+08	-8.11E+08	1.11E+09	-1.11E+09	2.06E+09
1	5.14E+08	-1.86E+09	1.87E+08	-8.16E+08	1.13E+09	-1.13E+09	2.09E+09
1.1	5.31E+08	-1.88E+09	1.94E+08	-8.21E+08	1.15E+09	-1.15E+09	2.11E+09
1.2	5.46E+08	-1.89E+09	2.00E+08	-8.26E+08	1.17E+09	-1.17E+09	2.13E+09
1.3	5.60E+08	-1.91E+09	2.05E+08	-8.30E+08	1.18E+09	-1.18E+09	2.16E+09
1.4	5.73E+08	-1.92E+09	2.10E+08	-8.34E+08	1.20E+09	-1.20E+09	2.18E+09
1.5	5.84E+08	-1.94E+09	2.14E+08	-8.37E+08	1.21E+09	-1.21E+09	2.21E+09
2	6.28E+08	-2.00E+09	2.28E+08	-8.53E+08	1.27E+09	-1.27E+09	2.32E+09

n	Center Deflection	Top Yield Count	Top Ultimate Count	Bottom Yield Count	Bottom Ultimate Count	Total Yield Count	Total Ultimate Count
0	0.0055084	56	52	82	82	138	134
0.2	0.0007373	86	86	82	82	168	168
0.5	-0.0098404	90	86	295	283	385	369
0.8	-0.011247	90	90	299	287	389	377
0.9	-0.011544	90	90	299	291	389	381
1	-0.011794	90	90	299	291	389	381
1.1	-0.012006	90	90	299	291	389	381
1.2	-0.012189	90	90	299	291	389	381
1.3	-0.012348	90	90	303	291	393	381
1.4	-0.012488	90	90	303	291	393	381
1.5	-0.012612	90	90	303	291	393	381
2	-0.013067	90	90	303	295	393	385

0.10" Ti-Zi (Partial Taper)

n	x11 Top (max)	x11 Top (min)	x22 Top (max)	x22 Top (min)	x12 Top (max)	x12 Top (min)	Top Mises (max)
0	3.52E+08	-6.84E+08	1.30E+07	-4.89E+08	3.17E+08	-3.17E+08	7.98E+08
0.2	3.31E+08	-7.01E+08	7.85E+06	-4.93E+08	3.31E+08	-3.31E+08	8.21E+08
0.5	3.16E+08	-7.19E+08	2.47E+06	-4.97E+08	3.45E+08	-3.45E+08	8.45E+08
0.8	3.08E+08	-7.32E+08	-9.34E+05	-5.01E+08	3.54E+08	-3.54E+08	8.62E+08
0.9	3.06E+08	-7.35E+08	-1.78E+06	-5.02E+08	3.56E+08	-3.56E+08	8.67E+08
1	3.05E+08	-7.39E+08	-2.52E+06	-5.02E+08	3.58E+08	-3.58E+08	8.70E+08
1.1	3.04E+08	-7.40E+08	-3.14E+06	-5.03E+08	3.60E+08	-3.60E+08	8.73E+08
1.2	3.03E+08	-7.44E+08	-3.75E+06	-5.04E+08	3.62E+08	-3.62E+08	8.77E+08
1.3	3.03E+08	-7.46E+08	-3.65E+06	-5.04E+08	3.63E+08	-3.63E+08	8.78E+08
1.4	3.02E+08	-7.48E+08	-2.69E+06	-5.04E+08	3.64E+08	-3.64E+08	8.80E+08
1.5	3.02E+08	-7.50E+08	-1.37E+06	-5.05E+08	3.65E+08	-3.65E+08	8.83E+08
2	3.01E+08	-7.58E+08	3.81E+06	-5.07E+08	3.70E+08	-3.70E+08	8.92E+08

n	x11 Bottom (max)	x11 Bottom (min)	x22 Bottom (max)	x22 Bottom (min)	x12 Bottom (max)	x12 Bottom (min)	Bottom Mises (max)
0	4.89E+08	-9.31E+08	1.12E+08	-6.26E+08	3.66E+08	-3.66E+08	1.03E+09
0.2	5.22E+08	-9.63E+08	1.23E+08	-6.35E+08	3.78E+08	-3.78E+08	1.06E+09
0.5	5.60E+08	-9.93E+08	1.39E+08	-6.43E+08	3.91E+08	-3.91E+08	1.10E+09
0.8	5.86E+08	-1.01E+09	1.50E+08	-6.47E+08	3.98E+08	-3.98E+08	1.12E+09
0.9	5.93E+08	-1.02E+09	1.53E+08	-6.48E+08	4.00E+08	-4.00E+08	1.12E+09
1	5.99E+08	-1.02E+09	1.56E+08	-6.49E+08	4.02E+08	-4.02E+08	1.13E+09
1.1	6.05E+08	-1.02E+09	1.59E+08	-6.50E+08	4.04E+08	-4.04E+08	1.13E+09
1.2	6.10E+08	-1.03E+09	1.61E+08	-6.50E+08	4.05E+08	-4.05E+08	1.13E+09
1.3	6.15E+08	-1.03E+09	1.64E+08	-6.51E+08	4.07E+08	-4.07E+08	1.14E+09
1.4	6.19E+08	-1.03E+09	1.66E+08	-6.52E+08	4.08E+08	-4.08E+08	1.14E+09
1.5	6.23E+08	-1.03E+09	1.68E+08	-6.53E+08	4.09E+08	-4.09E+08	1.14E+09
2	6.39E+08	-1.04E+09	1.76E+08	-6.55E+08	4.13E+08	-4.13E+08	1.15E+09

n	Center Deflection	Top Yield Count	Top Ultimate Count	Bottom Yield Count	Bottom Ultimate Count	Total Yield Count	Total Ultimate Count
0	0.010989	8	8	86	86	94	94
0.2	0.011075	12	8	86	86	98	94
0.5	0.0112	12	8	101	86	113	94
0.8	0.011304	16	8	105	86	121	94
0.9	0.011333	16	8	107	91	123	99
1	0.01136	16	8	107	93	123	101
1.1	0.011385	16	8	113	95	129	103
1.2	0.011406	16	8	119	97	135	105
1.3	0.011424	16	8	123	97	139	105
1.4	0.011443	16	8	127	99	143	107
1.5	0.011461	16	8	127	99	143	107
2	0.011534	16	8	137	101	153	109

0.20" Ti-Zi (Partial Taper)

n	x11 Top (max)	x11 Top (min)	x22 Top (max)	x22 Top (min)	x12 Top (max)	x12 Top (min)	Top Mises (max)
0	1.63E+08	-7.63E+08	1.23E+07	-5.08E+08	3.84E+08	-3.84E+08	9.01E+08
0.2	1.60E+08	-7.91E+08	4.43E+06	-5.15E+08	4.06E+08	-4.06E+08	9.39E+08
0.5	1.61E+08	-8.17E+08	8.60E+05	-5.22E+08	4.26E+08	-4.26E+08	9.74E+08
0.8	1.64E+08	-8.34E+08	8.88E+06	-5.26E+08	4.39E+08	-4.39E+08	9.96E+08
0.9	1.64E+08	-8.38E+08	1.10E+07	-5.27E+08	4.42E+08	-4.42E+08	1.00E+09
1	1.65E+08	-8.42E+08	1.30E+07	-5.28E+08	4.45E+08	-4.45E+08	1.01E+09
1.1	1.66E+08	-8.45E+08	1.48E+07	-5.29E+08	4.47E+08	-4.47E+08	1.01E+09
1.2	1.67E+08	-8.49E+08	1.64E+07	-5.30E+08	4.49E+08	-4.49E+08	1.02E+09
1.3	1.68E+08	-8.52E+08	1.79E+07	-5.30E+08	4.51E+08	-4.51E+08	1.02E+09
1.4	1.69E+08	-8.54E+08	1.93E+07	-5.31E+08	4.53E+08	-4.53E+08	1.02E+09
1.5	1.69E+08	-8.57E+08	2.06E+07	-5.32E+08	4.54E+08	-4.54E+08	1.02E+09
2	1.72E+08	-8.66E+08	2.59E+07	-5.34E+08	4.61E+08	-4.61E+08	1.04E+09

n	x11 Bottom (max)	x11 Bottom (min)	x22 Bottom (max)	x22 Bottom (min)	x12 Bottom (max)	x12 Bottom (min)	Bottom Mises (max)
0	5.06E+08	-1.16E+09	8.06E+07	-7.12E+08	4.20E+08	-4.20E+08	1.19E+09
0.2	5.54E+08	-1.21E+09	9.22E+07	-7.27E+08	4.43E+08	-4.43E+08	1.24E+09
0.5	6.11E+08	-1.25E+09	1.14E+08	-7.41E+08	4.69E+08	-4.69E+08	1.29E+09
0.8	6.51E+08	-1.28E+09	1.31E+08	-7.49E+08	4.84E+08	-4.84E+08	1.31E+09
0.9	6.62E+08	-1.28E+09	1.36E+08	-7.52E+08	4.88E+08	-4.88E+08	1.32E+09
1	6.72E+08	-1.29E+09	1.41E+08	-7.53E+08	4.92E+08	-4.92E+08	1.33E+09
1.1	6.80E+08	-1.29E+09	1.45E+08	-7.55E+08	4.95E+08	-4.95E+08	1.33E+09
1.2	6.88E+08	-1.30E+09	1.48E+08	-7.57E+08	4.98E+08	-4.98E+08	1.33E+09
1.3	6.95E+08	-1.30E+09	1.52E+08	-7.58E+08	5.00E+08	-5.00E+08	1.34E+09
1.4	7.02E+08	-1.31E+09	1.55E+08	-7.59E+08	5.02E+08	-5.02E+08	1.34E+09
1.5	7.08E+08	-1.31E+09	1.58E+08	-7.60E+08	5.04E+08	-5.04E+08	1.34E+09
2	7.31E+08	-1.32E+09	1.70E+08	-7.65E+08	5.12E+08	-5.12E+08	1.35E+09

n	Center Deflection	Top Yield Count	Top Ultimate Count	Bottom Yield Count	Bottom Ultimate Count	Total Yield Count	Total Ultimate Count
0	0.0097475	16	12	86	82	102	94
0.2	0.0098629	16	16	95	82	111	98
0.5	0.010065	20	16	117	93	137	109
0.8	0.010234	20	16	135	101	155	117
0.9	0.010282	20	16	139	109	159	125
1	0.010326	20	20	139	117	159	137
1.1	0.010366	20	20	141	121	161	141
1.2	0.010404	20	20	145	125	165	145
1.3	0.010438	20	20	147	127	167	147
1.4	0.01047	20	20	147	131	167	151
1.5	0.0105	20	20	151	131	171	151
2	0.010621	20	20	157	137	177	157

0.50" Ti-Zi (Partial Taper)

n	x11 Top (max)	x11 Top (min)	x22 Top (max)	x22 Top (min)	x12 Top (max)	x12 Top (min)	Top Mises (max)
0	3.60E+07	-1.17E+09	-1.42E+07	-6.21E+08	5.46E+08	-5.46E+08	1.32E+09
0.2	4.34E+07	-1.22E+09	-1.31E+07	-6.34E+08	5.79E+08	-5.79E+08	1.38E+09
0.5	6.48E+07	-1.26E+09	-1.31E+07	-6.47E+08	6.10E+08	-6.10E+08	1.44E+09
0.8	8.76E+07	-1.28E+09	-8.65E+06	-6.59E+08	6.28E+08	-6.28E+08	1.47E+09
0.9	9.49E+07	-1.29E+09	-7.12E+06	-6.62E+08	6.32E+08	-6.32E+08	1.47E+09
1	1.02E+08	-1.29E+09	-5.60E+06	-6.64E+08	6.36E+08	-6.36E+08	1.48E+09
1.1	1.09E+08	-1.30E+09	-4.10E+06	-6.67E+08	6.39E+08	-6.39E+08	1.48E+09
1.2	1.15E+08	-1.30E+09	-2.62E+06	-6.69E+08	6.42E+08	-6.42E+08	1.49E+09
1.3	1.21E+08	-1.30E+09	-1.18E+06	-6.71E+08	6.45E+08	-6.45E+08	1.49E+09
1.4	1.27E+08	-1.31E+09	2.48E+05	-6.73E+08	6.47E+08	-6.47E+08	1.49E+09
1.5	1.32E+08	-1.31E+09	1.62E+06	-6.74E+08	6.49E+08	-6.49E+08	1.50E+09
2	1.56E+08	-1.32E+09	7.86E+06	-6.80E+08	6.57E+08	-6.57E+08	1.51E+09

n	x11 Bottom (max)	x11 Bottom (min)	x22 Bottom (max)	x22 Bottom (min)	x12 Bottom (max)	x12 Bottom (min)	Bottom Mises (max)
0	2.11E+08	-1.41E+09	1.59E+07	-7.54E+08	5.67E+08	-5.67E+08	1.52E+09
0.2	2.01E+08	-1.47E+09	1.98E+07	-7.61E+08	6.04E+08	-6.04E+08	1.58E+09
0.5	2.16E+08	-1.53E+09	2.42E+07	-7.75E+08	6.40E+08	-6.40E+08	1.65E+09
0.8	2.42E+08	-1.55E+09	2.73E+07	-7.89E+08	6.61E+08	-6.61E+08	1.68E+09
0.9	2.51E+08	-1.56E+09	2.82E+07	-7.93E+08	6.67E+08	-6.67E+08	1.69E+09
1	2.60E+08	-1.57E+09	2.89E+07	-7.98E+08	6.72E+08	-6.72E+08	1.70E+09
1.1	2.69E+08	-1.58E+09	2.96E+07	-8.02E+08	6.76E+08	-6.76E+08	1.70E+09
1.2	2.78E+08	-1.60E+09	3.03E+07	-8.05E+08	6.79E+08	-6.79E+08	1.71E+09
1.3	2.86E+08	-1.61E+09	3.08E+07	-8.09E+08	6.83E+08	-6.83E+08	1.71E+09
1.4	2.94E+08	-1.62E+09	3.12E+07	-8.12E+08	6.86E+08	-6.86E+08	1.72E+09
1.5	3.01E+08	-1.63E+09	3.17E+07	-8.15E+08	6.89E+08	-6.89E+08	1.72E+09
2	3.35E+08	-1.68E+09	3.36E+07	-8.29E+08	6.99E+08	-6.99E+08	1.73E+09

n	Center Deflection	Top Yield Count	Top Ultimate Count	Bottom Yield Count	Bottom Ultimate Count	Total Yield Count	Total Ultimate Count
0	0.0040839	82	82	86	82	168	164
0.2	0.0038258	86	82	86	82	172	164
0.5	0.0038441	86	86	86	82	172	168
0.8	0.0040341	86	86	86	82	172	168
0.9	0.0041107	86	86	86	86	172	172
1	0.0041897	86	86	86	86	172	172
1.1	0.0042696	86	86	86	86	172	172
1.2	0.0043494	86	86	86	86	172	172
1.3	0.0044284	86	86	86	86	172	172
1.4	0.0044816	86	86	86	86	172	172
1.5	0.0045516	86	86	86	86	172	172
2	0.004861	86	86	86	86	172	172

0.10" Zi-Ti (Partial Taper)

n	x11 Top (max)	x11 Top (min)	x22 Top (max)	x22 Top (min)	x12 Top (max)	x12 Top (min)	Top Mises (max)
0	3.08E+08	-8.06E+08	2.81E+07	-5.20E+08	3.90E+08	-3.90E+08	9.40E+08
0.2	3.16E+08	-7.90E+08	1.48E+07	-5.16E+08	3.78E+08	-3.78E+08	9.20E+08
0.5	3.26E+08	-7.71E+08	1.46E+06	-5.12E+08	3.65E+08	-3.65E+08	8.95E+08
0.8	3.33E+08	-7.59E+08	1.88E+06	-5.09E+08	3.57E+08	-3.57E+08	8.80E+08
0.9	3.35E+08	-7.55E+08	2.59E+06	-5.08E+08	3.54E+08	-3.54E+08	8.76E+08
1	3.36E+08	-7.52E+08	3.24E+06	-5.07E+08	3.52E+08	-3.52E+08	8.72E+08
1.1	3.38E+08	-7.49E+08	3.82E+06	-5.06E+08	3.51E+08	-3.51E+08	8.68E+08
1.2	3.39E+08	-7.46E+08	4.35E+06	-5.05E+08	3.49E+08	-3.49E+08	8.65E+08
1.3	3.40E+08	-7.44E+08	4.83E+06	-5.05E+08	3.48E+08	-3.48E+08	8.62E+08
1.4	3.41E+08	-7.41E+08	5.27E+06	-5.04E+08	3.46E+08	-3.46E+08	8.60E+08
1.5	3.42E+08	-7.39E+08	5.66E+06	-5.04E+08	3.45E+08	-3.45E+08	8.57E+08
2	3.45E+08	-7.31E+08	7.20E+06	-5.02E+08	3.40E+08	-3.40E+08	8.48E+08

n	x11 Bottom (max)	x11 Bottom (min)	x22 Bottom (max)	x22 Bottom (min)	x12 Bottom (max)	x12 Bottom (min)	Bottom Mises (max)
0	7.09E+08	-1.06E+09	2.21E+08	-6.63E+08	4.36E+08	-4.36E+08	1.18E+09
0.2	6.70E+08	-1.03E+09	2.04E+08	-6.56E+08	4.20E+08	-4.20E+08	1.15E+09
0.5	6.34E+08	-1.00E+09	1.87E+08	-6.49E+08	4.07E+08	-4.07E+08	1.12E+09
0.8	6.10E+08	-9.88E+08	1.76E+08	-6.45E+08	4.00E+08	-4.00E+08	1.10E+09
0.9	6.03E+08	-9.84E+08	1.73E+08	-6.44E+08	3.98E+08	-3.98E+08	1.10E+09
1	5.98E+08	-9.81E+08	1.70E+08	-6.43E+08	3.96E+08	-3.96E+08	1.10E+09
1.1	5.92E+08	-9.77E+08	1.68E+08	-6.42E+08	3.95E+08	-3.95E+08	1.09E+09
1.2	5.88E+08	-9.75E+08	1.66E+08	-6.41E+08	3.93E+08	-3.93E+08	1.09E+09
1.3	5.83E+08	-9.72E+08	1.63E+08	-6.40E+08	3.92E+08	-3.92E+08	1.09E+09
1.4	5.80E+08	-9.70E+08	1.62E+08	-6.39E+08	3.91E+08	-3.91E+08	1.08E+09
1.5	5.76E+08	-9.67E+08	1.60E+08	-6.39E+08	3.90E+08	-3.90E+08	1.08E+09
2	5.62E+08	-9.59E+08	1.52E+08	-6.36E+08	3.85E+08	-3.85E+08	1.07E+09

n	Center Deflection	Top Yield Count	Top Ultimate Count	Bottom Yield Count	Bottom Ultimate Count	Total Yield Count	Total Ultimate Count
0	0.011912	20	16	161	143	181	159
0.2	0.011765	20	16	147	119	167	135
0.5	0.011625	20	8	137	101	157	109
0.8	0.011535	16	8	119	97	135	105
0.9	0.01151	16	8	107	95	123	103
1	0.011487	16	8	107	93	123	101
1.1	0.011467	12	8	107	91	119	99
1.2	0.011448	12	8	105	86	117	94
1.3	0.011431	12	8	105	86	117	94
1.4	0.011415	12	8	105	86	117	94
1.5	0.0114	12	8	105	86	117	94
2	0.011339	12	8	101	86	113	94

0.20" Zi-Ti (Partial Taper)

n	x11 Top (max)	x11 Top (min)	x22 Top (max)	x22 Top (min)	x12 Top (max)	x12 Top (min)	Top Mises (max)
0	1.95E+08	-9.19E+08	5.69E+07	-5.48E+08	4.86E+08	-4.86E+08	1.09E+09
0.2	1.93E+08	-8.96E+08	4.68E+07	-5.43E+08	4.67E+08	-4.67E+08	1.06E+09
0.5	1.91E+08	-8.73E+08	3.60E+07	-5.37E+08	4.50E+08	-4.50E+08	1.03E+09
0.8	1.89E+08	-8.56E+08	2.82E+07	-5.33E+08	4.38E+08	-4.38E+08	1.00E+09
0.9	1.88E+08	-8.52E+08	2.61E+07	-5.32E+08	4.34E+08	-4.34E+08	9.99E+08
1	1.88E+08	-8.47E+08	2.41E+07	-5.31E+08	4.32E+08	-4.32E+08	9.94E+08
1.1	1.88E+08	-8.43E+08	2.23E+07	-5.29E+08	4.29E+08	-4.29E+08	9.88E+08
1.2	1.88E+08	-8.41E+08	2.06E+07	-5.29E+08	4.26E+08	-4.26E+08	9.84E+08
1.3	1.87E+08	-8.37E+08	1.90E+07	-5.28E+08	4.24E+08	-4.24E+08	9.79E+08
1.4	1.87E+08	-8.33E+08	1.76E+07	-5.27E+08	4.22E+08	-4.22E+08	9.76E+08
1.5	1.86E+08	-8.31E+08	1.62E+07	-5.26E+08	4.21E+08	-4.21E+08	9.73E+08
2	1.84E+08	-8.19E+08	1.11E+07	-5.23E+08	4.14E+08	-4.14E+08	9.60E+08

n	x11 Bottom (max)	x11 Bottom (min)	x22 Bottom (max)	x22 Bottom (min)	x12 Bottom (max)	x12 Bottom (min)	Bottom Mises (max)
0	8.25E+08	-1.38E+09	2.33E+08	-7.83E+08	5.42E+08	-5.42E+08	1.38E+09
0.2	7.72E+08	-1.34E+09	2.11E+08	-7.71E+08	5.19E+08	-5.19E+08	1.34E+09
0.5	7.20E+08	-1.30E+09	1.89E+08	-7.58E+08	4.96E+08	-4.96E+08	1.30E+09
0.8	6.86E+08	-1.28E+09	1.73E+08	-7.49E+08	4.81E+08	-4.81E+08	1.28E+09
0.9	6.77E+08	-1.27E+09	1.69E+08	-7.47E+08	4.77E+08	-4.77E+08	1.27E+09
1	6.69E+08	-1.26E+09	1.65E+08	-7.45E+08	4.74E+08	-4.74E+08	1.27E+09
1.1	6.61E+08	-1.26E+09	1.61E+08	-7.44E+08	4.71E+08	-4.71E+08	1.26E+09
1.2	6.55E+08	-1.25E+09	1.58E+08	-7.42E+08	4.69E+08	-4.69E+08	1.26E+09
1.3	6.49E+08	-1.25E+09	1.55E+08	-7.41E+08	4.66E+08	-4.66E+08	1.25E+09
1.4	6.43E+08	-1.25E+09	1.53E+08	-7.39E+08	4.64E+08	-4.64E+08	1.25E+09
1.5	6.38E+08	-1.24E+09	1.50E+08	-7.38E+08	4.62E+08	-4.62E+08	1.25E+09
2	6.16E+08	-1.23E+09	1.41E+08	-7.34E+08	4.53E+08	-4.53E+08	1.24E+09

n	Center Deflection	Top Yield Count	Top Ultimate Count	Bottom Yield Count	Bottom Ultimate Count	Total Yield Count	Total Ultimate Count
0	0.011223	24	20	173	159	197	179
0.2	0.011031	20	20	163	149	183	169
0.5	0.010844	20	20	153	137	173	157
0.8	0.010714	20	16	145	127	165	143
0.9	0.010678	20	16	145	123	165	139
1	0.010645	20	16	145	117	165	133
1.1	0.010614	20	16	141	113	161	129
1.2	0.010582	20	16	139	103	159	119
1.3	0.010555	20	16	139	101	159	117
1.4	0.01053	20	16	135	101	155	117
1.5	0.010507	20	16	135	101	155	117
2	0.010407	20	16	121	97	141	113

0.50" Zi-Ti (Partial Taper)

n	x11 Top (max)	x11 Top (min)	x22 Top (max)	x22 Top (min)	x12 Top (max)	x12 Top (min)	Top Mises (max)
0	2.80E+08	-1.35E+09	6.18E+07	-7.00E+08	6.82E+08	-6.82E+08	1.54E+09
0.2	2.57E+08	-1.31E+09	6.00E+07	-6.82E+08	6.55E+08	-6.55E+08	1.49E+09
0.5	2.31E+08	-1.27E+09	5.54E+07	-6.63E+08	6.28E+08	-6.28E+08	1.44E+09
0.8	2.11E+08	-1.25E+09	5.04E+07	-6.51E+08	6.11E+08	-6.11E+08	1.41E+09
0.9	2.05E+08	-1.24E+09	4.88E+07	-6.48E+08	6.07E+08	-6.07E+08	1.40E+09
1	1.99E+08	-1.23E+09	4.72E+07	-6.45E+08	6.03E+08	-6.03E+08	1.39E+09
1.1	1.94E+08	-1.23E+09	4.56E+07	-6.42E+08	5.99E+08	-5.99E+08	1.38E+09
1.2	1.89E+08	-1.22E+09	4.41E+07	-6.40E+08	5.96E+08	-5.96E+08	1.38E+09
1.3	1.84E+08	-1.22E+09	4.26E+07	-6.38E+08	5.94E+08	-5.94E+08	1.38E+09
1.4	1.80E+08	-1.22E+09	4.12E+07	-6.37E+08	5.91E+08	-5.91E+08	1.37E+09
1.5	1.75E+08	-1.22E+09	3.98E+07	-6.35E+08	5.89E+08	-5.89E+08	1.37E+09
2	1.57E+08	-1.21E+09	3.37E+07	-6.29E+08	5.80E+08	-5.80E+08	1.35E+09

n	x11 Bottom (max)	x11 Bottom (min)	x22 Bottom (max)	x22 Bottom (min)	x12 Bottom (max)	x12 Bottom (min)	Bottom Mises (max)
0	5.51E+08	-1.91E+09	9.83E+07	-9.13E+08	7.37E+08	-7.37E+08	1.92E+09
0.2	5.15E+08	-1.85E+09	9.62E+07	-9.00E+08	7.04E+08	-7.04E+08	1.86E+09
0.5	4.81E+08	-1.79E+09	8.99E+07	-8.84E+08	6.71E+08	-6.71E+08	1.81E+09
0.8	4.60E+08	-1.74E+09	8.22E+07	-8.70E+08	6.50E+08	-6.50E+08	1.76E+09
0.9	4.54E+08	-1.73E+09	7.96E+07	-8.66E+08	6.45E+08	-6.45E+08	1.75E+09
1	4.47E+08	-1.72E+09	7.70E+07	-8.62E+08	6.40E+08	-6.40E+08	1.74E+09
1.1	4.41E+08	-1.71E+09	7.49E+07	-8.59E+08	6.36E+08	-6.36E+08	1.73E+09
1.2	4.35E+08	-1.70E+09	7.30E+07	-8.56E+08	6.32E+08	-6.32E+08	1.72E+09
1.3	4.29E+08	-1.69E+09	7.11E+07	-8.53E+08	6.29E+08	-6.29E+08	1.71E+09
1.4	4.23E+08	-1.68E+09	6.93E+07	-8.50E+08	6.26E+08	-6.26E+08	1.70E+09
1.5	4.18E+08	-1.67E+09	6.74E+07	-8.47E+08	6.23E+08	-6.23E+08	1.70E+09
2	3.94E+08	-1.63E+09	5.89E+07	-8.35E+08	6.12E+08	-6.12E+08	1.66E+09

n	Center Deflection	Top Yield Count	Top Ultimate Count	Bottom Yield Count	Bottom Ultimate Count	Total Yield Count	Total Ultimate Count
0	0.0065282	86	86	86	86	172	172
0.2	0.0064961	86	82	86	86	172	168
0.5	0.006438	82	82	86	86	168	168
0.8	0.0063206	82	82	86	86	168	168
0.9	0.0062784	82	82	86	86	168	168
1	0.0062354	82	82	86	86	168	168
1.1	0.006192	82	82	86	86	168	168
1.2	0.0061486	82	82	86	86	168	168
1.3	0.0061053	82	82	86	86	168	168
1.4	0.0060625	82	82	86	86	168	168
1.5	0.0060204	82	82	86	86	168	168
2	0.0058232	82	82	86	86	168	168

0.10" A286-Ti (Partial Taper)

n	x11 Top (max)	x11 Top (min)	x22 Top (max)	x22 Top (min)	x12 Top (max)	x12 Top (min)	Top Mises (max)
0	5.59E+08	-9.52E+08	2.87E+08	-5.43E+08	5.29E+08	-5.29E+08	1.16E+09
0.2	5.25E+08	-9.08E+08	2.29E+08	-5.34E+08	4.88E+08	-4.88E+08	1.09E+09
0.5	4.94E+08	-8.66E+08	1.73E+08	-5.26E+08	4.51E+08	-4.51E+08	1.03E+09
0.8	4.75E+08	-8.40E+08	1.37E+08	-5.22E+08	4.28E+08	-4.28E+08	9.93E+08
0.9	4.70E+08	-8.33E+08	1.27E+08	-5.20E+08	4.22E+08	-4.22E+08	9.83E+08
1	4.65E+08	-8.27E+08	1.19E+08	-5.19E+08	4.17E+08	-4.17E+08	9.74E+08
1.1	4.61E+08	-8.21E+08	1.11E+08	-5.18E+08	4.12E+08	-4.12E+08	9.66E+08
1.2	4.57E+08	-8.15E+08	1.03E+08	-5.17E+08	4.07E+08	-4.07E+08	9.59E+08
1.3	4.54E+08	-8.10E+08	9.69E+07	-5.16E+08	4.03E+08	-4.03E+08	9.52E+08
1.4	4.50E+08	-8.06E+08	9.08E+07	-5.15E+08	3.99E+08	-3.99E+08	9.46E+08
1.5	4.47E+08	-8.02E+08	8.52E+07	-5.14E+08	3.96E+08	-3.96E+08	9.40E+08
2	4.35E+08	-7.83E+08	6.25E+07	-5.11E+08	3.82E+08	-3.82E+08	9.15E+08

n	x11 Bottom (max)	x11 Bottom (min)	x22 Bottom (max)	x22 Bottom (min)	x12 Bottom (max)	x12 Bottom (min)	Bottom Mises (max)
0	1.24E+09	-1.37E+09	5.69E+08	-6.79E+08	5.97E+08	-5.97E+08	1.53E+09
0.2	1.10E+09	-1.28E+09	4.81E+08	-6.61E+08	5.51E+08	-5.51E+08	1.43E+09
0.5	9.69E+08	-1.19E+09	4.01E+08	-6.53E+08	5.06E+08	-5.06E+08	1.34E+09
0.8	8.87E+08	-1.14E+09	3.55E+08	-6.49E+08	4.76E+08	-4.76E+08	1.28E+09
0.9	8.66E+08	-1.13E+09	3.42E+08	-6.48E+08	4.69E+08	-4.69E+08	1.26E+09
1	8.47E+08	-1.12E+09	3.31E+08	-6.47E+08	4.63E+08	-4.63E+08	1.25E+09
1.1	8.29E+08	-1.11E+09	3.22E+08	-6.46E+08	4.57E+08	-4.57E+08	1.23E+09
1.2	8.14E+08	-1.10E+09	3.12E+08	-6.45E+08	4.52E+08	-4.52E+08	1.22E+09
1.3	7.99E+08	-1.09E+09	3.04E+08	-6.44E+08	4.47E+08	-4.47E+08	1.21E+09
1.4	7.86E+08	-1.08E+09	2.97E+08	-6.44E+08	4.43E+08	-4.43E+08	1.21E+09
1.5	7.74E+08	-1.07E+09	2.90E+08	-6.43E+08	4.39E+08	-4.39E+08	1.20E+09
2	7.26E+08	-1.04E+09	2.61E+08	-6.41E+08	4.24E+08	-4.24E+08	1.17E+09

n	Center Deflection	Top Yield Count	Top Ultimate Count	Bottom Yield Count	Bottom Ultimate Count	Total Yield Count	Total Ultimate Count
0	0.015128	78	68	269	255	347	323
0.2	0.014452	78	60	251	243	329	303
0.5	0.01381	60	48	235	199	295	247
0.8	0.013386	56	44	199	179	255	223
0.9	0.013273	56	44	181	175	237	219
1	0.013172	56	44	179	167	235	211
1.1	0.013079	52	40	179	167	231	207
1.2	0.012994	52	40	175	163	227	203
1.3	0.012917	52	40	175	163	227	203
1.4	0.012845	52	36	171	163	223	199
1.5	0.012778	48	36	171	157	219	193
2	0.012508	48	20	161	147	209	167

0.20" A286-Ti (Partial Taper)

n	x11 Top (max)	x11 Top (min)	x22 Top (max)	x22 Top (min)	x12 Top (max)	x12 Top (min)	Top Mises (max)
0	5.68E+08	-1.14E+09	3.51E+08	-5.94E+08	6.83E+08	-6.83E+08	1.41E+09
0.2	4.51E+08	-1.09E+09	2.93E+08	-5.83E+08	6.28E+08	-6.28E+08	1.32E+09
0.5	3.45E+08	-1.04E+09	2.42E+08	-5.72E+08	5.75E+08	-5.75E+08	1.24E+09
0.8	2.80E+08	-1.01E+09	2.07E+08	-5.64E+08	5.41E+08	-5.41E+08	1.19E+09
0.9	2.63E+08	-9.96E+08	1.97E+08	-5.62E+08	5.32E+08	-5.32E+08	1.17E+09
1	2.60E+08	-9.87E+08	1.88E+08	-5.60E+08	5.24E+08	-5.24E+08	1.16E+09
1.1	2.57E+08	-9.79E+08	1.79E+08	-5.59E+08	5.17E+08	-5.17E+08	1.15E+09
1.2	2.54E+08	-9.71E+08	1.72E+08	-5.57E+08	5.11E+08	-5.11E+08	1.14E+09
1.3	2.51E+08	-9.64E+08	1.65E+08	-5.56E+08	5.05E+08	-5.05E+08	1.13E+09
1.4	2.48E+08	-9.58E+08	1.58E+08	-5.54E+08	5.00E+08	-5.00E+08	1.12E+09
1.5	2.46E+08	-9.52E+08	1.52E+08	-5.53E+08	4.95E+08	-4.95E+08	1.11E+09
2	2.36E+08	-9.26E+08	1.27E+08	-5.47E+08	4.75E+08	-4.75E+08	1.08E+09

n	x11 Bottom (max)	x11 Bottom (min)	x22 Bottom (max)	x22 Bottom (min)	x12 Bottom (max)	x12 Bottom (min)	Bottom Mises (max)
0	1.56E+09	-1.61E+09	6.84E+08	-8.33E+08	7.95E+08	-7.95E+08	1.81E+09
0.2	1.38E+09	-1.49E+09	5.82E+08	-8.17E+08	7.21E+08	-7.21E+08	1.68E+09
0.5	1.20E+09	-1.43E+09	4.89E+08	-7.99E+08	6.53E+08	-6.53E+08	1.56E+09
0.8	1.09E+09	-1.40E+09	4.28E+08	-7.88E+08	6.10E+08	-6.10E+08	1.49E+09
0.9	1.06E+09	-1.39E+09	4.12E+08	-7.84E+08	5.99E+08	-5.99E+08	1.47E+09
1	1.03E+09	-1.38E+09	3.97E+08	-7.81E+08	5.89E+08	-5.89E+08	1.45E+09
1.1	1.01E+09	-1.37E+09	3.84E+08	-7.79E+08	5.80E+08	-5.80E+08	1.43E+09
1.2	9.85E+08	-1.36E+09	3.72E+08	-7.76E+08	5.72E+08	-5.72E+08	1.42E+09
1.3	9.65E+08	-1.35E+09	3.60E+08	-7.74E+08	5.65E+08	-5.65E+08	1.41E+09
1.4	9.47E+08	-1.35E+09	3.50E+08	-7.72E+08	5.58E+08	-5.58E+08	1.40E+09
1.5	9.30E+08	-1.34E+09	3.40E+08	-7.70E+08	5.52E+08	-5.52E+08	1.39E+09
2	8.62E+08	-1.32E+09	3.02E+08	-7.62E+08	5.28E+08	-5.28E+08	1.35E+09

n	Center Deflection	Top Yield Count	Top Ultimate Count	Bottom Yield Count	Bottom Ultimate Count	Total Yield Count	Total Ultimate Count
0	0.015445	44	40	301	281	345	321
0.2	0.014642	40	36	269	259	309	295
0.5	0.013853	36	32	255	247	291	279
0.8	0.013317	36	32	251	243	287	275
0.9	0.013172	32	24	243	239	275	263
1	0.013039	32	24	243	235	275	259
1.1	0.012917	32	24	243	223	275	247
1.2	0.012804	32	24	239	223	271	247
1.3	0.0127	28	24	239	215	267	239
1.4	0.012602	28	24	239	211	267	235
1.5	0.012512	28	24	231	207	259	231
2	0.012136	24	20	211	169	235	189

0.50" A286-Ti (Partial Taper)

n	x11 Top (max)	x11 Top (min)	x22 Top (max)	x22 Top (min)	x12 Top (max)	x12 Top (min)	Top Mises (max)
0	5.30E+08	-1.51E+09	3.35E+08	-7.14E+08	1.08E+09	-1.08E+09	2.08E+09
0.2	8.77E+08	-1.68E+09	4.00E+08	-7.75E+08	8.95E+08	-8.95E+08	1.95E+09
0.5	7.21E+08	-1.59E+09	3.47E+08	-7.30E+08	8.19E+08	-8.19E+08	1.80E+09
0.8	6.21E+08	-1.53E+09	3.11E+08	-7.10E+08	7.71E+08	-7.71E+08	1.72E+09
0.9	5.93E+08	-1.52E+09	3.02E+08	-7.06E+08	7.57E+08	-7.57E+08	1.69E+09
1	5.69E+08	-1.50E+09	2.94E+08	-7.02E+08	7.46E+08	-7.46E+08	1.68E+09
1.1	5.47E+08	-1.49E+09	2.86E+08	-6.99E+08	7.36E+08	-7.36E+08	1.66E+09
1.2	5.27E+08	-1.48E+09	2.78E+08	-6.97E+08	7.27E+08	-7.27E+08	1.64E+09
1.3	5.09E+08	-1.47E+09	2.71E+08	-6.94E+08	7.18E+08	-7.18E+08	1.63E+09
1.4	4.91E+08	-1.46E+09	2.64E+08	-6.92E+08	7.11E+08	-7.11E+08	1.62E+09
1.5	4.76E+08	-1.45E+09	2.57E+08	-6.90E+08	7.04E+08	-7.04E+08	1.61E+09
2	4.11E+08	-1.42E+09	2.27E+08	-6.82E+08	6.77E+08	-6.77E+08	1.56E+09

n	x11 Bottom (max)	x11 Bottom (min)	x22 Bottom (max)	x22 Bottom (min)	x12 Bottom (max)	x12 Bottom (min)	Bottom Mises (max)
0	2.05E+09	-2.13E+09	7.23E+08	-9.00E+08	9.73E+08	-9.73E+08	2.28E+09
0.2	1.50E+09	-2.72E+09	5.53E+08	-1.15E+09	1.03E+09	-1.03E+09	2.76E+09
0.5	1.27E+09	-2.46E+09	4.75E+08	-1.09E+09	9.22E+08	-9.22E+08	2.52E+09
0.8	1.12E+09	-2.29E+09	4.24E+08	-1.06E+09	8.55E+08	-8.55E+08	2.36E+09
0.9	1.08E+09	-2.25E+09	4.11E+08	-1.05E+09	8.39E+08	-8.39E+08	2.33E+09
1	1.04E+09	-2.21E+09	3.99E+08	-1.04E+09	8.24E+08	-8.24E+08	2.29E+09
1.1	1.01E+09	-2.18E+09	3.87E+08	-1.03E+09	8.11E+08	-8.11E+08	2.26E+09
1.2	9.79E+08	-2.15E+09	3.76E+08	-1.02E+09	7.98E+08	-7.98E+08	2.23E+09
1.3	9.49E+08	-2.12E+09	3.66E+08	-1.01E+09	7.87E+08	-7.87E+08	2.20E+09
1.4	9.23E+08	-2.09E+09	3.56E+08	-1.01E+09	7.78E+08	-7.78E+08	2.18E+09
1.5	8.97E+08	-2.07E+09	3.46E+08	-1.00E+09	7.68E+08	-7.68E+08	2.15E+09
2	7.93E+08	-1.97E+09	3.07E+08	-9.72E+08	7.33E+08	-7.33E+08	2.05E+09

n	Center Deflection	Top Yield Count	Top Ultimate Count	Bottom Yield Count	Bottom Ultimate Count	Total Yield Count	Total Ultimate Count
0	8.286E-05	272	242	355	341	627	583
0.2	0.011917	179	149	309	271	488	420
0.5	0.011062	131	91	267	259	398	350
0.8	0.010433	86	82	255	247	341	329
0.9	0.010251	82	82	255	239	337	321
1	0.010079	82	82	247	235	329	317
1.1	0.009921	82	82	243	227	325	309
1.2	0.0097667	82	82	235	219	317	301
1.3	0.009622	82	82	231	203	313	285
1.4	0.00949	82	82	219	195	301	277
1.5	0.0093562	82	82	215	181	297	263
2	0.0087926	82	82	163	149	245	231

0.10" Ti-A286 (Partial Taper)

n	x11 Top (max)	x11 Top (min)	x22 Top (max)	x22 Top (min)	x12 Top (max)	x12 Top (min)	Top Mises (max)
0	3.52E+08	-6.84E+08	1.30E+07	-4.89E+08	3.17E+08	-3.17E+08	7.98E+08
0.2	3.53E+08	-6.95E+08	1.63E+06	-4.88E+08	3.53E+08	-3.53E+08	8.37E+08
0.5	3.72E+08	-7.14E+08	6.11E+07	-4.88E+08	3.91E+08	-3.91E+08	8.83E+08
0.8	3.92E+08	-7.34E+08	1.01E+08	-4.91E+08	4.17E+08	-4.17E+08	9.19E+08
0.9	3.98E+08	-7.41E+08	1.11E+08	-4.92E+08	4.24E+08	-4.24E+08	9.29E+08
1	4.04E+08	-7.47E+08	1.21E+08	-4.93E+08	4.30E+08	-4.30E+08	9.38E+08
1.1	4.09E+08	-7.53E+08	1.29E+08	-4.94E+08	4.35E+08	-4.35E+08	9.47E+08
1.2	4.15E+08	-7.59E+08	1.36E+08	-4.95E+08	4.40E+08	-4.40E+08	9.54E+08
1.3	4.19E+08	-7.64E+08	1.43E+08	-4.97E+08	4.44E+08	-4.44E+08	9.62E+08
1.4	4.24E+08	-7.69E+08	1.49E+08	-4.98E+08	4.48E+08	-4.48E+08	9.68E+08
1.5	4.28E+08	-7.74E+08	1.55E+08	-4.99E+08	4.52E+08	-4.52E+08	9.75E+08
2	4.46E+08	-7.96E+08	1.77E+08	-5.04E+08	4.66E+08	-4.66E+08	1.00E+09

n	x11 Bottom (max)	x11 Bottom (min)	x22 Bottom (max)	x22 Bottom (min)	x12 Bottom (max)	x12 Bottom (min)	Bottom Mises (max)
0	4.89E+08	-9.31E+08	1.12E+08	-6.26E+08	3.66E+08	-3.66E+08	1.03E+09
0.2	5.95E+08	-1.03E+09	1.55E+08	-6.34E+08	3.96E+08	-3.96E+08	1.13E+09
0.5	7.25E+08	-1.13E+09	2.20E+08	-6.40E+08	4.31E+08	-4.31E+08	1.24E+09
0.8	8.18E+08	-1.20E+09	2.74E+08	-6.44E+08	4.62E+08	-4.62E+08	1.30E+09
0.9	8.42E+08	-1.21E+09	2.88E+08	-6.45E+08	4.70E+08	-4.70E+08	1.32E+09
1	8.64E+08	-1.22E+09	3.02E+08	-6.47E+08	4.77E+08	-4.77E+08	1.33E+09
1.1	8.84E+08	-1.24E+09	3.14E+08	-6.50E+08	4.83E+08	-4.83E+08	1.35E+09
1.2	9.02E+08	-1.25E+09	3.25E+08	-6.53E+08	4.89E+08	-4.89E+08	1.36E+09
1.3	9.18E+08	-1.26E+09	3.35E+08	-6.55E+08	4.94E+08	-4.94E+08	1.37E+09
1.4	9.33E+08	-1.26E+09	3.45E+08	-6.57E+08	4.99E+08	-4.99E+08	1.38E+09
1.5	9.46E+08	-1.27E+09	3.54E+08	-6.59E+08	5.03E+08	-5.03E+08	1.39E+09
2	1.00E+09	-1.30E+09	3.89E+08	-6.65E+08	5.20E+08	-5.20E+08	1.42E+09

n	Center Deflection	Top Yield Count	Top Ultimate Count	Bottom Yield Count	Bottom Ultimate Count	Total Yield Count	Total Ultimate Count
0	0.010989	8	8	86	86	94	94
0.2	0.011515	20	8	107	91	127	99
0.5	0.012199	24	16	161	143	185	159
0.8	0.012693	32	20	177	165	209	185
0.9	0.012825	40	20	177	167	217	187
1	0.012944	40	20	179	173	219	193
1.1	0.013051	44	24	183	173	227	197
1.2	0.013149	44	24	185	173	229	197
1.3	0.013238	52	24	215	175	267	199
1.4	0.013319	52	24	219	175	271	199
1.5	0.013394	52	24	223	183	275	207
2	0.013692	56	40	231	219	287	259

0.20" Ti-A286 (Partial Taper)

n	x11 Top (max)	x11 Top (min)	x22 Top (max)	x22 Top (min)	x12 Top (max)	x12 Top (min)	Top Mises (max)
0	1.63E+08	-7.63E+08	1.23E+07	-5.08E+08	3.84E+08	-3.84E+08	9.01E+08
0.2	1.72E+08	-7.73E+08	2.51E+07	-5.05E+08	4.38E+08	-4.38E+08	9.57E+08
0.5	1.88E+08	-7.99E+08	7.70E+07	-5.06E+08	4.95E+08	-4.95E+08	1.03E+09
0.8	2.62E+08	-8.27E+08	1.14E+08	-5.11E+08	5.32E+08	-5.32E+08	1.08E+09
0.9	2.82E+08	-8.36E+08	1.23E+08	-5.13E+08	5.41E+08	-5.41E+08	1.09E+09
1	2.99E+08	-8.45E+08	1.32E+08	-5.15E+08	5.49E+08	-5.49E+08	1.11E+09
1.1	3.14E+08	-8.54E+08	1.41E+08	-5.17E+08	5.56E+08	-5.56E+08	1.12E+09
1.2	3.28E+08	-8.62E+08	1.48E+08	-5.19E+08	5.63E+08	-5.63E+08	1.13E+09
1.3	3.41E+08	-8.70E+08	1.55E+08	-5.21E+08	5.69E+08	-5.69E+08	1.14E+09
1.4	3.52E+08	-8.78E+08	1.62E+08	-5.23E+08	5.74E+08	-5.74E+08	1.15E+09
1.5	3.63E+08	-8.85E+08	1.68E+08	-5.24E+08	5.79E+08	-5.79E+08	1.16E+09
2	4.03E+08	-9.17E+08	1.92E+08	-5.32E+08	5.98E+08	-5.98E+08	1.19E+09

n	x11 Bottom (max)	x11 Bottom (min)	x22 Bottom (max)	x22 Bottom (min)	x12 Bottom (max)	x12 Bottom (min)	Bottom Mises (max)
0	5.06E+08	-1.16E+09	8.06E+07	-7.12E+08	4.20E+08	-4.20E+08	1.19E+09
0.2	6.64E+08	-1.23E+09	1.34E+08	-7.34E+08	4.82E+08	-4.82E+08	1.34E+09
0.5	8.59E+08	-1.35E+09	2.28E+08	-7.55E+08	5.54E+08	-5.54E+08	1.48E+09
0.8	9.96E+08	-1.42E+09	3.01E+08	-7.69E+08	6.02E+08	-6.02E+08	1.56E+09
0.9	1.03E+09	-1.44E+09	3.21E+08	-7.73E+08	6.14E+08	-6.14E+08	1.59E+09
1	1.06E+09	-1.45E+09	3.40E+08	-7.76E+08	6.24E+08	-6.24E+08	1.60E+09
1.1	1.09E+09	-1.46E+09	3.57E+08	-7.79E+08	6.34E+08	-6.34E+08	1.62E+09
1.2	1.12E+09	-1.47E+09	3.72E+08	-7.81E+08	6.43E+08	-6.43E+08	1.63E+09
1.3	1.14E+09	-1.48E+09	3.86E+08	-7.84E+08	6.50E+08	-6.50E+08	1.64E+09
1.4	1.16E+09	-1.49E+09	3.99E+08	-7.86E+08	6.57E+08	-6.57E+08	1.65E+09
1.5	1.18E+09	-1.50E+09	4.11E+08	-7.88E+08	6.64E+08	-6.64E+08	1.66E+09
2	1.26E+09	-1.53E+09	4.59E+08	-7.95E+08	6.89E+08	-6.89E+08	1.70E+09

n	Center Deflection	Top Yield Count	Top Ultimate Count	Bottom Yield Count	Bottom Ultimate Count	Total Yield Count	Total Ultimate Count
0	0.0097475	16	12	86	82	102	94
0.2	0.010499	20	20	135	103	155	123
0.5	0.011481	28	24	177	155	205	179
0.8	0.012182	32	28	231	203	263	231
0.9	0.012368	32	28	235	211	267	239
1	0.012534	32	28	239	223	271	251
1.1	0.012684	32	28	243	227	275	255
1.2	0.01282	32	28	243	235	275	263
1.3	0.012943	32	28	247	235	279	263
1.4	0.013056	32	32	255	239	287	271
1.5	0.013159	32	32	255	239	287	271
2	0.013567	36	32	261	251	297	283

0.50" Ti-A286 (Partial Taper)

n	x11 Top (max)	x11 Top (min)	x22 Top (max)	x22 Top (min)	x12 Top (max)	x12 Top (min)	Top Mises (max)
0	3.60E+07	-1.17E+09	-1.42E+07	-6.21E+08	5.46E+08	-5.46E+08	1.32E+09
0.2	1.15E+08	-1.24E+09	-7.65E+06	-6.54E+08	6.37E+08	-6.37E+08	1.45E+09
0.5	2.31E+08	-1.31E+09	1.23E+07	-7.05E+08	7.31E+08	-7.31E+08	1.58E+09
0.8	3.45E+08	-1.42E+09	4.50E+07	-7.39E+08	7.89E+08	-7.89E+08	1.67E+09
0.9	3.81E+08	-1.45E+09	5.64E+07	-7.47E+08	8.02E+08	-8.02E+08	1.70E+09
1	4.14E+08	-1.48E+09	6.75E+07	-7.55E+08	8.14E+08	-8.14E+08	1.73E+09
1.1	4.46E+08	-1.50E+09	7.85E+07	-7.61E+08	8.24E+08	-8.24E+08	1.76E+09
1.2	4.76E+08	-1.52E+09	9.08E+07	-7.67E+08	8.33E+08	-8.33E+08	1.79E+09
1.3	2.36E+08	-1.55E+09	1.04E+08	-7.75E+08	8.64E+08	-8.64E+08	1.81E+09
1.4	5.30E+08	-1.56E+09	1.14E+08	-7.76E+08	8.48E+08	-8.48E+08	1.83E+09
1.5	5.55E+08	-1.58E+09	1.25E+08	-7.80E+08	8.54E+08	-8.54E+08	1.85E+09
2	6.53E+08	-1.63E+09	1.71E+08	-7.95E+08	8.77E+08	-8.77E+08	1.91E+09

n	x11 Bottom (max)	x11 Bottom (min)	x22 Bottom (max)	x22 Bottom (min)	x12 Bottom (max)	x12 Bottom (min)	Bottom Mises (max)
0	2.11E+08	-1.41E+09	1.59E+07	-7.54E+08	5.67E+08	-5.67E+08	1.52E+09
0.2	2.80E+08	-1.62E+09	4.23E+07	-8.11E+08	6.78E+08	-6.78E+08	1.74E+09
0.5	4.07E+08	-1.87E+09	7.16E+07	-8.86E+08	7.96E+08	-7.96E+08	1.96E+09
0.8	5.71E+08	-2.09E+09	9.17E+07	-9.49E+08	8.72E+08	-8.72E+08	2.08E+09
0.9	6.47E+08	-2.15E+09	9.70E+07	-9.67E+08	8.91E+08	-8.91E+08	2.12E+09
1	7.17E+08	-2.20E+09	1.19E+08	-9.83E+08	9.08E+08	-9.08E+08	2.17E+09
1.1	7.82E+08	-2.25E+09	1.44E+08	-9.98E+08	9.23E+08	-9.23E+08	2.22E+09
1.2	8.42E+08	-2.30E+09	1.66E+08	-1.01E+09	9.36E+08	-9.36E+08	2.26E+09
1.3	1.05E+09	-2.15E+09	1.15E+08	-9.61E+08	9.47E+08	-9.47E+08	2.28E+09
1.4	9.46E+08	-2.38E+09	2.04E+08	-1.04E+09	9.59E+08	-9.59E+08	2.34E+09
1.5	9.91E+08	-2.42E+09	2.21E+08	-1.05E+09	9.69E+08	-9.69E+08	2.37E+09
2	1.17E+09	-2.55E+09	2.94E+08	-1.09E+09	1.01E+09	-1.01E+09	2.50E+09

n	Center Deflection	Top Yield Count	Top Ultimate Count	Bottom Yield Count	Bottom Ultimate Count	Total Yield Count	Total Ultimate Count
0	0.0040839	82	82	86	82	168	164
0.2	0.0040407	86	86	86	82	172	168
0.5	0.004771	86	86	106	82	192	168
0.8	0.0059905	94	86	124	102	218	188
0.9	0.0063956	94	86	137	112	231	198
1	0.0067725	98	86	151	123	249	209
1.1	0.0071224	98	86	165	139	263	225
1.2	0.0074442	98	86	171	151	269	237
1.3	-0.0082145	123	113	187	179	310	292
1.4	0.0080072	98	90	185	161	283	251
1.5	0.0082526	98	90	191	169	289	259
2	0.009205	100	94	243	211	343	305

0.10" Ti-Zi (Full Taper)

n	x11 Top (max)	x11 Top (min)	x22 Top (max)	x22 Top (min)	x12 Top (max)	x12 Top (min)	Top Mises (max)
0	7.38E+08	-5.25E+08	1.36E+07	-4.47E+08	2.85E+08	-2.85E+08	8.18E+08
0.2	9.03E+08	-7.76E+08	-3.32E+07	-6.70E+08	4.00E+08	-4.00E+08	1.06E+09
0.5	9.97E+08	-9.91E+08	-3.62E+07	-8.63E+08	4.98E+08	-4.98E+08	1.25E+09
0.8	1.03E+09	-1.10E+09	-2.68E+07	-9.54E+08	5.48E+08	-5.48E+08	1.38E+09
0.9	1.03E+09	-1.12E+09	-2.44E+07	-9.71E+08	5.58E+08	-5.58E+08	1.41E+09
1	1.04E+09	-1.13E+09	-2.23E+07	-9.84E+08	5.66E+08	-5.66E+08	1.43E+09
1.1	1.04E+09	-1.14E+09	-2.05E+07	-9.93E+08	5.72E+08	-5.72E+08	1.44E+09
1.2	1.05E+09	-1.15E+09	-1.89E+07	-1.00E+09	5.77E+08	-5.77E+08	1.45E+09
1.3	1.05E+09	-1.15E+09	-1.73E+07	-1.01E+09	5.82E+08	-5.82E+08	1.46E+09
1.4	1.05E+09	-1.16E+09	-1.59E+07	-1.01E+09	5.85E+08	-5.85E+08	1.47E+09
1.5	1.05E+09	-1.16E+09	-1.46E+07	-1.01E+09	5.88E+08	-5.88E+08	1.48E+09
2	1.06E+09	-1.18E+09	-9.56E+06	-1.02E+09	5.99E+08	-5.99E+08	1.50E+09

n	x11 Bottom (max)	x11 Bottom (min)	x22 Bottom (max)	x22 Bottom (min)	x12 Bottom (max)	x12 Bottom (min)	Bottom Mises (max)
0	6.90E+08	-5.41E+08	1.28E+08	-4.52E+08	2.86E+08	-2.86E+08	7.81E+08
0.2	8.37E+08	-7.99E+08	1.37E+08	-6.78E+08	4.01E+08	-4.01E+08	1.01E+09
0.5	9.19E+08	-1.02E+09	1.50E+08	-8.72E+08	4.99E+08	-4.99E+08	1.27E+09
0.8	9.45E+08	-1.13E+09	1.60E+08	-9.65E+08	5.49E+08	-5.49E+08	1.40E+09
0.9	9.49E+08	-1.15E+09	1.63E+08	-9.82E+08	5.59E+08	-5.59E+08	1.43E+09
1	9.53E+08	-1.17E+09	1.66E+08	-9.96E+08	5.68E+08	-5.68E+08	1.45E+09
1.1	9.57E+08	-1.17E+09	1.70E+08	-1.00E+09	5.73E+08	-5.73E+08	1.46E+09
1.2	9.58E+08	-1.18E+09	1.72E+08	-1.01E+09	5.79E+08	-5.79E+08	1.47E+09
1.3	9.60E+08	-1.19E+09	1.74E+08	-1.02E+09	5.83E+08	-5.83E+08	1.49E+09
1.4	9.61E+08	-1.20E+09	1.76E+08	-1.02E+09	5.87E+08	-5.87E+08	1.49E+09
1.5	9.62E+08	-1.20E+09	1.78E+08	-1.03E+09	5.90E+08	-5.90E+08	1.50E+09
2	9.65E+08	-1.21E+09	1.87E+08	-1.03E+09	6.00E+08	-6.00E+08	1.52E+09

n	Center Deflection	Top Yield Count	Top Ultimate Count	Bottom Yield Count	Bottom Ultimate Count	Total Yield Count	Total Ultimate Count
0	0.011019	74	74	78	78	152	152
0.2	0.011106	76	74	80	78	156	152
0.5	0.011234	86	80	109	84	195	164
0.8	0.01134	98	90	115	97	213	187
0.9	0.011369	98	90	115	99	213	189
1	0.011396	98	90	127	101	225	191
1.1	0.011417	98	90	135	103	233	193
1.2	0.01144	98	90	139	105	237	195
1.3	0.011461	98	90	139	105	237	195
1.4	0.01148	98	90	145	107	243	197
1.5	0.011498	98	90	145	107	243	197
2	0.011571	98	90	153	109	251	199

0.20" Ti-Zi (Full Taper)

n	x11 Top (max)	x11 Top (min)	x22 Top (max)	x22 Top (min)	x12 Top (max)	x12 Top (min)	Top Mises (max)
0	7.94E+08	-5.04E+08	6.92E+06	-4.32E+08	3.23E+08	-3.23E+08	8.58E+08
0.2	9.48E+08	-7.39E+08	-1.22E+07	-6.51E+08	4.59E+08	-4.59E+08	1.09E+09
0.5	1.04E+09	-9.51E+08	1.33E+06	-8.41E+08	5.77E+08	-5.77E+08	1.29E+09
0.8	1.08E+09	-1.05E+09	1.07E+07	-9.29E+08	6.35E+08	-6.35E+08	1.43E+09
0.9	1.09E+09	-1.07E+09	1.32E+07	-9.45E+08	6.47E+08	-6.47E+08	1.46E+09
1	1.09E+09	-1.08E+09	1.54E+07	-9.58E+08	6.57E+08	-6.57E+08	1.48E+09
1.1	1.10E+09	-1.09E+09	1.75E+07	-9.67E+08	6.65E+08	-6.65E+08	1.50E+09
1.2	1.11E+09	-1.10E+09	1.93E+07	-9.75E+08	6.71E+08	-6.71E+08	1.51E+09
1.3	1.11E+09	-1.11E+09	2.11E+07	-9.80E+08	6.77E+08	-6.77E+08	1.53E+09
1.4	1.12E+09	-1.11E+09	2.27E+07	-9.84E+08	6.81E+08	-6.81E+08	1.53E+09
1.5	1.12E+09	-1.12E+09	2.41E+07	-9.87E+08	6.84E+08	-6.84E+08	1.54E+09
2	1.14E+09	-1.13E+09	3.00E+07	-9.94E+08	6.96E+08	-6.96E+08	1.56E+09

n	x11 Bottom (max)	x11 Bottom (min)	x22 Bottom (max)	x22 Bottom (min)	x12 Bottom (max)	x12 Bottom (min)	Bottom Mises (max)
0	7.00E+08	-5.69E+08	1.00E+08	-4.45E+08	3.25E+08	-3.25E+08	7.87E+08
0.2	8.21E+08	-7.94E+08	1.12E+08	-6.69E+08	4.62E+08	-4.62E+08	1.05E+09
0.5	8.85E+08	-1.02E+09	1.32E+08	-8.64E+08	5.79E+08	-5.79E+08	1.34E+09
0.8	9.12E+08	-1.13E+09	1.48E+08	-9.54E+08	6.38E+08	-6.38E+08	1.48E+09
0.9	9.18E+08	-1.15E+09	1.52E+08	-9.71E+08	6.50E+08	-6.50E+08	1.51E+09
1	9.23E+08	-1.17E+09	1.57E+08	-9.84E+08	6.60E+08	-6.60E+08	1.53E+09
1.1	9.28E+08	-1.18E+09	1.60E+08	-9.94E+08	6.67E+08	-6.67E+08	1.55E+09
1.2	9.32E+08	-1.19E+09	1.64E+08	-1.00E+09	6.74E+08	-6.74E+08	1.56E+09
1.3	9.36E+08	-1.20E+09	1.67E+08	-1.01E+09	6.79E+08	-6.79E+08	1.58E+09
1.4	9.40E+08	-1.20E+09	1.70E+08	-1.01E+09	6.83E+08	-6.83E+08	1.58E+09
1.5	9.44E+08	-1.20E+09	1.73E+08	-1.01E+09	6.87E+08	-6.87E+08	1.59E+09
2	9.58E+08	-1.22E+09	1.84E+08	-1.02E+09	6.99E+08	-6.99E+08	1.62E+09

n	Center Deflection	Top Yield Count	Top Ultimate Count	Bottom Yield Count	Bottom Ultimate Count	Total Yield Count	Total Ultimate Count
0	0.0097736	74	74	78	78	152	152
0.2	0.0098883	80	76	95	78	175	154
0.5	0.01009	94	92	135	105	229	197
0.8	0.010259	98	94	153	117	251	211
0.9	0.010307	98	94	157	131	255	225
1	0.010351	98	94	157	141	255	235
1.1	0.01039	98	94	157	141	255	235
1.2	0.010429	98	94	163	145	261	239
1.3	0.010464	98	94	163	147	261	241
1.4	0.010494	98	94	163	151	261	245
1.5	0.010524	98	94	167	151	265	245
2	0.010647	98	94	171	157	269	251

0.50" Ti-Zi (Full Taper)

n	x11 Top (max)	x11 Top (min)	x22 Top (max)	x22 Top (min)	x12 Top (max)	x12 Top (min)	Top Mises (max)
0	1.64E+08	-7.63E+08	-1.18E+07	-5.07E+08	4.18E+08	-4.18E+08	9.39E+08
0.2	9.48E+08	-7.39E+08	-1.22E+07	-6.51E+08	4.59E+08	-4.59E+08	1.09E+09
0.5	-1.46E+07	-1.44E+09	-1.33E+07	-9.76E+08	7.55E+08	-7.55E+08	1.76E+09
0.8	1.01E+07	-1.56E+09	-7.34E+06	-1.07E+09	8.32E+08	-8.32E+08	1.93E+09
0.9	1.80E+07	-1.58E+09	-5.35E+06	-1.08E+09	8.48E+08	-8.48E+08	1.96E+09
1	2.55E+07	-1.59E+09	-3.39E+06	-1.10E+09	8.61E+08	-8.61E+08	1.99E+09
1.1	3.28E+07	-1.60E+09	-1.46E+06	-1.10E+09	8.71E+08	-8.71E+08	2.00E+09
1.2	3.95E+07	-1.61E+09	4.06E+05	-1.11E+09	8.79E+08	-8.79E+08	2.01E+09
1.3	4.61E+07	-1.61E+09	2.23E+06	-1.11E+09	8.86E+08	-8.86E+08	2.02E+09
1.4	5.23E+07	-1.61E+09	3.99E+06	-1.12E+09	8.91E+08	-8.91E+08	2.03E+09
1.5	5.82E+07	-1.60E+09	5.69E+06	-1.12E+09	8.95E+08	-8.95E+08	2.03E+09
2	8.35E+07	-1.58E+09	1.33E+07	-1.11E+09	9.08E+08	-9.08E+08	2.04E+09

n	x11 Bottom (max)	x11 Bottom (min)	x22 Bottom (max)	x22 Bottom (min)	x12 Bottom (max)	x12 Bottom (min)	Bottom Mises (max)
0	1.37E+08	-8.22E+08	1.94E+06	-5.26E+08	4.21E+08	-4.21E+08	9.82E+08
0.2	8.21E+08	-7.94E+08	1.12E+08	-6.69E+08	4.62E+08	-4.62E+08	1.05E+09
0.5	1.59E+08	-1.55E+09	-1.28E+07	-1.01E+09	7.57E+08	-7.57E+08	1.84E+09
0.8	1.91E+08	-1.69E+09	-1.09E+07	-1.11E+09	8.34E+08	-8.34E+08	2.02E+09
0.9	2.02E+08	-1.71E+09	-9.54E+06	-1.13E+09	8.50E+08	-8.50E+08	2.05E+09
1	2.13E+08	-1.73E+09	-8.02E+06	-1.14E+09	8.63E+08	-8.63E+08	2.07E+09
1.1	2.23E+08	-1.74E+09	-6.37E+06	-1.15E+09	8.73E+08	-8.73E+08	2.09E+09
1.2	2.34E+08	-1.75E+09	-4.65E+06	-1.16E+09	8.81E+08	-8.81E+08	2.11E+09
1.3	2.47E+08	-1.75E+09	-2.69E+06	-1.16E+09	8.88E+08	-8.88E+08	2.11E+09
1.4	2.60E+08	-1.75E+09	8.62E+04	-1.16E+09	8.93E+08	-8.93E+08	2.12E+09
1.5	2.72E+08	-1.75E+09	2.80E+06	-1.16E+09	8.98E+08	-8.98E+08	2.13E+09
2	3.24E+08	-1.74E+09	1.52E+07	-1.16E+09	9.11E+08	-9.11E+08	2.13E+09

n	Center Deflection	Top Yield Count	Top Ultimate Count	Bottom Yield Count	Bottom Ultimate Count	Total Yield Count	Total Ultimate Count
0	0.0041608	32	20	32	28	64	48
0.2	0.0098883	80	76	95	78	175	154
0.5	0.003947	104	100	108	104	212	204
0.8	0.0041496	110	104	108	104	218	208
0.9	0.0042299	110	104	108	104	218	208
1	0.0043125	114	104	108	104	222	208
1.1	0.0043961	114	106	108	104	222	210
1.2	0.0044544	114	110	108	104	222	214
1.3	0.00453	114	110	108	104	222	214
1.4	0.0046033	114	110	108	104	222	214
1.5	0.0046739	114	110	108	104	222	214
2	0.004985	114	110	108	104	222	214

0.10" Zi-Ti (Full Taper)

n	x11 Top (max)	x11 Top (min)	x22 Top (max)	x22 Top (min)	x12 Top (max)	x12 Top (min)	Top Mises (max)
0	1.09E+09	-1.21E+09	1.37E+07	-1.03E+09	6.29E+08	-6.29E+08	1.55E+09
0.2	9.61E+08	-9.01E+08	1.92E+07	-7.57E+08	4.93E+08	-4.93E+08	1.18E+09
0.5	8.43E+08	-6.86E+08	4.60E+07	-5.73E+08	3.90E+08	-3.90E+08	9.70E+08
0.8	7.85E+08	-6.00E+08	5.01E+07	-5.00E+08	3.45E+08	-3.45E+08	8.86E+08
0.9	7.73E+08	-5.84E+08	4.99E+07	-4.87E+08	3.37E+08	-3.37E+08	8.70E+08
1	7.65E+08	-5.72E+08	4.94E+07	-4.77E+08	3.30E+08	-3.30E+08	8.58E+08
1.1	7.58E+08	-5.63E+08	4.87E+07	-4.70E+08	3.24E+08	-3.24E+08	8.49E+08
1.2	7.54E+08	-5.56E+08	4.78E+07	-4.64E+08	3.20E+08	-3.20E+08	8.42E+08
1.3	7.50E+08	-5.51E+08	4.69E+07	-4.60E+08	3.17E+08	-3.17E+08	8.37E+08
1.4	7.47E+08	-5.47E+08	4.59E+07	-4.57E+08	3.14E+08	-3.14E+08	8.34E+08
1.5	7.45E+08	-5.44E+08	4.49E+07	-4.54E+08	3.12E+08	-3.12E+08	8.31E+08
2	7.41E+08	-5.36E+08	4.03E+07	-4.49E+08	3.05E+08	-3.05E+08	8.24E+08

n	x11 Bottom (max)	x11 Bottom (min)	x22 Bottom (max)	x22 Bottom (min)	x12 Bottom (max)	x12 Bottom (min)	Bottom Mises (max)
0	9.97E+08	-1.24E+09	2.29E+08	-1.04E+09	6.30E+08	-6.30E+08	1.58E+09
0.2	8.87E+08	-9.30E+08	2.11E+08	-7.67E+08	4.94E+08	-4.94E+08	1.20E+09
0.5	7.82E+08	-7.08E+08	1.94E+08	-5.81E+08	3.92E+08	-3.92E+08	9.29E+08
0.8	7.31E+08	-6.20E+08	1.85E+08	-5.07E+08	3.46E+08	-3.46E+08	8.46E+08
0.9	7.20E+08	-6.03E+08	1.82E+08	-4.93E+08	3.38E+08	-3.38E+08	8.30E+08
1	7.13E+08	-5.91E+08	1.80E+08	-4.83E+08	3.31E+08	-3.31E+08	8.19E+08
1.1	7.07E+08	-5.81E+08	1.78E+08	-4.76E+08	3.25E+08	-3.25E+08	8.10E+08
1.2	7.03E+08	-5.74E+08	1.76E+08	-4.70E+08	3.21E+08	-3.21E+08	8.04E+08
1.3	7.00E+08	-5.69E+08	1.74E+08	-4.66E+08	3.18E+08	-3.18E+08	7.99E+08
1.4	6.97E+08	-5.64E+08	1.72E+08	-4.63E+08	3.15E+08	-3.15E+08	7.95E+08
1.5	6.96E+08	-5.62E+08	1.71E+08	-4.60E+08	3.13E+08	-3.13E+08	7.93E+08
2	6.92E+08	-5.58E+08	1.64E+08	-4.54E+08	3.06E+08	-3.06E+08	7.87E+08

n	Center Deflection	Top Yield Count	Top Ultimate Count	Bottom Yield Count	Bottom Ultimate Count	Total Yield Count	Total Ultimate Count
0	0.011954	94	88	163	153	257	241
0.2	0.011805	84	76	155	117	239	193
0.5	0.011664	74	74	129	95	203	169
0.8	0.011572	74	74	115	89	189	163
0.9	0.011546	74	74	111	89	185	163
1	0.011523	74	74	103	87	177	161
1.1	0.011503	74	74	99	85	173	159
1.2	0.011484	74	74	99	83	173	157
1.3	0.011467	74	74	99	81	173	155
1.4	0.01145	74	74	99	78	173	152
1.5	0.011436	74	74	97	78	171	152
2	0.011374	74	74	95	78	169	152

0.20" Zi-Ti (Full Taper)

n	x11 Top (max)	x11 Top (min)	x22 Top (max)	x22 Top (min)	x12 Top (max)	x12 Top (min)	Top Mises (max)
0	1.28E+09	-1.14E+09	6.18E+07	-9.95E+08	7.26E+08	-7.26E+08	1.61E+09
0.2	1.13E+09	-8.46E+08	4.92E+07	-7.31E+08	5.65E+08	-5.65E+08	1.29E+09
0.5	9.84E+08	-6.42E+08	6.20E+07	-5.53E+08	4.46E+08	-4.46E+08	1.08E+09
0.8	9.15E+08	-5.59E+08	5.98E+07	-4.82E+08	3.93E+08	-3.93E+08	9.89E+08
0.9	9.02E+08	-5.44E+08	5.82E+07	-4.69E+08	3.83E+08	-3.83E+08	9.72E+08
1	8.92E+08	-5.32E+08	5.67E+07	-4.59E+08	3.75E+08	-3.75E+08	9.59E+08
1.1	8.84E+08	-5.24E+08	5.51E+07	-4.52E+08	3.68E+08	-3.68E+08	9.48E+08
1.2	8.79E+08	-5.14E+08	5.40E+07	-4.45E+08	3.62E+08	-3.62E+08	9.41E+08
1.3	8.74E+08	-5.09E+08	5.24E+07	-4.41E+08	3.58E+08	-3.58E+08	9.35E+08
1.4	8.70E+08	-5.05E+08	5.09E+07	-4.38E+08	3.55E+08	-3.55E+08	9.30E+08
1.5	8.67E+08	-5.02E+08	4.94E+07	-4.36E+08	3.52E+08	-3.52E+08	9.27E+08
2	8.58E+08	-4.95E+08	4.27E+07	-4.31E+08	3.44E+08	-3.44E+08	9.16E+08

n	x11 Bottom (max)	x11 Bottom (min)	x22 Bottom (max)	x22 Bottom (min)	x12 Bottom (max)	x12 Bottom (min)	Bottom Mises (max)
0	1.09E+09	-1.23E+09	2.43E+08	-1.02E+09	7.29E+08	-7.29E+08	1.66E+09
0.2	9.73E+08	-9.14E+08	2.23E+08	-7.53E+08	5.68E+08	-5.68E+08	1.26E+09
0.5	8.61E+08	-6.95E+08	2.03E+08	-5.70E+08	4.48E+08	-4.48E+08	9.86E+08
0.8	8.05E+08	-6.10E+08	1.89E+08	-4.96E+08	3.95E+08	-3.95E+08	9.04E+08
0.9	7.94E+08	-6.08E+08	1.85E+08	-4.83E+08	3.85E+08	-3.85E+08	8.88E+08
1	7.85E+08	-6.05E+08	1.82E+08	-4.73E+08	3.77E+08	-3.77E+08	8.76E+08
1.1	7.79E+08	-6.03E+08	1.78E+08	-4.66E+08	3.70E+08	-3.70E+08	8.67E+08
1.2	7.75E+08	-6.02E+08	1.75E+08	-4.59E+08	3.64E+08	-3.64E+08	8.60E+08
1.3	7.71E+08	-6.01E+08	1.72E+08	-4.55E+08	3.60E+08	-3.60E+08	8.55E+08
1.4	7.68E+08	-5.99E+08	1.70E+08	-4.52E+08	3.57E+08	-3.57E+08	8.51E+08
1.5	7.66E+08	-5.98E+08	1.67E+08	-4.49E+08	3.54E+08	-3.54E+08	8.47E+08
2	7.59E+08	-5.92E+08	1.57E+08	-4.44E+08	3.46E+08	-3.46E+08	8.38E+08

n	Center Deflection	Top Yield Count	Top Ultimate Count	Bottom Yield Count	Bottom Ultimate Count	Total Yield Count	Total Ultimate Count
0	0.011255	98	94	185	173	283	267
0.2	0.011063	88	84	167	157	255	241
0.5	0.010876	74	74	149	139	223	213
0.8	0.010746	74	74	143	125	217	199
0.9	0.01071	74	74	143	123	217	197
1	0.010676	74	74	143	119	217	193
1.1	0.010646	74	74	137	115	211	189
1.2	0.010613	74	74	137	111	211	185
1.3	0.010587	74	74	137	95	211	169
1.4	0.010562	74	74	133	95	207	169
1.5	0.010538	74	74	133	95	207	169
2	0.010438	74	74	123	91	197	165

0.50" Zi-Ti (Full Taper)

n	x11 Top (max)	x11 Top (min)	x22 Top (max)	x22 Top (min)	x12 Top (max)	x12 Top (min)	Top Mises (max)
0	6.57E+08	-1.40E+09	7.05E+07	-1.05E+09	9.28E+08	-9.28E+08	1.94E+09
0.2	6.84E+08	-1.04E+09	6.69E+07	-7.74E+08	7.19E+08	-7.19E+08	1.46E+09
0.5	6.62E+08	-7.96E+08	6.06E+07	-5.86E+08	5.64E+08	-5.64E+08	1.13E+09
0.8	6.35E+08	-6.99E+08	5.43E+07	-5.12E+08	4.96E+08	-4.96E+08	1.00E+09
0.9	6.26E+08	-6.83E+08	5.23E+07	-5.00E+08	4.83E+08	-4.83E+08	9.74E+08
1	6.18E+08	-6.71E+08	5.03E+07	-4.90E+08	4.73E+08	-4.73E+08	9.53E+08
1.1	6.10E+08	-6.62E+08	4.85E+07	-4.83E+08	4.65E+08	-4.65E+08	9.37E+08
1.2	6.03E+08	-6.57E+08	4.67E+07	-4.78E+08	4.59E+08	-4.59E+08	9.25E+08
1.3	5.95E+08	-6.53E+08	4.49E+07	-4.75E+08	4.53E+08	-4.53E+08	9.14E+08
1.4	5.88E+08	-6.50E+08	4.33E+07	-4.72E+08	4.49E+08	-4.49E+08	9.06E+08
1.5	5.81E+08	-6.49E+08	4.17E+07	-4.71E+08	4.46E+08	-4.46E+08	8.99E+08
2	5.48E+08	-6.53E+08	3.46E+07	-4.69E+08	4.36E+08	-4.36E+08	8.86E+08

n	x11 Bottom (max)	x11 Bottom (min)	x22 Bottom (max)	x22 Bottom (min)	x12 Bottom (max)	x12 Bottom (min)	Bottom Mises (max)
0	5.61E+08	-1.59E+09	1.04E+08	-1.11E+09	9.33E+08	-9.33E+08	2.05E+09
0.2	5.22E+08	-1.18E+09	1.04E+08	-8.19E+08	7.23E+08	-7.23E+08	1.55E+09
0.5	4.80E+08	-9.02E+08	9.89E+07	-6.21E+08	5.68E+08	-5.68E+08	1.20E+09
0.8	4.47E+08	-7.91E+08	9.38E+07	-5.42E+08	5.00E+08	-5.00E+08	1.05E+09
0.9	4.43E+08	-7.72E+08	9.26E+07	-5.28E+08	4.87E+08	-4.87E+08	1.02E+09
1	4.38E+08	-7.58E+08	9.12E+07	-5.18E+08	4.76E+08	-4.76E+08	1.00E+09
1.1	4.33E+08	-7.47E+08	8.98E+07	-5.11E+08	4.68E+08	-4.68E+08	9.84E+08
1.2	4.29E+08	-7.40E+08	8.83E+07	-5.05E+08	4.62E+08	-4.62E+08	9.72E+08
1.3	4.24E+08	-7.35E+08	8.68E+07	-5.01E+08	4.57E+08	-4.57E+08	9.63E+08
1.4	4.19E+08	-7.31E+08	8.53E+07	-4.98E+08	4.53E+08	-4.53E+08	9.56E+08
1.5	4.13E+08	-7.29E+08	8.38E+07	-4.96E+08	4.49E+08	-4.49E+08	9.51E+08
2	3.87E+08	-7.29E+08	7.64E+07	-4.93E+08	4.39E+08	-4.39E+08	9.39E+08

n	Center Deflection	Top Yield Count	Top Ultimate Count	Bottom Yield Count	Bottom Ultimate Count	Total Yield Count	Total Ultimate Count
0	0.0066286	114	114	117	104	231	218
0.2	0.0065803	106	104	108	104	214	208
0.5	0.0065002	92	86	90	86	182	172
0.8	0.0063987	82	74	86	60	168	134
0.9	0.0063552	78	74	82	48	160	122
1	0.0063114	78	74	82	44	160	118
1.1	0.0062673	78	74	82	44	160	118
1.2	0.0062234	78	74	68	40	146	114
1.3	0.0061799	78	74	60	40	138	114
1.4	0.0061369	78	74	52	40	130	114
1.5	0.0060946	78	74	48	40	126	114
2	0.0058974	78	74	44	36	122	110

0.10" A286-Ti (Full Taper)

n	x11 Top (max)	x11 Top (min)	x22 Top (max)	x22 Top (min)	x12 Top (max)	x12 Top (min)	Top Mises (max)
0	8.93E+08	-2.08E+09	2.47E+08	-1.93E+09	1.09E+09	-1.09E+09	2.76E+09
0.2	1.02E+09	-1.26E+09	1.93E+08	-1.15E+09	7.80E+08	-7.80E+08	1.81E+09
0.5	1.00E+09	-7.67E+08	2.18E+08	-6.83E+08	5.59E+08	-5.59E+08	1.21E+09
0.8	9.52E+08	-5.98E+08	2.31E+08	-5.22E+08	4.63E+08	-4.63E+08	1.05E+09
0.9	9.39E+08	-5.74E+08	2.28E+08	-4.97E+08	4.46E+08	-4.46E+08	1.03E+09
1	9.28E+08	-5.53E+08	2.24E+08	-4.77E+08	4.30E+08	-4.30E+08	1.01E+09
1.1	9.18E+08	-5.38E+08	2.19E+08	-4.63E+08	4.17E+08	-4.17E+08	9.93E+08
1.2	9.09E+08	-5.27E+08	2.13E+08	-4.52E+08	4.07E+08	-4.07E+08	9.80E+08
1.3	9.01E+08	-5.19E+08	2.07E+08	-4.45E+08	3.98E+08	-3.98E+08	9.69E+08
1.4	8.95E+08	-5.13E+08	2.01E+08	-4.39E+08	3.90E+08	-3.90E+08	9.60E+08
1.5	8.89E+08	-5.09E+08	1.95E+08	-4.35E+08	3.83E+08	-3.83E+08	9.53E+08
2	8.66E+08	-5.00E+08	1.68E+08	-4.27E+08	3.59E+08	-3.59E+08	9.28E+08

n	x11 Bottom (max)	x11 Bottom (min)	x22 Bottom (max)	x22 Bottom (min)	x12 Bottom (max)	x12 Bottom (min)	Bottom Mises (max)
0	1.24E+09	-2.16E+09	5.62E+08	-1.96E+09	1.08E+09	-1.08E+09	2.79E+09
0.2	1.10E+09	-1.31E+09	4.80E+08	-1.16E+09	7.76E+08	-7.76E+08	1.83E+09
0.5	9.69E+08	-8.05E+08	4.05E+08	-6.95E+08	5.57E+08	-5.57E+08	1.23E+09
0.8	8.90E+08	-6.28E+08	3.57E+08	-5.32E+08	4.62E+08	-4.62E+08	1.01E+09
0.9	8.79E+08	-6.03E+08	3.44E+08	-5.06E+08	4.45E+08	-4.45E+08	9.82E+08
1	8.69E+08	-5.91E+08	3.33E+08	-4.86E+08	4.30E+08	-4.30E+08	9.63E+08
1.1	8.60E+08	-5.88E+08	3.23E+08	-4.71E+08	4.17E+08	-4.17E+08	9.48E+08
1.2	8.52E+08	-5.85E+08	3.14E+08	-4.60E+08	4.06E+08	-4.06E+08	9.36E+08
1.3	8.45E+08	-5.82E+08	3.06E+08	-4.53E+08	3.98E+08	-3.98E+08	9.26E+08
1.4	8.39E+08	-5.80E+08	2.98E+08	-4.47E+08	3.90E+08	-3.90E+08	9.17E+08
1.5	8.34E+08	-5.78E+08	2.91E+08	-4.43E+08	3.84E+08	-3.84E+08	9.10E+08
2	8.13E+08	-5.70E+08	2.63E+08	-4.34E+08	3.59E+08	-3.59E+08	8.87E+08

n	Center Deflection	Top Yield Count	Top Ultimate Count	Bottom Yield Count	Bottom Ultimate Count	Total Yield Count	Total Ultimate Count
0	0.015192	114	114	295	287	409	401
0.2	0.014512	96	88	269	249	365	337
0.5	0.013863	84	82	239	211	323	293
0.8	0.013434	82	78	207	171	289	249
0.9	0.013322	78	74	183	165	261	239
1	0.013219	74	74	173	165	247	239
1.1	0.013126	74	74	173	161	247	235
1.2	0.013041	74	74	171	161	245	235
1.3	0.012962	74	74	165	159	239	233
1.4	0.01289	74	74	161	155	235	229
1.5	0.012823	74	74	161	155	235	229
2	0.012551	74	74	155	145	229	219

0.20" A286-Ti (Full Taper)

n	x11 Top (max)	x11 Top (min)	x22 Top (max)	x22 Top (min)	x12 Top (max)	x12 Top (min)	Top Mises (max)
0	1.57E+09	-1.93E+09	3.50E+08	-1.86E+09	1.29E+09	-1.29E+09	2.92E+09
0.2	1.54E+09	-1.16E+09	2.94E+08	-1.09E+09	9.09E+08	-9.09E+08	1.94E+09
0.5	1.40E+09	-7.09E+08	3.31E+08	-6.50E+08	6.46E+08	-6.46E+08	1.50E+09
0.8	1.29E+09	-5.53E+08	3.14E+08	-4.96E+08	5.29E+08	-5.29E+08	1.33E+09
0.9	1.26E+09	-5.27E+08	3.05E+08	-4.71E+08	5.06E+08	-5.06E+08	1.30E+09
1	1.24E+09	-5.08E+08	2.95E+08	-4.52E+08	4.86E+08	-4.86E+08	1.27E+09
1.1	1.22E+09	-4.92E+08	2.85E+08	-4.38E+08	4.70E+08	-4.70E+08	1.25E+09
1.2	1.21E+09	-4.85E+08	2.75E+08	-4.29E+08	4.60E+08	-4.60E+08	1.23E+09
1.3	1.19E+09	-4.80E+08	2.65E+08	-4.22E+08	4.50E+08	-4.50E+08	1.21E+09
1.4	1.18E+09	-4.75E+08	2.56E+08	-4.18E+08	4.42E+08	-4.42E+08	1.20E+09
1.5	1.17E+09	-4.72E+08	2.47E+08	-4.14E+08	4.35E+08	-4.35E+08	1.19E+09
2	1.12E+09	-4.69E+08	2.09E+08	-4.09E+08	4.11E+08	-4.11E+08	1.14E+09

n	x11 Bottom (max)	x11 Bottom (min)	x22 Bottom (max)	x22 Bottom (min)	x12 Bottom (max)	x12 Bottom (min)	Bottom Mises (max)
0	1.57E+09	-2.10E+09	6.82E+08	-1.91E+09	1.27E+09	-1.27E+09	2.99E+09
0.2	1.38E+09	-1.28E+09	5.82E+08	-1.13E+09	9.04E+08	-9.04E+08	1.98E+09
0.5	1.23E+09	-7.91E+08	4.93E+08	-6.76E+08	6.44E+08	-6.44E+08	1.37E+09
0.8	1.15E+09	-6.42E+08	4.35E+08	-5.17E+08	5.30E+08	-5.30E+08	1.22E+09
0.9	1.13E+09	-6.36E+08	4.20E+08	-4.91E+08	5.06E+08	-5.06E+08	1.19E+09
1	1.11E+09	-6.31E+08	4.06E+08	-4.71E+08	4.87E+08	-4.87E+08	1.16E+09
1.1	1.09E+09	-6.28E+08	3.94E+08	-4.56E+08	4.72E+08	-4.72E+08	1.14E+09
1.2	1.08E+09	-6.22E+08	3.82E+08	-4.47E+08	4.61E+08	-4.61E+08	1.13E+09
1.3	1.07E+09	-6.18E+08	3.71E+08	-4.40E+08	4.52E+08	-4.52E+08	1.11E+09
1.4	1.06E+09	-6.15E+08	3.61E+08	-4.35E+08	4.44E+08	-4.44E+08	1.10E+09
1.5	1.05E+09	-6.12E+08	3.52E+08	-4.31E+08	4.37E+08	-4.37E+08	1.09E+09
2	1.00E+09	-6.00E+08	3.15E+08	-4.25E+08	4.13E+08	-4.13E+08	1.05E+09

n	Center Deflection	Top Yield Count	Top Ultimate Count	Bottom Yield Count	Bottom Ultimate Count	Total Yield Count	Total Ultimate Count
0	0.015505	122	118	327	293	449	411
0.2	0.014697	104	96	285	269	389	365
0.5	0.013904	88	84	255	251	343	335
0.8	0.013364	82	82	251	239	333	321
0.9	0.013218	82	82	247	235	329	317
1	0.013085	82	78	247	235	329	313
1.1	0.012963	82	74	247	223	329	297
1.2	0.01285	78	74	239	223	317	297
1.3	0.012743	78	74	231	215	309	289
1.4	0.012645	74	74	227	211	301	285
1.5	0.012554	74	74	223	203	297	277
2	0.012174	74	74	203	163	277	237

0.50" A286-Ti (Full Taper)

n	x11 Top (max)	x11 Top (min)	x22 Top (max)	x22 Top (min)	x12 Top (max)	x12 Top (min)	Top Mises (max)
0	2.05E+09	-1.76E+09	4.52E+08	-1.76E+09	1.56E+09	-1.56E+09	3.32E+09
0.2	1.94E+09	-1.13E+09	3.99E+08	-1.05E+09	1.12E+09	-1.12E+09	2.35E+09
0.5	1.71E+09	-7.51E+08	3.56E+08	-6.36E+08	8.02E+08	-8.02E+08	1.73E+09
0.8	1.55E+09	-6.20E+08	3.22E+08	-4.99E+08	6.65E+08	-6.65E+08	1.53E+09
0.9	1.51E+09	-5.98E+08	3.12E+08	-4.74E+08	6.35E+08	-6.35E+08	1.49E+09
1	1.47E+09	-5.89E+08	3.03E+08	-4.59E+08	6.13E+08	-6.13E+08	1.45E+09
1.1	1.44E+09	-5.85E+08	2.94E+08	-4.49E+08	5.95E+08	-5.95E+08	1.41E+09
1.2	1.40E+09	-5.83E+08	2.85E+08	-4.43E+08	5.80E+08	-5.80E+08	1.38E+09
1.3	1.37E+09	-5.85E+08	2.77E+08	-4.38E+08	5.68E+08	-5.68E+08	1.35E+09
1.4	1.35E+09	-5.87E+08	2.69E+08	-4.36E+08	5.57E+08	-5.57E+08	1.33E+09
1.5	1.32E+09	-5.91E+08	2.62E+08	-4.35E+08	5.49E+08	-5.49E+08	1.30E+09
2	1.21E+09	-6.16E+08	2.29E+08	-4.39E+08	5.19E+08	-5.19E+08	1.21E+09

n	x11 Bottom (max)	x11 Bottom (min)	x22 Bottom (max)	x22 Bottom (min)	x12 Bottom (max)	x12 Bottom (min)	Bottom Mises (max)
0	1.73E+09	-2.16E+09	6.30E+08	-1.89E+09	1.57E+09	-1.57E+09	3.33E+09
0.2	1.50E+09	-1.38E+09	5.51E+08	-1.14E+09	1.12E+09	-1.12E+09	2.29E+09
0.5	1.35E+09	-9.14E+08	4.82E+08	-6.94E+08	8.09E+08	-8.09E+08	1.64E+09
0.8	1.24E+09	-7.61E+08	4.33E+08	-5.44E+08	6.71E+08	-6.71E+08	1.35E+09
0.9	1.21E+09	-7.31E+08	4.21E+08	-5.18E+08	6.41E+08	-6.41E+08	1.30E+09
1	1.18E+09	-7.16E+08	4.09E+08	-5.00E+08	6.19E+08	-6.19E+08	1.26E+09
1.1	1.15E+09	-7.06E+08	3.98E+08	-4.88E+08	6.01E+08	-6.01E+08	1.23E+09
1.2	1.13E+09	-7.00E+08	3.88E+08	-4.80E+08	5.86E+08	-5.86E+08	1.20E+09
1.3	1.10E+09	-6.97E+08	3.77E+08	-4.75E+08	5.74E+08	-5.74E+08	1.18E+09
1.4	1.08E+09	-6.97E+08	3.68E+08	-4.71E+08	5.63E+08	-5.63E+08	1.16E+09
1.5	1.06E+09	-6.97E+08	3.58E+08	-4.69E+08	5.54E+08	-5.54E+08	1.14E+09
2	9.68E+08	-7.12E+08	3.23E+08	-4.70E+08	5.24E+08	-5.24E+08	1.07E+09

n	Center Deflection	Top Yield Count	Top Ultimate Count	Bottom Yield Count	Bottom Ultimate Count	Total Yield Count	Total Ultimate Count
0	0.01279	291	271	377	369	668	640
0.2	0.011955	235	197	361	299	596	496
0.5	0.011103	161	121	285	273	446	394
0.8	0.010477	102	96	265	247	367	343
0.9	0.010295	100	96	253	243	353	339
1	0.010125	96	96	251	239	347	335
1.1	0.0099706	96	88	247	235	343	323
1.2	0.0098141	96	84	243	227	339	311
1.3	0.0096695	96	84	239	219	335	303
1.4	0.0095427	92	82	235	211	327	293
1.5	0.0094068	88	78	231	191	319	269
2	0.0088349	82	78	173	143	255	221

0.10" Ti-A286 (Full Taper)

n	x11 Top (max)	x11 Top (min)	x22 Top (max)	x22 Top (min)	x12 Top (max)	x12 Top (min)	Top Mises (max)
0	7.38E+08	-5.25E+08	1.36E+07	-4.47E+08	2.85E+08	-2.85E+08	8.18E+08
0.2	6.95E+08	-1.03E+09	-1.60E+07	-9.64E+08	4.54E+08	-4.54E+08	1.27E+09
0.5	5.75E+08	-1.52E+09	3.78E+07	-1.48E+09	6.36E+08	-6.36E+08	1.86E+09
0.8	5.17E+08	-1.77E+09	7.44E+07	-1.73E+09	7.57E+08	-7.57E+08	2.19E+09
0.9	5.12E+08	-1.82E+09	8.39E+07	-1.78E+09	7.85E+08	-7.85E+08	2.26E+09
1	5.12E+08	-1.86E+09	9.24E+07	-1.82E+09	8.09E+08	-8.09E+08	2.31E+09
1.1	5.14E+08	-1.88E+09	1.00E+08	-1.85E+09	8.29E+08	-8.29E+08	2.35E+09
1.2	5.18E+08	-1.91E+09	1.07E+08	-1.87E+09	8.46E+08	-8.46E+08	2.39E+09
1.3	5.24E+08	-1.92E+09	1.13E+08	-1.88E+09	8.62E+08	-8.62E+08	2.42E+09
1.4	5.31E+08	-1.94E+09	1.19E+08	-1.90E+09	8.75E+08	-8.75E+08	2.44E+09
1.5	5.39E+08	-1.95E+09	1.24E+08	-1.90E+09	8.87E+08	-8.87E+08	2.46E+09
2	5.79E+08	-1.97E+09	1.45E+08	-1.92E+09	9.29E+08	-9.29E+08	2.53E+09

n	x11 Bottom (max)	x11 Bottom (min)	x22 Bottom (max)	x22 Bottom (min)	x12 Bottom (max)	x12 Bottom (min)	Bottom Mises (max)
0	6.90E+08	-5.41E+08	1.28E+08	-4.52E+08	2.86E+08	-2.86E+08	7.81E+08
0.2	6.26E+08	-1.07E+09	1.66E+08	-9.73E+08	4.55E+08	-4.55E+08	1.28E+09
0.5	7.29E+08	-1.57E+09	2.30E+08	-1.49E+09	6.37E+08	-6.37E+08	1.89E+09
0.8	8.19E+08	-1.83E+09	2.79E+08	-1.75E+09	7.56E+08	-7.56E+08	2.22E+09
0.9	8.43E+08	-1.88E+09	2.92E+08	-1.80E+09	7.83E+08	-7.83E+08	2.29E+09
1	8.64E+08	-1.92E+09	3.05E+08	-1.84E+09	8.07E+08	-8.07E+08	2.34E+09
1.1	8.84E+08	-1.95E+09	3.16E+08	-1.87E+09	8.27E+08	-8.27E+08	2.39E+09
1.2	9.02E+08	-1.97E+09	3.27E+08	-1.89E+09	8.44E+08	-8.44E+08	2.42E+09
1.3	9.18E+08	-1.99E+09	3.37E+08	-1.91E+09	8.59E+08	-8.59E+08	2.45E+09
1.4	9.33E+08	-2.00E+09	3.45E+08	-1.92E+09	8.72E+08	-8.72E+08	2.48E+09
1.5	9.47E+08	-2.01E+09	3.54E+08	-1.93E+09	8.83E+08	-8.83E+08	2.50E+09
2	1.00E+09	-2.04E+09	3.87E+08	-1.95E+09	9.25E+08	-9.25E+08	2.56E+09

n	Center Deflection	Top Yield Count	Top Ultimate Count	Bottom Yield Count	Bottom Ultimate Count	Total Yield Count	Total Ultimate Count
0	0.011019	74	74	78	78	152	152
0.2	0.011552	98	94	123	105	221	199
0.5	0.012235	114	110	197	179	311	289
0.8	0.012738	118	118	209	199	327	317
0.9	0.012871	118	118	213	203	331	321
1	0.012991	118	118	215	209	333	327
1.1	0.013099	118	118	217	209	335	327
1.2	0.013198	118	118	231	213	349	331
1.3	0.013287	118	118	255	213	373	331
1.4	0.013369	118	118	259	217	377	335
1.5	0.013445	118	118	267	217	385	335
2	0.013745	118	118	279	255	397	373

0.20" Ti-A286 (Full Taper)

n	x11 Top (max)	x11 Top (min)	x22 Top (max)	x22 Top (min)	x12 Top (max)	x12 Top (min)	Top Mises (max)
0	7.94E+08	-5.04E+08	6.92E+06	-4.32E+08	3.23E+08	-3.23E+08	8.58E+08
0.2	7.79E+08	-9.69E+08	2.18E+07	-9.23E+08	5.34E+08	-5.34E+08	1.29E+09
0.5	2.93E+08	-3.46E+09	4.46E+07	-2.23E+09	9.64E+08	-9.64E+08	3.04E+09
0.8	7.35E+08	-1.59E+09	1.14E+08	-1.65E+09	9.06E+08	-9.06E+08	2.26E+09
0.9	7.50E+08	-1.63E+09	1.25E+08	-1.70E+09	9.41E+08	-9.41E+08	2.33E+09
1	7.67E+08	-1.66E+09	1.34E+08	-1.73E+09	9.70E+08	-9.70E+08	2.39E+09
1.1	7.86E+08	-1.69E+09	1.43E+08	-1.76E+09	9.95E+08	-9.95E+08	2.44E+09
1.2	8.06E+08	-1.71E+09	1.51E+08	-1.78E+09	1.02E+09	-1.02E+09	2.48E+09
1.3	8.27E+08	-1.72E+09	1.58E+08	-1.79E+09	1.04E+09	-1.04E+09	2.51E+09
1.4	8.47E+08	-1.73E+09	1.65E+08	-1.81E+09	1.05E+09	-1.05E+09	2.54E+09
1.5	8.67E+08	-1.74E+09	1.71E+08	-1.81E+09	1.07E+09	-1.07E+09	2.56E+09
2	9.57E+08	-1.77E+09	1.98E+08	-1.83E+09	1.12E+09	-1.12E+09	2.64E+09

n	x11 Bottom (max)	x11 Bottom (min)	x22 Bottom (max)	x22 Bottom (min)	x12 Bottom (max)	x12 Bottom (min)	Bottom Mises (max)
0	7.00E+08	-5.69E+08	1.00E+08	-4.45E+08	3.25E+08	-3.25E+08	7.87E+08
0.2	6.67E+08	-1.01E+09	1.50E+08	-9.47E+08	5.36E+08	-5.36E+08	1.33E+09
0.5	3.40E+08	-3.21E+09	-1.40E+08	-2.15E+09	9.42E+08	-9.42E+08	2.84E+09
0.8	9.99E+08	-1.73E+09	3.09E+08	-1.70E+09	9.03E+08	-9.03E+08	2.32E+09
0.9	1.04E+09	-1.77E+09	3.28E+08	-1.75E+09	9.37E+08	-9.37E+08	2.39E+09
1	1.07E+09	-1.81E+09	3.46E+08	-1.78E+09	9.65E+08	-9.65E+08	2.45E+09
1.1	1.10E+09	-1.84E+09	3.62E+08	-1.81E+09	9.90E+08	-9.90E+08	2.50E+09
1.2	1.12E+09	-1.86E+09	3.77E+08	-1.83E+09	1.01E+09	-1.01E+09	2.54E+09
1.3	1.15E+09	-1.88E+09	3.90E+08	-1.85E+09	1.03E+09	-1.03E+09	2.58E+09
1.4	1.17E+09	-1.89E+09	4.03E+08	-1.86E+09	1.04E+09	-1.04E+09	2.61E+09
1.5	1.19E+09	-1.90E+09	4.15E+08	-1.87E+09	1.06E+09	-1.06E+09	2.63E+09
2	1.26E+09	-1.94E+09	4.61E+08	-1.88E+09	1.11E+09	-1.11E+09	2.71E+09

n	Center Deflection	Top Yield Count	Top Ultimate Count	Bottom Yield Count	Bottom Ultimate Count	Total Yield Count	Total Ultimate Count
0	0.0097736	74	74	78	78	152	152
0.2	0.010524	102	98	161	127	263	225
0.5	-0.014805	98	98	263	263	361	361
0.8	0.012209	118	118	267	251	385	369
0.9	0.012395	118	118	275	255	393	373
1	0.012563	118	118	279	267	397	385
1.1	0.012714	118	118	287	275	405	393
1.2	0.01285	118	118	287	275	405	393
1.3	0.012975	118	118	287	275	405	393
1.4	0.013088	118	118	291	279	409	397
1.5	0.013192	118	118	295	279	413	397
2	0.013604	118	118	299	283	417	401

0.50" Ti-A286 (Full Taper)

n	x11 Top (max)	x11 Top (min)	x22 Top (max)	x22 Top (min)	x12 Top (max)	x12 Top (min)	Top Mises (max)
0	1.64E+08	-7.63E+08	-1.18E+07	-5.07E+08	4.18E+08	-4.18E+08	9.39E+08
0.2	2.18E+07	-1.32E+09	-4.68E+06	-1.02E+09	7.21E+08	-7.21E+08	1.70E+09
0.5	1.34E+08	-1.78E+09	2.29E+07	-1.51E+09	1.04E+09	-1.04E+09	2.44E+09
0.8	2.46E+08	-1.94E+09	5.35E+07	-1.73E+09	1.23E+09	-1.23E+09	2.82E+09
0.9	2.80E+08	-1.96E+09	6.36E+07	-1.77E+09	1.27E+09	-1.27E+09	2.89E+09
1	3.17E+08	-1.96E+09	7.35E+07	-1.79E+09	1.30E+09	-1.30E+09	2.94E+09
1.1	3.60E+08	-1.96E+09	8.31E+07	-1.81E+09	1.33E+09	-1.33E+09	2.98E+09
1.2	4.00E+08	-1.95E+09	9.49E+07	-1.82E+09	1.36E+09	-1.36E+09	3.01E+09
1.3	4.36E+08	-1.94E+09	1.06E+08	-1.83E+09	1.37E+09	-1.37E+09	3.04E+09
1.4	4.69E+08	-1.93E+09	1.18E+08	-1.83E+09	1.39E+09	-1.39E+09	3.06E+09
1.5	4.99E+08	-1.92E+09	1.28E+08	-1.83E+09	1.41E+09	-1.41E+09	3.07E+09
2	6.14E+08	-1.86E+09	1.74E+08	-1.82E+09	1.45E+09	-1.45E+09	3.11E+09

n	x11 Bottom (max)	x11 Bottom (min)	x22 Bottom (max)	x22 Bottom (min)	x12 Bottom (max)	x12 Bottom (min)	Bottom Mises (max)
0	1.37E+08	-8.22E+08	1.94E+06	-5.26E+08	4.21E+08	-4.21E+08	9.82E+08
0.2	2.10E+08	-1.45E+09	-2.99E+07	-1.07E+09	7.21E+08	-7.21E+08	1.77E+09
0.5	3.67E+08	-2.01E+09	-9.99E+06	-1.58E+09	1.04E+09	-1.04E+09	2.55E+09
0.8	6.03E+08	-2.23E+09	3.98E+07	-1.82E+09	1.22E+09	-1.22E+09	2.94E+09
0.9	6.77E+08	-2.26E+09	6.02E+07	-1.86E+09	1.26E+09	-1.26E+09	3.02E+09
1	7.45E+08	-2.28E+09	8.69E+07	-1.89E+09	1.30E+09	-1.30E+09	3.08E+09
1.1	8.08E+08	-2.29E+09	1.12E+08	-1.91E+09	1.32E+09	-1.32E+09	3.12E+09
1.2	8.66E+08	-2.29E+09	1.35E+08	-1.93E+09	1.35E+09	-1.35E+09	3.15E+09
1.3	9.18E+08	-2.29E+09	1.57E+08	-1.94E+09	1.37E+09	-1.37E+09	3.18E+09
1.4	9.66E+08	-2.29E+09	1.77E+08	-1.94E+09	1.38E+09	-1.38E+09	3.20E+09
1.5	1.01E+09	-2.28E+09	1.96E+08	-1.95E+09	1.40E+09	-1.40E+09	3.22E+09
2	1.18E+09	-2.24E+09	2.73E+08	-1.94E+09	1.44E+09	-1.44E+09	3.26E+09

n	Center Deflection	Top Yield Count	Top Ultimate Count	Bottom Yield Count	Bottom Ultimate Count	Total Yield Count	Total Ultimate Count
0	0.0041608	32	20	32	28	64	48
0.2	0.0041837	118	106	112	104	230	210
0.5	0.0050227	126	122	142	126	268	248
0.8	0.0062461	130	122	161	142	291	264
0.9	0.0066367	130	126	177	153	307	279
1	0.0070019	130	126	195	167	325	293
1.1	0.0073388	130	126	205	179	335	305
1.2	0.0076474	130	126	215	193	345	319
1.3	0.0079292	134	126	221	203	355	329
1.4	0.0081861	134	126	229	209	363	335
1.5	0.0084202	134	126	245	211	379	337
2	0.0093313	141	130	287	263	428	393

Appendix E. Non-Linear Solution Example

The following example is taken directly from the ABAQUS user's manual. [6]

"The nonlinear response of a structure to a small load increment, ΔP, is shown in Figure 8.2.1–3. ABAQUS/Standard uses the structure's tangent stiffness, K_0, which is based on its configuration at u_0, and ΔP to calculate a *displacement correction*, c_a, for the structure. Using c_a, the structure's configuration is updated to u_a.

Figure 8.2.1–3 First iteration in an increment.

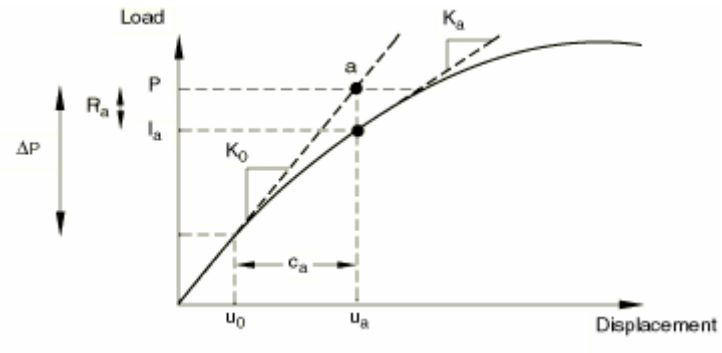

ABAQUS/Standard then calculates the structure's internal forces, I_a, in this updated configuration. The difference between the total applied load, P, and I_a can now be calculated as

$R_a = P - I_a$

where Ra is the force residual for the iteration.

If R_a is zero at every degree of freedom in the model, point "a" in Figure 8.2.1–3 would lie on the load-deflection curve and the structure would be in equilibrium. In a nonlinear problem R_a will never be exactly zero, so ABAQUS/Standard compares it to a tolerance value. If R_a is less than this force residual tolerance at all nodes, ABAQUS/Standard accepts the solution as being in equilibrium. By default, this tolerance value is set to 0.5% of an average force in the structure, averaged over time.

ABAQUS/Standard automatically calculates this spatially and time-averaged force throughout the simulation. This, and all other such tolerances, can be changed by using the *CONTROLS option..

If R_a is less than the current tolerance value, P and I_a are considered to be in equilibrium and u_a is a valid equilibrium configuration for the structure under the applied load. However, before ABAQUS/Standard accepts the solution, it also checks that the last displacement correction, c_a, is small relative to the total incremental displacement, $\Delta u_a = u_a - u_0$. If c_a is greater than a fraction (1% by default) of the incremental displacement, ABAQUS/Standard performs another iteration. Both convergence checks must be satisfied before a solution is said to have *converged* for that time increment.

If the solution from an iteration is not converged, ABAQUS/Standard performs another iteration to try to bring the internal and external forces into balance. First, ABAQUS/Standard forms the new stiffness, K_a, for the structure based on the updated configuration, u_a. This stiffness, together with the residual R_a, determines another displacement correction, c_b, that brings the system closer to equilibrium (point b in Figure 8.2.1–4).

Figure 8.2.1–4 Second iteration.

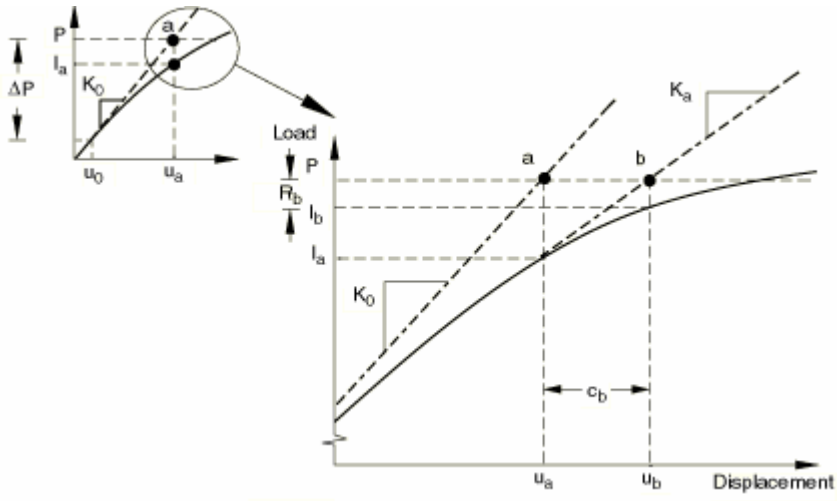

ABAQUS/Standard calculates a new force residual, R_b, using the internal forces from the structure's new configuration, u_b. Again, the largest force residual at any degree of freedom, R_b, is compared against the force residual tolerance, and the displacement correction for the second iteration, c_b, is compared to the increment of displacement, Δu_b. If necessary, ABAQUS/Standard performs further iterations.

For each iteration in a nonlinear analysis ABAQUS/Standard forms the model's stiffness matrix and solves a system of equations. Therefore, the computational cost of each iteration is close to the cost of conducting a complete linear analysis, making the computational expense of a nonlinear analysis potentially many times greater than the cost of a linear analysis. Since it is possible with ABAQUS/Standard to save results at each converged increment, the amount of output data available from a nonlinear simulation can also be much greater than that available from a linear analysis of the same geometry.” [6]

Bibliography

1. Cook, Robert D., Malkus, David S., Plesha, Michael E., and Witt, Robert J. *Concepts and Applications of Finite Element Analysis* (4th Edition). New York, NY: John Wiley & Sons, Inc., 2002

2. Reddy, J. N. "Analysis of functionally graded plated," *International Journal for Numerical Methods in Engineering, 47*:663-384 (2000)

3. Reddy, J. N. *Mechanics of Laminated Composite Plates and Shells* (2nd Edition). Boca Raton, FL: CRC Press, LLC, 2004

4. Gasik, M. M., Zhang, B.-S., Van der Biest, O., Vleuggels, J., Anne, G., and Put, S. "Design and Fabrication of Symmetric FGM Plates," *Materials Science Forums*, Vols. 423-425:23-28 (2003)

5. Palazotto, Anthony N. and Dennis, Scott T. *Nonlinear Analysis of Shell Structures.* Washington, DC: American Institute of Aeronautics and Astronautics, Inc., 1992

6. ABAQUS User's Manual. ABAQUS, Inc. 2003

7. Department of Defense. *Metallic Materials and Element for Aerospace Vehicle Structures*. MIL-HDBK-5J. Wright-Patterson Air Force Base: AFRL/MLSC, 31 January 2003.

8. Aerospace Specification Metals, Inc. "Titanium Ti-6Al-2Sn-4Zr-2Mo, Duplex Annealed." http://asm.matweb.com/search/SpecificMaterial.asp?bassnum=MTA641. 3 December 2003.

9. Incropera, Frank P. and DeWeitt, David P. *Fundamentals of Heat and Mass Transfer* (4th Edition). New York, NY: John Wiley & Sons, Inc., 1996

10. Ferro-Ceramic Grinding, Inc. http://65.108.128.37/pub/prodsvc/zirconia-properties.php. 22 February 2005

Vita

Captain W. Glenn Cooley graduated from Fort Collins High School in Fort Collins, Colorado. He entered undergraduate studies at the Colorado School of Mines in Golden, Colorado where he graduated with high scholastic honors in May 2000 with a Bachelor of Science degree in Engineering (Mechanical Specialty) and minors in Computer Science and Military Science. He was commissioned through the Detachment 105 AFROTC at the University of Colorado.

His first assignment was at Hill AFB as a T-37/T-38/F-4/F-5 Mechanical Systems Engineer in July 2000. He also served as and Aircraft Battle Damage Repair (ABDR) Engineer where he became the first engineer to be qualified on all three weapons systems supported at Hill AFB, the F-117, F-16, and A-10. In February 2004, he volunteered for deployment as an F-16 ABDR Engineer and deployed for three months in support of Iraqi Freedom. In August 2004, he entered the Graduate School of Aeronautics and Astronautics, Air Force Institute of Technology. Upon graduation, he will be assigned to the Air Force Research Laboratory in the Air Vehicles Directorate at Wright Patterson AFB, OH.

REPORT DOCUMENTATION PAGE

Form Approved
OMB No. 074-0188

1. REPORT DATE *(DD-MM-YYYY)*	2. REPORT TYPE	3. DATES COVERED *(From – To)*
21-03-2005	Master's Thesis	Aug 2003 - Mar 2005

4. TITLE AND SUBTITLE

Application of Functionally Graded Materials in Aircraft Structures

5a. CONTRACT NUMBER

5b. GRANT NUMBER

5c. PROGRAM ELEMENT NUMBER

6. AUTHOR(S)

Cooley, William G., Captain, USAF

5d. PROJECT NUMBER

5e. TASK NUMBER

5f. WORK UNIT NUMBER

7. PERFORMING ORGANIZATION NAMES(S) AND ADDRESS(S)

Air Force Institute of Technology
Graduate School of Engineering and Management (AFIT/EN)
2950 Hobson Way, Building 640
WPAFB OH 45433-8865

8. PERFORMING ORGANIZATION REPORT NUMBER

AFIT/GAE/ENY/05-M04

9. SPONSORING/MONITORING AGENCY NAME(S) AND ADDRESS(ES)

Dr. Ravinder Chona
AFRL/VASM
Bldg 65 Rm. 203W
2790 D Street
WPAFB, OH 45433

10. SPONSOR/MONITOR'S ACRONYM(S)

11. SPONSOR/MONITOR'S REPORT NUMBER(S)

12. DISTRIBUTION/AVAILABILITY STATEMENT

APPROVED FOR PUBLIC RELEASE; DISTRIBUTION UNLIMITED.

13. SUPPLEMENTARY NOTES

14. ABSTRACT

A Functionally Graded Material (FGM) is a material which has a continuous variation of material properties through-the-thickness. This thesis will explore analysis of FGM flat plates and shell panels, and use FGM's unique characteristics to retrofit a cracked exhaust wash structure.

FGMs are first characterized as flat plates under pressure and thermal loading. Next, FGM shell panels are characterized under thermal loading. Conclusions drawn from FGM characterization are used to develop a patch to retrofit a cracked aircraft exhaust wash structure. The exhaust wash structure is first analyzed to provide a baseline and then several FGM patches are evaluated on their ability to reduce stress and deflection. Finally, an exhaust wash panel made of FGM is analyzed.

15. SUBJECT TERMS

functionally graded materials, FGM, FGMs, exhaust wash structure, thermal protection

16. SECURITY CLASSIFICATION OF:			17. LIMITATION OF ABSTRACT	18. NUMBER OF PAGES	19a. NAME OF RESPONSIBLE PERSON
a. REPORT	b. ABSTRACT	c. THIS PAGE			Dr. A. N. Palazotto (ENY)
U	U	U	UU	189	19b. TELEPHONE NUMBER *(Include area code)* (937) 255-3069 anthony.palazotto@afit.edu